DI Theresa R. Hörmann, BSc

Development of a Continuous Manufacturing Line for the Tableting of Hot-Melt Extruded Pellets

DOCTORAL THESIS

to achieve the university degree of

Doktorin der technischen Wissenschaften

submitted to

Graz University of Technology

Supervisor

Univ.Prof. Dipl.-Ing. Dr.techn. Johannes G. Khinast

Institute for Process and Particle Technology

Research Center for Pharmaceutical Engineering GmbH

Graz, April 2019

Theresa Ruth Hörmann
Development of a Continuous Manufacturing Line
for the Tableting of Hot-Melt Extruded Pellets
Dissertation

First assessor
Univ.-Prof. Dipl.-Ing. Dr.techn. Johannes Khinast
Institute of Process and Particle Engineering
Research Center Pharmaceutical Engineering GmbH
Graz University of Technology

Second assessor
Assoz. Prof. Mag.pharm. Dr.rer.nat. Eva Roblegg
Institute of Pharmaceutical Sciences
University of Graz

Affidavit

I declare that I have authored this thesis independently, that I have not used other than the declared sources/resources, and that I have explicitly indicated all material which has been quoted either literally or by content from the sources used. The text document uploaded to TUGRAZonline is identical to the present doctoral thesis.

_____ _____

Date Signature

“Beim Mochn so wurdn.”

(Maria Fruhwirth)

Acknowledgements

First of all, I would like to thank Prof. Johannes Khinast, who provides an inspiring and challenging environment at his institute and research center, allowing to grow and develop oneself, according to one's talents. This environment creates a rare and positive working atmosphere which I enjoyed during my PhD.

I also want to acknowledge Assoz. Prof. Eva Roblegg, for being the second assessor of my thesis and the Austrian Federal Ministries and Funding Agencies (BMVIT, BMWFJ, SFG) for the financial support of my research.

Next, I deeply thank Daniel Treffer, who taught me to tackle problems by analytical thinking, an open mind and unwavering persistence in the search of solutions. Nevertheless, he also taught me not to miss out on any chance to have fun and make new friends along one's way.

Moreover, I would like to thank my colleagues at the Institute of Process and Particle Engineering, Tom Forgber, Bianca Grabner, Jakob Redlinger-Pohn, Federico Municchi and Mingqiu Wu for a great number of interesting discussions. Regarding my colleagues from the RCPE, special thanks go to Josip Matić and Andreas Eitzlmayr for long conversations on hot-melt extrusion, Alexander Troiss on melt rheology, Amrit Paudel on amorphous solid dispersions, Jakob Rehrl on PAT and control related aspects and Otto Scheibelhofer on basically everything.

Special thanks also go to Phillip Clarke for proof-reading parts of this thesis, to Hans Grubbauer for his support in the workshop and to Daniel Markl and Lukas Pichler for their support with the data management systems. Moreover, I want to thank Gerold Koscher for suggesting me to join this project as a PhD student and for teaching me a lot in project management. And I really need to thank my colleagues Mario Unterreiter, Markus Gamsriegler, Daniel Kaiser, Jelena Milinkovic, Andreas Freidl, Daniel Wiegele, Viktoria Magiosi, Viktoria Marko, Philipp Pernitsch, Michael Piller, Gudrun Hörl, Thomas Heller, Patrick Prugger, Michael Martinetz and Andreas Witschnigg for their help during experiments and characterization work.

In addition, I want to thank all the students that I (co-)supervised and which contributed to the findings and data in the thesis: Nina Jäger, Katrin Waldenhofer, Lukas Fölzer, Thomas Schmidt, Hannes Bauer, Josef Tausendschön, Stefan Naderer, Peter Prander, Alexander Meister, Petra Hainz, Sarah Koller and Jasmin Preininger.

I also enjoyed having the administrative team at the institute, Adela, Michaela and Silvia, as a great source of daily motivation and support. You provide such an open and friendly settings, that I think is

rare to find. In that context, I also want to tell all my colleagues Heidi, the Peters, Christian, Dani, Kathi, Christoph, Gernot, Stephan, the Stefans, and many more, that it was a pleasure working with you!

Finally, I also highly appreciate the valuable input to my work given by the project members in my consortium use-case project. Special thanks go to Reinhardt-Karsten Mürb and Adrian Funke for their continuous scientific input throughout the project and beyond.

Concluding, I want the express my gratitude to my love, Manuel, who accepted and supported my commitment to my scientific work during the last years and to my parents and grandparents, who equipped me with the confidence and will to do so.

Kurzfassung

Für viele pharmazeutische Produzenten wird es als unabdinglich gesehen, den Übergang zu kontinuierlichen Herstellungsverfahren und neuen Prozesstechnologien zu schaffen, um auch in Zukunft weiterhin den Patienten kostengünstige und sichere neue Medikamente zur Verfügung stellen zu können. Dieser Paradigmenwechsel in der pharmazeutischen Herstellung hat einen erhöhten Bedarf an Wissensaustausch zu diesen neuen Ansätzen und Technologien geweckt. Diese Arbeit ist Teil des European Consortium for Continuous Pharmaeutical Manufacturing (ECCPM), eines Konsortiums zur Erforschung kontinuierlicher Herstellungsverfahren in der Produktion von Medikamenten. In dessen Rahmen wurden drei verschiedene Routen zur Herstellung von Tabletten untersucht: i) über Direktverpressung, ii) über Feuchtgranulation und iii) über Schmelzextrusion in Kombination mit Pelletierung. Die Anwendungsfälle gaben Einblick in die verschiedenen Herausforderungen und Möglichkeiten, welche mit kontinuierlicher Prozessführung einhergehen.

Diese Arbeit beschäftigt sich mit der dritten Option, der Herstellung von Tabletten über Schmelzextrusion und Pelletierung. Die Produktentwicklung umfasste die Rezepturentwicklung, die Prozessentwicklung und die Charakterisierung der involvierten Prozesseinheiten. Die Route über Schmelzextrusion wurde in diesem Anwendungsfall gewählt, um eine Darreichungsform mit verbesserter Bioverfügbarkeit eines wasser-unlöslichen Wirkstoffes, Nimodipin (NMD), zu erreichen.

Im ersten Teil dieser Arbeit (Kapitel 2) wurde ein geeignetes Fenster für die Rezepturzusammensetzung mit 10 Gew.% NMD und verschiedenen Anteilen zweier Trägerpolymere, Aminoalkylmethacrylate-Copolymer (Euragit® E) und Hypromellose (Methocel® E5) (HPMC) gesucht, die gewünschten Eigenschaften des Zwischenprodukts zu erreichen. Das identifizierte Fenster der Rezepturzusammensetzung war geeignet um die gewünschte sofortige Freisetzung des Wirkstoffes von einer physikalisch stabilen amorphen Dispersion in Pelletform zu erreichen. Darüber hinaus wurden molekulare Wechselwirkungen untersucht um den Beitrag der einzelnen Komponenten tiefgehend zu verstehen. Da die Prozessroute vorgegeben war, wurde auch die Verarbeitbarkeit der Rezeptur in dieser berücksichtigt.

Im nächsten Abschnitt (Kapitel 3) werden die Versuche zur Konfiguration der Extrusions- und Pelletier-Prozesse diskutiert. Dabei standen zwei Möglichkeiten zur Verfügung, um die gewünschten Pellets als Zwischenprodukt herzustellen: i) die Strangpelletierung und ii) der Heißabschlag. Die Strangpelletierung ist aufgrund ihrer Robustheit weiter verbreitet. Die Anwendbarkeit des Heißabschlages wurde trotzdem getestet, weil mit diesem gerundete Pellets mit überlegenen Fließeigenschaften, im Vergleich zu den zylindrischen Pellets aus dem Strangpelletierer, hergestellt werden können. Schlussendlich wurde dennoch der Strangpelletierer gewählt, da die mehrphasige

Struktur der Formulierung mit zwei Erweichungstemperaturen einen Heißabschlag der Schmelze nicht erlaubte. Schließlich wurde eine Parameterstudie mit der finalen Prozesskonfiguration durchgeführt, mit dem Ziel Prozesseinstellungen zu finden, an welchen keine Bräunung des HPMCs in der Rezeptur auftrat. Aus dieser Parameterstudie wurden die optimalen Einstellungen abgeleitet, welche fortführend als Nominalwerte der Extrusions- und Pelletiereinheit dienten.

Kapitel 4 untersucht die Sensitivität des Extrusions- und Pelletierprozesses auf Kontrollmaßnahmen und Änderungen in der Zusammensetzung rund um die nominellen Prozesseinstellungen und der nominellen Rezeptur. Daraufhin wurde, basierend auf Pelletqualität und Prozesssabilität, ein Design-Space definiert. Außerdem wurde basierend auf beobachteten Effekten der getesteten Abweichungen auf die Prozessdynamik (d.h. die Verweilzeitverteilung) eine Kontrollstrategie vorgeschlagen.

Der nächste Abschnitt (Kapitel 5) handelt von der Charakterisierung der Verformungseigenschaften des Pelletbulks während der Kompaktierung und der Entwicklung einer Tablettenrezeptur zur Fertigung von mechanisch stabilen Tabletten auf einer Labor-Rundläufertablettenpresse. Diesbezüglich wurde Zusammensetzung einer Rezeptur bestehend aus mikrokristalliner Cellulose (Avicel® PH102), Crospovidone (Kollidon® CL) und Magnesium Stearat, im Hinblick auf Bruchfestigkeit, Friabilität, Gleichförmigkeit des Gewichtes und der Zerfallszeit der Tabletten, optimiert. Die größte Herausforderung dabei waren die elastischen Eigenschaften der Pellets während des Verpressens, welche Laminierung der Tabletten verursachte, wenn die Pulvermatrix die Verformung nicht ausreichend kompensieren konnte.

Schlussendlich enthält Kapitel 6 die Daten der Verweilzeitcharakterisierung des kontinuierlichen Mischers und der Tablettenpresse. Dabei wurde ein besonderes Augenmerk auf die Unterschiede im Materialtransport von Pellets und den Pulverkomponenten gelegt, indem die Verweilzeitverteilung dieser Komponenten getrennt bestimmt wurde. Es wurden Unterschiede festgestellt, welche bei der Nachverfolgung von Material im kontinuierlichen Prozess eine wesentliche Rolle zur Prozesskontrolle spielen.

Insgesamt konnte diese Arbeit erfolgreich einige Schritte der Pharmazeutischen Prozessentwicklung demonstrieren und dabei Vorteile und Herausforderungen der kontinuierlichen Herstellungsweise hervorheben. Besonders die Möglichkeit während Parameterstudien und der Prozessentwicklung für den Extrusions- und Pelletierprozess dynamisch die Einstellungen zu verändern, eröffnet ein beträchtliches Einsparungspotential für Entwicklungszeit und Materialbedarf, wenn man den Vergleich zu einem chargenweisen Wirbelschichtgranulationsprozess anstellt. Um dieses Potenzial jedoch voll ausschöpfen zu können, wäre es nötig, für alle entscheidenden Qualitätsattribute des Produktes Prozessanalytik mit Echtzeitüberwachung zur Verfügung zu haben. Hier eröffnet sich durch einen Mangel an geeigneten Methoden ein großes Potenzial für zukünftige Forschung.

Abstract

The adoption of continuous manufacturing (CM) and new technologies in pharmaceutical production is considered an indispensable step for many companies, in order to further successfully provide cost-efficient, safe and new medicines to patients. Therefore, a paradigm shift in pharmaceutical manufacturing is taking place which has generated a need for increased co-operation in terms of knowledge exchange and sharing of these new approaches and technologies. This work is part of a consortium for research on the CM of pharmaceutical products, the European Consortium for Continuous Pharmaceutical Manufacturing (ECCPM). Thereby, three continuous tablet production lines via different process routes were investigated: i) direct compaction (DC), ii) wet granulation (WG) and iii) hot-melt extrusion (HME) and pelletization. These use cases provided insight into the variety of challenges and solutions associated with CM.

This thesis investigates the third option, a tablet manufacturing line via HME and pelletization, including formulation development, process development and process characterization of all involved units. The route via HME was chosen in this use case, in order to provide a dosage form with enhanced bioavailability for a poorly water-soluble active pharmaceutical ingredient (API), nimodipine (NMD).

In the first part of this work (Chapter 2) a feasible composition window was determined for the desired intermediate product performance of a formulation with 10 wt.% of NMD and varying fractions of two carrier polymers, a copolymer of di-methyl-amino-ethyl-methacrylate, butyl-methacrylate and methyl-methacrylate (Eudragit® E) and hydroxyproyl methylcellulose (Methocel® E5) (HPMC). The identified composition window provided the required immediate API release from a physically stable amorphous solid dispersion (ASD) in pellet shape. Moreover, molecular interactions between the formulation components and their effect on performance were investigated, in order to thoroughly understand the contribution of each substance. Since the process route was preset, the processability of the formulation was also considered.

In the next section (Chapter 3), the process setup and a process parameter screening for the HME-pelletization unit are discussed. There were two options for the generation of the intermediate pellets: i) via strand pelletization and ii) via die-face pelletization. Strand pelletization is the more established and robust pelletization technology. However, die-face pelletization was also tested since it generates rounded pellets, with superior flow properties compared to the cylindrical pellets from strand pelletization. Ultimately, strand pelletization was selected, as the phase separated nature of the formulation with two softening points did not allow to pelletize the melt directly at the die-face. The process parameter screening focused on the identification of process parameter settings which did not

provoke browning of the HPMC in the formulation. The optimal settings derived from this screening were further used as a nominal set point for the HME-pelletization unit.

Chapter 4 investigates the sensitivity of the HME-pelletization process to control actions and composition deviations around the nominal process settings and formulation. Subsequently, the findings on pellet quality and the process stability were utilized for the definition of a design space. Moreover, a control strategy was suggested based on the observed effects of the tested variations on the process dynamics, i.e. the residence time distribution (RTD).

The next section (Chapter 5) details on the characterization of the bulk deformation behavior of the pellets during compression and also the development of a tableting formulation for the generation of mechanically stable tablets on a rotary, laboratory tablet press. To that end, a formulation comprising pellets, microcrystalline cellulose (Avicel® PH102), cross-linked polyvinylpyrrolidone (Kollidon® CL) and magnesium stearate was optimized with regard to final tablet resistance to crushing, friability, weight uniformity and disintegration time. The main challenge was the elastic behavior of the pellets upon compression, causing lamination of the tablets, if the powder matrix was not able to accommodate this deformation.

Finally, Chapter 6 contains the data on the characterization of the continuous blender and the tablet press with regard to their RTDs. Special focus was placed on understanding the differences in material transport for pellets and powder components, by characterizing their RTDs separately. The observed differences in RTD are crucial for material tracking as a basis for process control in a pharmaceutical CM line.

Overall, this work successfully demonstrated several stages of the pharmaceutical product development, highlighting the advantages and challenges of CM. Especially, the ability to perform dynamic set point changes during process screening and development of the HME-pelletization unit was found to carry significant potential to save time and material, when compared to the development of a batch fluidized bed granulation process. However, in order to take full advantage of this potential, the implementation of real-time process analytical tools (PAT) for all crucial product quality attributes would be required. In this regard, several limitations and consequently, significant potential for future work were identified.

Table of Contents

List of Figures

List of Tables

1. Introduction

Recently pharmaceutical companies are undergoing a transformation. This is not only due to the effect of globalization and digitalization as observed in other industries, but also due to a change in mindset concerning the manufacturing of pharmaceutical products (Plumb, 2005). This manufacturing change is driven by several aspects:

- The patent cliff, forcing pharmaceutical companies to innovate or increase efficiency in order to maintain revenue upon blockbuster drug patent expiration. Song and Han (2016) suggested several strategies to overcome this critical phase, where one option was to extend patent duration by improving manufacturing for better purity or efficiency after filing, or to maintain market dominance through competitive pricing, if the manufacturing process is cost efficient. The second suggestion extends the life cycle of a drug product in a sustainable manner.
- The "solubility challenge" is driving the development of more sophisticated manufacturing processes (Hywel D Williams et al., 2013). Due to systematic molecule screening, the low hanging fruits, i.e. small drug molecules from chemical synthesis with good bioavailability, have already been marketed and an increasing number of poorly soluble APIs are being discovered as potential candidates (Leuner et al., 2017). Thus, the fraction of drugs with poor bioavailability in the development pipeline has increased, comprising the majority of new molecular entities (NMEs) (Ku, 2008). These active pharmaceutical ingredients (APIs) require advanced formulations and dosage forms to overcome the bioavailability limitation.
- Recalls and drug shortages (Peters, 2019) have led to a change in the strategy of regulating agencies, with the goal of increasing the quality of pharmaceutical production in a way that those agencies need less involvement (FDA US Department of Health, 2011). Simultaneously, more room was provided for continuous improvement of manufacturing processes during patent protection and product life cycle. There were several initiatives launched and broadly discussed to achieve this goal (Yu et al., 2014). Today the industry is still in the process of adaption to these new possibilities and requirements.
- Finally, outdated and partially poorly understood batch processes were used by the pharmaceutical industry to a large extent, due to the strict regulation and pressure to return on investment during patent protection. There was a strong focus on developing new molecules in Research and Development, but not on improving manufacturing efficiency.

However, this has led to lower manufacturing capabilities compared to other industries (e.g. six sigma in semi-conductor production) and long product development lead times.

Thus, there has been strong activity in recent decades to investigate different approaches in pharmaceutical production. Continuous manufacturing (CM) processes were investigated as one promising route towards a more efficient manufacturing environment.

1.1. Continuous Manufacturing of Solid Oral Dosage Forms

The adoption of CM in pharmaceutical production is a response to several of the above mentioned trends. Continuous processes have the potential to increase flexibility, robustness and process control in primary, as well as in secondary manufacturing. Initially, expectations were very high as Sau L. Lee et al. (2015) states in a list of expected benefits: i) increased efficiency and reduced safety hazards due to smaller equipment, ii) lower cost of storage, faster response time to market shortage and less risk of intermediate degradation due to shorter supply chains and lean manufacturing, iii) less batch-to-batch variation, simpler process monitoring and control strategies and reduction of corrective steps downstream due to the steady state of production, and iv) ease of scale-up by increasing running time and potential improvements in synthesis reaction control and possibilities due to continuous flow production. However, a later article by McWilliams et al. (2018) highlights, that the adoption of CM was rather slow with a shift from batch to continuous processes between 0-5% over five years in primary manufacturing. This finding was based on an extensive survey among pharmaceutical companies and contract manufacturing organizations. The authors identified business considerations as a main reason for this, along with slow adaptations of culture, training and perception of regulatory risks. Especially the postreaction steps in API synthesis and real-time analytical tools were found to advance slowly, which was attributed to a lack of established approaches and little harmonization. No equivalent study was found for secondary manufacturing, but similar trends were observed (Johnston et al., 2017). In both mentioned publications, platform technologies for robust processes, and collaboration of industry, academia and regulatory agencies to expand the knowledge base in CM, were identified as solutions/requirements to successful adoption. Platform technologies and knowledge bases are needed for many different aspects of CM, such as: manufacturing route selection, process control strategy, process analytical technology (PAT) and real-time release testing (RTRT), batch definition, risk management, data handling and management, process validation and verification.

The proposal of a Manufacturing Classification System (MCS) (Leane et al., 2015) was an approach to simplify and rationalize the decision making with regard to manufacturing route selection. In this system, APIs with specific properties are classified with regard to percolation threshold and

developability, in order to identify the simplest possible, but robust, manufacturing route. The manufacturing routes are ranked with increasing complexity, but also increasing capability to process more difficult APIs:

- Direct Compression (DC)
- Dry Granulation (DG)
- Wet Granulation (WG)
- Other technologies (e.g. hot-melt extrusion (HME)).

The MCS can be used either to select a viable manufacturing route for a given API, or to design an API specifically for a desired manufacturing route. This set of processing routes also captures the most common routes investigated for CM. However, neither does the MCS consider processability in CM, nor does it explain process route decisions with regard to biopharmaceutical considerations (Leane et al., 2018).

Therefore, there is still a knowledge gap regarding the risk of transferring, for example, a batch WG formulation to a continuous process, and a lack of process route indications for APIs with bioavailability limitations that need rigorous transformation of their properties. Regarding the latter aspect, the Biopharmaceutics Classification System (BCS), introduced in 1995 (Amidon et al., 1995), already maps bioavailability limitations to aqueous solubility and/or intestinal permeability, guiding the correct formulation approach.

APIs with solubility limitations, but good permeability (class II) are especially relevant, due to the amount of NMEs in this class. Thus, extensive work has been completed to identify options to overcome this issue. Hywel D. Williams et al. (2013) published an in-depth review on the options to overcome low drug solubility. Amorphous solid dispersions (ASDs) are one on these options for oral dosage forms.

1.2. Amorphous Solid Dispersions

ASDs are systems containing the API in an amorphous state, that is in an unordered state with increased free energy. The aqueous solubility is increased because the energy for solubilization is reduced by the energy required for breaking crystalline bonds between API molecules. Moreover, the effective particle size of the API is reduced and wetting improved. However, the amorphous state is thermodynamically unstable and, therefore, needs to be well controlled for solid-state transitions, in order to provide increased dissolution performance for a sufficient time. Polymers can be used to stabilize the amorphous state by intermolecular interaction with the API or increased local viscosity. Both routes reduce the mobility of the drug molecules or hinder crystal nucleation (Hywel D. Williams et al., 2013). This stabilization is not only required to achieve the desired shelf-life of the drug product, but also during dissolution of the drug in the body. Recrystallization needs to be prevented at the wetted surface with increased molecular mobility, as well as precipitation in the intestinal fluids due to super-saturation.

The performance of ASD systems is largely determined by their structure, which is governed by API concentration, polymer selection and ASD preparation method (Janssens et al., 2010). The most stable and fastest dissolution of API is achieved from solid solutions or glass solutions, where the API is solubilized molecularly in the carrier polymer, typically at low concentration levels. With increasing API content, systems with amorphous or crystalline API clusters or particles are created. Depending on the state of the polymeric carrier, different systems of amorphous/crystalline API and amorphous/crystalline carrier polymer can be achieved, that is eutectic systems, solid amorphous suspensions, glass suspensions, or glass amorphous suspensions (Leuner et al., 2017; Hywel D. Williams et al., 2013). The solid and glass amorphous suspensions with amorphous API clusters typically outperform eutectic systems and glass suspensions with crystalline API particles, with regard to dissolution enhancement (Mohammed et al., 2012).

Even though the use of ASDs is a widely accepted approach to overcome the solubility challenge, there are a limited amount of ASD products on the market (Jermain et al., 2018). This is attributed to the manufacturing complexity and the need to adopt more sophisticated quality testing approaches (Hywel D. Williams et al., 2013).

There are two main approaches for the generation of polymeric ASDs: the solvent evaporation and the fusion method. Examples of an industrial process resembling the evaporation method is spray drying, while HME is an industrial technology for applying the fusion method. Solvent evaporation is used in the case of thermally labile APIs, dissolving the API and the polymer in an organic solvent, then evaporating the solvent at slightly increased temperature and under vacuum. However, it is crucial to remove the solvent completely due to toxicity and ASD stability considerations. Moreover, ASD

stability can be critically influenced by changing manufacturing conditions, due to the sensitivity of the ASD structure to the rate of solvent removal (Hywel D. Williams et al., 2013). The fusion method in contrast, typically applies higher temperatures, heating the mixture above the melting or glass transition temperature of the components, followed by rapid cooling to freeze the molecules in the disordered state. Thereby, a fast cooling rate minimizes the time for diffusion processes, leading to clustered API molecules and an increased risk of recrystallization. Moreover, intensive mixing of the melt is crucial for the generation of a stable ASD, in order to avoid API or polymer-enriched domains. Co-rotating twin-screw extruders (TSE) are an inherently continuous process technology offering excellent mixing capability, at simultaneously short residence times, minimizing thermal stress (Breitenbach, 2002; Crowley et al., 2007; Martin, 2013a). Thus, it has firmly established itself in the industrial production of ASD systems (Albers, 2008; Patil et al., 2016; Repka et al., 2008; Shah and Repka, 2013).

1.3. Hot-Melt Extrusion and Pelletization

HME is mainly applied for the preparation of advanced dosage forms, since the process requires more specific understanding of product and equipment compared. to, for example, a tablet from a DC line. Censi et al. (2018) provide a comprehensive overview of physicochemical factors that need to be specifically considered, when designing an HME process:

- chemical and thermal stability of raw materials and products,
- the solid state and stability of the product,
- drug-polymer interaction, miscibility and solubility,
- the rheological behavior of the melt, and
- the physicochemical properties of the products.

However, it combines the advantage of being inherently continuous and is superior for providing tailored drug release, or solubility enhancement in one process step, due to the melting, mixing and shaping options (Repka et al., 2018). It has also been used for taste masking in pediatric applications (Keating et al., 2018; D. C. T. Tan et al., 2018), for the preparation of abuse resistant dosage forms (Baronsky-Probst et al., 2016; Jedinger et al., 2016, 2014), for the production of nano-based systems (Khinast et al., 2013; Patil et al., 2015), the combination of several drugs in one dosage unit (Chowdhury et al., 2018) and for personalized medicine in combination with 3D printing (D. Tan et al., 2018) for oral application. An extensive overview of applications and marketed products can be found elsewhere (Ren et al., 2019; Repka et al., 2018; Stanković et al., 2015).

HME is frequently used to shape the melt directly to matrix tablets, that is the final dosage form (Bruce et al., 2005; Crowley et al., 2004; Desai et al., 2017; Fukuda et al., 2006; Kipping and Rein, 2013; Liu et

al., 2001; Nokhodchi et al., 2012; Patil et al., 2016). However, this approach is usually chosen for sustained release applications, since the matrix of HME products is typically dense with a lack of pores for the dissolution medium to provide fast API release (Crowley et al., 2004; Roblegg et al., 2011). If immediate API release should be achieved, pore formers, or disintegrants can be added to the matrix, or the extrudate can be milled prior to tableting in order to increase the surface area for dissolution (Albers, 2008; Démuth et al., 2015; Grymonpré et al., 2016; Kalivoda, 2012; Mohammed et al., 2012). A risk associated with the latter approach is that the milling process may influence the solid state, which is especially critical for ASD formulations (Albers, 2008) and the advantage of gaining superior ASD stability by HME processing could be lost. Moreover, the lowered glass transition temperature of ASDs often requires cryogenic milling, (Démuth et al., 2015) which is laborious and not possible to achieve in a continuous mode. Finally, there is also the option to pelletize the extrudate in order to increase the surface to volume ratio, accelerating dissolution, and to use the pellets for further processing. Pelletization is less widely applied, due to the dominance of tablets as the final dosage form for oral application. Most pellets though, are either filled in sachets for direct oral use, or filled into capsules (Kalivoda, 2012; Mohammed et al., 2012; Vithani and Douroumis, 2019).

However, multiple unit pellet system (MUPS) tablets make use of coated or uncoated pellets in combination with tablet compression. A fast disintegration of such tablets into many small pellets helps to avoid locally high API concentration in the gastrointestinal (GI) tract, causing irritation or precipitation risk, or problems in esophageal transport (Abdul et al., 2010; Bodmeier, 1997; Mehta et al., 2012). However, no literature is available on such use of HME prepared pellets. The published work was mainly performed with pellets generated by different types of granulation and spheronization (Abbaspour et al., 2008; Dukić-Ott et al., 2009; Dukić et al., 2007; Mehta et al., 2012).

Basically, there are two ways to pelletize the melt after the extrusion: either directly at the die via die-face pelletization, or after a certain distance from the die via strand pelletization (Case, 2003). Die-face pelletization has been applied for preparing pellets using different APIs in starches (Bialleck and Rein, 2011), sugar in corn starch (Yeung and Rein, 2015), antipyrine and codeine phosphate in corn starch and antipyrine in xanthan and gum arabic (Jedinger et al., 2016), paracetamol in calcium stearate (CaSt) (Treffer et al., 2014) and carbamazepine in Soluplus® (Alshetaili et al., 2016). Strand pelletization has been used for formulations composed of CaSt and paracetamol (Roblegg et al., 2011), of a combination of Eudragit® RSPO, hydroxypropyl methylcellulose (HMPC) and stearic acid as a carrier for anhydrous theophylline (Vo et al., 2016), of combinations of Eudragit®, MCC and PEG with anhydrous theophylline (Young et al., 2002) and of copovidone, Soluplus® and HPMC with fenofibrate (Kalivoda et al., 2012).

The applicability of these two pelletization techniques largely depends on the viscoelastic properties of the strand at extrusion temperature and the mechanical properties in the solidified state. During

die-face pelletization, the glass transition temperature of the melt, where it changes its behavior from liquid to solid-like, must not be too high, in order to allow pelletization without sticking of the melt (Treffer and Khinast, 2017). In contrast, for strand pelletization, the cutting behavior of the solidified strand is critical, since brittle materials tend to fracture before or upon cutting, leading to poor size uniformity of the product.

1.3.1. Challenges and Limitations

Besides the variety of products developed via HME the number of pharmaceutical companies adopting this technology is limited, due to the following reasons:

- The process and its products require specifically educated product development personnel and trained operators.
- There are limitations for processing thermo-labile and shear sensitive APIs and excipients.
- Only a limited number of carrier materials are registered for oral use.

Regarding the latter point, a list of polymers, waxes and lipids used as functional carrier excipients or processing aids for HME is provided elsewhere (Crowley et al., 2007; Leuner et al., 2017). In order to overcome performance limitations offered by single polymer systems, there has been increased attention on the application of polymer mixtures as carriers (Kalivoda et al., 2012; Marks et al., 2014).

However, the limitations in available polymers are problematic for pelletization as well. For example, several of the registered polymers exhibit very sticky behavior and smear at HME processing temperatures, diminishing the feasibility of die-face pelletization (Bialleck and Rein, 2011; Treffer, 2016; Witschnigg et al., 2016). Moreover, the addition of large fractions of API to the polymers often complicates the properties of the melt further, either by plasticizing the melt, increasing stickiness (Witschnigg et al., 2016) or by increasing the brittleness in solid state (Abbaspour et al., 2007). Nevertheless, significant progress has been made by Treffer (2016) who developed a thermally decoupled die plate allowing pelletization of some of these problematic polymers. The challenge is to identify a sweet spot between decreased stickiness and increased melt pressure levels for successful die-face pelletization. The focus during the application of strand pelletization is on the formulation properties at the cutting temperature and the stability of the strand when drawn into the pelletizer.

Finally, the application cases of pelletization technology are limited due to the dominance of tablets on the pharmaceutical market and a lack of literature on the tableting of HME pellets.

1.4. From Pellet to Tablet

The tableting of HME pellets is an interesting research field, as it combines the advantages of tablets with the improved bioavailability and handling properties of ASD pellets. The advantages of MUPS tablets were already discussed extensively in 1997 by Bodmeier (Bodmeier, 1997). The more uniform distribution of many dosage units in the GI tract was reasoned as an option to accelerate the onset of the therapeutic effect, to mitigate side effects of drugs, to stabilize the bioavailability and to reduce food effects. In comparison to capsules, which are an alternative option for MUPS, tablets can be prepared at lower cost, carry a lower risk of tampering and have higher patient compliance (Bodmeier, 1997).

Even though, there is a large number of publications investigating the mechanical properties of pellets from different material combinations (Abbaspour et al., 2007; Bashaiwoldu et al., 2011, 2004a, 2004b; Dukić-Ott et al., 2009; Lundqvist et al., 1997; Sousa et al., 2002; Thommes and Kleinebudde, 2006a, 2006b), there is a lack of information on the intrinsic properties of raw materials which would be required to engineer the optimal pellet composition for tablet compression, without extensive experimental work (Bashaiwoldu et al., 2004a). A lot of focus was placed on the mechanical stability or ideal deformation behavior with regards to coated pellets for controlled drug release, that is plastic or slightly elastic behavior, in order to support the integrity of the coating upon compression. However, if immediate release is desired from the final tablet, fracturing of the pellets is also acceptable. However, bond formation by fusion is critical, as it may lead to a large, dense agglomerate of pellets with insufficient surface for fast API dissolution. Moreover, the latter would obliterate the positive effects of disintegrating pellets in the GI tract. Thereby, differences in microstructure and shape of single pellets from different manufacturing technologies, for example granulation-spheronization and HME, are expected to cause significant differences in the overall properties of the pellet bed, which are not very well understood, further complicating the knowledge transfer on excipient performance from one method to another.

However, typically it is not possible to compress tablets purely from pellets on industrial tableting equipment due to a lack of final tablet strength (Bodmeier, 1997; Braun, 2003). Under the assumption, that pellets do not contribute to the bond formation, the minimum volume fraction of binder required to fill the voids in a closely packed bed of spheres is 29% (Bodmeier, 1997). Thus, it is crucial to select appropriate tableting aids, in order to compensate for the lack of compressibility of the pellets, and to provide desired disintegration performance.

Moreover, two of the main concerns when processing pellets into tablets is weight and content uniformity, and segregation of pellets and tableting aids during processing. Research in the field of MUPS tablets indicate, that content and weight uniformity issues are minimized at specific optimal

mixture compositions, depending on the material combinations (Bodmeier, 1997; Braun, 2003). Additionally, segregation has to be controlled either by increasing particle size of the tableting aids, or by minimizing the pellet size. The reduction of pellet size further increases weight and content uniformity due to the lower relative contribution of single pellets to the overall content and weight. In that regard, it is crucial to investigate the smallest achievable pellet size to mitigate these risks.

1.4.1. Continuous Bending and Tableting

The process of tableting is inherently continuous, with tablets being produced as long as material resides in the hopper of the tablet press. However, tablet presses have been optimized for batch-processing. A characterization of dynamic properties, that is their RTD, and performance at changing tableting speeds, has only recently gained significant attention (Dülle et al., 2018a, 2018b; Grymonpré et al., 2018a; Manley and Shi, 2018; Martinetz et al., 2018, 2017).

Continuous blenders are well established, with regard to blending technology, and have been characterized extensively (Gao et al., 2011; Portillo et al., 2010; Toson et al., 2018; Vanarase and Muzzio, 2011). Blenders are characterized by their ability to mix the incoming materials radially and also to a certain degree along their axis, in order to dampen input fluctuation. However, there is a lack of literature on the continuous blending of pellet-powder blends.

1.5. Research Objectives and Content of the Dissertation

1.5.1. Overall Objectives

As introduced above, industry, academia and regulating agencies have reached the conclusion, that a successful adoption of CM in pharmaceutical production is possible only through knowledge exchange. This thesis is part of an academic-industrial consortium, the European Consortium for Continuous Pharmaceutical Manufacturing (ECCPM – find more information at www.eccpm.com). This consortium aims at providing a platform for the exchange of knowledge on overarching topics in CM by means of three use-cases representing typical tableting manufacturing routes via:

i) direct compression,
ii) wet granulation and
iii) hot-melt extrusion.

This work investigates the production of tablets via the compression of HME pellets.

Therefore, a BCS class II model API, nimodipine, was used with the target of providing immediate release from the final tablet via the formation of a physically stable ASD. A Quality Target Product Profile (QTPP) was defined (Table 1-1) and a QbD approach was taken to develop the desired tablet, as illustrated in Figure 1-1 and Figure 1-2.

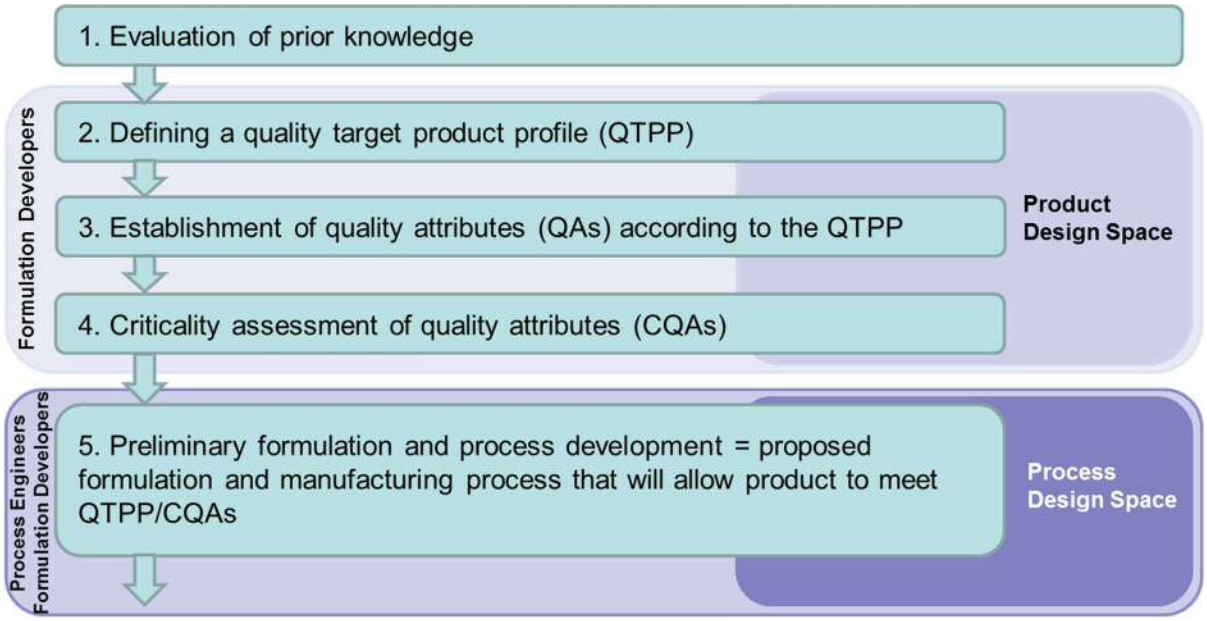

Figure 1-1. QbD strategy for the development of a pharmaceutical manufacturing process (part 1).

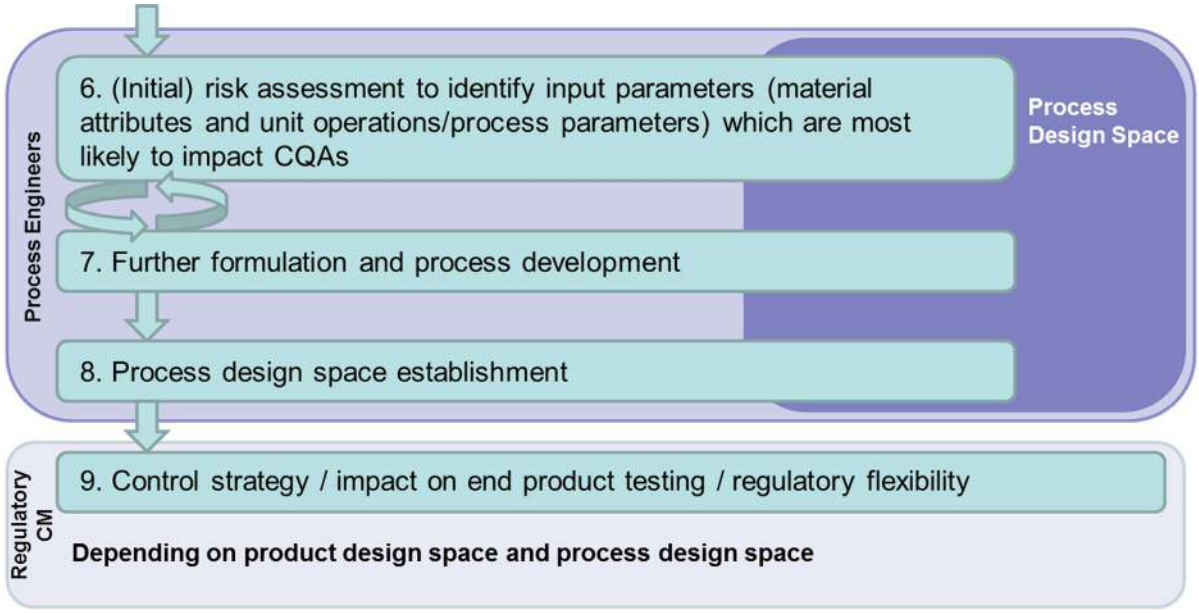

Figure 1-2. QbD strategy for the development of a pharmaceutical manufacturing process (part 2).

Table 1-1. QTPP for final tablet.

Parameter	Specifications release	Criticality assessment	Method
Description, Appearance	Round tablet Ø 6 to 10 mm, shape not specified	Critical	Tablet weight Size testing
Potency Assay	Not fixed	Critical	Inline: combined PAT tools Offline: HPLC (according to in-house-method)
Impurities: degradation products and impurities	Nitropyridine compound max. 0.5%; Unspecified degradation product 0.2%; Sum of all degradation products max. 1.0%;	Critical	Inline: Spectroscopy (PAT) Offline: HPLC (according to in-house-method)
Water:	Max. 1%	Critical	Inline: spectroscopy (PAT) Offline: Karl-Fischer titration
Identity: identification	Positive for amorphous Nimodipine	Critical	Inline: combined PAT tools Offline: HPLC
Uniformity of dosage units: content uniformity or weight variation	Meets Ph.Eur./USP	Critical	Inline: combined PAT tools Offline: HPLC According to Ph. Eur. 2.9.40
Dissolution	Consistent with immediate release, 85% (Q80) in 30 min	Critical	Dissolution testing according to Ph. Eur. 2.9.3
Disintegration	10 min	Critical	Disintegration testing according to Ph. Eur. 2.9.1
Resistance to crushing, Hardness*	40 to 120 N (depending on tablet size)	Critical	Hardness testing according to Ph. Eur. 2.9.8
Friability*	*0.1 to 0.2%*	Critical	Friability testing according to Ph. Eur. 2.9.7
Stability	*Shelf life 3 years*	Critical	Dissolution testing according to Ph. Eur. 2.9.3, HPLC
*Hardness and Friability combined to “Mechanical strength”			

An initial outline for the continuous process line is shown in Figure 1-3. The initial draft comprised a mill as an optional process step, in case direct compression of the HME pellets was not possible.

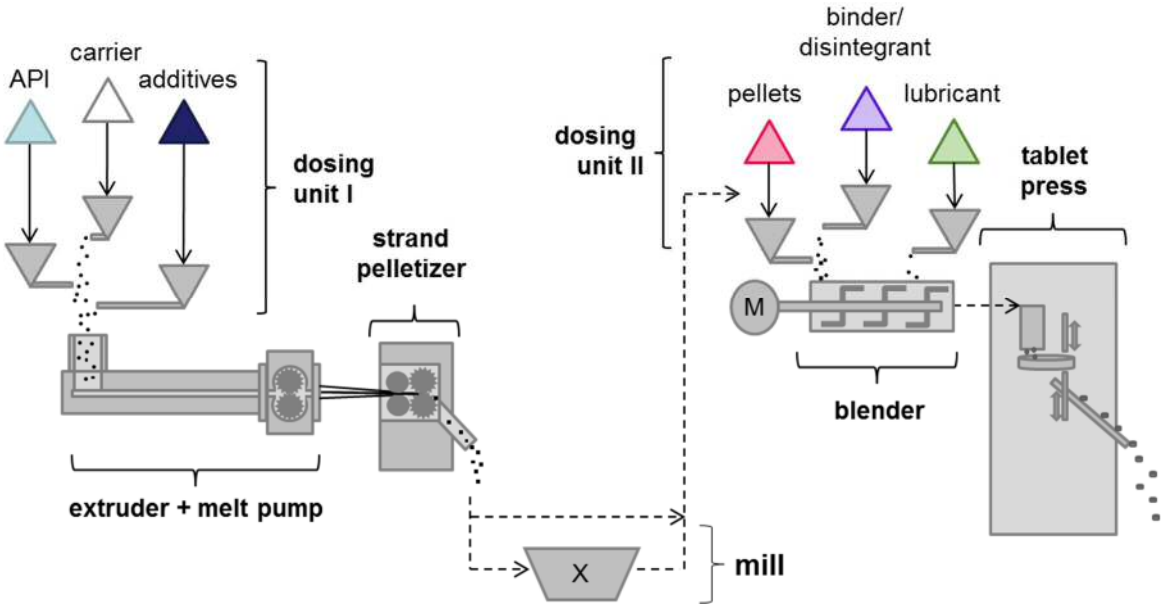

Figure 1-3. Initial outline of the continuous tablet manufacturing line via HME and pelletization.

1.5.2. Content of the Dissertation

The content of this work is structured into the following chapters and associated research questions:

- Chapter 2 - Formulation Performance and Processability Window for Manufacturing a Dual-Polymer Amorphous Solid Dispersion via Hot-Melt Extrusion and Strand Pelletization
    - Identification of a formulation composition providing a stable ASD with immediate release and properties appropriate for pelletization
    - Characterization of molecular interactions contributing to the performance of the ASD
- Chapter 3 - Hot-Melt Extrusion and Pelletization Process Setup and Parameter Screening
    - Identification of a stable HME process setup
    - Final selection of pelletization technology
    - Selection of nominal process settings for the HME-pelletization unit
- Chapter 4 - Sensitivity of a Continuous Hot-Melt Extrusion and Strand Pelletization Line to Control Actions and Composition Variation
    - Assessment of the sensitivity of process parameters and product quality to control actions and process deviations
    - Definition of a design space for the HME-pelletization unit
    - Establishment of a control strategy for the implementation of the process unit into a CM line for the production of tablets
- Chapter 5 - Tableting Formulation Development for the Compression of Elastic Hot-Melt Extruded Pellets

    - Characterization of the mechanical properties/compactability of the HME pellets
    - Identification of a formulation for a pilot-scale compression of the pellets into mechanically stable tablets with IR profile
- Chapter 6 - Residence Time Distributions of a Powder-Pellet Blend in a Continuous Blending and Tableting Unit
    - Pellets and powder component RTD characterization in blender and tablet press
    - Investigation of for material tracking-relevant differences in powder and pellet RTD, and sources thereof
- Chapter 7 - Conclusions and Future Directions

This is a cumulative thesis, where Chapter 2 has been published in the International Journal of Pharmaceutics (Hörmann et al., 2018) and Chapter 4 (Hörmann et al., n.d.) has been submitted to the same journal. Chapter 5 is in preparation for the submission to the International Journal of Pharmaceutics. A part of the work presented in Chapter 6 has been published in the International Journal of Pharmaceutics, as part of a joint publication with the other two academic partners in the consortium, the University of Ghent and the University of Eastern Finland (Karttunen et al., 2019).

1.6. References

Abbaspour, M.R., Sadeghi, F., Afrasiabi Garekani, H., 2008. Design and study of ibuprofen disintegrating sustained-release tablets comprising coated pellets. Eur. J. Pharm. Biopharm. 68, 747–59.

Abbaspour, M.R., Sadeghi, F., Afrasiabi Garekani, H., 2007. Thermal treating as a tool to produce plastic pellets based on Eudragit RS PO and RL PO aimed for tableting. Eur. J. Pharm. Biopharm. 67, 260–7.

Abdul, S., Chandewar, A. V, Jaiswal, S.B., 2010. A flexible technology for modified-release drugs: multiple-unit pellet system (MUPS). J. Control. Release 147, 2–16.

Albers, J., 2008. Hot-melt extrusion with poorly soluble drugs. Heinrich-Heine-Universität Düsseldorf.

Alshetaili, A.S., Almutairy, B.K., Alshahrani, S.M., Ashour, E.A., Tiwari, R. V., Alshehri, S.M., Feng, X., Alsulays, B.B., Majumdar, S., Langley, N., Kolter, K., Gryczke, A., Martin, S.T., Repka, M.A., 2016. Optimization of hot melt extrusion parameters for sphericity and hardness of polymeric face-cut pellets. Drug Dev. Ind. Pharm. 42, 1833–1841.

Amidon, G.L., Lennernas, H., Shah, V.P., Crison, J.R., 1995. A Theoretical Basis for a Biopharmaceutics Drug Classification: The Correlation of In Vitro Drug Product Dissolution and In Vivo Bioavaiability. Pharm. Res. 12, 413–420.

Baronsky-Probst, J., Möltgen, C.-V. V., Kessler, W., Kessler, R.W.W., 2016. Process design and control of a twin screw hot melt extrusion for continuous pharmaceutical tamper-resistant tablet production. Eur. J. Pharm. Sci. 87, 14–21.

Bashaiwoldu, A.B., Podczeck, F., Michael Newton, J., 2011. Compaction of and drug release from coated pellets of different mechanical properties. Adv. Powder Technol. 22, 340–353.

Bashaiwoldu, A.B., Podczeck, F., Newton, J.M., 2004a. Application of dynamic mechanical analysis (DMA) to determine the mechanical properties of pellets. Int. J. Pharm. 269, 329–342.

Bashaiwoldu, A.B., Podczeck, F., Newton, J.M., 2004b. A study on the effect of drying techniques on the mechanical properties of pellets and compacted pellets. Eur. J. Pharm. Sci. 21, 119–129.

Bialleck, S., Rein, H., 2011. Preparation of starch-based pellets by hot-melt extrusion. Eur. J. Pharm. Biopharm. 79, 440–8.

Bodmeier, R., 1997. Tableting of coated pellets. Eur. J. Pharm. Biopharm. 43, 1–8.

Braun, M., 2003. Einflussfaktoren bei der Tablettierung magensaftresistent überzogener Pellets auf Exzenter- und Rundlauftablettenpresse. Ph. D. Diss. Friedrich-Wilhelms-Universität Bonn, Ger. 1–168.

Breitenbach, J., 2002. Melt extrusion: from process to drug delivery technology. Eur. J. Pharm. Biopharm. 54, 107–117.

Bruce, L.D., Shah, N.H., Waseem Malick, A., Infeld, M.H., McGinity, J.W., 2005. Properties of hot-melt extruded tablet formulations for the colonic delivery of 5-aminosalicylic acid. Eur. J. Pharm. Biopharm. 59, 85–97.

Case, C.C., 2003. Melt Pelletization, in: Ghebre-Sellassie, I., Martin, C. (Eds.), Pharmaceutical Extrusion Technology. Dekker, New York, pp. 171–181.

Censi, R., Gigliobianco, M., Casadidio, C., Di Martino, P., Censi, R., Gigliobianco, M.R., Casadidio, C., Di Martino, P., 2018. Hot Melt Extrusion: Highlighting Physicochemical Factors to Be Investigated While Designing and Optimizing a Hot Melt Extrusion Process. Pharmaceutics 10, 89.

Chowdhury, N., Vhora, I., Patel, K., Bagde, A., Kutlehria, S., Singh, M., 2018. Development of Hot Melt Extruded Solid Dispersion of Tamoxifen Citrate and Resveratrol for Synergistic Effects on Breast Cancer Cells. AAPS PharmSciTech 19, 3287–3297.

Crowley, M.M., Schroeder, B., Fredersdorf, A., Obara, S., Talarico, M., Kucera, S., McGinity, J.W., 2004. Physicochemical properties and mechanism of drug release from ethyl cellulose matrix tablets prepared by direct compression and hot-melt extrusion. Int. J. Pharm. 269, 509–522.

Crowley, M.M., Zhang, F., Repka, M.A., Thumma, S., Upadhye, S.B., Kumar, S., McGinity, J.W., Martin, C., 2007. Pharmaceutical Applications of Hot-Melt Extrusion: Part I. Drug Dev. Ind. Pharm. 33, 909–926.

Démuth, B., Nagy, Z.K., Balogh, A., Vigh, T., Marosi, G., Verreck, G., Van Assche, I., Brewster, M.E., 2015. Downstream processing of polymer-based amorphous solid dispersions to generate tablet formulations. Int. J. Pharm. 486, 268–286.

Desai, P.M., Hogan, R.C., Brancazio, D., Puri, V., Jensen, K.D., Chun, J.-H.H., Myerson, A.S., Trout, B.L., 2017. Integrated hot-melt extrusion – injection molding continuous tablet manufacturing platform: Effects of critical process parameters and formulation attributes on product robustness and dimensional stability. Int. J. Pharm. 531, 332–342.

Dukić-Ott, A., Thommes, M., Remon, J.P., Kleinebudde, P., Vervaet, C., 2009. Production of pellets via extrusion–spheronisation without the incorporation of microcrystalline cellulose: A critical review. Eur. J. Pharm. Biopharm. 71, 38–46.

Dukić, A., Mens, R., Adriaensens, P., Foreman, P., Gelan, J., Remon, J.P., Vervaet, C., 2007. Development of starch-based pellets via extrusion/spheronisation. Eur. J. Pharm. Biopharm. 66, 83–94.

Dülle, M., Özcoban, H., Leopold, C.S., 2018a. Investigations on the residence time distribution of a three-chamber feed frame with special focus on its geometric and parametric setups. Powder Technol. 331, 276–285.

Dülle, M., Özcoban, H., Leopold, C.S., 2018b. Analysis of the powder behavior and the residence time distribution within a production scale rotary tablet press. Eur. J. Pharm. Sci. 125, 205–214.

FDA US Department of Health, 2011. Guidance for Industry: 21 CFR Part 11, Electronic Records; Electronic Signatures, Glossary of Terms, Vol. 1. ed.

Fukuda, M., Peppas, N.A., McGinity, J.W., 2006. Properties of sustained release hot-melt extruded tablets containing chitosan and xanthan gum. Int. J. Pharm. 310, 90–100.

Gao, Y., Vanarase, A., Muzzio, F., Ierapetritou, M., 2011. Characterizing continuous powder mixing using residence time distribution. Chem. Eng. Sci. 66, 417–425.

Grymonpré, W., Blahova Prudilova, B., Vanhoorne, V., Van Snick, B., Detobel, F., Remon, J.P., De Beer, T., Vervaet, C., 2018. Downscaling of the tableting process: Feasibility of miniaturized forced feeders on a high-speed rotary tablet press. Int. J. Pharm. 550, 477–485.

Grymonpré, W., De Jaeghere, W., Peeters, E., Adriaensens, P., Remon, J.P., Vervaet, C., 2016. The impact of hot-melt extrusion on the tableting behaviour of polyvinyl alcohol. Int. J. Pharm. 498, 254–262.

Hörmann, T.R., Jäger, N., Funke, A., Mürb, R.-K., Khinast, J.G., Paudel, A., 2018. Formulation Performance and Processability Window for Manufacturing a Dual-Polymer Amorphous Solid Dispersion via Hot-Melt Extrusion and Strand Pelletization. Int. J. Pharm. 553, 408–421.

Hörmann, T.R., Rehrl, J., Scheibelhofer, O., Schaden, L.-M., Funke, A., Makert, C., Khinast, J.G., submitted. Sensitivity of a Hot-Melt Extrusion and Strand Pelletization Line to Control Actions and Composition Variation. Int. J. Pharm.

Janssens, S., De Zeure, A., Paudel, A., Van Humbeeck, J., Rombaut, P., Van Den Mooter, G., 2010. Influence of preparation methods on solid state supersaturation of amorphous solid dispersions: A case study with itraconazole and eudragit E100. Pharm. Res. 27, 775–785.

Jedinger, N., Khinast, J., Roblegg, E., 2014. The design of controlled-release formulations resistant to alcohol-induced dose dumping – A review. Eur. J. Pharm. Biopharm. 87, 217–226.

Jedinger, N., Schrank, S., Fischer, J.M., Breinhälter, K., Khinast, J., Roblegg, E., 2016. Development of an Abuse- and Alcohol-Resistant Formulation Based on Hot-Melt Extrusion and Film Coating. AAPS PharmSciTech 17, 68–77.

Jermain, S. V., Brough, C., Williams, R.O., 2018. Amorphous solid dispersions and nanocrystal technologies for poorly water-soluble drug delivery – An update. Int. J. Pharm. 535, 379–392.

Johnston, C., Cooney, C.L., Konstantinov, K., Mascia, S., Trout, B.L., Nasr, M.M., Florence, A., Krumme, M., Matsuda, Y., Badman, C., Jensen, K.D., Lee, S.L., 2017. Regulatory Perspectives on Continuous Pharmaceutical Manufacturing: Moving from Theory to Practice. September 26-27, 2016, International Symposium of the Continuous Manufacturing of Pharmaceuticals. J. Pharm. Sci. 106, 3199–3206.

Kalivoda, A., 2012. Solubility enhancement of poorly water-soluble drugs by solid dispersion a comparison of two manufacturing methods. Heinrich-Heine Universität Düsseldorf.

Kalivoda, A., Fischbach, M., Kleinebudde, P., 2012. Application of mixtures of polymeric carriers for dissolution enhancement of fenofibrate using hot-melt extrusion. Int. J. Pharm. 429, 58–68.

Karttunen, A.-P., Hörmann, T.R., De Leersnyder, F., Ketolainen, J., De Beer, T., Hsiao, W.-K., Korhonen, O., 2019. Measurement of residence time distributions and material tracking on three continuous manufacturing lines. Int. J. Pharm. 563, 184–197.

Keating, A. V., Soto, J., Forbes, C., Zhao, M., Craig, D.Q.M., 2018. Solid state characterisation and taste masking efficiency evaluation of polymer based extrudates of isoniazid for paediatric administration. Int. J. Pharm. 536, 536–546.

Khinast, J.G., Baumgartner, R., Roblegg, E., 2013. Nano-extrusion: a One-Step Process for Manufacturing of Solid Nanoparticle Formulations Directly from the Liquid Phase. AAPS PharmSciTech.

Kipping, T., Rein, H., 2013. A new method for the continuous production of single dosed controlled release matrix systems based on hot-melt extruded starch: analysis of relevant process parameters and implementation of an in-process control. Eur. J. Pharm. Biopharm. 84, 156–71.

Ku, M.S., 2008. Use of the Biopharmaceutical Classification System in Early Drug Development. AAPS J. 10, 208–212.

Leane, M., Pitt, K., Reynolds, G., 2015. A proposal for a drug product Manufacturing Classification System (MCS) for oral solid dosage forms. Pharm. Dev. Technol. 20, 12–21.

Leane, M., Pitt, K., Reynolds, G.K., Dawson, N., Ziegler, I., Szepes, A., Crean, A.M., Dall Agnol, R., 2018. Manufacturing classification system in the real world: factors influencing manufacturing process choices for filed commercial oral solid dosage formulations, case studies from industry and considerations for continuous processing. Pharm. Dev. Technol. 23, 964–977.

Lee, S.L., O'Connor, T.F., Yang, X., Cruz, C.N., Chatterjee, S., Madurawe, R.D., Moore, C.M. V, Yu, L.X., Woodcock, J., 2015. Modernizing Pharmaceutical Manufacturing : from Batch to Continuous Production. J. Pharm. Innov. 10, 191–199.

Leuner, C., Dressman, J., 2000. Improving drug solubility for oral delivery using solid dispersions. Eur. J. Pharm. Biopharm. 50, 47–60.

Liu, J., Zhang, F., McGinity, J.W., 2001. Properties of lipophilic matrix tablets containing phenylpropanolamine hydrochloride prepared by hot-melt extrusion. Eur. J. Pharm. Biopharm. 52, 181–90.

Lundqvist, A.E.K., Podczeck, F., Newton, J.M.., 1997. Influence of disintegrant type and proportion on the properties of tablets produced from mixtures of pellets. Int. J. Pharm. 147, 95–107.

Manley, L., Shi, Z., 2018. Characterizing drug product continuous manufacturing residence time distributions of major/minor excipient step changes using near infrared spectroscopy and process parameters. Int. J. Pharm. 551, 60–66.

Marks, J.A., Wegiel, L.A., Taylor, L.S., Edgar, K.J., 2014. Pairwise polymer blends for oral drug delivery. J. Pharm. Sci. 103, 2871–2883.

Martin, C., 2013. Twin Screw Extrusion for Pharmaceutical Processes, in: Repka, M.A., Langley, N., DiNunzio, J. (Eds.), Melt Extrusion - Materials, Technology and Drug Product Design. American Association of Pharmaceutical Scientists, New York.

Martinetz, M.C., Karttunen, A.-P., Sacher, S., Wahl, P., Ketolainen, J., Khinast, J.G., Korhonen, O., 2018. RTD-based material tracking in a fully-continuous dry granulation tableting line. Int. J. Pharm. 547, 469–479.

Martinetz, M.C., Rehrl, J., Aigner, I., Sacher, S., Khinast, J., 2017. A Continuous Operation Concept for a Rotary Tablet Press Using Mass Flow Operating Points. Chemie-Ingenieur-Technik 89, 1006–1016.

McWilliams, J.C., Allian, A.D., Opalka, S.M., May, S.A., Journet, M., Braden, T.M., 2018. The Evolving State of Continuous Processing in Pharmaceutical API Manufacturing. Org. Process Res. Dev. 22, 1143–1166.

Mehta, S., De Beer, T., Remon, J.P., Vervaet, C., 2012. Effect of disintegrants on the properties of multiparticulate tablets comprising starch pellets and excipient granules. Int. J. Pharm. 422, 310–7.

Mohammed, N.N., Majumdar, S., Singh, A., Deng, W., Murthy, N.S., Pinto, E., Tewari, D., Durig, T., Repka, M.A., 2012. KlucelTM EF and ELF polymers for immediate-release oral dosage forms prepared by melt extrusion technology. AAPS PharmSciTech 13, 1158–69.

Nokhodchi, A., Raja, S., Patel, P., Asare-Addo, K., 2012. The role of oral controlled release matrix tablets in drug delivery systems. BioImpacts 2, 175–187.

Patil, H., Feng, X., Ye, X., Majumdar, S., Repka, M.A., 2015. Continuous Production of Fenofibrate Solid Lipid Nanoparticles by Hot-Melt Extrusion Technology: A Systematic Study Based on a Quality by Design Approach. AAPS J. 17, 194–205.

Patil, H., Tiwari, R. V., Repka, M.A., 2016. Hot-Melt Extrusion: from Theory to Application in Pharmaceutical Formulation. AAPS PharmSciTech 17, 20–42.

Peters, R.C., 2019. Identifying Incentives to Adopt Advanced Manufacturing. BioPharm Int. 32, 10–14.

Plumb, K., 2005. Continuous Processing in the Pharmaceutical Industry. Chem. Eng. Res. Des. 83, 730–738.

Portillo, P.M., Vanarase, A.U., Ingram, A., Seville, J.K., Ierapetritou, M.G., Muzzio, F.J., 2010. Investigation of the effect of impeller rotation rate, powder flow rate, and cohesion on powder flow behavior in a continuous blender using PEPT. Chem. Eng. Sci. 65, 5658–5668.

Ren, Y., Mei, L., Zhou, L., Guo, G., 2019. Recent Perspectives in Hot Melt Extrusion-Based Polymeric Formulations for Drug Delivery: Applications and Innovations. AAPS PharmSciTech 20, 92.

Repka, M.A., Bandari, S., Kallakunta, V.R., Vo, A.Q., McFall, H., Pimparade, M.B., Bhagurkar, A.M., 2018. Melt extrusion with poorly soluble drugs – An integrated review. Int. J. Pharm. 535, 68–85.

Repka, M.A., Majumdar, S., Battu, S.K., Srirangam, R., Upadhye, S.B., 2008. Applications of hot-melt extrusion for drug delivery. Inf. Healthc. 5, 1357–1376.

Roblegg, E., Jäger, E., Hodzic, A., Koscher, G., Mohr, S., Zimmer, A., Khinast, J., 2011. Development of sustained-release lipophilic calcium stearate pellets via hot melt extrusion. Eur. J. Pharm. Biopharm. 79, 635–645.

Shah, S., Repka, M.A., 2013. Melt Extrusion in Drug Delivery: Three Decades of Progress, in: Repka, M.A., Langley, N., DiNunzio, J. (Eds.), Melt Extrusion - Materials, Technology and Drug Product Design. American Association of Pharmaceutical Scientists, New York.

Song, C.H., Han, J.W., 2016. Patent cliff and strategic switch: exploring strategic design possibilities in the pharmaceutical industry. Springerplus 5, 1–14.

Sousa, J.J., Sousa, A., Podczeck, F., Newton, J.M., 2002. Factors influencing the physical characteristics of pellets obtained by extrusion-spheronization. Int. J. Pharm. 232, 91–106.

Stanković, M., Frijlink, H.W., Hinrichs, W.L.J., 2015. Polymeric formulations for drug release prepared by hot melt extrusion: application and characterization. Drug Discov. Today 20, 812–823.

Tan, D., Maniruzzaman, M., Nokhodchi, A., Tan, D.K., Maniruzzaman, M., Nokhodchi, A., 2018. Advanced Pharmaceutical Applications of Hot-Melt Extrusion Coupled with Fused Deposition Modelling (FDM) 3D Printing for Personalised Drug Delivery. Pharmaceutics 10, 203.

Tan, D.C.T., Ong, J.J., Gokhale, R., Heng, P.W.S., 2018. Hot melt extrusion of ion-exchange resin for taste masking. Int. J. Pharm. 547, 385–394.

Thommes, M., Kleinebudde, P., 2006a. Use of κ-carrageenan as alternative pelletisation aid to microcrystalline cellulose in extrusion/spheronisation. I. Influence of type and fraction of filler. Eur. J. Pharm. Biopharm. 63, 59–67.

Thommes, M., Kleinebudde, P., 2006b. Use of κ-carrageenan as alternative pelletisation aid to microcrystalline cellulose in extrusion/spheronisation. II. Influence of drug and filler type. Eur. J. Pharm. Biopharm. 63, 68–75.

Toson, P., Siegmann, E., Trogrlic, M., Kureck, H., Khinast, J., Jajcevic, D., Doshi, P., Blackwood, D., Bonnassieux, A., Daugherity, P.D., am Ende, M.T., 2018. Detailed modeling and process design of an advanced continuous powder mixer. Int. J. Pharm. 552, 288–300.

Treffer, D., Wahl, P.R., Hörmann, T.R., Markl, D., Schrank, S., Jones, I., Cruise, P., Mürb, R.-K., Koscher, G., Roblegg, E., Khinast, J.G., 2014. In-line implementation of an image-based particle size measurement tool to monitor hot-melt extruded pellets. Int. J. Pharm. 466, 181–9.

Treffer, D.F., 2016. Pharmaceutical Hot Melt Extrusion - Novel Tools for Screening and Processing. Graz University of Technology.

Treffer, D.F., Khinast, J.G., 2017. Why hot melts do not stick to cold surfaces. Polym. Eng. Sci. 57, 1083–1089.

Vanarase, A.U., Muzzio, F.J., 2011. Effect of operating conditions and design parameters in a continuous powder mixer. Powder Technol.

Vithani, K., Douroumis, D., 2019. Hot-melt extruded lipidic pellets for pediatric applications: An investigation of the effects and stability on drug dissolution. J. Drug Deliv. Sci. Technol. 49, 43–49.

Vo, A.Q., Feng, X., Morott, J.T., Pimparade, M.B., Tiwari, R. V., Zhang, F., Repka, M.A., 2016. A novel floating controlled release drug delivery system prepared by hot-melt extrusion. Eur. J. Pharm. Biopharm. 98, 108–121.

Williams, H.D., Trevaskis, N.L., Charman, S. a, Shanker, R.M., Charman, W.N., Pouton, C.W., Porter, C.J.H., 2013. Strategies to address low drug solubility in discovery and development. Pharmacol. Rev. 65, 315–499.

Williams, H.D., Trevaskis, N.L., Charman, S.A., Shanker, R.M., Charman, W.N., Pouton, C.W., Porter, C.J.H., 2013. Strategies to address low drug solubility in discovery and development. Pharmacol. Rev. 65, 315–499.

Witschnigg, A., Koscher, G., Treffer, D., Mürb, R., Laske, S., Khinast, J., 2016. Micro-pelletizing of pharmaceutical HME formulations using a die face pelletizer. AIP Conf. Proc. 1779.

Yeung, C.-W., Rein, H., 2015. Hot-melt extrusion of sugar-starch-pellets. Int. J. Pharm. 493, 390–403.

Young, C.R., Koleng, J.J., McGinity, J.W., 2002. Production of spherical pellets by a hot-melt extrusion and spheronization process. Int. J. Pharm. 242, 87–92.

Yu, L.X., Amidon, G., Khan, M.A., Hoag, S.W., Polli, J., Raju, G.K., Woodcock, J., 2014. Understanding Pharmaceutical Quality by Design. AAPS J. 16, 771–783.

2. Formulation Performance and Processability Window for Manufacturing a Dual-Polymer Amorphous Solid Dispersion via Hot-Melt Extrusion and Strand Pelletization[1]

This work evaluates several compositions of an amorphous solid dispersion (ASD) comprising nimodipine (NMD) as poorly soluble model API in a dual-polymer carrier system. HPMC E5 and Eudragit E were used for the two polymeric carriers. The formulation was designed for hot-melt extrusion (HME) and subsequent strand pelletization. The aim was to identify a formulation window with desired functional ASD performance, i.e. physical stability and immediate API release, as well as processability in strand pelletization. Samples were prepared using small-scale methods, such as vacuum compression molding (VCM) and benchtop extrusion. Miscibility and phase studies were performed for a wide range of polymer ratios and three levels of API content (10% to 30% w/w). Ternary ASD formulations were phase-separated, yet physically stable upon exposure to elevated temperature/humidity. A study of phase composition showed that the drug molecules were predominantly solubilized in the Eudragit E fraction of the formulation. The miscibility study and Fourier-transform infrared spectroscopy indicated hydrogen (H)-bond interactions between NMD and Eudragit E. In HPMC, the amorphous API was dispersed in polymeric matrix and stabilized due to anti-plasticization and the disruption of intermolecular H-bonding between API molecules. Concerning processability in strand pelletization the formulation is limited at high Eudragit E content. NMD and EE-rich phases exhibit low mixture glass transition, low melt stability and brittle breaking behavior upon strand cutting. The high viscosity and yield point of HPMC contributes to the mechanical robustness of the strand at temperatures relevant for processing. Formulation-intrinsic dissolution rates in VCM ASDs developed as an irregular function of polymer ratio, associated with diverse and competitive dissolution mechanisms in the polymers. With regard to the binary system of NMD with HPMC E5, surface crystallization was observed in VCM ASDs. For extruded pellets this was not the case, and a steady trend of formulation-intrinsic dissolution rate across different polymer ratios was observed. These discrepancies indicated a major influence of shear stress during sample preparation on HPMC-based ASD performance. Finally, a feasible formulation window within a polymer ratio of 1:2 to 2:3 Eudragit E:HPMC was identified in which Eudragit E acts as a dissolution rate enhancer and ASD stabilizer during dissolution.

[1] This chapter was published in Hörmann et al., 2018. Formulation Performance and Processability Window for Manufacturing a Dual-Polymer Amorphous Solid Dispersion via Hot-Melt Extrusion and Strand Pelletization. Int. J. Pharm. 553, 408–421.

2.1. Introduction

Amorphous solid dispersions (ASDs) are widely used to enhance bioavailability of poorly water-soluble active pharmaceutical ingredients (APIs) (Newman et al., 2012; Van Den Mooter, 2012; Hywel D. Williams et al., 2013). Polymers can stabilize the amorphous API and maintain increased apparent solubility (super saturation) of the API during dissolution. Two common industrial processes for manufacturing ASD intermediates are spray drying and hot melt extrusion (HME) (DiNunzio and Miller, 2013; Li et al., 2014; Maniruzzaman et al., 2015; Paudel et al., 2013; Hywel D. Williams et al., 2013). In HME, processed materials are first forced to mix in the molten state by applying shear and heat. Next, the melt is extruded through a die into strand shape and cooled down rapidly to generate a solid ASD material. Depending on the downstream process and the equipment, extrudates can be processed into powders, flakes, films, pellets, tablets, rods and other forms. In this case pellets are desirable as they offer good flowability and handling properties and can be filled directly into sachets or capsules or can be compressed to tablets.

Pelletization, as a downstream process of extrusion, can be performed in two ways: die-face pelletization directly at the extrusion die, or strand pelletization at a certain cooling distance from the die (Martin, 2013b). Pellets from strand pelletization are roughly cylindrical, whereas die-face pelletization yields rounded shapes. Processability of a formulation via die-face pelletization is determined by the stickiness of the melt, melt viscosity and glass transition temperature (T_g) of the formulation. In strand pelletization, the cutting process is thermally and spatially separated from the extrusion process. Therefore, mechanical properties of the strand at cutting temperature are crucial. The strands must not adhere to each other or other surfaces after the die and must tolerate some bending and mechanical stress in the intake zone of the pelletizer, where intake rolls grip the strands and push them into the cutting zone. Moreover, the strand must not show fragmentation at the cutting temperature, as this creates an undesired fines fraction and dusting. Glass transition temperature (T_g) and viscoelastic properties of a formulation can be used to estimate processability, or the required cooling period before pelletization, respectively.

Formulation development, however, is governed by physicochemical performance considerations. The major functional requirements for an ASD are dissolution and physical and chemical stability of the system. In order to address the diverse requirements, the application of dual-polymer ASDs is increasingly chosen as a formulation strategy (Marks et al., 2014). Dual-polymer ASDs are ternary combinations of one API and two polymers (hence “dual-polymer”), which allow to combine the advantageous properties of both polymers. Over the last decade, this formulation approach with rapid, or tailored release properties and simultaneously crystallization-inhibiting properties have generated increasing interest (Janssens et al., 2008b, 2008a; Marks et al., 2014; Prodduturi et al., 2007; Ueda et

al., 2018; Xie and Taylor, 2016; Yang et al., 2013). In this work, a combination of two polymers is also desired from a processing point of view.

Nimodipine (NMD) was selected as a poorly soluble model API of BCS class II. This API has already been reported to form ASDs with increased dissolution efficiency via HME processing with several polymers. However, dual-polymer systems and their effect on downstream processability have not been studied yet. ASDs with nimodipine (NMD) in polyethylene glycols (PEG 2000 (Urbanetz and Lippold, 2005), PEG 4000 (Docoslis et al., 2007) and PEG 2000 with povidone K17 (Smikalla and Urbanetz, 2007; Urbanetz, 2006)) were shown to increase the solubility of NMD. Yet, the mechanical stability of the extrudate strand makes it not feasible as a polymeric carrier for strand pelletization due to the low melting point of PEG. Other investigated polymers were poly(1-vinylpyrrolidone-co-vinyl acetate) (PVP-VA) (Jijun et al., 2010; Sun et al., 2008; Zheng et al., 2007a, 2007b), poly-(butylmethacrylate-co-(2-dimethylaminoethyl)methacrylate-co-methyl methacrylate) (Eudragit® E) and hydroxypropyl methylcellulose (HPMC, Methocel™ E5) (Zheng et al., 2007a, 2007b). The effect of these polymers in physical stability, dissolution and HME processability-determining properties were reported. However, in all studies the extrudates were milled for further processing, or used for the production of semi-solid capsules, in the case of (Sun et al., 2008). Therefore, formulation properties indicating downstream processability were not investigated. This means, that the selection of the polymeric carrier for downstream processes such as strand pelletization has to be done empirically and based on raw material properties. Hygroscopicity of PVP-VA and the low T_g in Eudragit® E-based formulations are considered disadvantageous. Both properties potentially corrupt downstream processability and physical stability of the formulation. One disadvantage of ASDs from NMD in HPMC E5 is their limited miscibility. A single T_g was observed by Zheng et al. (Zheng et al., 2007a) solely at a drug load of 10% and the same miscibility limit was confirmed by Riekes et al. (Riekes et al., 2014) in ASD stability tests. Eudragit® E and PVP-VA based ASDs, in contrast offer good miscibility for up to 50 % NMD load (Zheng et al., 2007a). Eudragit® E-based systems were also shown to be in-vivo bioequivalent to reference Nimotop® tablets in beagle dogs (Zheng et al., 2007b). Therefore, Eudragit® E is chosen as a formulation component in this study, being crucial for the physicochemical performance of the drug. For the compensation of the low T_g (48°C) of Eudragit® E, HPMC was selected as a second carrier polymer. It exhibits a high T_g (146°C) and forms strong, flexible networks, which is considered beneficial for strand pelletization.

Therefore, this study investigates different dual combinations of HPMC E5 and Eudragit® E (EE) as polymeric carrier for NMD. On one hand, the performance requirements are thermal and mechanical properties indicating robust processability in strand pelletization. And on the other hand, there is the target of immediate API release via a physico-chemically stable ASD formulation.

The feasibility of a NMD-EE SD system for achieving bioavailability similar to the originator in beagle dogs has been shown already by Zheng (Zheng et al., 2007b). Therefore, understanding the molecular-level interactions and phase arrangement, and their effects on recrystallization in an ASD, is important to prevent unexpected discrepancies in the *in-vitro* and *in-vivo* performance (Craig, 2002; Newman et al., 2012; Qian et al., 2010). To that end, we investigated miscibility and phase arrangement via modulated differential scanning calorimetry (mDSC) for a wide range of formulation component combinations in physical mixtures and ASDs. Melting point depression and T_g shifts were evaluated using theoretical models for ideal systems (Gordon-Taylor/Kelley-Bueche) (Marsac et al., 2009). Molecular interactions between the components were assessed via attenuated total reflection Fourier-transformed spectroscopy (ATR-FTIR) to detect the presence of hydrogen (H-)bonds, ionic interactions or dipole-dipole interactions (Marsac et al., 2006a). While binary combinations of the formulation components are reported in literature already (Marks et al., 2014; Riekes et al., 2014; Zheng et al., 2007a, 2007b), the focus lies on investigating the interplay of competing material pairs on the formulation, especially on dissolution. Formulation-intrinsic dissolution studies considered the effect of the dissolution mechanisms exhibited by the two polymers (Eudragit® E eroding and HPMC swelling), regardless of the sample size and shape. ASD characterization methods were applied to melt specimens prepared via vacuum compression molding technology (VCM, MeltPrep GmbH, Austria), which is a tool to achieve reproducible melt rheology characterization results with only a small amount of material (Treffer et al., 2015). The specimens are formed under vacuum and exhibit a perfectly flat platelet-like shape, without any inclusions of vapor or air. This flat shape allows to achieve excellent contact between the sample and the DSC pan in mDSC measurements. This improves the sensitivity of the measurement for weak thermal signals, such as the glass transition of HPMC. In contrast to extrusion, mixing in this sample preparation method is driven by diffusive mass transport only. This of course affects miscibility data and the representativeness of findings for HME processed systems. However, other miniaturized ASD preparation methods, such as solvent casting or melt film preparation also differ e.g. in miscibility data and H-bonding due to different mechanisms upon preparation (Paudel et al., 2012). For the present formulation melt film preparation was not feasible due to a lack of flowability of HPMC (viscous behavior with yield point), even at high temperatures. Therefore, the VCM method applied to cryogenically milled formulation blends, was considered the most appropriate approach for this study.

Concerning pelletization performance, thermo-physical formulation properties and observations of strand properties during and after benchtop extrusion were utilized to estimate processability in a larger production scale. The results eventually lead to a window in the formulation composition for the desired performance, based on understanding of the contribution made by each component.

2.2. Materials and Methods

2.2.1. Materials

Nimodipine (NMD), kindly donated by Bayer AG, Germany, was chosen as model API. The polymeric carriers were HPMC E5 (Methocel™ E5) and Eudragit® EPO obtained from DOW Chemical (USA) and Evonik AG (Germany), respectively.

2.2.2. Formulation Selection

The formulations were prepared using the API and polymer ratios listed in Table 2-1. Tested compositions of API and polymeric carriers in weight percent and the ratio of the carries.. Binary (containing the API and only one polymer) and ternary blends were investigated to capture the influence of each polymer and their mixtures. Different loadings of polymers were combined in ternary mixtures to assess the performance of the formulation across the full range of carrier compositions. To assess the effect of API loading, blends with an increased NMD content (20% and 30% w/w) were prepared with a 1:1 ratio of the polymers. Binary formulations at increased API content were not considered, as studies on their ASD properties are published already (Riekes et al., 2014; Zheng et al., 2007a).

Table 2-1. Tested compositions of API and polymeric carriers in weight percent and the ratio of the carries.

No.	Nimodipine (NMD) [% w/w]	Eudragit® E (EE) [% w/w]	Methocel™ E5 (HPMC) [% w/w]	Ratio of Polymers EE:HPMC
F1	10	90	0	- (EE)
F2	10	72	18	4:1
F3	10	60	30	2:1
F4	10	54	36	3:2
F5	10	45	45	1:1
F6	10	36	54	2:3
F7	10	30	60	1:2
F8	10	18	72	1:4
F9	10	0	90	- (HPMC)
F10	20	40	40	1:1
F11	30	35	35	1:1

2.2.3. Preparation of Physical Mixtures

30 g of physical mixtures were prepared for miscibility studies using tumble blending (Turbula® TypT2F, Willy Bachofen AG, Switzerland) with a mixing time of 10 min at a blender speed of 75 rpm. Physical mixtures contained the components with the original particle size distribution (Table A-1 in the Supplemental Material section A).

2.2.4. Preparation of Amorphous Solid Dispersions

Vacuum Compression Molding (VCM)

To achieve homogeneous specimen, all powder blends were cryogenically milled (CryoMill, Retsch, Germany) before sample preparation. Portions of 5 g of powder blend were filled into the 50 mL stainless steel grinding beaker. Milling was conducted with one stainless steel ball (diameter 25 mm) in 3 cycles of 2.5 min at a milling frequency of 25 Hz. Intercooling for one minute was performed at a shaking frequency of 5 Hz.

The milled powder blends were weighed into the VCM device (MeltPrep GmbH, Austria) and deaerated by evacuation (5 min), heated (3 - 8 min) and cooled (3 - 5 min) to generate the ASD. The time was adapted for each formulation, since the larger amount of Methocel™ E5 the longer the heating time required. The temperature of the hot plate was set to 170 - 180°C, depending on the formulation. After sample preparation, the final weight of specimen was determined once again. The samples were stored in a desiccator over silica gel at room temperature (RT) until analysis.

Phase arrangement studies of all formulations and stability studies of selected formulations (F1, F3, F5, F6 and F9) were performed using 5 mm VCM specimen with 10 mg of cryogenically-milled mixture (n=2). For dissolution testing under sink conditions, disc-shaped VCM specimen with a diameter of 10 mm were prepared for all formulation compositions with 60 mg of powder mixture for each sample (n=3).

Benchtop Extrusion

Benchtop HME was applied for selected formulations, to investigate mechanical strand properties and to prepare pellets for reference ASD characterization (hereinafter referred to as HME ASDs). A co-rotating twin-screw benchtop extruder (ZE 9, Three Tec GmbH, Switzerland) with a screw diameter of 9 mm and an L/D ratio of 20 was used. The extrusion die had a diameter of 1.5 mm. The screw speed was set to 150 rpm and the temperatures of the three sections heated barrels from feeding to the exit zone were 120°C, 140°C and 130°C. The physical mixtures were prepared in portions of 30 g in a tumble blender (Turbula® TypT2F, Willy Bachofen AG, Switzerland) for 10 min at 75 rpm and fed into the extruder manually. The extruded strands were collected and cooled down at ambient temperature. For dissolution testing, pellets were manually cut from the strands to achieve an approximate length of 5 mm (diameter and surface specifications are provided in Table A-2 in Supplemental Material A).

2.2.5. Analysis of Miscibility, Molecular Interactions and Processability

Dynamic and Modulated Differential Scanning Calorimetry

Dynamic (DSC) and modulated DSC (mDSC) experiments were carried out with physical mixtures, and ASDs prepared via VCM (hereinafter referred to as VCM ASDs) and via HME. A differential scanning calorimeter (DSC 204F1 Phoenix®, Netzsch GmbH, Germany) was used. The samples (n=2) were characterized in crimped standard alumina crucibles with manually pierced lids. The physical mixtures were tested during two heating runs. During the first heat run, a quench-cooled ASD was generated by melting and cooling at a dynamic rate of 10°C/min at temperatures from -10°C to +180°C. Pure nitrogen was applied as a purge gas at a flow rate of 50 mL/min. During the second heating run, characterization of the quench-cooled ASD (hereinafter referred to as QC ASD) was performed at a modulated heating rate of 5°C/min (period of 40 s and amplitude of ± 0.531°C) and temperatures from -10°C to +180°C. The VCM specimen before and after stability testing were examined via the mDSC program identical to the second heating cycle as for the QC ASDs. The same mDSC program was applied to scan HME ASDs in two modulated heating cycles.

The NETZSCH Proteus Thermal Analysis V.6.1.0 software was applied for data treatment and evaluation. The reversing heat flows (rev. HF) and their derivatives were smoothed via the smoothing degree “F”, respectively “H” for HME ASD of formulation F9 in the software. In the mDSC thermograms, the glass transition temperatures were evaluated based on the midpoint of the event in the RHF curves. Peaks in the derivative of the reversing heat flow aided in identifying thermal events, in setting the limits for onset and endset temperatures for the evaluation and in interpretation. For dynamic DSC runs, the total heat flow was evaluated. Melting temperature was assessed based on the onset and offset temperature. Enthalpy of fusion was determined via a linear baseline or, in the case of the binary mixture with HPMC and samples with increased API content, a tangential baseline. For HME ASDs, the second heat run was performed to evaluate T_g for reasons of improved contact of pan and sample and enhanced signal intensity during the second run. The exact sample mass was taken into account during the evaluation.

The DSC was calibrated using an Indium standard to compare onset temperature and area of fusion at heat rates of 2, 5 and 10 K/min.

Attenuated Total Reflectance-Fourier Transform Infrared (ATR-FTIR) Spectroscopy

ATR-FTIR spectroscopy was used to investigate the molecular arrangement of pure substances, physical mixtures and VCM ASDs (before and after stability studies). In order to record FTIR-spectra of amorphous NMD, a small amount of crystalline API was molten on a hot plate in an aluminium DSC crucible and subsequently swiftly cooled down on ice. The amorphous drug sample was analysed immediately. Absorbance spectra were recorded with a Bruker VERTEX 70 spectrometer (Bruker, Germany) using an ATR unit and the following settings: spectral resolution 4 cm^{-1}, 64 scans,

4500 - 600 cm^{-1}. The Spekwin32 optical spectroscopy software V.1.72.2 and MATLAB 2014b (The MathWorks, USA) were applied for spectra evaluation and presentation. Spectra of replicates were peak height-normalized and averaged. Spectra of physical mixtures, pure HPMC powder and VCM samples from the stability test after 1 week were smoothed using a third-order Savitzky-Golay filter for a span of 15 spectra.

Physical Stability Studies

VCM ASDs were characterized before and after stress conditions via mDSC and FTIR using the analysis methods described above. Stressing of the ASD (n=2) was performed for one and four weeks under accelerated conditions at 40°C and 75% relative humidity (RH). Storage under accelerated conditions was carried out in a climate cabinet (Binder GmbH, Germany), with the VCM specimen kept in an uncovered DSC crucible. The aim for the stress test was to determine possible changes in ASD phase arrangement after stress testing. Since the thermal signal indicating the T_g of HPMC is very weak, samples were stored in a desiccator under vacuum for two days prior to analysis. Removing the water minimized disturbances due to water evaporation during ASD characterization.

2.2.6. Dissolution Studies

Dissolution tests were performed for pellets and VCM discs under sink conditions. Pellet dissolution was done in a USP dissolution apparatus I (basket, 100 rpm) and, for VCM specimen, USP dissolution apparatus II (paddle, 75 rpm) apparatus, both in an Erweka DT820LH Dissolution Tester (Erweka, Germany). All tests were performed at 37 ± 0.5°C with 500 mL of dissolution medium. The dissolution medium was chosen according to the specification for NMD tablets in the British Pharmacopoeia (British Pharmacopoeia, 2009) and consisted of a sodium acetate buffer with pH 4.5 ± 0.1 and 0.3% of sodium lauryl sulfate (SLS). The dissolved API concentration from samples over time was determined via UV/Vis spectroscopy (Lambda 950, PerkinElmer, USA). Absorbance measurements were carried out in 10 mm polymethyl methacrylate (PMMA) semi-micro cuvettes at 360 nm. Each sample was measured against a blank of dissolution medium. All work was executed under light protection or yellow light.

Intrinsic Dissolution Studies

Formulation-intrinsic dissolution studies for VCM discs were performed in triplicates (n=3) as given above for all formulations listed in Table 2-1. The goal was to achieve a layer-wise dissolution in order to calculate the dissolution rate per area as a shape- and size-independent value. The resulting formulation specific intrinsic dissolution rate can be used to estimate dissolution from differently shaped geometries. To that end, VCM discs were pressed into custom-made PTFE sample holders, which covered the lateral and base surfaces, while the top area remained uncovered. The PTFE holder sinks to the bottom of the vessel, remaining in this position throughout the whole dissolution test

(sample surface approximately 14 mm below paddle). This way, similar hydrodynamic conditions were maintained in all tests. Samples of dissolution medium of 2 mL were collected manually every 10 min over 70 min and filtered using 0.22 µm nylon filters. Formulation-intrinsic dissolution rate was calculated via a linear regression of the cumulative amount dissolved within 30 min, from the slope of the fit [kg/s] divided by the surface area of the specimen exposed to the dissolution medium.

Pellet Dissolution Studies

Dissolution tests were performed in triplicates (n=3) using 100 mg pellets from selected formulations (F1, F3, F5, F6 and F9). The aim was to achieve immediate release from the pellets and therefore, samples of 1.5 mL were collected automatically at 0, 5, 15, 30, 45, 60, 80 and 100 min and filtered through 0.10 µm poroplast filters. Since viscosity and strand thickness varied across the formulations and pellets were cut manually to an approximate length of 5 mm, the exact dimensions of three pellets and the average pellet weight of ten pellets were used to estimate the available surface during dissolution testing (Table A-2 in the Supplemental Material section A).

2.2.7. Oscillatory Rheology Measurements

VCM samples from formulation F1 (10% NMD and EE) and F6 (10% NMD in 2:3 HPMC:EE) were characterized for their viscoelastic properties. The sample disks had a diameter of 25 mm and each formulation was tested in duplicate. Measurements were performed using an oscillatory rheometer (MCR 301, Anton Paar, Austria) and a plate-plate measurement setup (diameter 25 mm). For formulation F6 it was necessary to use a constant normal force of 25 N and a rough bottom plate, in order to avoid slipping of the sample during measurement. Temperature sweeps between 140°C to 160°C were performed with a linear heating rate of 0.016667°C/s and an oscillation frequency of 10 Hz. The amplitude was selected in the linear viscoelastic range of each formulation, which was 2% for F1 and 0.05% for F6. During the measurement, the heating chamber was purged with nitrogen (~ 50 L^3_N/h).

The rheometer's software (Rheoplus/32 V3.40, Anton Paar, Austria) was used to evaluate storage modulus (G') and loss modulus (G'').

2.3. Results and Discussion

The results section is structured in a way, that characteristics of the used formulations components are given first, followed by observations from sample preparation and benchtop extrusion. Then, results from mDSC investigations on miscibility, phase arrangement and thermal properties of ASDs prepared by different methods (QC, VCM, HME) are given. The observations in miscibility and phase arrangement are deeper discussed in the following chapter about molecular interactions, based on FTIR data. Stability test data concludes the solid-state characterization. The last results section details on dissolution results, investigating the effect of different dissolution mechanisms on formulation-intrinsic dissolution. Finally, the comparison of dissolution performance of VCM versus HME processed ASD leads to a conclusion on a suitable formulation window.

2.3.1. Characteristics of the Selected API and Polymers

NMD is a dihydropyridine derivative, which appears in two crystalline modifications with slightly different solubility and melting point (Grunenberg et al., 1995). Modification I (mod I) is a metastable racemic crystal with two optical antipodes, whereas the stable modification II (mod II) is a conglomerate of four NMD units (Wang et al., 1989). Both modifications are practically insoluble in water (Grunenberg et al., 1995). In this study, NMD modification II was used. Since NMD is light-sensitive, sample preparation and characterizations were performed in a light-protected environment and under yellow light. EE is a cationic, amorphous statistical copolymer, comprising di-methyl-amino-ethyl-methacrylate, butyl-methacrylate and methyl-methacrylate monomers (Quinteros et al., 2008). HPMC is a non-ionic cellulose ether with hydroxy-propyl- and methoxy-side groups. The chemical structures of API and polymers are illustrated in Figure 2-1 and the relevant physical properties are listed in Table 2-2. From glass transition data it can be seen, that amorphous NMD can be expected to act as a plasticizer for both polymers, which is relevant for processing, as well as physical stability of the ASD.

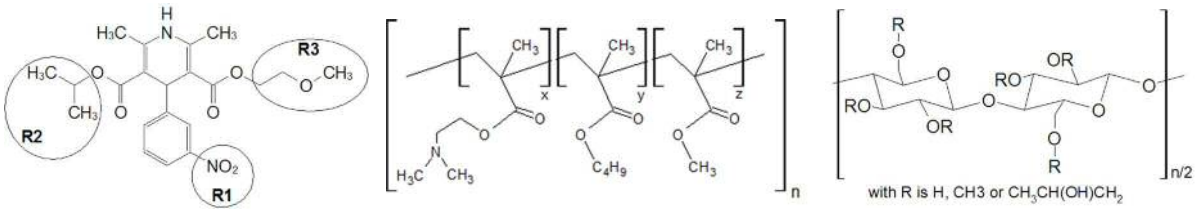

a) b) c)

Figure 2-1. Chemical structure of a) NMD with three side chain residues (R1-R3), b) Eudragit® E and c) Methocel™ E5.

Table 2-2. Raw material properties of the formulation components.

	Molecular weight [g/mol]	**T_g [a] [°C]**	**$T_{m,onset}$ [°C]**	**ΔH_f [J/g]**	**Density [g/cm³]**
Nimodipine (mod II)	418.44	16.2	116.7	-117.0	cryst.: 1.300 (Grunenberg et al., 1995) amorph.: 1.150 [b]
HPMC E5	~ 35000 (The Dow Chemical Company, 2002)	146.4	-	-	1.326 (Rowe et al., 2009)
Eudragit® E (EE)	47000 (Paudel et al., 2013)	48.4	-	-	0.821 (Rowe et al., 2009)

[a] measured T_g; [b] calculated according to (Van Krevelen et al., 2009)

2.3.2. VCM Sample Preparation and Benchtop Extrusion

Visual information on transparency of ASDs during sample preparations is an indicator for miscibility of a formulation. Different observations during melt specimen preparation and benchtop extrusion are summarized in Table 2-3 for all formulations with 10% API content. Pictures from the extruded strands are shown in Figure 2-2.

Table 2-3. Observations on transparency and strand properties (n=3, mean ± SD) during sample preparation.

No.	NMD content [% w/w]	Ratio of Polymers EE:HPMC	VCM Specimen	HME Strands		
			Transparency & Color	Transparency & Color	Diameter [mm]	Mechanical Properties
F1	10	- (EE)	transparent	transparent, light yellow	1.12 ± 0.12 uniform	brittle upon cutting
F2	10	4:1	transparent with light dots	-	-	-
F3	10	2:1	opaque	opaque, light yellow	1.24 ± 0.09 uniform	well cuttable
F4	10	3:2	opaque	-	-	-
F5	10	1:1	opaque	opaque, light yellow	1.48 ± 0.01 air inclusions	well cuttable
F6	10	2:3	opaque	opaque, light yellow	1.53 ± 0.03 many air inclusions	well cuttable
F7	10	1:2	opaque	-	-	-
F8	10	1:4	opaque	-	-	-
F9	10	- (HPMC)	opaque, with light regions	opaque, slightly darkened	1.83 ± 0.01 uniform	well cuttable

For both, VCM specimen and HME strands, the same trend in transparency was observed across the tested formulation compositions. The binary formulation of NMD with EE (F1) led to clear, light yellow products. In contrast, the presence of HPMC immediately resulted in opaque, or dotted melt product. This observation indicated already a lack of miscibility for HPMC with the other two components.

Additionally, observations from benchtop extrusion offer crucial information on processability. As both binary formulations are known to be processable in HME (Zheng et al., 2007a), this work focuses on pelletization performance of different ternary formulation compositions. Prerequisites for a successful strand pelletization process are:

- Formation of a uniform, solid-like strand downstream of the extrusion die.
- Mechanical melt stability, which is the capability of the strand to bear some longitudinal force (correlating to general viscosity).
- Slightly elastic, or no brittle mechanical behavior respectively, to tolerate slight bending and compression in the intake zone of the pelletizer and to avoid extensive dust formation during strand cutting.

- A formulation glass transition temperature that can be undercut by air-cooling over a limited distance before the pelletizer intake to avoid sticking of the strands.

Formation of a solid-like strand depends on the formulation, as well as processing temperature. It was possible to choose benchtop extrusion temperatures in a way, that all formulations yielded stable strands. However, three critical observations were made:

1) The strand formed by the binary formulation F1 with NMD and EE was very soft and tacky at the extrusion die. Its low mechanical melt stability caused significant strand thinning after the die (d_{Strand} = 1.12 mm after a die with d_{Die} = 1.5 mm).
2) The cool strand received from formulation F1 was showing fragmentation when cutting it to pellets and
3) formulation F6 with a polymer ratio of 2:3 EE:HPMC exhibited a large amount of vapor inclusions.

The latter observation of vapor inclusions is a result of humidity in the raw material. Due to the small scale of the benchtop extruder, devolatilization is not possible in the process. In technical lab or production scale extruders though, a vacuum devolatilization zone is common, and this observation therefore not considered critical for the large-scale pelletization process.

The second point about strand fragmentation in contrast is critical, as it does not allow to control the resulting particle size. The production of fines by fragmentation of the strand is not desired, eading to increased cleaning effort, problems in flow, and in material tracking through continuous processes. Its origin lies within a small process window between upper and lower end of the glass transition temperature range. It can be overcome with a strict temperature control and cooling scheme, like varying cooling rates along the free strand. Finding optimal parameters needs further research and development.

The first point, concerning the soft and tacky strand obtained for formulation F1, is expected to cause processing challenges in a large-scale process as well. In benchtop scale a single strand is coming from the die, allowing to cool it down separately on a slowly moving conveyor belt (approx. 1 m length). In production scale processes though, multiple strands are leaving the extrusion die next to each other and a significant amount of heat is transported to the direct environment. Without a specific strand handling unit with active cooling, this could lead to strand rupture or strands sticking to each other before pelletization. Softness of the strand decreased significantly with increasing amount of HPMC in the formulation.

The robustness of a melt strand at the extrusion die can be assessed by characterizing viscoelastic properties of the melt. Oscillatory rheology measurements were performed with samples from the

binary formulation F1 (with EE) and the ternary formulation with a polymer ratio of 2:3 EE:HPMC (F6) (Figure 2-3). For formulation F1 the storage modulus (elastic contribution to deformation) is lower than the loss modulus (viscous contribution to deformation) across the range of relevant melt temperatures. This indicates, that the melt acts liquid-like. In contrast, formulation F6 exhibits a storage modulus which is 100 times higher and also higher than the loss modulus of the formulation. This shows, that the strand can endure significant mechanical stress, acting more as a deformable solid. This is beneficial, as this can be used to elongate the strand in a controlled manner in the final process, to achieve smaller pellet diameters. However, it must be noted, that the characterization of melts with HPMC content in oscillatory rheology measurements does not exactly represent the situation in the extrusion die. HPMC acts like a filler in the formulation not only increasing melt viscosity (see benchtop extrusion torque data in Table A-3 in the Supplemental Material section A), but also causing a yield point. For such a highly complex flow behavior, the Cox-Merz rule is not fulfilled using plate-plate measurement systems. The application of cone-plate systems however is not possible due to the high flow resistance of the formulation. Moreover, characterization of the binary system F9 with 10% API with HPMC was not possible at all, due to significant browning of HPMC during the long measurement time. Therefore, processability will be assessed quantitatively in the next results section based on thermal properties determined from mDSC curves for VCM and HME ASDs. The work of Treffer and Khinast (Treffer and Khinast, 2017) showed, that sticking of melts to other surfaces depends on the contact temperature between the two bodies. If the contact temperature is above a critical temperature, where the melt is able to “wet” the other body, sticking occurs. Below this critical temperature the melt behaves as a solid. For ASDs, this critical temperature is considered to be in the range of glass transition (Treffer and Khinast, 2017). As sticking is most likely to occur between two hot strands, both need to have a surface temperature well below their T_g.

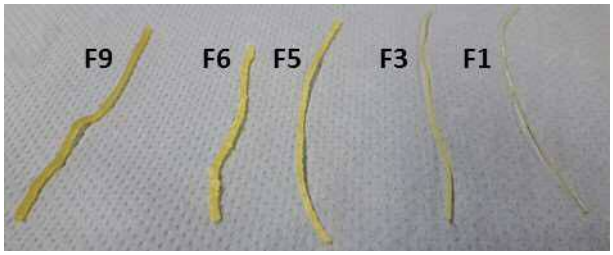

Figure 2-2. Benchtop extruded strands from selected formulations with 10% API and EE (F1), 2:1 EE:HPMC (F3), 1:1 EE:HPMC (F5), 2:3 EE:HPMC (F6) and HPMC (F9).

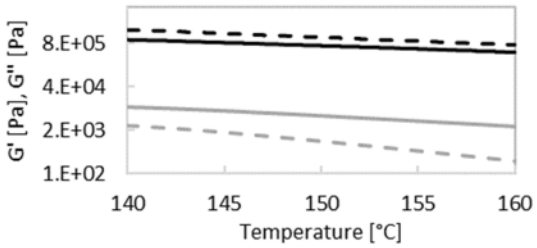

Figure 2-3.Storage (G’ - dashed lines) and loss modulus (G’’ – solid lines) for 10% API and EE (F1 - grey lines) and 10% API and 2:3 EE:HPMC (F6 - black lines).

2.3.3. Miscibility Estimation from Physical Mixture Thermograms

To assess miscibility of the formulation components, the first DSC heating run with physical mixtures was analyzed, where all thermal events from the raw materials can be observed. API melting peak intensity and position provide information about the miscibility of a formulation (Janssens et al., 2010; Li et al., 2014; Marsac et al., 2009). Moreover, this is an indication for HME processing temperatures needed to achieve melting of the API. Figure 2-4 shows the total heat flow for all formulations. The T_g of EE, followed by an enthalpic recovery endotherm, is clearly visible, whereas the T_g of HPMC appears rather weak. It was established that the melting point of NMD was depressed in all formulations. This indicates, that an extrusion temperature around 120°C and below the melting point of pure NMD would allow fusion of the API already (Li et al., 2014). However, since the T_g of HPMC E5 was not depressed, higher temperatures are needed to ensure softening of this component. Binary mixtures (F1 with melting onset at 83.8°C, and F9 at 107.5°C) had the most pronounced peak intensity, whereas the peak almost vanished in the ternary mixture with equal polymer content (F5). Thus, evaluating offset temperature and heat of fusion is challenging in formulations with polymer ratios around 1:1 EE:HPMC. With increasing NMD content at a polymer ratio of 1:1 EE:HPMC (right diagram in Figure 2-4), peak intensity increases accordingly at significantly depressed onset temperatures.

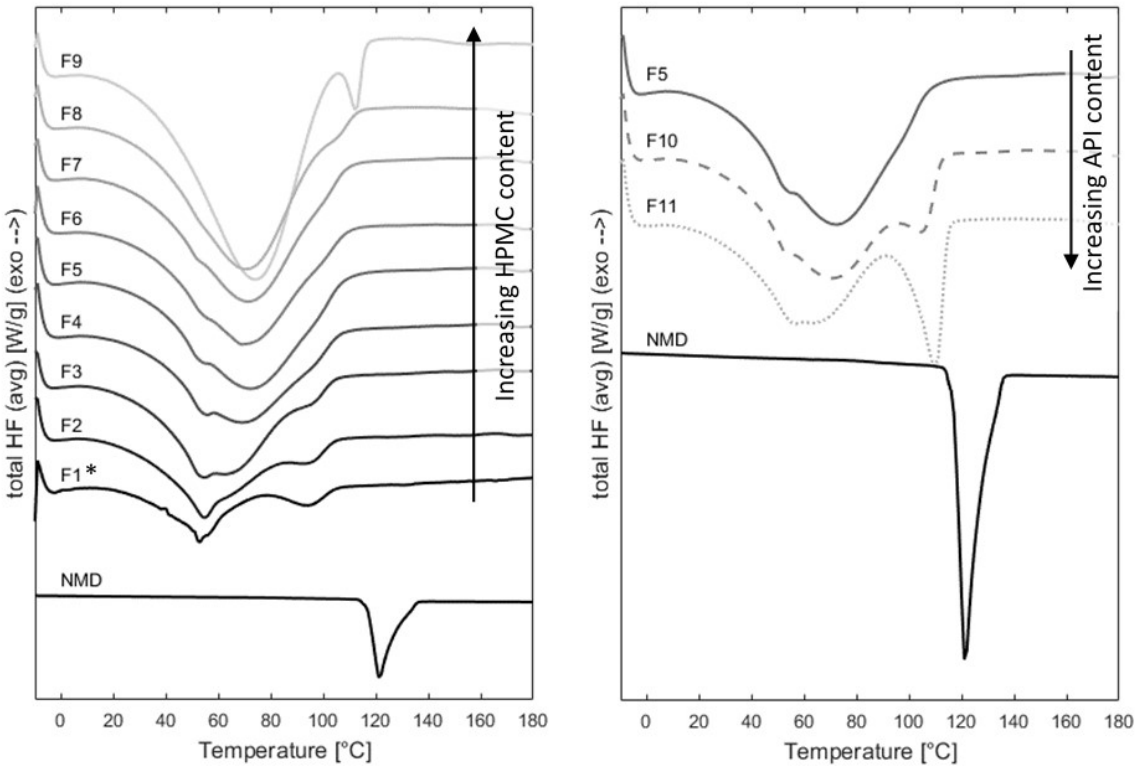

*Figure 2-4. Total heat flow during the 1st heating run for physical mixtures. Left: formulations with 10% (w/w) API content and variable polymer ratio. Right: formulations with variable API content and a polymer ratio of 1:1 (EE:HPMC). References (black) from pure NMD scaled to 10% (w/w) (left) and 30% (w/w) (right), respectively. (*n=1).*

Figure 2-5 displays the evolution of fusion enthalpy across all formulations in comparison to the fusion enthalpy of pure NMD. The formulation range is shown over the composition of the carrier (stated as

a percentage of EE in the carrier, with the remaining fraction made up by HPMC E5) for an NMD content of 10%. As such, an EE content of 50% (w/w) in the carrier corresponds to a polymer ratio of 1:1. A decrease in the fusion enthalpy indicates that less energy is required to transfer the crystalline API into its liquid state. This was observed in all formulations, suggesting miscibility of NMD in both polymeric carriers. Although samples with a higher API content (F10, F11) have a higher enthalpy of fusion in Figure 2-4, it is still significantly lower than even a 10% scaled value of pure NMD. In Figure 2-5, at 10% API content, a minimum fusion enthalpy was observed in dual-polymer blends with a similar EE and HPMC content.

Figure 2-5 also shows endset temperatures of the melting endotherm across the formulation range. The melting temperature of a substance indicates the point at which the chemical potential of the solid state is equal to that of the liquid state. The chemical potential of the drug can decrease due to interactions with other molecules, such as the polymers (Li et al., 2014; Marsac et al., 2006b). The endset temperature was used since it gives the temperature at which all of the API is molten, providing a more reliable indication of miscibility than the onset temperature (Marsac et al., 2009). All formulations had a melting endset temperature lower than that of the pure API, suggesting a miscible system again. The trend of the endset temperature across the EE content appears to be almost constant for higher EE contents. This however, does not agree with the miscibility observations for the melting endotherm data, which indicated the best miscibility in the range of 30 to 50% (w/w) of EE in the carrier. Melting point depression depends on the ability of components to physically interact (Marsac et al., 2006b). Since glass transition and softening of HPMC occurs above the melting temperature of NMD, “wetting” between the molten particles can hardly occur in formulations with more HPMC. Thus, the degree of physical interaction is limited. This could explain the kink in the melting point depression trend below 50% of EE in the carrier (polymer ratio of 1:1 EE:HPMC).

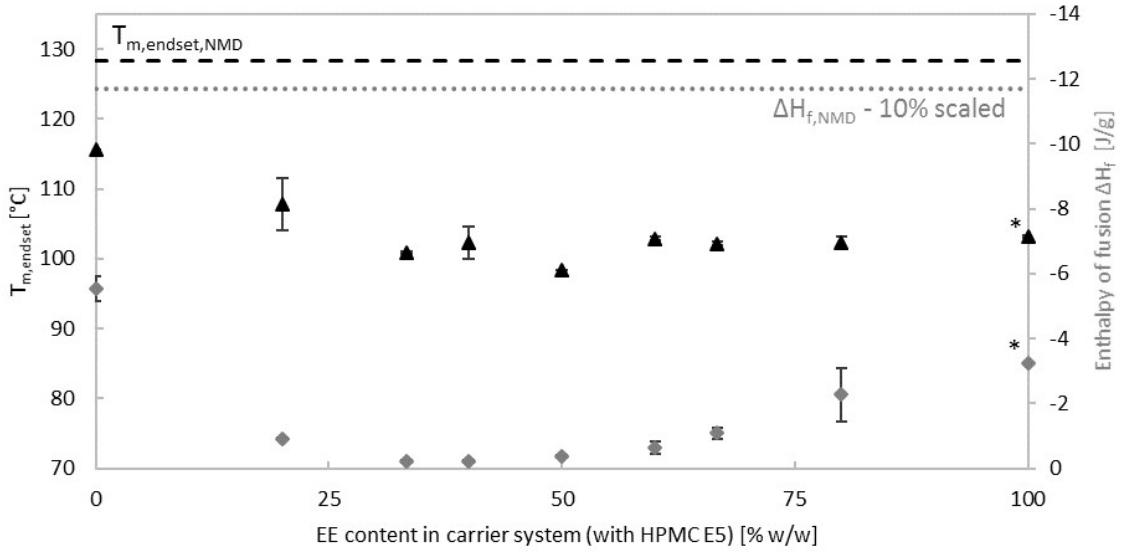

*Figure 2-5. Melting endset temperature (▲) and enthalpy of fusion (◆) of NMD versus the EE content in the polymeric carrier (mean ± span, n=2). Scaled enthalpy of fusion of pure NMD (dashed line) and pure NMD (dashed line). (*n=1)*

2.3.4. ASD Phase Arrangement and Thermal Property Characterization

In order to further investigate miscibility and understand phase arrangement, mDSC curves for QC, VCM and HME ASDs were analyzed thoroughly. With regard to miscibility, a single T_g of an ASD indicates mixedness at a molecular level and a single-phase amorphous system. If several glass transitions are detected, a multiphase amorphous system is present, with regions that have different compositions. In a binary formulation, these regions are API-rich or polymer-rich, whereas in a ternary formulation additional phases can occur. A single-phase system is considered to exhibit better ASD stability than a phase-separated system due to the lack of phase interfaces at which recrystallization is likely to occur.

Theoretically, the T_g of an ideal binary or ternary mixture can be estimated using the Gordon-Taylor/Kelley-Bueche equation (Gordon and Taylor, 1952; Kelley and Bueche, 1961):

$$T_{g,\text{binary } mix} = \frac{w_1 T_{g,1} + K_1 w_2 T_{g,2}}{w_1 + K_1 w_2} \qquad \text{Eq. 2-1}$$

$$T_{g,\text{ternary } mix} = \frac{w_1 T_{g,1} + K_1 w_2 T_{g,2} + K_2 w_3 T_{g,3}}{w_1 + K_1 w_2 + K_2 w_3} \qquad \text{Eq. 2-2}$$

where w_i is the weight fraction and $T_{g,i}$ is the glass transition temperature in Kelvin of a pure component *i*. Indices 1, 2 and 3 represent NMD, EE and HPMC, respectively. Water was not considered in our calculations. It can be assumed that all water content was removed from the physical mixtures during the first heating run and the VCM specimen were stored dry prior to analysis. Constants K_i were calculated using the Simha-Boyer rule (Simha and Boyer, 1962) with ρ representing the density of each component. Indices 1 and 2 represent the amorphous component with the lowest T_g and highest T_g, respectively:

$$K_1 = \frac{\rho_1 T_{g,1}}{\rho_2 T_{g,2}} \qquad \text{Eq. 2-3}$$

K_1 was calculated for NMD and EE, yielding a value of 1.261. K_2 was calculated for NMD and HPMC and results in a value of 0.598. The raw material properties used in the calculation are taken from Table 2-2.

Predicting T_g by this approach relies on an ideal behavior of polymeric mixture (Gordon and Taylor, 1952). Measured T_gs deviating positively from the predicted value suggest enthalpic contributions to mixing, such as strong intermolecular H-bonding or negative excess volume of mixing. Negative deviations may indicate positive excess of mixing volume due to either moderate-to-strong or weak-to-moderate heteromolecular interactions (Paudel et al., 2014).

Figure 2-6 shows reversing heat flows for all ASDs prepared via quench cooling (first heating and subsequent cooling run in DSC for physical mixtures) and VCM technology (data in Table A-4 in the

Supplemental Material section A). Arrows indicate the occurrence of a T_g. For all QC formulations, only one T_g was detected, whereas for most of VCM ASDs, two or three glass transitions were observed. Detection of more than one T_g indicates a multiphase system. Glass transitions around 145 °C suggest an HPMC phase. Lower range glass transitions may point to the presence of a phase rich in EE and/or API, whereas T_g at around 100°C may signify a phase rich in HPMC and API. Surprisingly, the binary system with EE and NMD showed a second step-change at 94.2°C. Parikh et al. (Parikh et al., 2014) reported a second cross-over point in the viscosity measurements of EE but no corresponding thermal event. Parikh et al. connected this second cross-over point to flow onset in the main block chain of the polymers. Observations via a hot-stage microscope at a heat rate of 5 K/min at 40°C-120°C with pictures taken every 5°C (Figure A-1 in the Supplemental Material section A) support this hypothesis, since a coalescence of softened EE particles was observed only at above 95°C.

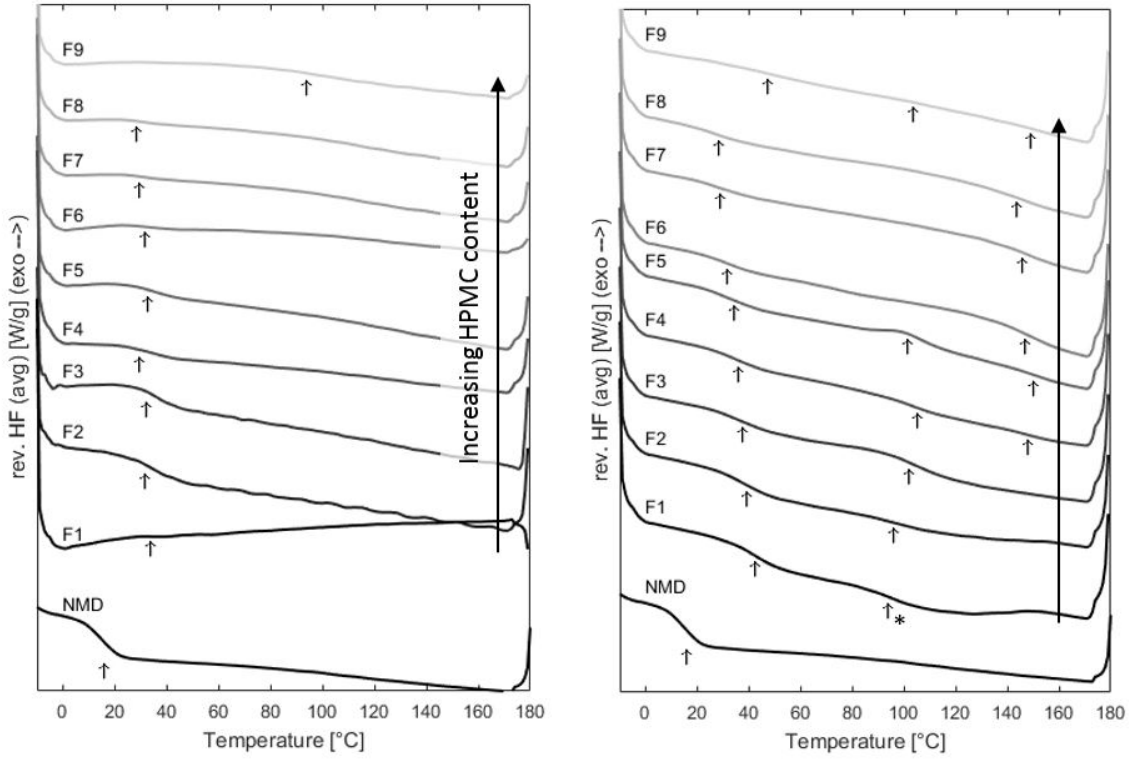

*Figure 2-6. Averaged reversing heat flow (n=2) based on the mDSC measurement of QC (left) and VCM ASDs (right) for all formulations and a polymer ratio of 1:1 (EE:HPMC) at 10% (w/w) API content. * Thermal event other than T_g.*

Overall, when comparing QC ASDs with VCM ASDs, the lowest T_g detected in the EE-containing VCM samples was always close to T_g in the QC samples. For the binary NMD-HPMC system, the middle T_g in the VCM samples correlated well to QC data. The detection of additional glass transitions in VCM discs is possible due to better contact between sample and pan, ensuring a more sensitive measurement of weak thermal events. Another possible reason is some degree of phase separation occurring only in VCM-processed ASDs.

Analysis of HME processed ASDs (F1, F3, F5, F6 and F9) was done with thin pieces cut from the strands and placed in the DSC pans. Just as for QC ASDs, only one mixture T_g could be detected. The obtained T_g values agree well with data for QC-prepared ASDs and the lowest T_g in VCM samples, except for F9 with NMD and HPMC only. This indicates similar phase arrangement for EE containing samples. It is assumed, that it is not possible to detect the glass transitions from HPMC containing phases in extruded ternary mixtures, since overall signal intensity was rather weak due to poorer sample contact to the pan (Figure A-4 in the Supplemental Material section A).

Comparing measured T_gs in a multiphase system with predictions for a ternary system based on the Gordon-Taylor/Kelley-Bueche equation is not feasible (Figure 2-7). Thus, T_gs were predicted for binary systems of NMD and EE, and of NMD and HPMC. In the weight fractions of these hypothetical binary formulations, the other (neglected) polymer is considered an inert, immiscible filler. For example, weight fractions for the prediction of the binary NMD-EE blend T_g in F5, with an actual composition of 10% NMD, 45% EE and 45% HPMC (50% (w/w) EE in carrier system), are calculated to be 18.18% (w/w) NMD and 81.82% (w/w) EE. As can be seen in the Figure, predictions of the binary model with NMD and EE agree well with the experimental values for the NMD-EE-rich phase in all ASDs. The same is observed in samples with variable NMD content (Figure A-3 in the Supplemental Material section A). This suggests, that all NMD in the formulation is solubilized in EE. The model still slightly overestimates T_g, possibly indicating a molecular interaction between NMD and EE.

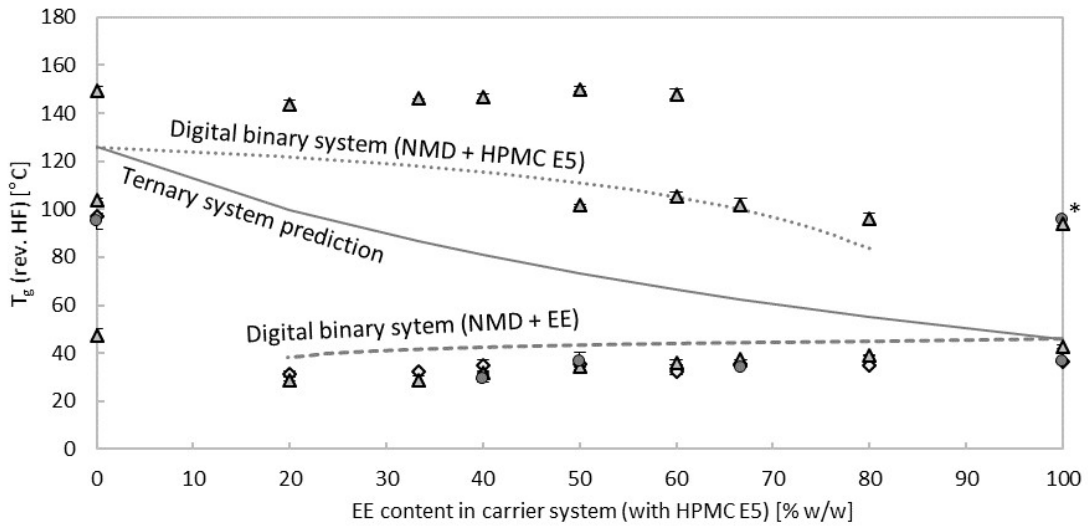

*Figure 2-7. Measured T_g values (rev. HF) (mean ± span, n=2) versus EE content in the polymeric carrier for QC ASD (◇), VCM ASD (△) and HME ASD (●) versus "digital" values calculated using the Gordon-Taylor model for ternary (solid line) and binary mixtures of NMD and EE (dashed line) and NMD and HPMC (dotted line). * Thermal event other than T_g.*

The binary model with HPMC yields T_g predictions close to those at medium level in VCM samples with low HPMC content. Due to the condition of mass fraction closure though, it impossible for NMD to be simultaneously present in the NMD-EE-rich phase (indicated by lower T_g) and the NMD-HPMC-rich phase, as suggested e.g. for F3 – 67% (w/w) EE in carrier. Moreover, at high HPMC content in ternary blends, no T_gs are detected in the vicinity of binary NMD-HPMC and ternary model predictions. This supports a hypothesis, that NMD is solely miscible with EE and that the medium level T_gs may originate from the second relaxation of EE polymers. However, another possible, less likely explanation for the medium level T_gs in ternary formulations is NMD mobility that facilitates a transfer from an EE-rich to HPMC-rich phase in VCM ASDs during the heating run. This option cannot be certainly excluded, as a T_g at similar position is present in the binary NMD-HPMC VCM ASD. Measured T_gs in the binary NMD-HPMC system can be used to estimate the composition of the phases based on the Gordon-Taylor model, under the assumption that T_g is not influenced by heteromolecular interactions. Apparent compositions indicate a HPMC-rich phase without NMD for the highest T_g and two mixture phases for the lower T_gs. Their composition is estimated with an NMD content of approximately 66% (w/w) (T_g at 47.3°C) and 23% (w/w) (T_g at 103.7°C), indicating some miscibility of NMD and HPMC.

In any case, these findings indicate a multiphase system in all ternary formulations, with NMD-EE rich and HPMC-containing phases. This also has a significant effect on processability. The low T_g of the NMD-EE rich phase poses a challenge for pelletization, as it is close to room temperature. Since cooling efficiency depends on the temperature difference between the hot and the cold medium, cooling becomes very slow close to ambient temperature. However, the T_g of the HPMC phase around 145°C in ternary formulations below 60% of EE in the carrier (F4-F9), can easily be undercut by ambient cooling before a pelletization. Therefore, these formulations can be considered to offer the mechanical robustness needed for strand pelletization.

2.3.5. Molecular Interaction Study

In order to better understand the multiphase system in ternary formulations, FTIR data were used to investigate the presence of molecular interactions in the ASDs. In H-bonding interactions, NMD can act as a proton donor and acceptor. In the crystalline lattice of NMD, H-bonds between the NH-group in 1,4-dihydro-pyridine ring and ether oxygen on the R3 side chain prevail (Drużbicki et al., 2016; Grunenberg et al., 1995; Tang et al., 2002; Wang et al., 1989). Stretching bands of the NH-group in N-H…O bonds are weakened in the amorphous form, as indicated by a shift towards higher wavenumbers and significant broadening (Figure 2-8, left). This suggests that the drug-drug H-bonds present in the crystalline form are significantly weakened or broken by amorphization (Drużbicki et al., 2016). The N-H stretching band from the dispersed NMD is even more blue-shifted (Figure 2-8). This demonstrates a more pronounced weakening of H-bond interactions in the N-H moiety and a lack of H-bonds interactions within these groups in the formulation.

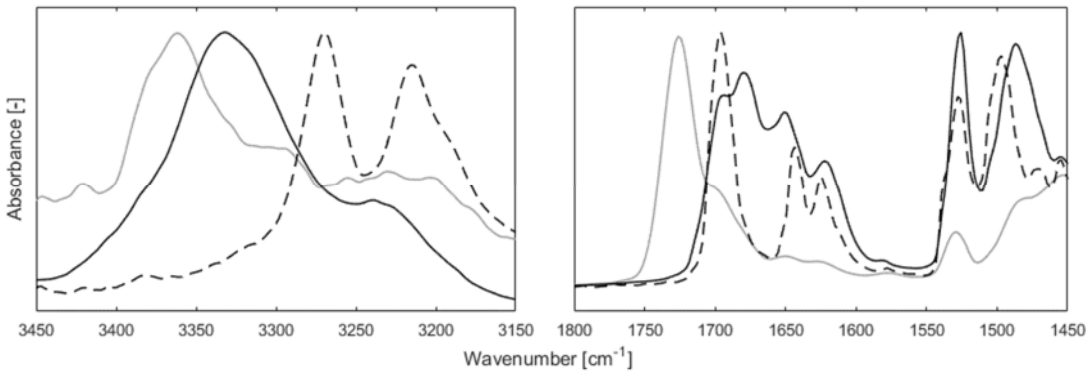

Figure 2-8. FTIR spectra (averaged, n=3) from crystalline (dashed black), amorphous (solid black) and dispersed (F5 – solid grey) NMD. Left: N-H stretching band region. Right: region with overlaid stretching vibrations and bending bands of N-H, C=O and C=C bonds. Spectrum of dispersed NMD (F5) smoothed using a third-degree Savitzky-Golay filter with a span of 15 spectra.

To investigate the possible interactions in the carbonyl groups, the wavenumber range of 1450-1800 cm^{-1} was examined. Drużbicki et al. (Drużbicki et al., 2016) applied molecular dynamics simulations to NMD (modification I) to facilitate the interpretation of FTIR spectra based on a mechanistic background, making a detailed assignment of FTIR bands possible. Bands relevant to molecular interaction via H-bonds and their shifts or changes in appearance are listed in Table 2-4. The band shifts are evaluated in relation to the bands observed in the crystalline NMD (here, modification II), with examples provided for the two binary formulations (F1 and F9), the ternary formulation with equal polymeric carrier content (F5) and the formulations with an increased API content (F10 and F11, spectra shown in Figure A-6). The band at 1696 cm^{-1} is significantly broadened, separating into two peaks in the amorphous API and in formulation F9. The carbonyl stretching band at this frequency is slightly red-shifted in the amorphous state. The second peak is assigned to the N-H in-plane bending band. It shifts towards lower wavenumbers (1680 cm^{-1}). In dispersed NMD (F5), there is only one small peak visible in the flank of the polymer band. Figure 2-9 shows FTIR spectra of all formulations with

10% (w/w) NMD and a trend in the position of this band across the different compositions, shifting to the right with increasing HPMC content. At 1644 cm^{-1}, the band is assigned to the C=C double bonds from the dihydropyridine ring. The dihydropyridine ring is distorted when NMD is in its crystalline form (Drużbicki et al., 2016), whereas, if NMD is amorphous, C=C bond interactions are weakened. Thus, the band shifts to higher wavenumbers in the amorphous form. In the spectra of dispersed API, broadening of peaks is enhanced.

Table 2-4. Shifts and changes in IR bands (averaged, n=3) for amorphous NMD, binary formulations (F1, F9) and ternary formulation with 1:1 EE:HPMC ratio and 10%, 20% and 30%(w/w) API (F5, F10 and F11). (ν: stretching, δ: in-plane bending)

	ν(N-H) [cm^{-1}]	**δ(N-H…O) + ν(C=O)^{R2} + ν(C=O)^{R3} [cm^{-1}]**		**ν(C=C) + ν(C=O)^{R2} [cm^{-1}]**	**δ(N-H…O) + ν(C=O)^{R2} + ν(C=O)^{R3} [cm^{-1}]**	**ν(NO_2) [cm^{-1}]**	**δ(N-H …O) [cm^{-1}]**
cryst. NMD	3269	1696 [b]		1644	1624	1528	1497
	Band shifts compared to crystalline NMD [cm^{-1}]						
amorph NMD	64 broader	-3 separated	-16 broader	7 broader	-2 broader	-2	-10 broader
F1	97	-	-	6	-	2	-
F5	93	5 [b]		7	4	2	-12
F9	-	2	-10	-	0	2	-
F10	95	2 [b]		7	2	2	-10
F11[a]	100 (6)	2[b]		6	0	2	-10

[a] data for duplicate measurements (n=2); [b] overlaid C=O and N-H…O bands

Formulations with an increased NMD content (F10 and F11) have higher peak intensities. Moreover, the peak at 3275 cm^{-1} indicates H-bonding in the N-H group of NMD (blue-shift). This may suggest recrystallization or interactions at a similar strength to NMD-NMD interactions in crystalline form. Since there was no evidence for recrystallization in mDSC measurements, this is considered a sign of some molecular interaction with the excipient(s). To confirm this interpretation, bands of moieties in the polymers were investigated that could interact with the API molecule.

The functional groups of interest in EE are the carbonyl group (C=O) at 1720 cm^{-1} (Moustafine et al., 2006; Zheng et al., 2007a) and the dimethyl amino peaks at 2822 and 2770 cm^{-1}. With regard to HPMC, the hydroxyl group occurring at 3447 cm^{-1} and -O- at 1733 cm^{-1} have the potential to interact with the drug molecule as a proton donor or acceptor. Spectra of powder and VCM-prepared pure polymers are provided in Figure A-5 in the Supplemental Material section A. Although the spectra are mainly superimposed without any peak shifts, the appearance of several peaks is slightly different. Table 2-5 summarizes the changes in band positions and appearance of VCM discs for pure polymers and binary formulations (F1 and F9), as well as the formulation with a polymer ratio of 1:1 EE:HPMC with various API contents (F5, F10 and F11). Since HPMC does not exhibit any significant band shifts in any formulation, it appears not to interact with the other components. This is in line with the results of

Marks et al. (Marks et al., 2014) who reported a miscibility gap for HPMC and EE. However, H-bond interaction with NMD has been reported by Riekes et al. (Riekes et al., 2014; Zheng et al., 2007a), indicated by the disappearance of NMD N-H stretching vibrations. EE bands in contrast show significant shifts with increasing NMD content at 1724 cm^{-1}, representing the carbonyl group. At 2822 and 2770 cm^{-1}, the ternary amine bands are observed. There is a slight shift to higher wavenumbers, indicating some interaction with NMD. Therefore, FTIR elucidated weak H-bonding between the API and EE. Moreover, amorphization and an intense dispersion effect for all formulations for NMD molecules were observed.

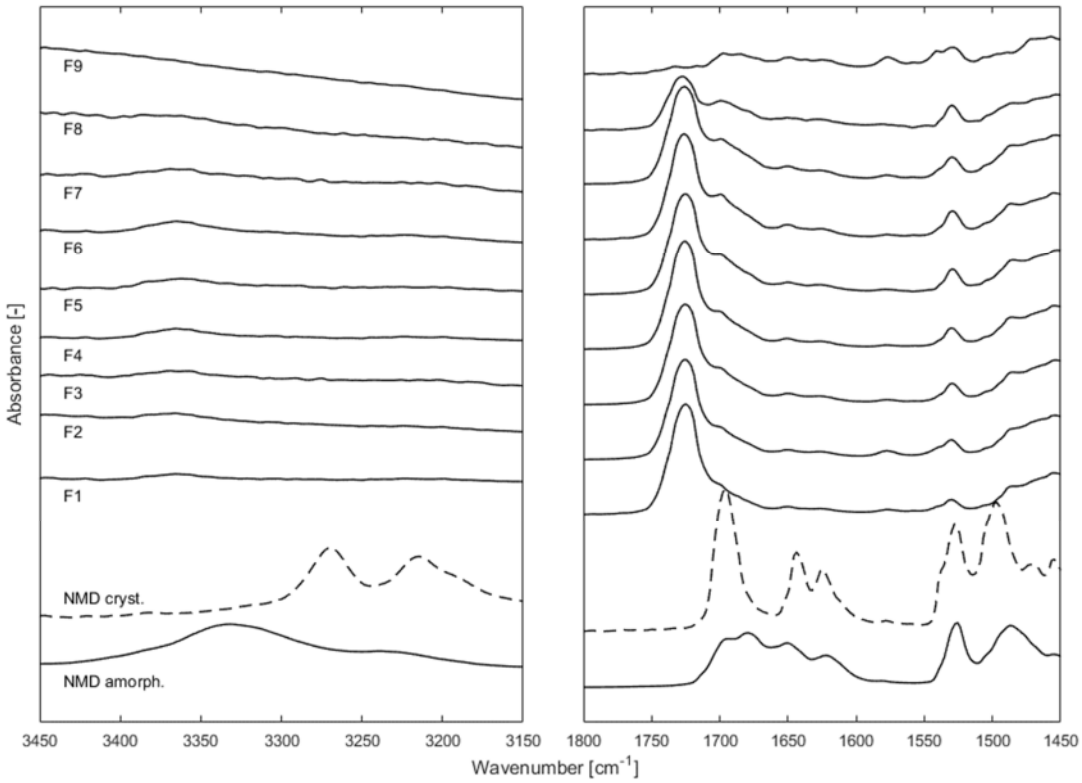

Figure 2-9. FTIR-spectra (averaged, n=3) of all VCM ASDs containing 10%(w/w) NMD (F1-F9).

Table 2-5. Shifts and changes in IR bands (averaged, n=3) for EE and HPMC in VCM discs, binary (F1, F9) and ternary formulation with 1:1 EE:HPMC ratio and 10%, 20% and 30%(w/w) API (F5, F10 and F11). (v: stretching, δ: in-pane bending)

	HPMC ν(OH) [cm^{-1}]	**EE (-N(CH_3)$_2$) [cm^{-1}]**		**HPMC ν(C=O) [cm^{-1}]**	**EE ν(C=O) [cm^{-1}]**
powder	3447	2822	2770	1733	1724
	Band shifts compared to powder spectrum [cm^{-1}]				
VCM disc	9	0	0	5 broader	1
F1		0	0		1
F5	-	0	0	-	2
F9	0			-1	
F10	0	0	2	-	3
F11[a]	0	2	2	-	3

[a] data for duplicate measurement (n=2)

2.3.6. Stability Studies

Molecular interactions between API and polymers are considered to be crucial for ASD stability (Li et al., 2014). DSC signals of stability-tested formulations did not indicate any recrystallization but rather some changes in the phase arrangement of the ASDs. Figure 2-10 presents the T_gs of VCM discs before and after storage under accelerated conditions. The binary formulation with HPMC had a reduced number of phases after stress conditions. While the T_g at the medium level vanished, the high level and the low level remain unchanged, showing that these two-phase compositions may be thermodynamically preferable. The binary formulation with EE did not significantly change the mixture's T_g, indicating good physical stability of the EE-rich phase. The second T_g which indicates a relaxation of the block-chain polymers increased slightly over storage time under accelerated conditions. In the ternary system with a polymer ratio of 2:1 EE:HPMC (F3), a HPMC-rich phase was formed suggesting some phase separation. Other ternary formulations (F5 and F6) did not show any changes in T_g after storage, indicating a stable-phase configuration. FTIR spectra (Figure A-7) support the findings regarding stability based on the DSC thermograms. Characteristic band wavenumbers of binary formulations (shown in Figure A-7 in the Supplemental Material section A) and the ternary formulation with a polymer ratio of 1:1 EE:HPMC remain the same.

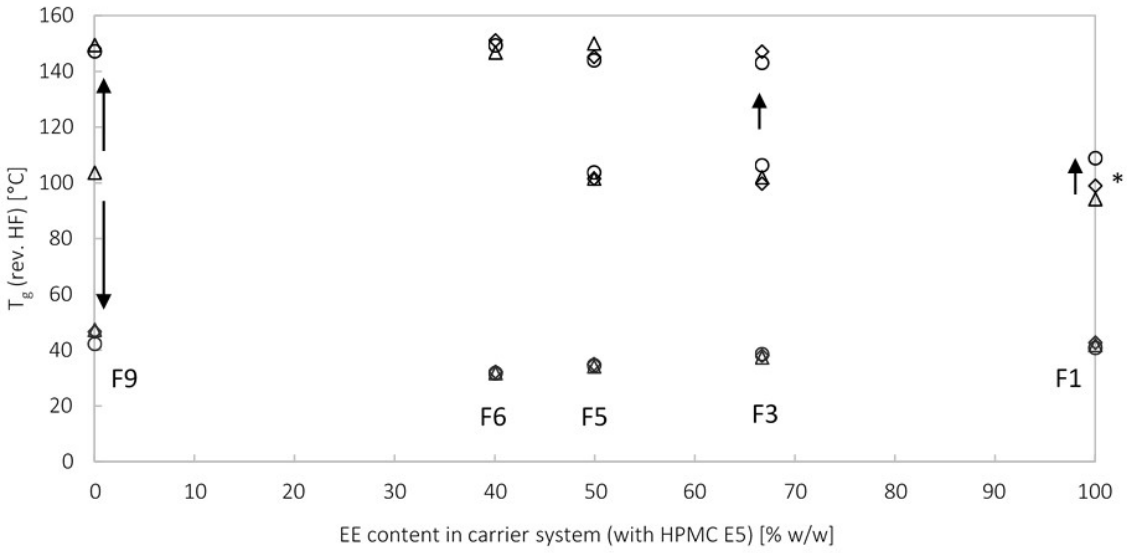

*Figure 2-10. T_gs (rev. HF) of VCM ASDs (mean ± span, n=2) versus EE content in the polymeric carrier before stability testing (Δ), after 1 week (◇) and after 4 weeks (o) of storage under accelerated conditions. Arrows indicating changes. * Thermal events other than T_g.*

2.3.7. Dissolution Studies

Formulation-Intrinsic Dissolution Studies with VCM discs

Formulation-intrinsic dissolution studies were performed to assess the formulation performance, regardless of shape and size of samples. The dissolution profile is considered formulation-intrinsic, since dissolution conditions were kept constant for all samples and the layer-by-layer dissolution in the PTFE holder allows a normalization of the dissolution rate by the interfacial area of the samples.

Two main observations were made in formulation-intrinsic dissolution profiles (Figure A-8 in the Supplemental Material section A) of VCM-prepared samples: 1) Samples containing predominantly one of the polymers show a linear release profile of the API, whereas samples with similar amounts of both polymers show flattening of the profile after 30 min. 2) Variability in the dissolution profile increased with increasing EE content. Concerning the first observation, the appearance of samples after 70 min of dissolution testing indicated that the emergence of flattening after 30 min correlated with a change in dissolution mechanism. HPMC is a swelling polymer that releases the API from a gel-like surface via diffusion, and EE is a polymer that releases the API via surface erosion. While formulations F1 and F2 with 100% (w/w) and 80% (w/w) EE in the carrier eroded almost completely, much of the sample was preserved in the sample holder for all other formulations. Therefore, the API dissolution is at least partially controlled via diffusion above a HPMC content of 33.3% (w/w) in the carrier. The second observation on variability has to do with the low T_g in the EE-rich domains of the formulation, causing surface deformation after a certain time at dissolution temperature. To compare all formulations, the intrinsic dissolution rates were calculated via a linear regression of the dissolved API fraction over the first 30 min (Table 2-6).

The trend for intrinsic dissolution rates across the EE content in the polymeric carrier at 10% (w/w) NMD (Figure 2-11) reflects the effects of the different dissolution mechanisms of the two polymers used. The binary formulation with EE exhibited the fastest dissolution rate. In formulations with more than 50% (w/w) EE in the carrier, the eroding mechanism of EE dissolution is slowed down for increasing HPMC content. HPMC polymer swelling appears to hinder the erosion of NMD-EE rich phases. However, an unexpected trend of the dissolution rates was observed at equal content of both polymeric carriers (F5 - 1:1 EE:HPMC), which represented the minimum of dissolution rates for all ternary formulations. ASD stability during dissolution can be excluded as a reason for this observation, since the dissolution test of samples with increased API content (F10 and F11 – Figure A-9 in the Supplemental Material section A), and the same polymer ratio of 1:1 EE:HPMC led to a faster intrinsic dissolution rate. Therefore, it is suggested, that the competing dissolution mechanisms of the two polymers are source of this observation. Ueda et al. (Ueda et al., 2018) recently investigated a miscible dual-polymer system, observing a maximum in drug release rate a similar polymer content. Observations in this work suggest, that the opposite effect can be achieved by the selection of an

immiscible dual-polymer system. However, the exact mechanism of this interplay and possible applications should be investigated more thoroughly in another study.

In samples with higher HPMC content the effect of further decreasing EE content turned out to be more complex. At first, a steep increase of the dissolution rate was observed in formulations F6 and F7. At higher HPMC content, the dissolution rate levels off (F8) and finally drops significantly to the lowest level for the binary system of NMD and HPMC (F9). Polarized light microscope images from NMD-HPMC dispersions after various times of dissolution testing (Figure A-2 in the Supplemental Material section A), revealed recrystallization of API at the surface of the sample. Therefore, drug dissolution from this formulation was controlled not only by the dissolution mechanism of HPMC, but also by the kinetics of crystallization towards equilibrium and the dissolution on the polymer surface. As such, HPMC did not act as a crystallization inhibitor for amorphous NMD, as reported for other poorly soluble APIs (Xie et al., 2017; Xie and Taylor, 2016). To prevent matrix or surface crystallization, close contact between polymer and API is required upon dissolution and swelling. Phase separation observed in this formulation during the miscibility study appears to result in a lack of ASD stabilization during dissolution. However, the presence of EE even in low fractions stabilizes the ASD successfully during dissolution. The validity of this observation in non-sink conditions needs to be assessed in future studies. However, as the ability of EE-based NMD formulations has been shown already to provide bioavailability similar to the originator, this study focuses on the comparison of the sink-condition data only.

Pellet Dissolution

Dissolution testing of pellets prepared via benchtop extrusion was performed to determine if the miniaturized formulation screening could be transferred to a small-scale extrusion process and if the goal of immediate API release can be achieved. Dissolution profiles of pellets are shown in Figure 2-12 together with dissolution data for crystalline NMD. It can be observed, that the amount of dissolved API after 30 min from the crystalline state can be exceeded manifold by all ASD formulations. Immediate release was observed for formulations F1, F3, and F6, while F5 was slightly below the target of 85% NMD dissolved within 30 min. As a pilot-scale or manufacturing-scale extruder coupled with a pelletization system certainly will produce pellets smaller than 5 mm in length, the immediate release target is expected to be achieved by the final process also for this formulation.

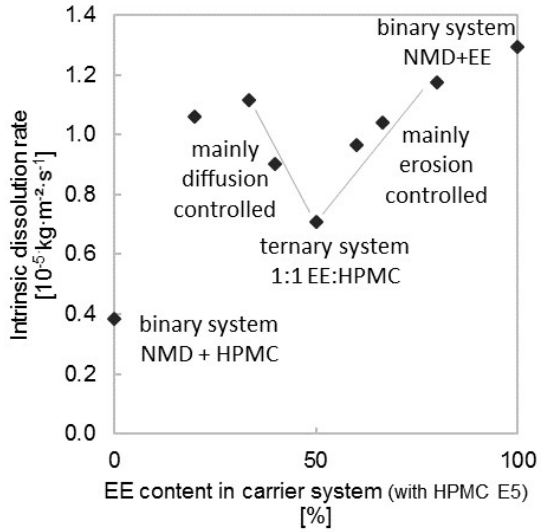

Figure 2-11. Formulation-intrinsic dissolution rates (averaged, n=3) versus EE content in the polymeric carrier for all formulations with 10%(w/w) API content (F1-F9).

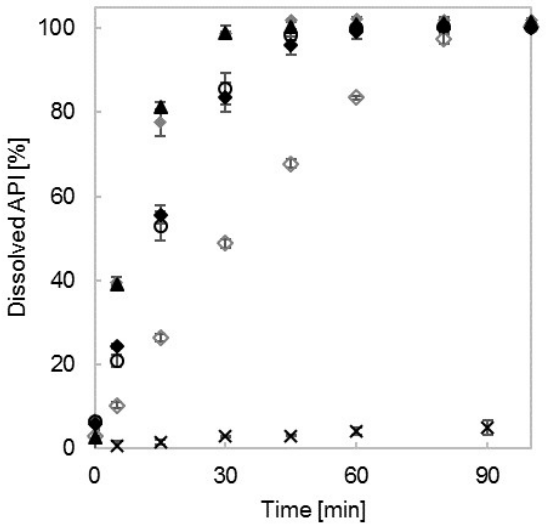

Figure 2-12. Dissolution profiles (mean ± SD, n=3) of HME pellets and crystalline NMD (USP Type 2, mean ± span, n=2). Pellets from formulations with 10% API and EE (◆ - F1), 2:1 EE:HPMC (▲ - F3), 1:1 EE:HPMC (◆ - F5), 2:3 EE:HPMC (○ - F6) and HPMC (◊ - F9).

Concerning the dissolution performance across the screened compositions, a similar trend was observed as for intrinsic dissolution samples. API release from the binary formulation with HPMC (F9) was the slowest, and dissolution from EE (F1) was very fast. Nevertheless, there were two significant differences arising: 1) 100% of the API was dissolved from all pellets within 120 min, strongly indicating that in this case the surface crystallization was inhibited by the binary system of NMD and HPMC E5; and 2) the trend across the tested ternary formulations shows a clear tendency towards a slower API release at increasing HPMC content. Especially the formulation with a polymer ratio of 1:1 EE:HPMC performed significantly better than in the intrinsic dissolution tests. The difference is assigned to the effect of shear during sample preparation. For systems exhibiting a yield point such as formulations with HPMC, shear forces are considered to facilitate homogenization of the sample and improve interaction at a molecular basis. Thus, intense intermixing of all components via benchtop extrusion is necessary to achieve representative information on the effect of HPMC on dissolution.

Table 2-6 additionally provides a quantitative comparison of formulation-intrinsic drug release rates within the first 5 min of dissolution testing for VCM ASDs and the pellet-shaped HME ASDs. To facilitate the comparison, a short timeframe was chosen to minimize the effect of pellet erosion on interface size. Dissolution of pellets was faster for all formulations, with the smallest increase observed in the NMD-EE system. Note that, compared to VCM specimen dissolution testing (using a paddle method and a more or less fixed sample position in a sample holder), fundamentally different hydrodynamic conditions were applied in pellets testing via a basket method. Therefore, no direct comparison of absolute values should be attempted.

Table 2-6. Formulation-intrinsic dissolution rates (averaged, n=3) of VCM ASD based on linear regression of dissolution profile within the first 30 min for all formulations and surface related dissolution rate of pellets (HME ASD) based on linear regression of the dissolution profile within the first 5 min for selected formulations.

No.	Ratio of Polymers (EE:HPMC)	VCM API release rate [10^{-5}·kg/(m²·s)]	Pellet API release rate [10^{-5}·kg/(m²·s)]
F1	EE	1.294	2.150 (166% of VCM ASD)
F2	4:1	1.174	
F3	2:1	1.040	2.664 (256% of VCM ASD)
F4	3:2	0.965	
F5	1:1	0.707	2.264 (320% of VCM ASD)
F6	2:3	0.903	1.677 (186% of VCM ASD)
F7	1:2	1.114	
F8	1:4	1.060	
F9	HPMC	0.385	1.167 (303% of VCM ASD)
F10	1:1 (20% w/w NMD)	0.707	
F11	1:1 (30% w/w NMD)	2.326	

2.4. Conclusion

A miniaturized formulation screening was performed to study the interplay of the three components and its effect on physicochemical performance and stability, and on processability in strand pelletization. The investigation of T_gs in ASDs generated by different preparation methods, namely

i) in-situ quench cooling (QC ASD),
ii) small-scale vacuum-compression molding (VCM ASD) and
iii) benchtop-extrusion (HME ASD)

lead to the identification of a phase separated system. A NMD-EE-rich phase was identified, which contributes to physical and physico-chemical stability of the ASDs during stability and dissolution testing, respectively. The role of HPMC in the formulation was more difficult to investigate, as an effect of sample preparation on dissolution performance was observed. However, a strong dispersion effect of HPMC on NMD-NMD interactions was identified by FTIR data.

Since the formulation is intended to be processed via HME and strand pelletization, the investigation of processability was one of the main aspects in this work. With regard to strand pelletization, formulations with very high EE content were found to be unfavorable. Extrudates with mainly EE in the polymeric carrier exhibited poor mechanical stability and tackiness at high temperatures, both aspects being critical for manufacturing-scale pelletization. Moreover, the strand was showing fragmentation when cooled down and cut to pellets. Both properties indicate poor pelletization performance on production scale unless the production parameters are tightly fitted to a small production window. The viscoelastic properties of HPMC (such as the yield point) which were challenging during miniaturized sample preparation, give the strand the required mechanical stability to achieve good processability in strand pelletization.

In summary, the screening aided in thorough understanding of phase arrangement, ASD stability and dissolution performance and allows a rational selection of the best formulation. Especially considering the tackiness of the NMD-EE rich phase, a formulation composition with a polymer ratio around 1:4 to 2:3 of EE:HPMC (20-40% w/w EE in carrier) should be chosen. For these formulations a good pelletization performance can be expected at a simultaneously fast dissolution rate and good ASD stability.

Future studies should further extend the knowledge on the interplay of binary carrier systems on ASD stability, dissolution profiles and processability, as the number of available pharmaceutical polymers is limited. This approach, in combination with the application of new technologies, such as strand pelletization in pharmaceutical manufacturing, will facilitate tailoring of product performance to diverse requirements.

2.5. References

British Pharmacopoeia, 2009. British Pharmacopoeia (2009).

Craig, D.Q.., 2002. The mechanisms of drug release from solid dispersions in water-soluble polymers. Int. J. Pharm. 231, 131–144.

DiNunzio, J.C., Miller, D.A., 2013. Formulation Development of Amorphous Solid Dispersions, in: Repka, M.A., Langley, N., DiNunzio, J.C. (Eds.), Hot-Melt Extrusion: Pharmaceutical. Springer Verlag, New York, pp. 161–203.

Docoslis, A., Huszarik, K.L., Papageorgiou, G.Z., Bikiaris, D., Stergiou, D., Georgarakis, E., 2007. Characterization of the distribution, polymorphism, and stability of nimodipine in its solid dispersions in polyethylene glycol by micro-Raman spectroscopy and powder X-ray diffraction. AAPS J. 9, E361-70.

Drużbicki, K., Pajzderska, A., Kiwilsza, A., Jenczyk, J., Chudoba, D., Jarek, M., Mielcarek, J., Wąsicki, J., 2016. In search of the mutual relationship between the structure, solid-state spectroscopy and molecular dynamics in selected calcium channel blockers. Eur. J. Pharm. Sci. 85, 68–83.

Gordon, M., Taylor, J.S., 1952. Ideal Copolymers and the Second-Order Transitions of Synthetic Rubbers. I. Non-Crystalline Copolymers. J. Appl. Chem. 2, 493–500.

Grunenberg, A., Keil, B., Henck, J.-O., 1995. Polymorphism in binary mixtures, as exemplified by nimodipine. Int. J. Pharm. 118, 11–21.

Janssens, S., de Armas, H.N., Roberts, C.J., Van den Mooter, G., 2008a. Characterization of Ternary Solid Dispersions of Itraconazole, PEG 6000, and HPMC 2910 E5. J. Pharm. Sci. 97, 2110–2120.

Janssens, S., De Zeure, A., Paudel, A., Van Humbeeck, J., Rombaut, P., Van Den Mooter, G., 2010. Influence of preparation methods on solid state supersaturation of amorphous solid dispersions: A case study with itraconazole and eudragit E100. Pharm. Res. 27, 775–785.

Janssens, S., Nagels, S., Armas, H.N. de, D'Autry, W., Van Schepdael, A., Van den Mooter, G., 2008b. Formulation and characterization of ternary solid dispersions made up of Itraconazole and two excipients, TPGS 1000 and PVPVA 64, that were selected based on a supersaturation screening study. Eur. J. Pharm. Biopharm. 69, 158–166.

Jijun, F., Lili, Z., Tingting, G., Xing, T., Haibing, H., 2010. Stable nimodipine tablets with high bioavailability containing NM-SD prepared by hot-melt extrusion. Powder Technol. 204, 214–221.

Kelley, F.N., Bueche, F., 1961. Viscosity and glass temperature relations for polymer-diluent systems. J. Polym. Sci. 50, 549–556.

Li, Y., Pang, H., Guo, Z., Lin, L., Dong, Y., Li, G., Lu, M., Wu, C., 2014. Interactions between drugs and polymers influencing hot melt extrusion. J. Pharm. Pharmacol. 66, 148–166.

Maniruzzaman, M., Nair, A., Scoutaris, N., Bradley, M.S.A., Snowden, M.J., Douroumis, D., 2015. One-step continuous extrusion process for the manufacturing of solid dispersions. Int. J. Pharm. 496, 42–51.

Marks, J.A., Wegiel, L.A., Taylor, L.S., Edgar, K.J., 2014. Pairwise polymer blends for oral drug delivery. J. Pharm. Sci. 103, 2871–2883.

Marsac, P.J., Konno, H., Taylor, L.S., 2006a. A comparison of the physical stability of amorphous felodipine and nifedipine systems. Pharm. Res. 23, 2306–2316.

Marsac, P.J., Li, T., Taylor, L.S., 2009. Estimation of drug-polymer miscibility and solubility in amorphous solid dispersions using experimentally determined interaction parameters. Pharm. Res. 26, 139–151.

Marsac, P.J., Shamblin, S.L., Taylor, L.S., 2006b. Theoretical and practical approaches for prediction of drug-polymer miscibility and solubility. Pharm. Res. 23, 2417–2426.

Martin, C., 2013. Twin-Screw Extrusion for Pharmaceutical Processes, in: Repka, M.A., Langley, N., Dinunzio, J.C. (Eds.), Melt Extrusion - Materials, Technology and Drug Product Design. American Association of Pharmaceutical Scientists, New York, pp. 47–79.

Moustafine, R.I., Zaharov, I.M., Kemenova, V.A., 2006. Physicochemical characterization and drug release properties of Eudragit® E PO/Eudragit® L 100-55 interpolyelectrolyte complexes. Eur. J. Pharm. Biopharm. 63, 26–36.

Newman, A., Knipp, G., Zografi, G., 2012. Assessing the performance of amorphous solid dispersions. J. Pharm. Sci. 101, 1355–1377.

Parikh, T., Gupta, S.S., Meena, A., Serajuddin, A.T.M., 2014. Investigation of thermal and viscoelastic properties of polymers relevant to hot melt extrusion - III: Polymethacrylates and polymethacrylic acid based polymers. J. Excipients Food Chem. 5, 56–64.

Paudel, A., Meeus, J., Van den Mooter, G., 2014. Structural Characterization of Amorphous Solid Dispersions, in: Shah, N., Sandhu, H., Choi, D.S., Chokshi, H., Malick, A.W. (Eds.), Amorphous Solid Dispersions: Theory and Practice. Springer Verlag, p. 421-485.

Paudel, A., Nies, E., Van den Mooter, G., 2012. Relating hydrogen-bonding interactions with the phase behavior of naproxen/PVP K 25 solid dispersions: evaluation of solution-cast and quench-cooled films. Mol. Pharm. 9, 3301–3317.

Paudel, A., Worku, Z.A., Meeus, J., Guns, S., Van den Mooter, G., 2013. Manufacturing of solid dispersions of poorly water soluble drugs by spray drying: formulation and process considerations. Int. J. Pharm. 453, 253–284.

Prodduturi, S., Urman, K.L., Otaigbe, J.U., Repka, M.A., 2007. Stabilization of hot-melt extrusion formulations containing solid solutions using polymer blends. AAPS PharmSciTech 8, E152–E161.

Qian, F., Huang, J., Hussain, M.A., 2010. Drug-Polymer Solubility and Miscibility: Stability Consideration and Practical Challenges in Amorphous Solid Dispersion Development. J. Pharm. Sci. 99, 2941–2947.

Quinteros, D.A., Rigo, V.R., Kairuz, A.F.J., Olivera, M.E., Manzo, R.H., Allemandi, D.A., 2008. Interaction between a cationic polymethacrylate (Eudragit E100) and anionic drugs. Eur. J. Pharm. Sci. 33, 72–79.

Riekes, M.K., Kuminek, G., Rauber, G.S., De Campos, C.E.M., Bortoluzzi, A.J., Stulzer, H.K., 2014. HPMC as a potential enhancer of nimodipine biopharmaceutical properties via ball-milled solid dispersions. Carbohydr. Polym. 99, 474–482.

Rowe, R.C., Sheskey, P.J., Quinn, M.E., 2009. Handbook of Pharmaceutical Excipinets, 6th ed. Pharmaceutical Press, London.

Simha, R., Boyer, R.F., 1962. On a General Relation Involving the Glass Temperature and Coefficients of Expansion of Polymers. J. Chem. Phys. 37, 1003–1007.

Smikalla, M.M., Urbanetz, N.A., 2007. The influence of povidone K17 on the storage stability of solid dispersions of nimodipine and polyethylene glycol. Eur. J. Pharm. Biopharm. 66, 106–112.

Sun, Y., Rui, Y., Wenliang, Z., Tang, X., 2008. Nimodipine semi-solid capsules containing solid dispersion for improving dissolution. Int. J. Pharm. 359, 144–149.

Tang, X.C., Pikal, M.J., Taylor, L.S., 2002. A Spectroscopic Investigation of Hydrogen Bond Patterns in Crystalline and Amorphous Phases in Dihydropyridine Calcium Channel Blockers. Pharm. Res. 19, 477–4830.

The Dow Chemical Company, 2002. METHOCEL Cellulose Ethers in Aqueous Systems for Tablet Coating.

Treffer, D., Troiss, A., Khinast, J.G., 2015. A novel tool to standardize rheology testing of molten polymers for pharmaceutical applications. Int. J. Pharm. 495, 474–481.

Treffer, D.F., Khinast, J.G., 2017. Why hot melts do not stick to cold surfaces. Polym. Eng. Sci. 57, 1083–1089.

Ueda, K., Yamazoe, C., Yasuda, Y., Higashi, K., Kawakami, K., Moribe, K., 2018. Mechanism of enhanced nifedipine dissolution by polymer-blended solid dispersion through molecular-level characterization. Mol. Pharm. 15, 4099–4109.

Urbanetz, N.A., 2006. Stabilization of solid dispersions of nimodipine and polyethylene glycol 2000. Eur. J. Pharm. Sci. 28, 67–76.

Urbanetz, N.A., Lippold, B.C., 2005. Solid dispersions of nimodipine and polyethylene glycol 2000: dissolution properties and physico-chemical characterisation. Eur. J. Pharm. Biopharm. 59, 107–18.

Van Den Mooter, G., 2012. The use of amorphous solid dispersions: A formulation strategy to overcome poor solubility and dissolution rate. Drug Discov. Today Technol. 9, e79–e85.

Van Krevelen, D.W., Te Nijenhuis, K., Van Krevelen, D.W., Te Nijenhuis, K., 2009. Chapter 4 – Volumetric Properties, in: Properties of Polymers. pp. 71–108.

Wang, S.D., Herbette, L.G., Rhodes, D.G., 1989. Structure of the calcium channel antagonist, nimodipine. Acta Crystallogr. Sect. C Cryst. Struct. Commun. 45, 1748–1751.

Williams, H.D., Trevaskis, N.L., Charman, S.A., Shanker, R.M., Charman, W.N., Pouton, C.W., Porter, C.J.H., 2013. Strategies to address low drug solubility in discovery and development. Pharmacol. Rev. 65, 315–499.

Xie, T., Gao, W., Taylor, L.S., 2017. Impact of Eudragit EPO and Hydroxypropyl Methylcellulose on Drug Release Rate, Supersaturation, Precipitation Outcome and Redissolution Rate of Indomethacin Amorphous Solid Dispersions. Int. J. Pharm.

Xie, T., Taylor, L.S., 2016. Improved Release of Celecoxib from High Drug Loading Amorphous Solid Dispersions Formulated with Polyacrylic Acid and Cellulose Derivatives. Mol. Pharm. 13, 873–884.

Yang, Z., Nollenberger, K., Albers, J., Craig, D., Qi, S., 2013. Microstructure of an immiscible polymer blend and its stabilization effect on amorphous solid dispersions. Mol. Pharm. 10, 2767–2780.

Zheng, X., Yang, R., Tang, X., Zheng, L., 2007a. Part I: Characterization of Solid Dispersions of Nimodipine Prepared by Hot-Melt Extrusion. Drug Dev. Ind. Pharm. 33, 791–802.

Zheng, X., Yang, R., Zhang, Y., Wang, Z., Tang, X., Zheng, L., 2007b. Part II: Bioavailability in Beagle Dogs of Nimodipine Solid Dispersions Prepared by Hot-Melt Extrusion. Drug Dev. Ind. Pharm. 33, 783–789.

3. Hot-Melt Extrusion and Pelletization Process Setup and Parameter Screening

This chapter provides a transition between the formulation development and the hot-melt extrusion (HME) and pelletization process design space definition. In the formulation development phase, different compositions of a ternary formulation with 10 wt.% of NMD, and a carrier system of Eudragit® E (EE) and Methocel™ E5 (HPMC) have been investigated, yielding an optimal carrier polymer ratio between 1:4 and 2:3 of EE:HPMC. With a formulation composition within this range, two steps were taken in this first stage of process development: i) testing of different setups, with a special focus on the feasible pelletization technology, and ii) a process parameter screening.

In the setup experiments, the intake of the Eudragit® EPO powder with low bulk density and the rheology and degradation propensity of HPMC constituted a challenge. The change from Eudragit® in powder form (EPO) to its pellet grade Eudragit® E100 largely resolved the extruder intake issue. This selection further lead to the application of a split-feeding strategy, dosing each component by a separate feeder. With regard to pelletization technology, strand pelletization is known to provide wider processing windows due to the thermal decoupling of the cutting from the extrusion process. However, die-face pelletization was tested, since it offers rounded pellets with even better flow properties compared to cylindrical pellets. Finally, strand pelletization remained the best option for this formulation, as the formulation's phase separated nature did not allow to apply die-face pelletization.

The most important parameters of the HME process were varied in a design of experiments (DoE) in order to assess their effect on relevant process responses and product quality attributes, such as pellet API content and content uniformity, dissolution performance, shape and size, as well as degradation of the API and HPMC. A critical aspect for product quality was the browning of pellets at screw speed levels above 120 rpm, indicating degradation of HPMC. The degradation resulted in decreased melt flowability and consequently, in issues with elevated and inconsistent die melt pressure. Moreover, the uniformity of strand velocities was found to be sensitive to the condition of the extrusion dies. A change in their condition was observed over repeated cleaning cycles, resulting in non-uniform strand velocities. This had a critical effect on pellet size and shape. The other pellet quality attributes were not affected by the investigated process parameters.

Finally, the nominal process parameter settings for producing 4 kg/h of pellets in the HME-pelletization unit were determined: 120 rpm screw speed, 140°C die temperature and 30 bar inlet pressure for the melt pump. Moreover, stainless steel dies should be used instead of the soft copper dies in order to decrease their sensitivity to cleaning.

3.1. Introduction

Hot-melt extrusion (HME) and pelletization are widely applied in polymer processing. HME enables melting, mixing, and shaping of thermoplastic materials in one step and is an inherently continuous process. Moreover, extruders have been successfully adapted for many different applications, such as compounding, food extrusion and as reactors. Pellets exhibit excellent handling properties due to superior flowability and uniformity compared to powders and are thus the most common shape for intermediate products in the polymer industry.

The application of HME in the pharmaceutical industry has gained significant interest after a publication of Breitenbach in the early 2000s (Breitenbach, 2002). He was promoting this technology especially for the preparation of amorphous solid dispersion (ASDs) with increased bioavailability of poorly water-soluble active pharmaceutical ingredients (APIs). Since then, several HME prepared products were brought on the market (Repka et al., 2018), among them, for example an oral medication for HIV therapy (Breitenbach, 2006).

Most oral dosage forms, that is tablets, with HME-prepared intermediates were manufactured via milling of the extrudate (Démuth et al., 2015; Grymonpré et al., 2017a). Milling has been reported to decrease ASD stability (Kalivoda, 2012) and in many cases cryogenic milling was required (Démuth et al., 2015; Gryczke et al., 2011), which demands complex process technology and cannot be executed continuously. The preparation of tablets from pellets offers several biopharmaceutical advantages, as discussed in on the context of multiple pellet unit systems (MUPS) (Abdul et al., 2010; Bodmeier, 1997). The disintegration of tablets into multiple pellets in the stomach allows to distribute the API better in the gastrointestinal (GI) tract and decreases the passage time in the stomach. Nevertheless, there have been challenges observed in their production, associated with segregation and uniformity of the final dosage form. These challenges were overcome by an appropriate selection of the tableting formulation (Braun, 2003; Wagner et al., 2000).

The aim of this work was to execute the first two steps of a pharmaceutical process development on an HME and pelletization unit, following the principles of Quality-by-Design (QbD). First, initial experiments were performed, determining the feasible setup of the process and second, a process parameter screening was executed to build a knowledge space. Thereby, a special focus was put on the following two aspects:

i. The decision between die-face pelletization and strand pelletization technology.
ii. The identification of a nominal set point for the process line, yielding desired pellet properties at a target throughout of 4 kg/h.

The target throughput of 4 kg/h was given by the minimum throughput required for units that will be used downstream of the HME-pelletization line. The formulation used in this study had been developed in Chapter 2, comprising 10 wt.% of a poorly water-soluble API, nimodipine, and two polymers, Eudragit® E and Methocel™ E5 in an optimized ratio of 1:4 to 2:3. Even though the processability of the formulation for strand pelletization had been considered specifically during formulation development, the applicability of die-face pelletization was assessed in the study at hand. The technology of die-face pelletization would be beneficial since it yields round pellets with superior flowability compared to the cylindrical pellets of strand pelletization. Die-face pelletization has already been successfully applied to produce pharmaceutical pellets (Roblegg et al., 2011; Treffer et al., 2014) and micro-pellets (Witschnigg et al., 2016) using the pelletizer Sphero® THA by Maag Automatik (Germany). However, in general strand pelletization is considered to be more robust, due to the thermal decoupling of the extrusion and the pelletization process. The only limitation for the strand pelletization technology are melts with brittle fracture behavior at the cutting temperature.

The process screening was performed by means of a design of experiments (DOE), varying screw speed, die plate temperature and the inlet pressure for the melt pump. Responses of the process state variables, such as motor load, die melt pressure and die melt temperature were collected, as well as product quality responses, i.e. API content, content uniformity, dissolution performance, shape and size of the pellets, and the degradation of API and HPMC. Moreover, the uniformity of the exit velocity of the extruded strands was an important response of the process. Eventually, the findings from the screening were used to define the nominal settings for the HME-pelletization line for preparing uniform pellets with immediate release (IR) of the API.

In the following section, a short review is given on HME and pelletization technologies, as well as the critical process parameters (CPPs) of each unit.

3.1.1. Technology and Process Parameters

Twin-Screw Extruders

The principle of HME is to melt and mix the input materials by shearing them in one or more rotating screws in a heated barrel. Thereby, the screws are divided into zones, which can be included or excluded as needed, depending on the requirements of the product: intake, melting, conveying, mixing, devolatilization and pressure build-up. At the screw end, the melt is forced though one or more dies by increased pressure. The extrusion die(s) can be round, flat, or in any other arbitrary shape, or it (they) can be directly connected to a mold, in the case of injection molding.

There is a large variety of extruder types available on the market, e.g. single-screw, co-rotating twin-screw and counter-rotating twin-screw extruders. A list of laboratory and production scale equipment for pharmaceutical application is given in Muehlenfeld and Thommes (2012) and Patil et al. (2016). In general, the co-rotating TSE is the preferred extrusion technology in pharmaceutical production, due to its excellent mixing characteristics in combination with a short residence time distribution (RTD) and good scalability (Maniruzzaman and Nokhodchi, 2017).

The twin screws of a co-rotating TSE are self-cleaning and they can be configured in a modular manner, allowing for a product-specific design. The screw design is composed by single elements with different functionality (Figure 3-1). The barrels of the extruder are typically divided into segments, which are temperature controlled and can be equipped with additional feeding or devolatilization ports.

In the plastics industry there is also a large variety of accessories available, in order to further adapt the HME-setup to material specific requirements: stuffing screws and side-feeders for feeding materials with very low bulk density into the extrusion screw, start-up valves which allow to divert material before the die and melt pumps in order to increase the processable melt pressure range. However, these accessories have not yet been established in pharmaceutical production.

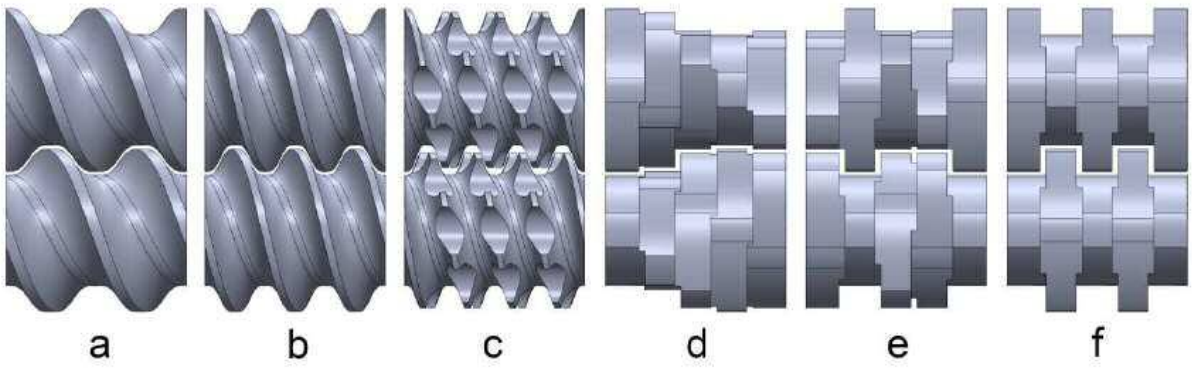

Figure 3-1. Common types of screw elements with different functionality: a and b are conveying elements with different pitch length, c is a mixing element and d to f are kneading elements with different staggering angle (30°, 60° and 90°). Taken with permission from (Eitzlmayr, 2015).

The CPPs of a HME process are well known (Schenk et al., 2011; Thiry et al., 2015) and given in Table 3-1. However, the criticality of each parameter needs to be assessed for every specific product by applying QbD principles, i.e. by establishing a knowledge space.

In general, the continuous nature and well-controlled RTD of HME technology is considered especially well-suited to adopt QbD principles and for the application of process analytical technology (PAT) (Maniruzzaman and Nokhodchi, 2017; Patil et al., 2016). Process monitoring applications were extensively reported (Markl et al., 2013; Saerens et al., 2014; Wahl et al., 2013), highlighting the suitability of this process for continuous pharmaceutical production.

Treffer et al. (2014) demonstrated an approach for inline monitoring of pellet size by installing an Eyecon™ camera after the pelletizer's outlet, supervising the pelletization process.

Die-Face Pelletization

The die-face pelletization processes cuts the hot strands emerging from the extrusion dies by a rotating knife head (Figure 3-2 A). At the moment of cutting, the melt is still soft, giving the pellet a rounded shape due to the surface tension and molecular relaxation processes (Figure 3-2 B) (Bialleck and Rein, 2011; Treffer et al., 2014). Subsequently, the pellets are carried out of the cutting chamber by the cooling air stream while solidifying rapidly (Figure 3-2 C).

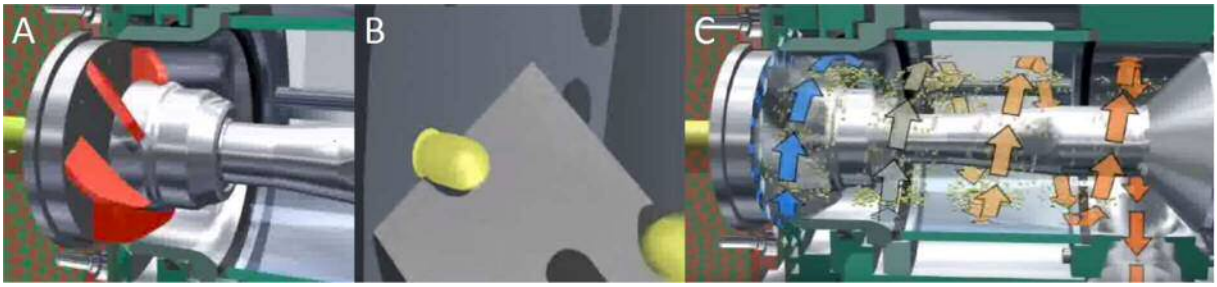

Figure 3-2. Die-face pelletizer Sphero® THA: exemplary configuration of a knife head (A), animation picture of a knife cutting the soft melt directly at the die (B) and cooling air, transporting the pellets from the cutting chamber (C). All pictures taken with permission from a YouTube video by *Maag Automatik (2015)*.

The pellet size is determined by the die diameter, the die length and the rotating speed of the knife head. The die diameter and length determine the final diameter of the strand. For short extrusion dies, the time in the die is not sufficient for the polymer molecules to relax and thus, die-swelling occurs. For longer dies, i.e. when the relaxation time of the molecules is shorter than the residence time in the die, no or less die swell occurs, depending on the viscoelasticity of the melt.

The smallest applicable die size is typically determined by the viscosity of the melt at extrusion temperature, since the pressure drop increases dramatically with decreasing die diameter and increasing die length. Thereby, high pressure drops may exceed the pressure specification limits of the equipment. However, micro-pellets were already generated by using sieve die systems instead of single dies, as demonstrated by Witschnigg and co-workers (Witschnigg et al., 2016).

Treffer has investigated thoroughly the conditions under which die-face pelletization is successful, i.e. pellets can be produced without any defects (Treffer, 2016). Especially sticking of the melt to the knives and smearing of polymers on the die-face (Figure 3-3) leads to pelletization failures, such as tailed pellets, pellet agglomerates, or the formation of pellet chains. In order to avoid sticking, the contact temperature between the pellets and the pelletizer knives must remain below a critical temperature, or more precisely the glass transition temperature for thermoplastic materials (Treffer and Khinast, 2017). The contact temperature depends on the initial temperatures, as well as the heat effusivity of the two bodies in contact. Thus, for a given material combination, i.e. pellets and knives, especially the initial temperatures need to be well controlled. The melt temperature is determined by the extrusion process and dissipation when forcing the material through the small dies. The temperature of the knives is governed by the rotational speed of the knife head, the air cooling system of the cutting chamber and the heat conduction into the knife running surface and knife head driving shaft (Treffer, 2016). The formation of a melt film on the running surface reduces the heat conductive heat flow from the knives. Melt films are formed by many pharmaceutical polymers due to a complex interplay of their rheology, the knife geometry, the contact pressure between the knives and the running surface and the temperature of the running surface (Mürb, 2015). The contribution of the heat conduction into the running surface to the cooling of the pelletizer knifes was significantly increased by Treffer through the development of a thermally decoupled die plate (Treffer, 2016). This thermally decoupled die plate has allowed to pelletize sticky polymers (Treffer, 2016) and to prepare micro-pellets from selected formulations containing API (Witschnigg et al., 2016).

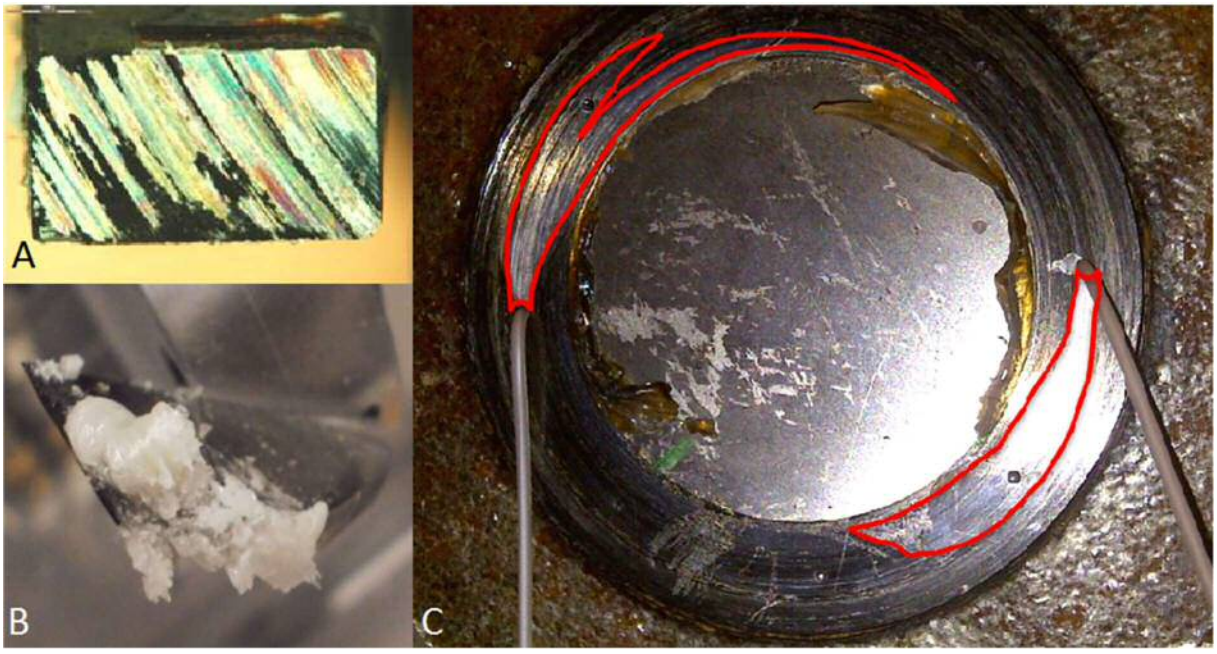

Figure 3-3. Critical aspects in die-face pelletization: A melt film on running face of pelletization knife (A) and a melt film on the running surface of the die plate (C), both decreasing the heat conduction from the knife into the cooled running surface, if covering the whole contact surfaces (both from Mürb (2015)*). Pellet agglomerates sticking to the pelletizer knife (B), as a results of insufficient cooling.*

An attempt to capture the potentially critical process parameters of a die-face pelletization process is made in Table 3-1.

Table 3-1. A list of potential CPPs for the HME, the strand pelletization and the die-face pelletization process.

Process step	Potential CPPs
Hot-melt extrusion	Throughput
	Screw speed
	Specific mechanical energy consumption (SMEC), or motor load
	Barrel temperature profile
	Screw configuration
Die-face pelletization	Throughput per die
	Die diameter and length
	Rotational speed of the pelletizer knife head
	Number of knives on knife head
	Contact pressure between knife head and knife running surface
	Cooling air flow and velocity (i.e. inlet gap size)
Strand pelletization	Strand diameter
	Stand cooling length and method (e.g. ambient cooling, cooling channel)
	Strand intake speed relative to exit velocity of strands
	Pellet length setting, i.e. strand cutting frequency

Strand Pelletization

In contrast to die-face pelletization, strand pelletization cuts the cooled strands after a certain distance from the die, yielding cylindrical pellets. The pellet diameter, that is the strand diameter, is a function of die geometry, as introduced above. A possibility to reduce the strand diameter is to pull the strands faster into the pelletizer than they emerge from the die. This results in an extension and thinning of the strand. The length of the cylindrical pellets is given by the cutting frequency and the intake speed of the pelletizer. The configuration of a strand pelletizer is shown in Figure 3-4.

The lower number of potential CPPs shown in Table 3-1 indicates already, the simplicity of the strand pelletization process compared to die-face pelletization.

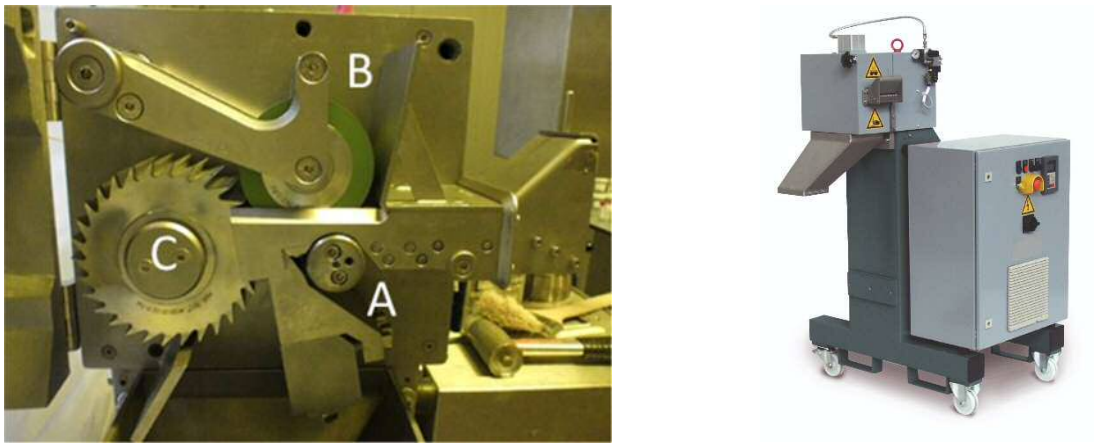

Figure 3-4. Left: Configuration of a strand pelletizer with a grooved intake roll (A), a rubber wheel pressing the strands down onto the intake wheel (B) and the knife roll (C). Right: Strand pelletizer Primo® E by Maag Automatik (Germany).

3.2. Materials and Methods

3.2.1. Materials

Nimodipine (NMD) was received from Bayer AG (Germany), Methocel™ E5 (HPMC) and both grades of Eudragit®, EPO as well as E100 (EE), were purchased from Dow Chemicals (USA), and Evonik (Germany) respectively. The formulation composition range providing IR from HME pellets has been determined in Chapter 2. A NMD content of 10 wt.% was used in all runs of this study, but the carrier composition was slightly varied during the process setup runs. During the process parameter screening a fixed formulation composition with 54 wt.% of HPMC and 36 wt.% of EE was used. Since NMD is light-sensitive, all processing and analysis was performed under yellow light and were samples stored light protected.

3.2.2. Pellet Characterization Methods

API Content and Content Uniformity

Pellet API content and content uniformity were determined by means of HPLC analysis (1260 Infinity II LC System, Agilent with a Purospher® STAR RP-18 encapped (5 µm) Hibar® 125-4 column, Merck KGaA). 100 mg of pellets (n=10) were extracted in methanol (MeOH) and filtered (MCE filter, 0.22 µm) prior to analysis. The mobile phase consisted of 20% MeOH, 20% tetrahydrofuran (THF) and 60% purified water. All chemicals were used in analytical grade. The flow was set to 2 mL/min and the injection volume was 20 µL. The column temperature was 40°C and pressure approximately 320 bar. The UV wavelength in the detector was set to 235 nm.

API and HPMC Degradation

The investigation of API degradation was performed by analyzing the peak of impurity A in the HPLC chromatograms according to the monograph in the Ph.Eur. 8.0 (Council of Europe, 2014a). Therefore, samples from the experiments with the highest and the lowest stress conditions in the process screening DoE were used. HPLC analysis was performed as described above for API content analysis.

HPMC degradation by browning was evaluated via colorimetric analysis. Therefore, a picture of the pellets was taken and the redness of the samples compared to each other by means of the a*-value in L*a*b*-color space. The average a*-value of each selected picture region was determined in Matlab (Matlab 2014b, MathWorks®, USA) using the function “imread”.

In-Vitro Dissolution Testing

Dissolution was performed in sink conditions at 37 ± 0.5°C using an USP apparatus I (DT820LH Dissolution Tester, Erweka, Germany). The dissolution vessels were filled with 500 mL of dissolution medium, a sodium acetate buffer with pH 4.5 ± 0.1 and 0.3% of sodium lauryl sulfate (SLS). The medium has been selected based on the specification for testing NMD tablets in the British Pharmacopoeia (British Pharmacopoeia, 2009). Dissolution tests were performed in triplicates (n=3)

using 100 mg of pellet in each dissolution vessel. Samples of 1.5 mL were collected automatically at 0, 5, 15, 30, 45, 60 and 90 min and filtered through 0.10 µm poroplast filters. The API concentration dissolved in the dissolution medium over time was determined via UV/Vis spectroscopy (Lambda 950, PerkinElmer, USA). Absorbance measurements were carried out in 10 mm polymethyl methacrylate (PMMA) semi-micro cuvettes at 360 nm. Each sample was measured against the fresh dissolution medium from the same vessel. The dissolution profiles were normalized for comparison, using the API content determined in the HPLC analysis and the pellet mass in each vessel.

Particle Size and Shape Measurement

Pellet geometries were determined using the dynamic image particle analyzer PartAn^{3D} (Microtrac, USA). A detailed description of the functionality of the particle sizer is given in Chapter 4. The median D_{50} of the projection area equivalent diameter $D_A = \sqrt{4 \cdot A_P/\pi}$ distribution was used as measure for pellet size. The span (Eq. 3-1) was used as a parameter for the particle size distribution (PSD) width.

$$span\ [mm] = D_{90} - D_{10} \qquad \textit{Eq. 3-1}$$

The values D_{10} and D_{90} represent the 10%- and 90%-quantile of the D_A distribution. Mean sphericity of total volume ($\psi = D_A/D_P$, with D_P the projection perimeter equivalent diameter) was used as pellet shape parameter.

The pellet samples for size and shape analysis were taken over a period of 20 seconds during steady-state operation at each DoE setting, that is at 0, 10, 20 and 30 min of run time.

3.2.3. Process Equipment and Data Collection

In total, three different loss-in-weight (LIW) powder feeders, a side feeder, an extruder, a melt pump and two types of pelletizers were used. The used feeders were of two different scales: a micro-feeder (MT-S Hyg, Brabender Technologie, Germany) and two lab-scale feeders (K-PH-CL-SFS-KT20 and K-CL-KT20, Coperion-KTron, Switzerland). The extruder was a pilot-scale co-rotating TSE (ZSK 18 MI with L/D = 40, Coperion, Switzerland) with ten heated barrels. The side feeder ZS-B (Coperion, Switzerland) was mounted in barrel 2 for one set of the setup testing experiments. The melt pump Extrex® and both pelletizers, the die-face pelletizer Sphero® THA and the strand pelletizer Primo 60E® were all from the same manufacturer (Maag-Automatik Plastics Machinery, Germany). In all runs, a die plate with eight dies was mounted at the end of the extrusion line.

Several pressure and temperature sensors were included in the process equipment, at the end of the extruder, before the melt pump and in the connection part holding the die plate. The process data was collected by SIMATIC SIPAT V4.0 (Siemens, Germany) at a frequency of 1 Hz. The die melt temperature sensor was not integrated into SIPAT during the screening experiments and the data was logged manually every 10 min.

Data that were available in SIPAT, such as actual feed rates from the LIW feeders, screw speed, motor load, and die melt pressure, were later exported and further processed in Matlab (Matlab 2014b, MathWorks®, USA). Statistical analysis was performed for selected responses using MODDE 11 (Umetrics, Sweden). Partial least squares (PLS) models were fit for each response and fine-tuned by manual exclusion of insignificant factors and the auto-tune function of the software.

The exit velocity distribution of the strands could not be measured directly as a process response. Thus, the number of strands at similar velocity was manually noted and indicated as the "number of stable strands". Those strands were pulled into the strand pelletizer for the production of pellets.

RTD Characterization

In addition, the RTD of the extrusion process was characterized during the process parameter screening by means of tracer experiments. Approximately 35 mg of Fe_2O_3 (Sigma Aldrich) were used as tracer material. The mass was accurately weighed and filled in a manually shortened HPMC capsule (Coni-snap®, size 0, Capsugel). Pouring the tracer directly into the intake funnel, e.g. using a spoon, the actual amount of tracer entering the extrusion screw was never accurately known, due to adhesion of small tracer particles to inlet walls. Using the capsule, the tracer stayed entrapped during free-fall until it was broken up in the intake zone of the extruder, giving an ideal tracer impulse.

The tracer signal in the melt was detected by a near-infrared (NIR) probe mounted in the connection part holding the die plate at the end of the extrusion line. Spectra were collected in reflectance mode by the process spectrometer SentroPAT FO (Sentronic, Germany) via a fibre-optic probe (DR-NIR Dynisco, Germany). An integration time of 9 ms was used for each collected spectrum and 60 spectra were averaged. The spectra containing the signals from the tracer material were extracted to perform a principal component analysis (PCA). The spectral wavelengths between 1150 to 1982 nm were used for determining the first three principal components. The curve of the first principal component (PC1) over time was directly used as the tracer signal indicating the RTD.

3.2.4. Experimental Schedule for Process Screening

A full-factorial design was applied in the process parameter screening with three two-level factors and a triplicate center point. The factors and factor levels are given in Table 3-2, the settings from all runs and the run order in Table 3-3. All screening experiments were performed at the desired nominal throughput of 4 kg/h, using the barrel temperature profile fixed during the process setup experiments. The optimal screw configuration was determined as well in the setup stage.

Table 3-2. Screening DoE with full factorial design.

	Low level (-)	Mid level (0)	High level (+)
Screw speed [rpm]	120	200	280
Melt pump pressure [bar]	50	60	70
Die plate temperature [°C]	120	130	140

With regard to the pelletization parameters, the distance between the extrusion dies and the strand pelletizer inlet was fixed to 1400 mm. This was the length available for the strands to cool down at ambient conditions. The cutting frequency of the pelletizer was adjusted automatically by the pelletizer when selecting a desired pellet length. Pellet length was set to the shortest possible value of 0.5 mm. The intake velocity was manually adjusted during the experiments to fit the largest number of strands emerging from the extrusion dies at a similar velocity (see “number of stable strands” explained above in section 3.2.3).

Table 3-3. Screening DoE run schedule with factor settings and run order. Bold rows represent replicate runs.

Exp Name	Run Order	Screw speed	Melt pump pressure	Die plate temperature
N2	1	120	70	120
N3	**7**	**200**	**60**	**130**
N4	8	120	70	140
N5	11	280	70	120
N6	3	120	50	140
N7	**10**	**200**	**60**	**130**
N8	6	120	50	120
N9	**9**	**200**	**60**	**130**
N12	2	280	50	140
N13	4	280	50	120
N14	5	280	70	140

3.3. Results

The first part of the results section is a summary of the main findings from the setup experiments and illustrates the decision-making process on the pelletization technology. The second section details on the findings from the process parameter screening and the definition of the nominal process settings.

3.3.1. Process Setup Experiments

Several aspects are especially relevant for setting up an HME process line: i) the feeding strategy, ii) the screw and barrel configuration, i.e. the temperature profile and use of special barrel types, and iii) the die plate configuration. Initially, all experiments were performed in combination with the die-face pelletizer. Later the strand pelletizer was tested in order to make a decision on the feasible pelletization technology.

Feeding Strategy

Initial process setup experiments were performed at a throughput levels of 1.5 to 2 kg/h to save material during this phase. The aim was to eventually increase the throughput to a level of 4 kg/h. Two KT20 feeders were used to feed premixes, while testing different formulation compositions. Both feeders were mounted above the inlet to the first barrel of the extruder. Thereby, the maximum intake capacity of the extrusion screw was reached when the flow rate of the low-density EE powder reached approximately 0.5 kg/h. At this point, a backlog of material was formed, which started to soften due to the increased temperature and humidity in this zone. Consequently, a different strategy was tested by mounting a side feeder at the second barrel, for pre-compressing and feeding the EE powder containing premix through this port. However, also the twin-screws of the side feeder did not provide a consistent mass flow into the extruder, due to the softening of EE before the side-feeder outlet. This resulted in high HPMC fractions in the melt, followed by a process shut-down due to pressure overload and subsequently, by severe HPMC degradation, e.g. in the distributor channel before the die plate, as shown in Figure 3-5 (left hand side).

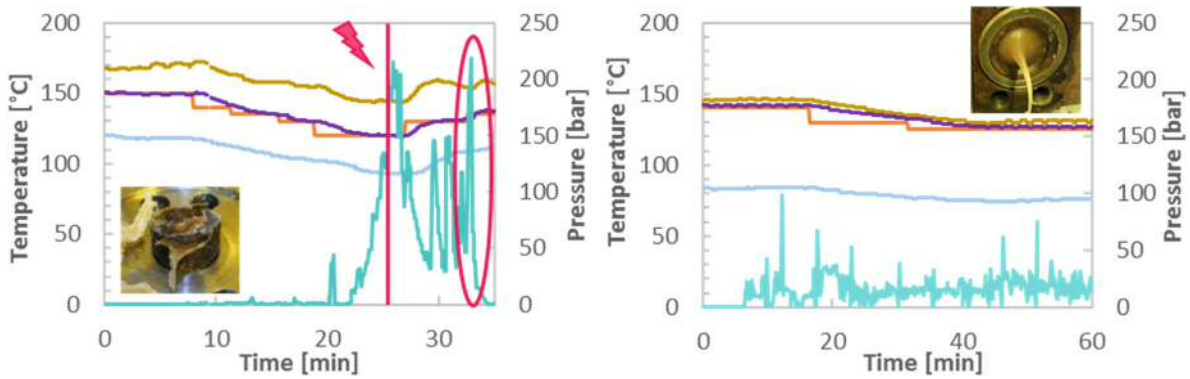

Figure 3-5. Process parameters collected from runs with the initial (left) and the optimized process setup (right). The circled area in the left graph highlights a process shut-down due to pressure overload after intake problems of EE powder. Small images show melt with degraded and non-degraded HPMC. (Line colors: brown…melt temperature, orange…set die plate temperature, purple…actual die plate temperature, light blue…running surface temperature and turquoise…die melt pressure)

The degraded melt had to be removed mechanically from the extruder, since it did not flow anymore even at high pressures and increased temperature.

Ultimately, EE pellets were tested instead of the EE powder grade. The use of pellets did not allow to prepare a premix with the other components anymore but increased the feeding consistency and the mass flow that could be taken in by the extruder significantly. Finally, a split feeding strategy was applied, feeding all components by separate feeders. All material streams were merged into a funnel on the inlet at the first barrel. The feeder types and setup were chosen according to the fraction of each component in the formulation. NMD was fed by the small-scale feeder MT-S Hyg, using coarse concave screws, and the polymers by the pilot-scale KT20 feeders with pellet screws for EE pellet feeding and fine concave screws for feeding of the HPMC powder.

Screw and Barrel Configuration

The initially used screw configuration and temperature profile are shown in Figure 3-6 A. All setup experiments were performed at a screw speed of 200 rpm. The first block of kneading elements in the screw configuration was used to thoroughly melt the raw materials, while the second block of kneading elements was used to provide intensive mixing. The temperature profile up to 160°C was chosen, in order to soften the HPMC, which has a glass transition point of 146.4°C (see section 2.3.1).

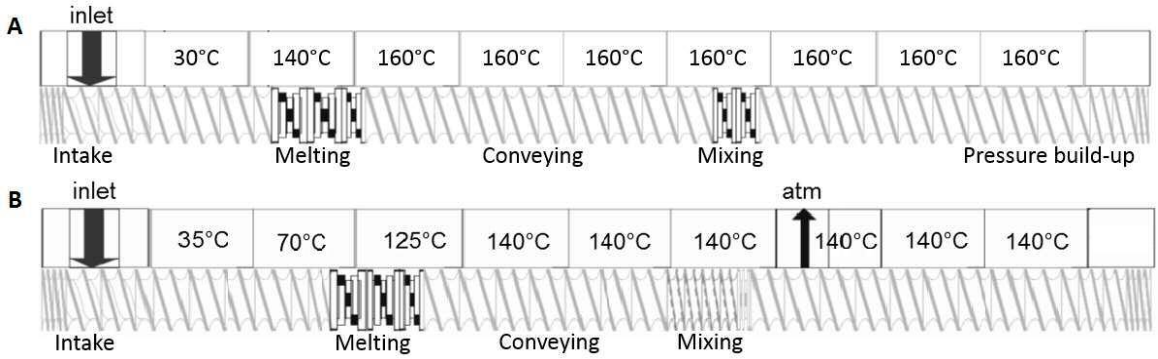

Figure 3-6. Initial screw configuration (A) with intake zone, a melting and a mixing zone equipped with kneading elements (30° staggering angle) and a temperature profile up to 160°C barrel temperature. Final screw configuration (B) with longer intake zone, a low-shear mixing zone with toothed mixing elements and a narrow kneading element with 90° staggering angle, a devolatilization zone with atmospheric pressure and a temperature profile only up to 140°C.

Extrusions using this first setup yielded extrudates showing different degrees of browning. This was an indication of HPMC degradation, either caused by shear stress or by thermal stress in the process. Consequently, the screw design was changed towards less mechanical energy input. The kneading elements in the mixing zone of the screw configuration were replaced by toothed mixing elements and a narrow kneading block (Figure 3-6 B). The temperature profile was lowered to reduce the input of thermal energy into the melt. The temperature profile with a maximal temperature of 140°C, did not provoke HPMC degradation anymore, even during process interruptions, where the melt remained in the process for longer time periods.

The risk of softening EE in the intake zone was mitigated by elongating this zone and heating it with a slower incline in barrel temperature. At the same time, complete melting of the API was ensured in the melting zone, by setting the barrel temperature above the melting temperature of the API (T_m=116°C). Finally, a devolatilization port was added in the eighth barrel in order to remove any moisture from the raw materials before the strand formation.

Die Plate Configuration

The thermally decoupled die plate used in the experiments was equipped with eight copper dies. Dies with different diameter and cylindrical length could be mounted in this die plate, in order to meet the different requirements. One requirement was to produce pellets in the desired size range and with a narrow size distribution. The desired size range of 0.6 to 1.0 mm was given, according to the specification to produce tablets with a diameter of 6 to 10 mm (Table 1-1 given in section 1.5.1). A rule of thumb says that the particle size should be below 1/10 of the tableting die diameter, in order to achieve consistent filling during tableting. The PSD was considered narrow, when the ratio of the 10%-quantile to the 90% quantile of the distribution was below 1.5 (Merkus, 2009), or when a low absolute difference , i.e. a span (acc. to Eq. 3-1) below 0.4 mm, was obtained.

The second requirement was to achieve a stable process with well-controlled die pressure levels. Since there had been high melt pressure levels observed already at low throughput and there had been a process emergency shut-down provoked by pressure overload due to a formulation composition deviation, a melt pump was used to increase process stability. The melt pump could achieve melt pressure levels up to 250 bar, whereas the extruder could provide only up to 100 bar without an emergency shut-down. The melt pump consists of two gear wheels pumping the melt from one side to the other. The speed of these wheels is controlled by the specified melt pressure levels at the pump inlet side. Moreover, the pump was temperature controlled and set to 140°C, according to the observations during optimization of the temperature profile of the extruder barrels.

Since the pressure drop across the die plate and the achievable pellet size also depends on the used pelletization technology, the discussion of the best die plate configuration and temperature settings is given in the next section.

Die-Face Pelletization Runs

The goal of the pelletization setup was to generate uniform pellets with desired size in a long-term stable process. In order to achieve the desired particle size range of 0.6 to 1.0 mm, dies with a diameter of 0.8 mm and 1 mm cylindrical length were initially used. The pelletizer knife head was equipped with six knives, mounted at an angle of 45° on the knife head. Thereby, pellet chains (Figure 3-8) were formed. This was attributed to the formation of a melt film, after inspecting the running surface and the knives (Figure 3-7 A and B). Additionally, melt pressure was strongly fluctuating, caused by the

freezing of single die. Adaptations in contact pressure, die plate temperature and cooling air flow did not improve the performance sufficiently. Applying higher contact pressures, in order to remove the melt film, actually resulted in increasing melt film thickness. This was finally attributed to the bending of the knives upon higher contact pressures, causing the knife tips to lift off the running surface.

Thus, a knife head design with knives mounted at an angle of 90° was subsequently tested, allowing to maintain tight contact of the knife tips also at increased contact pressure. In order to stabilize the melt pressure, dies with 1 mm in diameter and a cylindrical length of 0.5 mm were used.

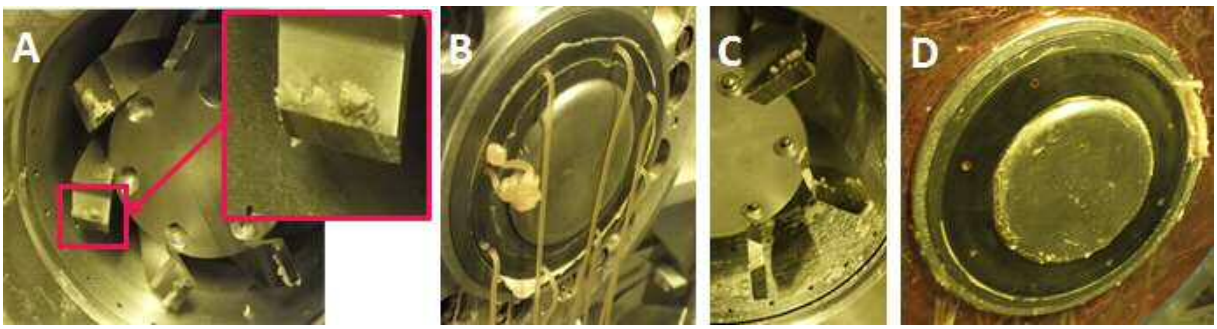

Figure 3-7. Pelletizer knife head with 45° angled knives (A) resulting in a thick melt film on the running surface (B) and knife head with 90° angled knives (C) yielding reduced melt film thickness on running surface (D).

These adaptations allowed to significantly reduce melt film thickness (Figure 3-7 C and D) and the formation of pellet chains in the product. It was possible to produce pellets with a minimum of pellet chains at a die plate temperature of 130°C and intensified knife cooling by pressing a copper ring between the knife running surface and the water-cooled pelletizer housing. However, the pellets exhibited tails (Figure 3-8 B) and the process was very sensitive to minor deviations in formulation composition and difficult to handle during start-up (145°C die plate temperature needed). Moreover, the melt film did not rip off between the die holes but was merely displaced to the outer diameter of the knife head, forming melt agglomerates there. Thus, it was concluded, that a long-term stable process window cannot be found for die-face pelletizing this formulation. Consequently, strand pelletization was tested.

Figure 3-8. Two types of pelletization problems in die-face pelletization: Pellet chains (A) and tailed and irregularly shaped pellets (B). Cylindrical pellets from strand pelletization (C).

Strand Pelletization Runs

The process data from the strand pelletization setup runs are shown in Figure 3-9. Extrusion dies with 0.8 mm diameter were used in this run and different die temperatures were tested. In preparation for the process screening DoE, also different screw speeds were set, that is initially 120 rpm and later 500 rpm (after 11:30 am).

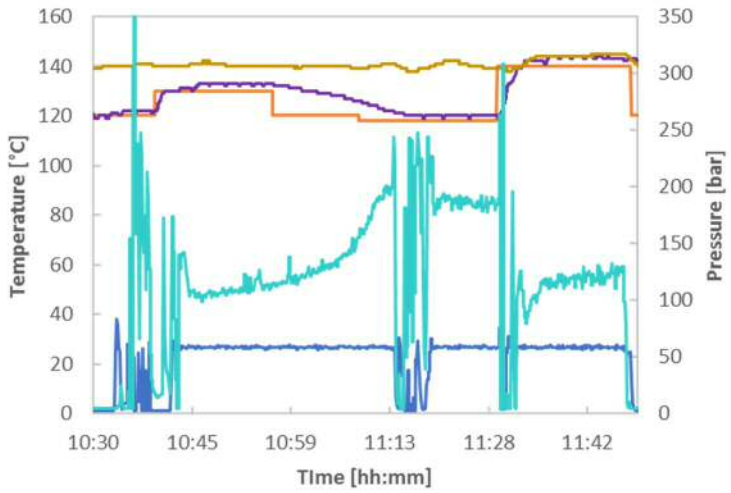

Figure 3-9. Process data collected during strand pelletization runs with a die diameter of 0.8 mm and different die plate temperatures and extruder screw speeds. (Line colors: brown…melt temperature, orange…set die plate temperature, purple…actual die plate temperature, blue…melt pump inlet pressure and turquoise…die melt pressure)

Several findings regarding process stability were obtained during this process setup run:

i. Starting the process at a die plate temperature of 120°C was not possible, due to extremely high melt pressure drops across the extrusion dies. An increase of the die temperature to 130°C allowed to start the process without any problems (shortly after 10:40 am).

ii. At 130°C die plate temperature it was only possible to pelletize five out of eight strands. Three dies showed irregular strand velocities, which did not allow to pull the strands into the pelletizer at the same intake velocity.

iii. Lowering the die plate temperature to 120°C resulted in elevated melt pressure levels. Thereby, the maximal acceptable melt pressure level of 250 bar was closely approached. An attempt to receive more uniform strand velocities by locally cooling and heating single dies provoked a process shut-down (shortly after 11:13 am). However, it was possible to restart the process and achieve a stable process, pelletizing five strands.

iv. Around 11.30 am the extrusion screw speed was increased to 500 rpm (screw speed not shown in Figure 3-9) and the die plate temperature was elevated to 140°C. At this set point, the number of strands with uniform velocity increased to six.

Ultimately, the cooling length, i.e. the machine distance between extrusion dies and the pelletizer intake, was reduced in order to test the process boundaries. A reduction from 1400 mm cooling length to 830 mm provoked the strands started to stick to each other in the intake section of the pelletizer, resulting in pelletization failures.

Subsequently, experiments with 1 mm die diameter were performed, based on the challenges during process start-up and the high pressure levels at 120°C die plate temperature. This successfully lowered the melt pressure level and stabilized the melt flow through the dies. Thus, this die diameter was used in all further experiments, that is in the process screening. Pellets produced with these dies at an extrusion screw speed of 200 rpm and a die plate temperature of 146°C are shown in Figure 3-8.

Pelletization Technology Decision

The decision on the feasible pelletization technology was performed by comparing the two technologies in several categories relevant for the final product performance, the process stability and safety aspects in pharmaceutical processing (Table 3-4).

Table 3-4. Comparison of the pelletization technologies with regard to formulation, product and process aspects.

	Die-face pelletizing	**Strand pelletizing**
Formulation / product aspects		
Possible pellet size / shape / morphology	0.8 - 1 mm / round / amorphous	(0.5) – 1 mm /cylindrical / amorphous
Mechanical properties of strand	Not sensitive	Sensitive (brittleness – not relevant)
Properties of melt	Sensitive to tackiness	Sensitive to very low viscosity (not relevant)
Process aspects		
Process window size	narrow (limited by die plate temp., contact pressure, air cooling)	robust (limited by very high melt temperature – not relevant)
Closed containment of intermediates	✓	✗ (possible, but not necessary in this project)
Start-up complexity / Cleaning	high complexity / high effort	less complexity / less effort

A comparison of the achievable pellet sizes was relevant, since they were critical for the downstream processing of the intermediate product. In this regard, strand pelletization offers the potential to decrease the pellet size by elongating and thinning the strand when drawing it into the pelletizer at higher speed, than the speed with which the strands are emerging from the extrusion die. However, the cylindrical shape of the pellet constitutes a disadvantage for uniform filling of tableting matrices and may also decrease the compactability of the intermediate.

The sensitivity of the strand pelletization process to the brittle cutting behavior of the strand and low melt viscosities were not critical for the used formulation, since it was originally optimized for this pelletization method by adding HPMC to the formulation (see Chapter 2). In contrast, the thermal properties of the melt did pose a challenge for die-face pelletization. The low mixture T_g around 30°C of the NMD-EE rich phase of the formulation, which was identified in the study in Chapter 2, did not allow to avoid, or rip off the melt film between the dies. Thus, the melt film was smeared along the whole knife running surface, resulting in pelletization failures such as pellet chain formation and tailing.

Die melt pressure was the most critical process parameter, determining the process window for a stable process. In the runs with the die-face pelletizer this parameter was highly sensitive to die plate temperature, contact pressure of the knife head and the settings for the cooling system (inlet gap width, air flow rate). It was basically not possible to obtain a stable process while producing pellets with desired properties. Decreasing the die plate temperature in order to improve the pelletization, led to the “freezing” of single die holes and melt pressure fluctuations or overload. The freezing of dies was caused by the high T_g of the HPMC rich phase in the given formulation. For strand pelletization, the die melt pressure was influenced by die temperature as well, but not with the same severity.

Finally, aspects especially relevant when producing pharmaceutical products were considered as well. That is the possibility to maintain all material in a closed system on one hand, and on the other hand, the complexity of process start-up and equipment cleaning. In this work, strand pelletization was not carried out in a closed containment. However, this could be changed if necessary, e.g. by using a closed cooling channel for the distance between the extrusion dies and the pelletizer intake. Concerning the complexity of process start-up and cleaning, strand pelletization is also preferable over die-face pelletization.

Concluding, strand pelletization was clearly found to be the preferable pelletization technology for this specific application.

3.3.2. Process Parameter Screening

Based on the findings from the setup experiments, a melt pump temperature of 140°C, and a die plate configuration with eight copper dies with 1 mm diameter and 0.5 mm cylindrical length were used in the screening. Moreover, a formulation composition of 10 wt.% NMD, 54 wt.% HPMC and 36 wt.% of EE was found to result in the desired processability performance during setup experiments.

The experiments were performed partially by changing dynamically from one DoE set point to the other and partially by starting up the cleaned extruder. After reaching steady state in all process parameters, the process was operated for 30 min at the respective set point for collecting process data for statistical evaluation. During this time, pellets were sampled as well for the later analysis of product quality attributes. After the 30 min, the tracer RTD experiments were performed, by adding the tracer capsule in the feeding port of the extruder. The experiment ended when no tracer color was visible in the extruded strands anymore.

Process Parameter Responses

The process parameter responses from all DoE runs are shown in Table 3-5. Motor load did not exhibit a strong variation across the different DoE runs, varying only between 41.1. and 45.7%. Thus, only a limited effect of the back-pressure length of the melt before the melt pump on mechanical energy input was observed. The other parameters, average die melt pressure and melt pressure standard deviation (SD), die melt temperature and the number of stable strands in contrast did show more sensitivity to the tested factors.

Table 3-5. Process responses from screening DoE. Bold rows represent replicate runs.

Exp	Motor load [%]	Die melt pressure [bar]	Die melt pressure SD [bar]	Die melt temperature* [°C]	# of stable strands [-]
N2	45.7	147.3	9.92	133.7	6
N3	**44.3**	**140.9**	**5.30**	**140.3**	**8**
N4	45.1	77.5	5.31	140.8	5
N5	45.9	(152*)	-	141.8	5
N6	42.5	84.2	4.15	143	8
N7	**44.2**	**109.4 (110.5*)**	**4.72**	**142**	**5-6**
N8	42.8	122.5	8.02	136.8	8
N9	**45.1**	**147.5**	**7.16**	**141**	**8**
N12	41.1	122.8	7.73	147	7
N13	42.5	198.8	8.89	140	7-8
N14	44.9	113.6	4.54	149.3	8

* manually logged data (n=4) was used for cases where no data was available from SIPAT.

By investigating the data from the replicate runs, significant variation was observed in the die melt pressure level. The die melt pressure in run N7 was significantly reduced compared to the runs N3 and N9. At the same time, the number of stable strands, i.e. number of strands leaving the extrusion dies at similar velocity, was reduced. The same effect was observed for the runs N13 and N5, which were

both executed at 280 rpm screw speed and a die plate temperature of 120°C (run order and settings are given in Table 3-3). After careful consideration, both observations were related to wear of the dies due to the cleaning procedure. The different solubility of the formulation components in available cleaning agents made some mechanical cleaning of the dies necessary. Thereby, the diameter and surface of single dies was changed, resulting in a slightly different effect on flow resistance of each single die.

Product Quality Attribute Responses

API content and content uniformity of pellets produced in all DoE runs was determined in order to assess, if the combination of the selected feeding system and the HME screw configuration were appropriate to produce pellets with uniform content. All samples were passing the content uniformity test according to the acceptance value AV (the data is given in Table B-1 in the Supplemental Material section B), as defined in the European Pharmacopoeia (Council of Europe, 2014b). Therefore, the feeding system did provide a sufficiently accurate composition of the inlet material stream to the extruder and existing fluctuations could be dampened by the used screw configuration.

Moreover, API degradation was assessed by comparing the chromatograms of a pellet sample from run N2, with lowest stress conditions, to a sample from run 14, with highest stress conditions (both chromatograms shown in Figure B-1 in the Supplemental Material section B). In both cases it was not possible to detect any impurity, indicating that the API was stable at the tested process conditions.

Investigation on HPMC degradation

Since degradation of HPMC has been found to increase the risk of process interruptions during the process setup experiments, the investigation of its cause depicts an important aspect in the process screening. The investigation on HPMC degradation was performed based on the color change of the pellets at different process settings. Figure 3-10 shows a picture from all pellet samples and the cut picture regions which were used for colorimetric analysis. The differences in the a*-value (redness) of all pellets compared to the pellet with the lowest redness (N6) is given in Table 3-6 and Figure B-2 in the Supplemental Material section B.

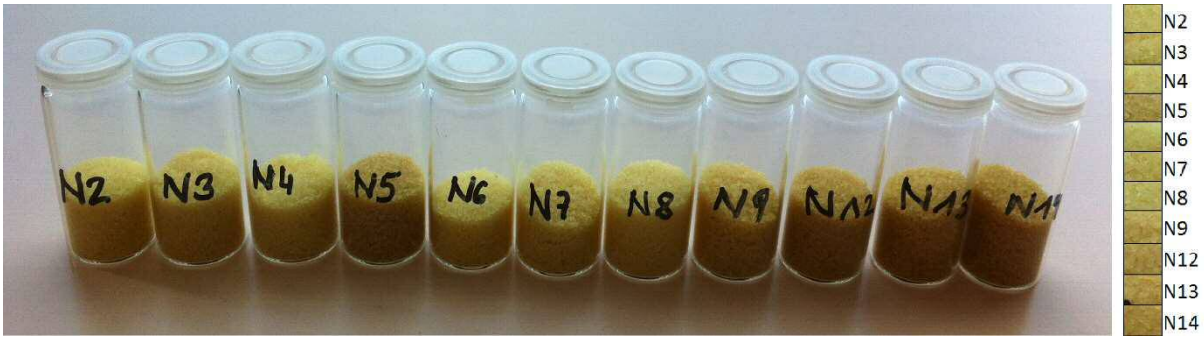

Figure 3-10. Pellets from all screening DoE runs, with different levels of HPMC browning for pellets produced at different screw speeds. Right: picture regions used for colorimetric analysis.

The reason for the color change in HPMC was investigated by researching on a correlation between die melt temperature and screw speed with the intensity of browning. The aim was to understand if thermal stress or shear stress were the main origin of the decomposition. Melt temperature did not show a consistent correlation with the browning of pellets. However, as it was significantly influenced by the set die plate temperature the measured temperature probably did not represent the actual bulk volume temperature in the flow channel. However, a clear correlation of HPMC browning with the set screw speed was observed. When investigating the RTDs of the HME line (Figure 3-11), screw speed is further supported as the main influential factor on HPMC decomposition. While the DoE runs with the lowest screw speed exhibited the longest residence times of the material in the heated environment of the extruder, this did not cause browning of the samples. In contrast, the sample N12 with a short and narrow RTD did clearly show a brown color. The possible relevance of other factors in the DoE on HPMC degradation will be discussed in the statistical analysis section.

Another relevant observation from the tracer experiments was, that the runs with higher screw speed exhibited more irregular RTD shape. This indicated that flow instabilities occurred, potentially caused by the decomposition of HPMC. In any case, the RTD was mainly determined by screw speed and no effect of different melt pump inlet pressure levels was observed.

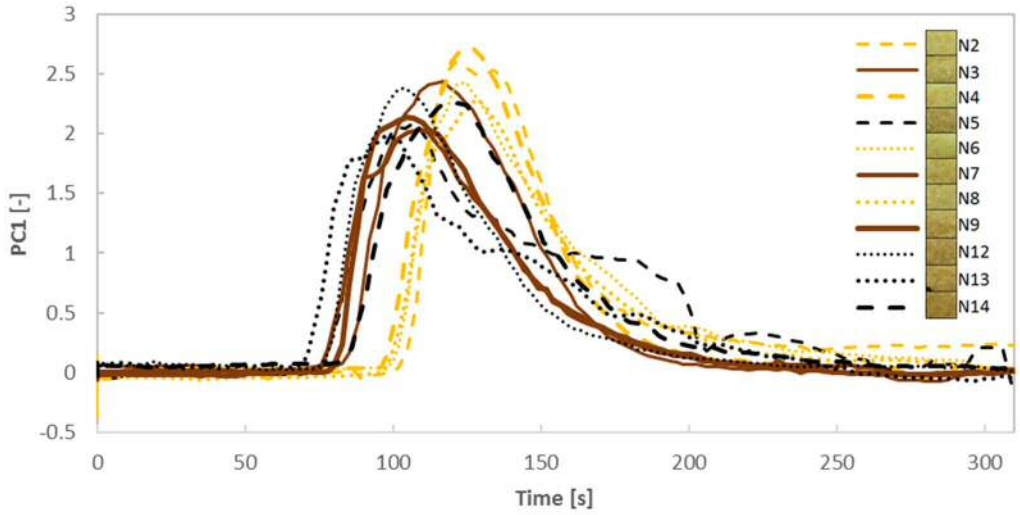

Figure 3-11. Tracer RTDs of the process screening experiments. Dotted lines represent runs at low melt pump pressure, dashed lines high melt pump pressure and solid lines the replicated center point settings. Yellow line color represents runs at low screw speed, black at high screw speed and brown again the center point settings.

Pellet API Dissolution

Besides the investigation of the DoE factor effects on API dissolution, it was also important to understand whether the degradation of HPMC affected the API dissolution from the pellets. The dissolution profiles from the pellet samples are shown in Figure 3-12. It can be observed, that there was some variation between the profiles, especially in the plateau value that was reached after full pellet dissolution. However, all pellets reached immediate release (85% in 30 min). Thus, it can be concluded, that neither the process parameters, nor the degradation of HPMC had a critical influence on API dissolution from the final pellets. Therefore, this response was not included in further statistical analysis of the DoE data.

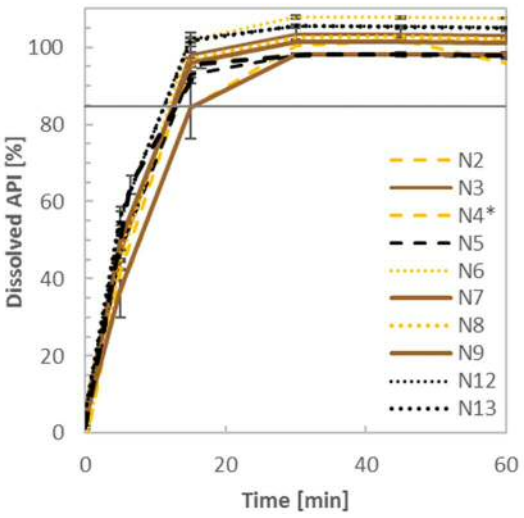

Figure 3-12. Average dissolution profiles from pellets for all DoE runs (n=3). (for N4: n=1)*

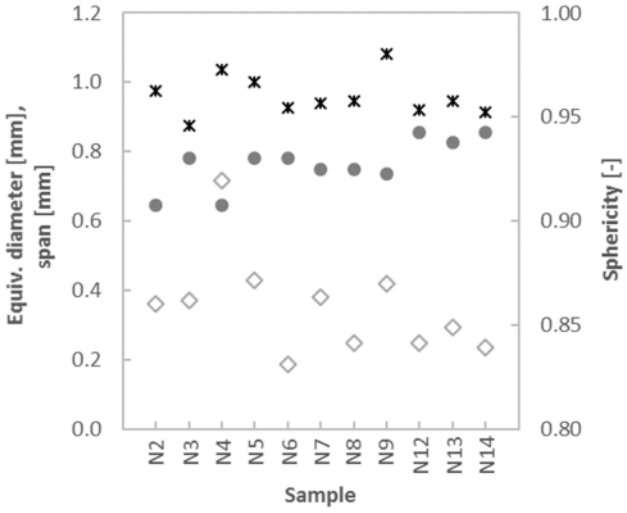

Figure 3-13. Average pellet equiv. diameter (D_{50} - black stars), PSD width (span- grey diamonds) and pellet shape data (sphericity- grey circles) for all DoE runs (n=4).

Pellet Size and Shape

The effects of process parameters on pellet size, size distribution and shape were investigated and all response data is shown in Figure 3-13. Pellet size was in the range of 0.88 to 1.08 mm for all DoE runs. The majority of samples had a PSD span in the range of 0.19 to 0.43 mm, indicating a narrow (below 0.4 mm), or medium PSD distribution. In contrast, sample N4 was a clear outlier, with a span of 0.72 mm. Since there had been only five stable strands available for pelletization at this run, this deviation was considered a consequence of a poor pelletization conditions. A process interruption occurred directly before this run, which may have affected the melt flow in the extrusion dies.

Whether there was a significant correlation between the tested factors and pellet size and PSD, will be assessed in statistical analysis. Sphericity however, indicated a second run, run N2, to be an outlier as well, since this sample exhibited the same lower sphericity as N4, compared to the other runs. All product quality responses used for statistical analysis were summarized in Table 3-6.

Table 3-6. Product responses from screening DoE. Bold rows represent replicate runs.

Exp.	D50 [mm]	Span [mm]	Sphericity [-]	Color change [-]	Die age [-]
N2	0.98	0.36	0.91	1.31	3
N3	**0.88**	**0.37**	**0.93**	**3.26**	**2**
N4	1.04	0.72	0.91	0.35	2
N5	1.00	0.43	0.93	6.68	3
N6	0.93	0.19	0.93	Ref	0
N7	**0.94**	**0.38**	**0.93**	**3.23**	**3**
N8	0.95	0.25	0.93	1.77	1
N9	**1.08**	**0.42**	**0.92**	**6.98**	**2**
N12	0.92	0.25	0.94	9.69	0
N13	0.95	0.30	0.94	9.91	1
N14	0.91	0.24	0.94	11.79	1

Statistical Analysis

Statistical analysis was used to investigate the significance of factor effects on selected, relevant process and product responses. The investigated process responses were motor load, die melt pressure and die melt pressure variability, as well as the number of stable strands. Motor load indicates how much shear stress was applied to the processed material and is linked to the important HME process characteristic of SMEC. Die melt pressure was investigated, because it is a critical parameter for HME process stability. At the event of reaching 250 bar, or higher, the melt pump and the extruder shut down immediately. The variability of die melt pressure constitutes an indicator for the consistency and uniformity of melt flow through the extrusion dies. Similarly, the number of stable strands correlates with the uniformity of strand exit velocities from the extrusion dies, which is obviously critical for the performance of the pelletization process.

The investigated product responses were: color change, sphericity, median size and PSD span of the pellets. API content uniformity and dissolution performance were not investigated in statistical analysis, since there was no relevant variability observed.

In order to capture the effect of die wear, the number of cleaning cycles was included as an uncontrolled factor (“die age” - DA) into the dataset for statistical modeling (Table 3-6).

The coefficients of the fit PLS models (Figure 3-14) were used to investigate the main factors on the different responses. The details of correlation analysis (Table B-2) and PLS model coefficients and performance (Table B-3) are given in the Supplemental Material section B.

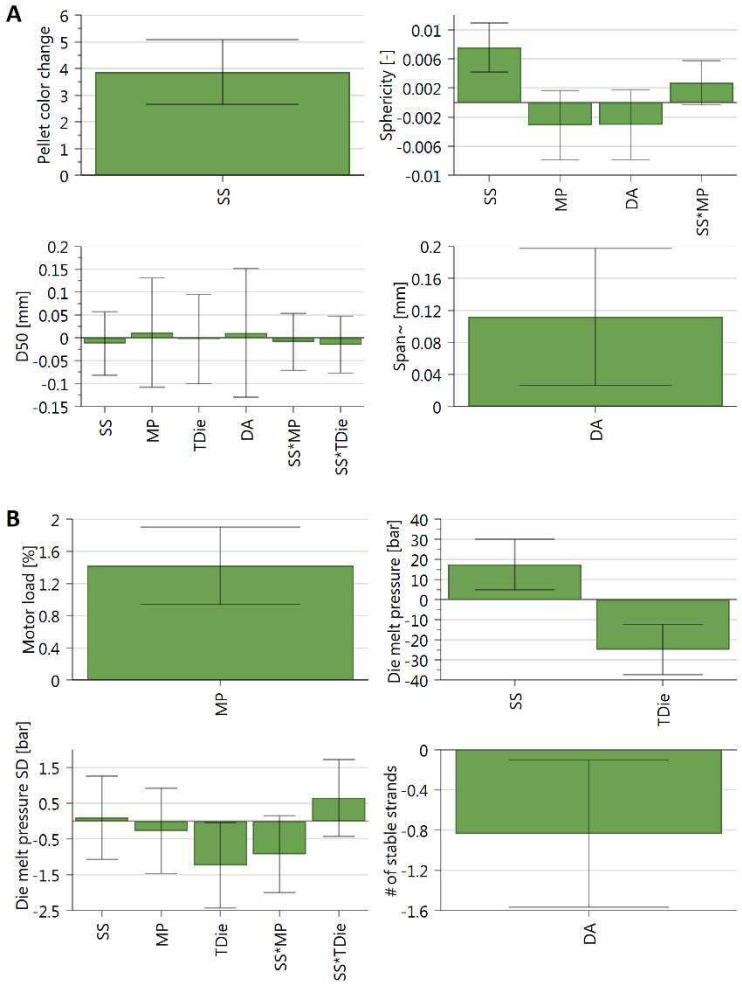

Figure 3-14. Coefficient plots of PLS models for relevant product responses (A) and process responses (B). (SS…screw speed, MP…melt pump inlet pressure, TDie…die plate temperature, DA…die age)

The model for the change of pellet color clearly allowed to correlate this response to screw speed, as already indicated in the previous investigations. Thus, it is crucial, to operate the HME line at low screw speed in order to avoid the degradation of HPMC.

All shape and size related pellet quality attributes included the uncontrolled factor of die age in the model. The PLS model for span even performed best, when including only die age as an input parameter to the model, highlighting that this factor was the main reason for wider PSD distributions. Thus, this factor needs to be tightly controlled in future experiments.

However, span and the measure for median pellet size, D_{50}, both yielded very poor models ($Q^2 = 0.127$ for D_{50} and $Q^2 = 0.433$ for span). Thus, the predictive power of these models is very little and needs to be interpreted with care. The model for D_{50} did moreover not contain a single significant factor. An attempt was made to improve these models by excluding run N4 from the data set, treating it as an outlier. This only gave little improvement in model performance and the data is therefore not shown. One reason for the poor model performance was, that the pelletization conditions had not been very

well controlled, as pelletizer intake speed was adjusted manually to the strand velocities at the different runs. Thus, the intake speed should be a controlled factor in future investigations.

However, sphericity actually yielded an excellent model ($Q^2 = 0.811$ and $R^2 = 0.903$), containing screw speed as significant factor. The sign of the coefficients in the plot, indicated that pellets had a higher sphericity with increasing screw speed, decreasing melt pump inlet pressure and low die age. The positive effect of higher screw speed and positive correlation with pellet color change in the correlation matrix (Table B-2 in the Supplemental Materials section B) suggest, that the degradation of HPMC led to pellets with more uniform dimensions. Since the set pellet length was the same for all DoE runs, die swell may have been influenced by the degradation of HPMC. However, sphericity as shape parameter does not resolve the different dimensions of the pellet, so deeper investigations on this effect were not possible.

With regard to the process parameter responses (Figure 3-14 right hand side), the models for motor load and the number of stable strands contained only one significant factor. Motor load was only a function of the melt pump inlet pressure, as expected. However, this parameter was not in a critical range and the melt pump inlet pressure is therefore not a CPP for the investigated process. The model for the number of stable strands contained the die age as a significant, negatively correlated factor, confirming the conclusions from the previous discussion of the process data.

The models for die melt pressure and die melt pressure variability contained more than one factor, with the die temperature being significant for both responses. Both responses increased with lowered die temperature. Thus, die plate temperature was a CPP for the investigated process. Both responses also showed a positive correlation with screw speed.

Selection of Nominal Settings

Combining all findings from the screening DoE, some adaptations of the process setup and a nominal set point for the HME and pelletization process were defined. The aim was to establish a process which reliably produces pellets with desired performance in terms of content uniformity, API dissolution and pellet geometry at a throughput of 4 kg/h.

API content uniformity and dissolution performance were found to be very robust against variation of all DoE factors. Moreover, the absence of API degradation upon HME processing was confirmed. However, some sensitivity of the pellet geometry and PSD was observed. The majority of produced pellet samples did provide acceptable quality, but the “die age” played a critical role, decreasing the quality of the pellets in terms of their geometrical properties. Thus, with regard to pelletization process stability, the sensitivity of the dies to the cleaning procedure needs to be eliminated. Therefore, steel dies should be used in the final process setup.

HME process stability is only critically depending on the die melt pressure level. Motor load and other pressure levels in the process, were never in a critical range. By statistical analysis it was demonstrated that higher die plate temperature can be utilized to lower the die melt pressure level and its variability. Consequently, the nominal set point for this CPP was selected at the highest level that was tested, at 140°C.

Additionally, there was a positive correlation of die melt pressure and screw speed observed. This is attributed to a change of flow properties of HPMC upon degradation. Thus, even though the degradation did not influence the pellet performance negatively, it should be eliminated to increase process stability. Consequently, the lowest tested screw speed was chosen as nominal set point, that is 120 rpm, which is also the lowest possible screw speed for the used HME equipment.

Melt pump inlet pressure was not critical, neither for process stability, nor for product quality. Nevertheless, there was an effect observed on die melt pressure variability, suggesting a high nominal value setting for this parameter. Yet, the melt pump requires the melt pressure level to increase from its inlet side to the outlet side and a low inlet pressure gives the process more stability in the case of lowered melt viscosity. This would be relevant in case of feeding deviations, resulting in an increased fraction of plasticizing materials in the melt. Thus, the nominal melt pump inlet pressure was set to 30 bar.

Finally, the poor model performance of the pellet size and PSD model highlighted the need to determine a nominal setting for the intake speed of the pelletizer. By investigating the pelletizer intake speed settings in runs, where all strands were stable, a target intake speed setting of 13.2 m/min was determined for processing 4 kg/h of pellets.

3.4. Conclusion

It was possible to set up a stable HME-pelletization process at a targeted throughput of 4 kg/h for the production of IR pellets for subsequent tableting by using a split-feeding strategy, a screw configuration with low mechanical energy input, a melt pump and a strand pelletizer.

A knowledge space was established by systematically investigating the CPPs for this specific setup in a DoE, revealing the criticality of extruder screw speed and die plate temperature. The melt pump inlet pressure was found not to be critical, neither for product quality, nor for process stability. However, the condition of the extrusion dies was identified as a critical uncontrolled parameter which will be eliminated by replacing the soft copper dies by more robust stainless steel dies in the future.

Finally, nominal process settings were established based on the findings on pellet quality and process stability during the DoE.

3.5. References

Abdul, S., Chandewar, A. V, Jaiswal, S.B., 2010. A flexible technology for modified-release drugs: multiple-unit pellet system (MUPS). J. Control. Release 147, 2–16.

Bialleck, S., Rein, H., 2011. Preparation of starch-based pellets by hot-melt extrusion. Eur. J. Pharm. Biopharm. 79, 440–8.

Bodmeier, R., 1997. Tableting of coated pellets. Eur. J. Pharm. Biopharm. 43, 1–8.

Braun, M., 2003. Einflussfaktoren bei der Tablettierung magensaftresistent überzogener Pellets auf Exzenter- und Rundlauftablettenpresse. Ph. D. Diss. Friedrich-Wilhelms-Universität Bonn, Ger. 1–168.

Breitenbach, J., 2006. Melt Extrusion Can Bring New Benefits to HIV Therapy. Am. J. Drug Deliv. 4, 61–64.

Breitenbach, J., 2002. Melt extrusion: from process to drug delivery technology. Eur. J. Pharm. Biopharm. 54, 107–117.

British Pharmacopoeia, 2009. British Pharmacopoeia (2009).

Démuth, B., Nagy, Z.K., Balogh, A., Vigh, T., Marosi, G., Verreck, G., Van Assche, I., Brewster, M.E., 2015. Downstream processing of polymer-based amorphous solid dispersions to generate tablet formulations. Int. J. Pharm. 486, 268–286.

Eitzlmayr, A., 2015. Modeling of High-Viscous Flow and Mixing in Co-Rotating Twin-Screw Extruders. Graz University of Technology.

European Commission, 2014a. Nimodipine 01/2008: 1245, in: European Pharmacopoeia 8.0. European Commission, pp. 2857–2858.

European Commission, 2014b. 2.9.40. Uniformity of Dosage Units, in: European Pharmacopoeia 8.0. European Commission, pp. 357–359.

Grymonpré, W., Bostijn, N., Herck, S. Van, Verstraete, G., Vanhoorne, V., Nuhn, L., Rombouts, P., Beer, T. De, Remon, J.P., Vervaet, C., 2017. Downstream processing from hot-melt extrusion towards tablets: A quality by design approach. Int. J. Pharm. 531, 235–245.

Maag Automatik, 2015. Pharma Pelletizer Sphero® THA [WWW Document]. Commer. Video. URL https://www.youtube.com/watch?v=24cWLYHV4q8 (accessed 7.22.15).

Maniruzzaman, M., Nokhodchi, A., 2017. Continuous manufacturing via hot-melt extrusion and scale up: regulatory matters. Drug Discov. Today 22, 340–351.

Markl, D., Wahl, P.R., Menezes, J.C., Koller, D.M., Kavsek, B., Francois, K., Roblegg, E., Khinast, J.G., 2013. Supervisory control system for monitoring a pharmaceutical hot melt extrusion process. AAPS PharmSciTech 14, 1034–44.

Merkus, H.G., 2009. Particle Size, Size Distributions and Shape, in: Particle Size Measurements. Springer Netherlands, Dordrecht, pp. 13–42.

Muehlenfeld, C., Thommes, M., 2012. Miniaturization in Pharmaceutical Extrusion Technology: Feeding as a Challenge of Downscaling. AAPS PharmSciTech 13, 94–100.

Mürb, R.-K., 2015. Zur Bedeutung der Anpressdruckaufbringung bei Heißabschlägen.

Patil, H., Tiwari, R. V., Repka, M.A., 2016. Hot-Melt Extrusion: from Theory to Application in Pharmaceutical Formulation. AAPS PharmSciTech 17, 20–42.

Repka, M.A., Bandari, S., Kallakunta, V.R., Vo, A.Q., McFall, H., Pimparade, M.B., Bhagurkar, A.M., 2018. Melt extrusion with poorly soluble drugs – An integrated review. Int. J. Pharm. 535, 68–85.

Roblegg, E., Jäger, E., Hodzic, A., Koscher, G., Mohr, S., Zimmer, A., Khinast, J., 2011. Development of sustained-release lipophilic calcium stearate pellets via hot melt extrusion. Eur. J. Pharm. Biopharm. 79, 635–645.

Saerens, L., Vervaet, C., Remon, J.P., De Beer, T., 2014. Process monitoring and visualization solutions for hot-melt extrusion: A review. J. Pharm. Pharmacol. 66, 180–203.

Schenk, L., Troup, G.M., Lowinger, M., Li, L., McKelvey, C., 2011. Achieving a HME design space for the production of solid solutions, in: am Ende, D.J. (Ed.), Chemcial Engineering in the Pharmaceutical Industry: R&D to Manufacturing. John Wiley & Sons, Inc., pp. 819–836.

Thiry, J., Krier, F., Evrard, B., 2015. A review of pharmaceutical extrusion: Critical process parameters and scaling-up. Int. J. Pharm. 479, 227–240.

Treffer, D., Wahl, P.R., Hörmann, T.R., Markl, D., Schrank, S., Jones, I., Cruise, P., Mürb, R.-K., Koscher, G., Roblegg, E., Khinast, J.G., 2014. In-line implementation of an image-based particle size measurement tool to monitor hot-melt extruded pellets. Int. J. Pharm. 466, 181–9.

Treffer, D.F., 2016. Pharmaceutical Hot Melt Extrusion - Novel Tools for Screening and Processing. Graz University of Technology.

Treffer, D.F., Khinast, J.G., 2017. Why hot melts do not stick to cold surfaces. Polym. Eng. Sci. 57, 1083–1089.

Wagner, K.G., Krumme, M., Beckert, T.E., Schmidt, P.C., 2000. Development of disintegrating multiple-unit tablets on a high-speed rotary tablet press. Eur. J. Pharm. Biopharm. 50, 285–292.

Wahl, P.R., Treffer, D., Mohr, S., Roblegg, E., Koscher, G., Khinast, J.G., 2013. Inline monitoring and a PAT strategy for pharmaceutical hot melt extrusion. Int. J. Pharm. 455, 159–68.

Witschnigg, A., Koscher, G., Treffer, D., Mürb, R., Laske, S., Khinast, J., 2016. Micro-pelletizing of pharmaceutical HME formulations using a die face pelletizer. AIP Conf. Proc. 1779.

4. Sensitivity of a Continuous Hot-Melt Extrusion and Strand Pelletization Line to Control Actions and Composition Variation[2]

The purpose of this work was to develop a robust hot-melt extrusion and strand pelletization process for manufacturing pellets with an immediate active pharmaceutical ingredient (API) release (IR). The robustness of pharmaceutical continuous manufacturing processes and of its control strategy is vital for competitiveness to traditional batch-manufacturing. Therefore, first the sensitivity of product quality, process stability, and process monitoring tools to i) parameter changes due to control actions and ii) typical process deviations, i.e., feeding errors, was investigated in a design of experiments (DoE). Second, a design space for the production of IR pellets for later tableting was established and finally, a technical control strategy developed to ensure a robust process.

The used formulation consisted of a poorly-water-soluble API, nimodipine, and two polymers, Methocel™ E5 (HPMC) and Eudragit® E100. Deviations in HPMC content were considered especially critical, since HPMC has highly viscous and complex flow behavior. To that end, die melt pressure was found to be highly sensitive to composition deviations, i.e. a limiting factor for process stability. A melt pump was applied to achieve extrusion die pressure levels of up to 250 bar, but even these process limits were approached during the DoE. Pelletization, or pellet size and size distribution respectively, were found to be sensitive to an increased throughput, due to the resulting insufficient strand cooling before the pelletizer. However, API dissolution was found to be very robust across the entire investigated range. Near-infrared (NIR) spectroscopy was applied to monitor API content and the sensitivity of the residence time distribution (RTD) was investigated by means of tracer measurements. NIR-based API content monitoring and RTD models for material tracking were found to be at risk after processing melt with high HPMC content, due to a lack of purging by less viscous formulation compositions. Eventually, a feed rate control strategy relative to the HPMC feeder was suggested as a promising option to improve process and process monitoring robustness.

[2] This chapter is based on the publication Hörmann et al.. Sensitivity of a Continuous Hot-Melt Extrusion and Strand Pelletization Line to Control Actions and Composition Variation. Submitted to Int.J.Pharm.

4.1. Introduction

In order to improve the product robustness and quality in pharmaceutical manufacturing, regulatory agencies, as well as the International Council for Harmonization (ICH) promote a quality-by-design (QbD) product and process development (Sau L Lee et al., 2015). This approach emphasizes the need to understand the effects of critical process parameters (CPPs) and material attributes (CMAs) on the product's critical quality attributes (CQAs) (Desai et al., 2017; Patwardhan et al., 2015). The evaluation of CPPs and their effects on CQAs should be performed in a systematic way, e.g., by applying the Design of Experiments (DoE) during process development, aiming for a robust process. Process robustness is defined as "the ability of a process to tolerate variability in materials and changes of the process and equipment without negative impact on quality" (International Conference on Harmonisation of Technical Requirements for Registration of Pharmaceuticals for Human Use, 2009), i.e. CQAs must remain within specification limits. This approach can be applied to both batch and continuous manufacturing (CM). In contrast to batch manufacturing, in CM varying process input typically arises from interdependencies between various process units. For example, feeder deviations are considered a main source of process variation in CM (Engisch and Muzzio, 2014; Meier et al., 2016), causing downstream changes in the formulation composition and throughput. Process units downstream of the feeding step can merely dampen such fluctuations, depending on their process dynamics (Schenck et al., 2010). Common aspects, only relevant in integrated CM lines are first, the alignment of the process units' throughputs, second, the effect of discharging deviating material and the resulting throughput decrease in downstream processes and third, the ability of a process to recover from a deviation. While the first two points have an effect on the optimal line throughput (range) and can be considered aspects of process design and control, the third is a matter of process stability.

This study intends to establish a continuous hot-melt extrusion (HME) and strand pelletization line for the production of amorphous solid dispersion (ASD) pellets with immediate release (IR) of a poorly soluble active pharmaceutical ingredient (API), which is robust with regard to:

i) control actions, i.e., throughput changes; and
ii) typical process variation, i.e., formulation composition and throughput variability induced by feeder deviations.

Pellets produced in this HME and pelletization unit are intended to be used for subsequent tableting in a semi-continuous manufacturing line, as shown in Figure 4-1. Based on the specification for the final tablet and the requirements of the downstream units, target properties for the intermediate pellets are given, i.e. for API release, pellet size and size distribution, and shape. Therefore, one main aspect of this study was to evaluate the sensitivity of the intermediate product to those intentional and unintentional disturbances. The process is considered robust, if the target properties of the

intermediate pellets are within the requirements. While the definition of robustness given above and much of the literature focuses on the sensitivity of product attributes (Desai et al., 2017; Roth et al., 2017) to input changes, this study specifically investigates – in addition - the sensitivity of the process state variables and process control tools, such as near-infrared (NIR) spectroscopy. While for intermediate CQAs tight limits are defined by the product specification, the acceptable limits for process state variables are given by the feasible equipment operating range.

For example, for the HME equipment the process state variable limits include a maximal melt pressure and motor load level as well as intake capacity limitations. The strand pelletization process does not have any limiting state variables, but its performance depends on the mechanical stability and temperature of the strand at the cutting zone, potentially causing pelletization failures, such as fragmentation or sticking.

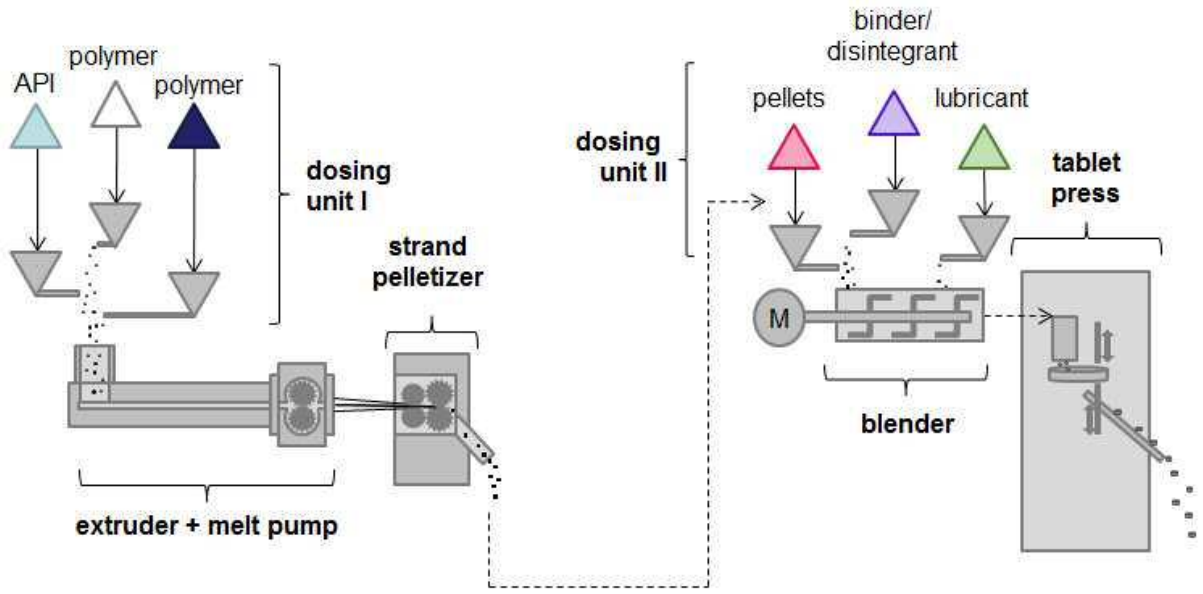

Figure 4-1. Schematic representation of the full process line for tablet manufacturing via hot-melt extrusion and strand pelletization.

Moreover, the sensitivity of the residence time distribution (RTD) was investigated, since it characterizes the transient behavior of continuous processes and is increasingly utilized in process monitoring, e.g., for tracking of material and out-of-specification (OOS) material segregation (Almaya et al., 2017; Engisch and Muzzio, 2015; Sau L Lee et al., 2015; Reitz et al., 2013). It also serves as a basis for process control strategy development, e.g., via process simulation (Kruisz et al., 2017). Thus, it is critical to understand for which situations (disturbances, feed variability) the RTD model remains valid for material tracking or for assigning process analytical technology (PAT) data to specific material portions (e.g., for real-time release from inline PAT measurements, or for material deviation decisions). Concerning the use of NIR for API content monitoring, the sensitivity to process input changes, i.e., throughput or formulation composition changes needs to be understood.

The model API used by us was nimodipine (NMD), a poorly water-soluble compound. An immediate API release (IR) from the final tablet was desired. HME is an established, inherently continuous manufacturing method of oral dosage forms, especially for more advanced drug products, such as ASD, sustained or controlled release and nano-based formulations (Ghebremeskel et al., 2007; Jaeghere et al., 2015; Khinast et al., 2013; Roblegg et al., 2011; Zheng et al., 2007a).

In our previous work an amorphous solid dispersion (ASD) formulation of NMD with two carrier polymers, Eudragit E (EE) and HPMC E5, was demonstrated to provide IR from the HME pellets for a range of polymer ratios (Hörmann et al., 2018). EE was found to act as a carrier for amorphous NMD, ensuring ASD stability, while HPMC is required in the formulation to increase the mechanical melt stability in strand pelletization. However, HPMC has a complex flow behavior above its yield point, as well as a narrow HME processing window between softening and degradation (Hughey et al., 2012; LaFountaine et al., 2016). The presence of a yield point in a formulation is especially challenging during the HME process start-up phase and can cause motor load and pressure peaks. In the case of additional melt composition fluctuations due to momentary feeding failures, the risk of a process shut-down increases. This is highly critical since in CM each downtime undermines the competitiveness with batch processing.

Co-rotating twin-screw extruders (TSEs) are limited in terms of pressure build-up capability since the extrusion shaft generally has a bearing only on the material inlet side. High pressure at the outlet can cause decentering of the shafts and damage to the extrusion screws. Nevertheless, this type of extruder is preferred in pharmaceutical manufacturing since it offers good radial mixing and a narrow well-defined RTD (Crowley et al., 2007).

To overcome pressure peaks and decrease the risk during process start-up, a melt pump was installed at the end of the extruder. Melt pumps are commonly used in the plastics industry to achieve high pressure levels. Moreover, they reduce the melt pressure pulsations caused by the rotating movement of the screws, resulting in lower strand velocity and thickness fluctuations. Melt pumps can only operate correctly if there is a positive pressure change across the pump with a higher pressure level at its outlet, before the extrusion die. By using the melt pump, the processable melt pressure window is increased significantly compared to an extruder alone. However, still a two-sided process limit on acceptable melt pressure levels remains.

Strand pelletization is one option for the production of pellets downstream of HME. Tableting of HME products is mostly performed by milling the extruded intermediate (Gryczke et al., 2011; Grymonpré et al., 2016; Zheng et al., 2007a). However, pellets have the advantage of a more or less uniform particle shape and size, as well as low friability, resulting in less dust formation during subsequent processing. Moreover, especially in ASD formulations, milling can induce changes in the solid state of

API, requiring a thorough investigation of this effect. The pellet size should be small since the influence of a single pellet on the mass and content uniformity of a dosage unit depends on the pellet size to the third power. Additionally, there is a risk of segregation if the pellets are blended with powder in a downstream unit, again as a function of size. Thus, pellet size is a CQA of the intermediate product.

Since strand pelletization is thermally decoupled from the extrusion process, it typically offers a wide processing window for non-brittle formulations. If a formulation is brittle at the pelletization temperature, the mechanical stress in the intake zone can cause fragmentation. This may result in long pieces of strand in the product or even a complete strand rupture. Although there are no process state variables limiting the pelletization process space, deviations in formulation composition, melt temperature and strand velocity affect the mechanical stability of the strands and the strand temperature at the cutting zone. Strand rupture has to be avoided since in this case an operator needs to be present during the process.

The setup selection and process parameter screening of the process were performed in advance of this study, resulting in a nominal formulation composition and nominal process parameter settings. A DoE plan was developed to investigate the sensitivity of this HME-pelletization line with regard to control actions and process variations. Thus, the aim was to develop statistical models that are valid in a wider range of process states and formulation compositions around the nominal set point. Based on the response surface models for several process and product responses, the criticality of specific process deviations was assessed. Finally, a design space for manufacturing pellets with nominal formulation composition on this HME pelletization line was defined, based on the intermediate product property responses and process limits.

In addition, RTD characterization and API content monitoring was performed in this study to understand the sensitivity of the process dynamics and PAT tools. Eventually, the results led to an outline for a control strategy for the process unit to improve robustness, when integrated in the continuous tablet manufacturing line.

4.2. Materials and Methods

4.2.1. Materials

Nimodipine (NMD) was donated by Bayer AG (Germany). Methocel™ E5 (HPMC) and Eudragit® E100 (EE) were purchased from Dow Chemicals (USA) and Evonik (Germany), respectively. The nominal formulation contained 10 wt% NMD, 54 wt% HPMC and 36 wt% EE. This formulation composition was chosen based on a previous study investigating properties of the ASD system (Hörmann et al., 2018) and on observations made during the process setup experiments. Since NMD is light-sensitive, all processing and analysis were performed under yellow light and samples were stored in a light-protected environment.

HME RTD measurements were performed using 35 mg Fe_2O_3 (Sigma Aldrich) in a manually-shortened HPMC capsule (Coni-snap®, size 0, Capsugel) which was added to the intake section of the extruder.

4.2.2. Rheology and pVT-Measurement

Rheological properties of the nominal formulations were characterized using a high-pressure capillary rheometer (Rheograph 2002, Göttfert Werkstoff Prüfmaschinen GmbH). The measurements were executed according to ISO 11443 inside a temperature range of 135 - 155°C. Die lengths of 10, 20 and 30 mm and a die diameter of D=1 mm were used to cover a shear rate range of 10 s^{-1} to 10,000 s^{-1}. Entrance pressure loss p_E was determined via a linear extrapolation in the Bagley-diagram and the Weißenberg-Rabinowitsch correction applied to account for the non-Newtonian melt flow behavior according to Kulka et al. (2018). Fitting of the viscosity curves was performed in Excel (Microsoft Corporation, USA) using the generalized-reduced-gradient (GRG) algorithm for non-linear regression, available in the Solver tool.

Specific volume was measured at various pressures and temperatures using a measurement device PVT00 (SWO Polymertechntik GmbH) to determine pVT-data according to ISO 17744. Measurements were performed at a constant cooling rate of 6 K/min within a pressure range of 200-325 bar and a temperature range of 40°C to 140°C.

Both the rheology and the pVT-measurements were performed using pellets with a nominal formulation composition (10 wt% NMD, 36 wt% EE and 54 wt% HPMC E5) dried for 24 h at 50°C and 2 mbar.

4.2.3. Pellet Characterization

Pellet Size and Shape Characterization

The size and shape characterization was performed using samples collected for 5 s every 5 min at the pelletizer outlet for each set point. This sample collection time resulted in 6000 - 33,000 pellets, depending on throughput and formulation.

The pellets were analyzed using the dynamic image particle analyzer PartAn^{3D} (Microtrac, USA). A camera captures images of particles falling from a vibrating chute and tumbling past the camera. Several images of each particle are taken from different sides during tumbling fall. A software is used to track each particle in a series of pictures. Based on particle projection area and dimensions, the software evaluates the size, the shape and the roughness parameters. Based on this information on single particle projections from different sides, three-dimensional properties are calculated, i.e., the length, the width and the thickness. The size and shape analysis was performed using 163 logarithmic bins in a size range from 0.063 to 4 mm. To avoid the evaluation of dust particles on the lens of the camera during pellet tracking, a minimal size threshold of 0.1 mm was used. The maximum bin size of 4 mm was chosen in order to achieve a good resolution for (desired) pellet sizes between 0.6 to 1.2 mm. Pellet fragments longer than 4 mm were categorized as being in the maximum bin size, slightly biasing the total volume calculation. Cross-checking the effect for the selected samples with a maximum bin size of 10 mm showed that this approach did not to change results significantly.

From the size parameters reported by the particle sizer, the projection area equivalent diameter $D_A = \sqrt{4 \cdot A_P/\pi}$, (with A_P being the projected area of the particle), Feret length (FL), width (FW) and thickness (FT) were chosen to characterize the pellets. The particle size distribution information was obtained based on the particle volume in all classes, where volume is computed by the software using the three Feret dimensions. Mean sphericity by total volume ($\psi = D_A/D_P$, with D_P the projection perimeter equivalent diameter) and mean L/T ratio by total volume were selected from several available shape factors offered by the particle sizer. For statistical evaluation of the DoE runs, different parameters were used and models were compared in order to select the most reliable and sensitive measure of size and shape. Concerning PSD width characterization, spans of 10%- and 90%-quantiles and uniformity index UI [%] of the D_A distribution were investigated.

$$span\ [mm] = D_{90} - D_{10} \qquad \textit{Eq. 4-1}$$

$$UI[\%] = D_5/D_{95} * 100 \qquad \textit{Eq. 4-2}$$

In-Vitro Dissolution Testing

Pellets used for dissolution were taken from the samples collected continuously over the steady-state runtime at each set point. Dissolution was performed under sink conditions using an USP apparatus I (DT820LH Dissolution Tester, Erweka, Germany) in 500 mL at 37 ± 0.5°C. The dissolution medium consisted of a sodium acetate buffer with pH 4.5 ± 0.1 and 0.3% of sodium lauryl sulfate (SLS), as noted in the specification for testing NMD tablets in the British Pharmacopoeia (British Pharmacopoeia, 2009). Dissolution tests were performed in triplicates (n=3) using pellet masses according to an API mass of 10 mg in each dissolution vessel. Samples of 1.5 mL were collected automatically at 0, 5, 15, 30, 45, 60 and 90 min and filtered through 0.10 µm poroplast filters. The dissolved API concentration in the dissolution medium over time was determined via UV/Vis spectroscopy (Lambda 950, PerkinElmer, USA). Absorbance measurements were carried out in 10 mm polymethyl methacrylate (PMMA) semi-micro cuvettes at 360 nm against pure dissolution medium from the same vessel.

In order to compare the dissolution profile from pellets with different API content, the dissolution curves were normalized by the average API content calculated from the real-time feeder data for each respective DoE run and the weighed pellet mass in each vessel. The time-shift between the API concentration at the extruder inlet (feeding unit) to the pelletizer outlet (pellet sample collection) was corrected using the mean residence time of each run.

4.2.4. Extrusion and Pelletization Process

A co-rotating TSE ZSK 18 MI extruder (L/D = 40, Coperion, Switzerland) was used in combination with a split-feeding unit (Figure 4-1). The latter consisted of three loss-in-weight (LIW) twin-screw feeders operated in gravimetric mode. NMD was dosed by a small-scale feeder (MT-S Hyg, Brabender, Germany) and the two carriers by larger KT20 feeders (K-PH-CL-SFS-KT20 and K-CL-KT20, Coperion-KTron, Switzerland). All feeders were mounted above the first extruder barrel, with a funnel merging all three material streams.

HME process settings and screw configuration were optimized prior to this study. The final screw design and process setup is described in detail in Section I in the Supplemental Material section C. A temperature-controlled melt pump Extrex® (Maag-Automatik, Germany) was mounted at the end of the extruder. After the melt pump, an adapter plate held the die plate with eight steel dies with a diameter of 1 mm and a cylindrical length of 1 mm. In the adapter plate, a melt pressure sensor, an immersion melt temperature sensor and a fiber-optic NIR probe (DR-NIR Dynisco, Germany) were mounted. The fiber-optic probe was used to collect the reflectance NIR spectra (process spectrometer SentroPAT FO, Sentronic, Germany) from the melt stream. The spectra were collected with an integration time of 9 ms and averaging of 60 spectra. The NIR probe was used for determining the RTD in the HME and melt pump unit, and for the API content monitoring.

The strand pelletizer Primo 60E® (Maag-Automatik Plastics Machinery, Germany) was located 2 m after the extrusion dies. The strand surface temperature was determined directly before the pelletizer intake using a hand-held IR thermometer pistol (IR 845, Testo). The ratio of the intake speed to the speed by which the strands exit the extrusion dies, determines the tension and possible dilation applied to the strands. In order to achieve the smallest possible pellet size, the strand cut length was set to 0.5 mm, which is the smallest possible size of this pelletizer configuration.

Nominal extrusion settings were determined previously in a process screening DoE (further details can be found in section I in the Supplemental Material). The screening gave an optimal screw speed level of 120 rpm and a pressure level of 30 bar before the melt pump to minimize shear stress on the melt. The nominal die plate temperature was set to 140°C and the intake speed setting of the pelletizer according to an intake speed-to-throughput ratio (in short: intake speed ratio) of 3.3 m·h/(kg·min). The investigations on sensitivity were made at or around these center point settings, respectively.

4.2.5. Process Data Collection and Processing

Accessible process data from feeders and the extruder were monitored and collected at a frequency of 1 Hz using a PAT software solution (SIMATIC SIPAT V4.0, Siemens, Germany). Although such a high collection frequency is not desirable in production, it is required for process development, especially when investigating process dynamics. The collected data were later exported and further processed in Matlab (Matlab 2014b, MathWorks®, USA). The values of response process parameters were averaged over 10 min of run-time in the steady state and subsequently implemented in MODDE 11 (Umetrics, Sweden) for statistical evaluation.

4.2.6. Processing of Spectral Data for RTD Measurements and API Monitoring

The RTD from extruder inlet to the NIR probe was captured experimentally. NIR spectra containing the tracer information were processed according to Rehrl et al. (2018). Selected wavelengths between 1200 nm and 2100 nm were standard normal variate (SNV) corrected and used in the principal component analysis (PCA). The impulse response of a fourth-order transfer function (Eq. 4-3) was fit to the first principal component (PC_1) profile over time. Choosing PC_1 to represent the tracer concentration ($PC_1 \approx f \cdot c_{Tracer}(t)$) during the RTD model fitting implies that the correlation of tracer concentration and PC_1 is linear and PC_1 is influenced by no other parameter then tracer concentration. The appropriateness to predict dynamic API content changes for this particular process equipment line based of this approach was shown by Rehrl et al. (2018).

$$P(s) = \frac{\bar{y}(s)}{\bar{u}(s)} = \frac{k}{(1+sT)^4} e^{-sT_d} \qquad \textit{Eq. 4-3}$$

The impulse response of $P(s)$ was normalized by setting the gain $k = 1$, yielding the RTD $E(t)$. $E(t)$ was used to calculate the mean residence time T_m (Eq. 4-4) and the standard deviation s_{RT} (Eq. 4-5). Lag time T_d (from Eq. 4-3), mean residence time T_m and standard deviation s_{RT} are used as responses for the statistical evaluation.

$$T_m = \int_0^\infty t\, E(t)\, dt \qquad \textit{Eq. 4-4}$$

$$s_{RT} = \sqrt{\int_0^\infty (t - T_m)^2 E(t)\, dt} \qquad \textit{Eq. 4-5}$$

For API monitoring, spectra from the steady state in each experimental setting were used to build the chemometric model. Additionally, the calibration dataset contained average API concentrations, calculated based on time-shifted feed rate data in the steady-state operation. To reduce non-chemically induced variations in the spectral data, the wavelength range of 1550 nm to 1850 nm was selected, pre-treated using the SNV correction and the first derivative determined by applying a Savitzky-Golay filter (second order, seven points with a step size of 2 nm). The centered spectral variables in the wavelength range between 1556 nm to 1746 nm were used for partial least squares (PLS) model regression.

The predictions of the chemometric model for the entire dataset are used in the discussion concerning the sensitivity of NIR spectroscopy as a PAT tool for the product monitoring in this process.

4.2.7. Design of Experiments

The aim of the experimental design was to simultaneously assess the effect of control actions and process deviations on several relevant process and product responses. The formulation composition or weight fraction of each component was varied to capture the effect of feeding deviations, affecting momentary compositions and throughput. The other relevant case for throughput changes (without composition changes) are process control actions.

Other process factors, namely the adapter temperature and the pellet intake speed ratio were investigated as tuning parameters. Changes in the adapter temperature can be used as a control measure if the die melt pressure is close to a processing limit (either too low or too high). Sensitivity of pellet geometry on intake speed ratio is relevant since faster intake speeds could result in thinner cylinders, while cylinder length remains constant at 0.5 mm as set by the pelletizer cutting speed. This may be utilized to fine-tune pellet size. A summary of the controlled DoE factors is given in Table 4-1.

*Table 4-1. Factors, factor levels (**bold** values represent the nominal settings) and DoE responses.*

Factors	Factor levels	DoE Responses
API fraction (API) [wt%]	2 / 6 / **10** / 14	Extruder motor load [%]
HPMC fraction (HPMC) [wt%]	46 / 50 / **54** / 58	Die melt pressure [bar]
EE fraction (EE) [wt%]	28 / 32 / **36** / 40	Die melt temperature [°C]
Throughput (mf) [kg/h]	3.2 / 3.6 / **4.0** / 4.4 / 4.8	RTD parameters
Die temperature (T_{Die}) [°C]	130 / **140** / 150	Pellet size [mm]
Intake speed ratio (v_{in}/mf) [m·min^{-1}/kg·h^{-1}]	3.0 / **3.3** / 3.6	Pellet shape
		PSD width

The DoE responses were chosen according to their relevance as process limits and to product quality. Motor load and die melt pressure were already discussed as parameters potentially causing an emergency shut-down of the line, and RTD parameters as responses relevant for process monitoring. The pelletization process is not limited by any process state variable, and strand rupture as a qualitative process limitation cannot be included into a statistical model. As such, the product attributes pellet size and shape, and PSD span were used to evaluate pelletizer performance. These parameters were also used as product responses during design space definition. Dissolution from the pellets was characterized as well, but no statistical model built due to a lack of variation.

A D-optimal DoE design with split objective for a quadratic mixture and a process model (interaction model) was chosen. Four formulation mixture levels (Figure 4-2a) and three process parameter levels (die plate temperature, intake speed ratio) were used, while the number of throughput levels was manually set to 5 (Figure 4-2b) in order to receive a higher resolution for the effect of this input parameter. The center point of the design was run in triplicate. Factor settings of all 31 runs are given in Table 4-2. G-efficiency of the selected design was 64.124 and condition number 15.399.

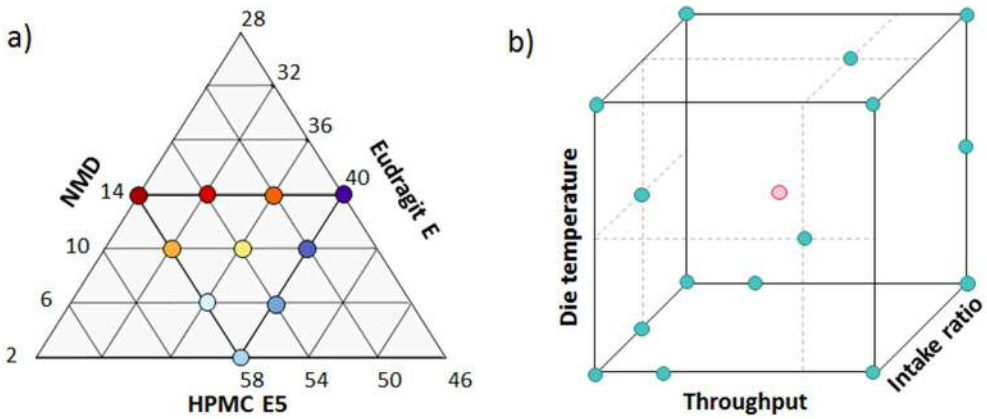

Figure 4-2. a) Mixture design with 4 levels for each component fraction and triplicate center point (yellow, n=3). b) Process design with 3 levels for intake ratio and die temperature and 5 levels for throughput. Center point (pink) with n=3.

Table 4-2. DoE schedule.

Run	Run Order	Die temp. [°C]	Throughput [kg/h]	Intake speed ratio [m·h/(min·kg)]	NMD frac. [-]	HPMC frac. [-]	EE frac. [-]
N1	24	130	3.2	3.0	0.02	0.58	0.40
N2	18	130	3.2	3.0	0.14	0.58	0.28
N3	8	150	3.2	3.0	0.14	0.54	0.32
N4	27	150	3.2	3.0	0.06	0.58	0.36
N5	11	150	3.2	3.0	0.10	0.50	0.40
N6	21	130	3.2	3.6	0.14	0.50	0.36
N7	23	130	3.2	3.6	0.10	0.58	0.32
N8	26	150	3.2	3.6	0.14	0.46	0.40
N9	28	150	3.2	3.6	0.02	0.58	0.40
N10	14	150	3.2	2.8[a]	0.14	0.58	0.28
N11	20	130	3.2	3.3	0.14	0.46	0.40
N12	6	140	3.2	3.3	0.10	0.54	0.36
N13	19	130	3.6	3.0	0.14	0.46	0.40
N14	4	130	3.6	3.6	0.06	0.54	0.40
N15	12	150	4.4	3.3	0.14	0.50	0.36
N16	17	140	4.4	3.0	0.02	0.58	0.40
N17	22	130	4.8	3.0	0.14	0.50	0.36
N18	5	130	4.8	3.0	0.10	0.58	0.32
N19	16	130	4.8	3.0	0.06	0.54	0.40
N20	13	150	4.8	3.0	0.14	0.46	0.40
N21	29	150	4.8	3.0	0.02	0.58	0.40
N22	10	150	4.8	3.0	0.14	0.58	0.28
N23	3	130	4.8	3.6	0.14	0.46	0.40
N24	31	130	4.8	3.6	0.02	0.58	0.40
N25	25	150[b]	4.8	3.6	0.14	0.58	0.28
N26	9	150	4.8	3.6	0.14	0.54	0.32
N27	7	150	4.8	3.6	0.06	0.58	0.36
N28	2	140	4.8	3.6	0.10	0.50	0.40
N29	15	*140*	*4.0*	*3.3*	*0.10*	*0.54*	*0.36*
N30	30	*140*	*4.0*	*3.3*	*0.10*	*0.54*	*0.36*
N31	1	*140*	*4.0*	*3.3*	*0.10*	*0.54*	*0.36*

[a] Setting with an intake speed ratio of 3.6 not possible without strand rupture, [b] temp. set to 150°C instead of 130°C suggested by MODDE.

4.2.8. Statistical Model Regression

A partial least-squares regression (PLS) model was fitted to the experimental response data. The model's fine-tuning was performed by excluding manually physically or statistically non-significant factors. The optimization target was to maximize the cross-validated coefficient of determination Q^2. Moreover, it was ensured that a small difference between R^2 and Q^2 and a normal distribution of residuals across the modelled range was achieved. Q^2, as a measure of the model's predictive ability is determined in MODDE by cross-validation.

All responses were scaled and centered prior to the model regression using the nominal formulation (center point) as a reference mixture. Moreover, some responses were transformed in order to achieve a normal distribution of responses (Table 4-3). Contour plots and sweet spot graphs were created in MODDE. After identifying the limiting process parameters and the indicative pellet properties, a design space was defined using a DPMO (defects per million opportunities) level of 66,000. DPMO level contours were calculated via Monte-Carlo simulation (n=20,000) by MODDE, also taking factor precision (2*std.dev. of factor settings as calculated from monitored process data) into account.

Table 4-3. DoE response details.

Name	Abbreviation	Units	Transform
Motor load	ML	%	Log: $Log_{10}(Y)$
Die melt pressure	DMP	bar	Log: Log_{10} (Y)
Die melt temperature	DMT	°C	None
RTD lag T_d(RTD model)	T_d	s	None
RTD mean T_m(RTD model)	T_m	s	None
RTD width s(RTD model)	s_{RT}	s	None
Pellet size x50(Dv)	Dv50	mm	Log: Log_{10} (10*Y+0.01)
Pellet size x50(Feret length)	FL50	mm	Log: Log_{10} (Y+0.01)
PSD width span	Span	mm	Log: Log_{10} (Y+0.001)
PSD width UI	UI	%	NegLog: -Log_{10} (10-0.1*Y)

4.3. Results and Discussion

4.3.1. DoE Process Data and Pellet Characterization

Figure 4-3 shows an exemplary set of process data collected during a full day of experiments. As can be seen the dataset contains six DoE runs. The process data are displayed in three diagrams: on the left-hand side are data from the split-feeding unit, in the middle are data from the extruder and on the right-hand side are data collected from melt pump and die plate. Similarly, factor and response parameters, such as feed rates, melt pressures and melt temperature, were displayed in real time during the experiments and used by the operator to decide when the process was in steady state. After achieving the steady state, pellet sampling was performed for 20 min, with four samples taken after 5, 10, 15 and 20 min for PSD analysis. Steady-state values of motor load and die melt pressure are summarized in Table C-1 in the Supplemental Material section C. After 20 min, the RTD was characterized by means of a tracer impulse test before switching to the new set point for the next run. Additionally, to displaying the process parameters, SIPAT can be used to calculate parameters in real time, based on the collected data. Examples of this are the API content momentarily fed by the split-feeding unit, or the specific mechanical energy consumption (SMEC).

Figure 4-3 shows a brief deviation in the EE feeding data (just before 11:00) after changing to the second run. The process data collected from the extruder, melt pump and die plate illustrate how such an event affects the downstream process parameters. Since EE acts a plasticizer, first, the extrusion motor load and, subsequently, the extruder melt pressure (sensor location shown in Figure C-2 in the Supplemental Material section C), the melt pump inlet pressure and finally die melt pressure exhibit a short peak. Although in this case the height of the peak is not putting the process at risk, a longer or more pronounced deviation could extend to the process limits (extrusion motor load > 80%, extruder melt pressure > 100 bar, die melt pressure > 250 bar).

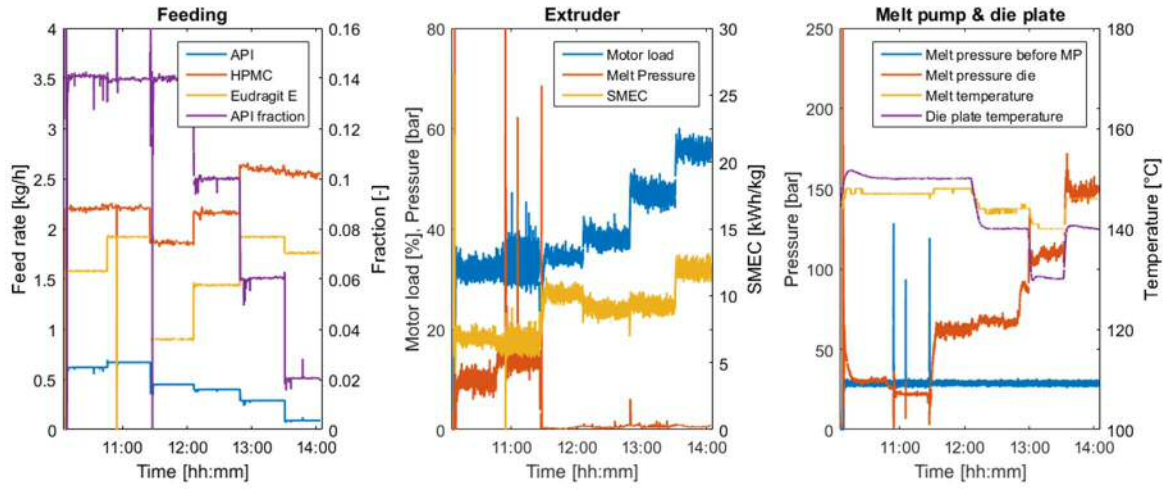

Figure 4-3. Exemplary set of process data for six sequential DoE runs. After each change of settings, approximately 10 min were needed to reach steady state again. After these 10 min, pellet sample and steady-state data collection was started for 20 min.

In two runs, N22 and N25, collecting the pellets was impossible: the strands were too soft for pelletization, breaking close to the dies even at lower intake speeds. In both cases, the same formulation and extrusion settings were applied, with a high NMD and HPMC content and at high die temperature and throughput level. All other setting yielded pellets, which were used in the pellet size and shape analysis.

Pellet Size and Shape

The aim for the pellet size and shape characterization was to provide indicators that can be used to correlate the respective property with process parameters via statistical analysis. The following goals were relevant in selecting the appropriate size and shape responses:

- The evaluation of the intake speed ratio as fine-tuning parameter for the strand diameter.
- A reliable detection of changes in the average pellet size and shape for the DoE settings.
- A robust quantitative measure of the size distribution center. This will be serving as critical intermediate quality attribute, which can be related to performance in future downstream processing and used for design space definition.

With regard to the investigation of the effect of intake speed ratio on pellet diameter, a reliable measure of strand diameter was required. Therefore, Feret width (FW) and Feret thickness (FT) were investigated. In general, FW_{2D} is the minimal length perpendicular to the maximum length between two tangents at each two-dimensional (2D) projection of a particle, as shown schematically in Figure 4-4a. While the FW_{2D} value is evaluated for each single projection of a pellet, the FT value can only be determined from the sum of projections collected for each pellet during the measurement (3D data), as it is the minimum of all projection FW_{2D} values. The 3D pellet width FW is the maximum FW_{2D} value from all projections of a single particle. However, as the schematics in Figure 4-4a illustrate, the 2D pellet length and width are assigned differently by the particle sizer, depending on the ratio of the actual cylindrical height to the actual cylindrical diameter. This occurs since the particle sizer software does not recognize the orientation of the cylindrical shape and perceives the actual pellet diameter as length if it is larger than the cylindrical height. Figure 4-4b illustrates two cases of pellets, where FT and FW for a strand fragment from sample N17 do represent the diameter of the pellet, while in the projections from the pellet in N8 the diameter of the pellet is captured in FL.

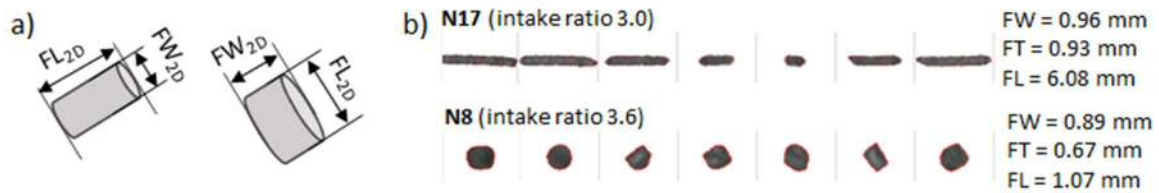

Figure 4-4. a) Illustration of Ferret dimensions of 2D projections from pellets with different proportions: Feret length FL and Feret width FW. b) Images from two selected pellets (DoE run N17 and 8, different zoom factor) taken during tumbling fall.

This occurred in several runs since the pelletizer's length setting is 0.5 mm of the pellet diameters of approx. 1 mm. As such, no parameter provided by the particle sizer can be used to evaluate the pellet diameter specifically. Thus, the effect of the intake speed ratio on the strand thickness should be assessed in future studies by measuring strand diameter before pelletization.

The other target of the pellet size, size distribution and shape characterization was to detect the effect of all other process and formulation parameters and to determine which indicators are feasible for design space definition. To that end, the median Feret length (FL) and the median projection area based equivalent diameter D_A, both were found to discriminate well between high-quality (e.g. sample N8) and low-quality pellet samples (e.g. N17). Feret dimensions and quantiles of the D_A distribution for all DoE runs are shown in Figure C-7 and Figure C-8 in the Supplemental Material section C.

Both, FL and D_A showed similar trends in the width of the distribution inside the respective samples (Figure 4-5a) and b)), while the center of the D_A distribution is at lower pellet size compared to the FL distribution.

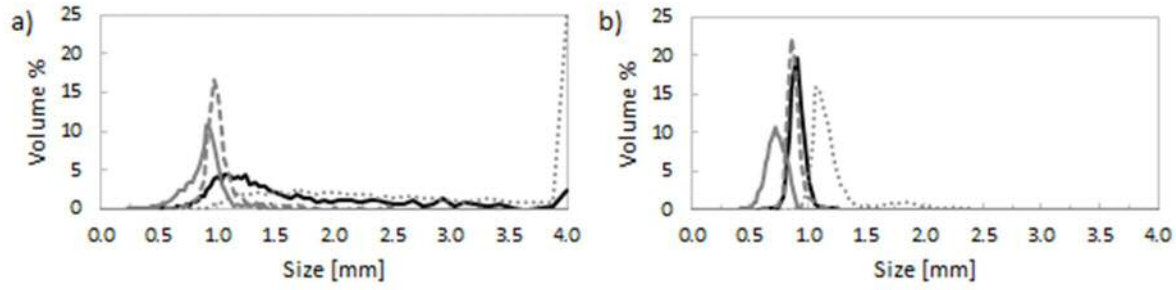

Figure 4-5. Volume distributions of particle size parameters D_A (black), FT (solid grey), FW (dashed grey) and FL (dotted grey) for samples from runs a) N17 and b) N8.

With regard to pellet shape data, both investigated shape parameters, namely sphericity and L/T ratio, showed good discrimination between the high-quality and low-quality pellets.

Pellet Size Distribution Width

PSD span (see Eq. 4-1) and uniformity index UI (Eq. 4-2) were evaluated as measures for the PSD width, a CQA of the intermediate pellets. PSD distribution data was thoroughly examined to establish reliable limits for the PSD span parameters to detect pelletization failures, i.e. strand fragments in the intermediate product. It was observed, that a span below 0.4 mm and an UI above 60% indicate presence of an unimodal pellet size distribution. Tailed or multimodal distributions were characterized by values crossing those limits. The majority of pellet samples was unimodally distributed, as shown in Figure C-9 in the Supplemental Material section C together with exemplary uni- and multimodal PSD distributions.

Since both PSD width parameters, span and UI, indicate good or poor performance in the same samples, the decision for one of these two parameters as a process and product response will be based on the quality of statistical models.

Pellet Dissolution

In pellet dissolution studies it was observed that from all pellets more than 85% of API were dissolved in less than 30 min (percentage of dissolved API at 5, 15 and 30 min for all runs shown in Figure C-10 in the Supplemental Material section C). Moreover, API content normalized dissolution profiles appeared very similar, reaching a plateau after 30 min.

To quantify similarity, $f1$ and $f2$ test values were calculated for selected dissolution profiles according to (Diaz et al., 2016). The dissolution profile from run N29 with nominal formulation and process settings was used as the reference dataset. First, the dissolution profile of pellets with the nominal formulation but produced at different process settings (N12) was selected. Then, the two most deviating dissolution profiles were included for similarity testing.

The fastest dissolution was achieved for pellets in run N2, which was performed at low throughput and low die temperature, processing the formulation with the maximal API and HPMC content. The slowest dissolution was achieved in N21, performed at a high die temperature and throughput with the formulation with lowest API content and the highest HPMC content. Since both extremes represented the formulation compositions located in the corners of the investigated formulation triangle, a dissolution from the third formulation corner composition was also selected: run N11 with the same HME processing conditions as N2. All profiles used for similarity testing are shown in Figure 4-6.

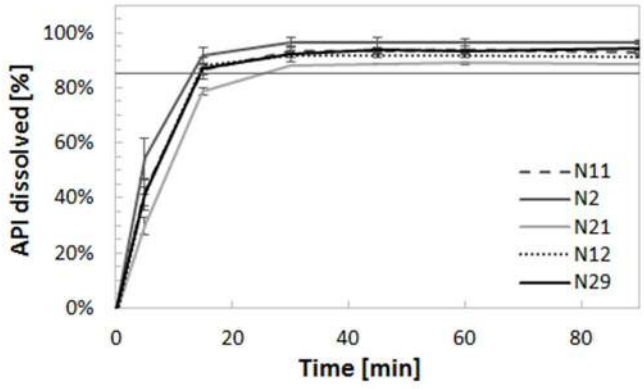

Figure 4-6. Dissolution profiles (mean ± std.dev., n=3) of nominal formulation pellets (N12 and N29) produced in different process settings and of pellets from the formulation triangle corner points (N11 – 14 wt.% NMD, 46 wt.% HPMC -, N2 – fastest dissolution, 14 wt.% NMD, 58 wt.% HPMC - and N21 – slowest dissolution - 2 wt.% NMD, 58 wt.% HPMC; N11 and N2 produced with equal HME settings, N21 with opposite combination of HME settings).

$f1$ and $f2$ values of the tested profiles are shown in Table 4-4, indicating similarity between the profiles. The highest $f1$ value was 7.87 for the dissolution profile of N21, which is well below the value of 15, ensuring sameness, according to most regulatory agencies (Diaz et al., 2016). The same conclusion was reached in the $f2$ test, where the minimal value was 99.95 (N21), which is indicating almost identical profiles (for $f2 = 100$). Since dissolution profiles were very similar, it was also not possible to generate a good statistical model for this product response. Moreover, since IR was achieved in all cases, the API release can be considered robust across the entire investigated process and even formulation space and a surface response model is thus not required for the later definition of a design space.

Table 4-4. Similarity test results for dissolution profiles of corner point (N11, N2, N21) and nominal formulation (N12) processed in different process settings, in comparison to the dissolution profile of pellets produced in the nominal center point settings (N29).

	N29	**N11**	**N2**	**N21**	**N12**
$f1$	ref.	0.88	6.05	7.87	1.60
$f2$	ref.	100.00	99.96	99.95	100.00

4.3.2. Process Limits and Product Quality Sensitivity

In this chapter statistical modeling was utilized to investigate the impact of process and formulation parameters, or combinations thereof, and specifically the degree of their potential to disturb the process. By generating response surfaces from the fitted statistical models for product responses (pellet size, PSD width and pellet shape) and stability-limiting process responses (motor load, die melt pressure), the design space were then established by imposing specific acceptance limits.

Statistical models for relevant process and pellet responses are discussed in detail below. The process responses, motor load and die melt pressure potentially limit the process stability. However, since motor load was found to take values between 20% and 60% in the DoE, it was well below the critical level of 80%. With respect to this parameter, the impact of investigated process conditions on motor load was not limiting, i.e. endangering process stability. Therefore, the statistical model is shown only in the Supplemental Material (section C IV). Pellet size, pellet shape and PSD width parameters were included to assess pelletization process and product performance.

Relevant Factors

A summary of the fitted PLS regression models and the model performance statistics can be found in the Supplemental Material section C (Table C-2 and Table C-3). Since several interactions and the factor intake speed ratio were found to be insignificant in terms of process and product performance, these factors were removed from the models.

The throughput was included in all process parameter, as well as in all pellet response models. Moreover, the formulation composition was not excluded as well from any statistical model. The interaction parameters between the formulation component fractions and the throughput were found to be significant in most process responses as well. This emphasizes the complexity of predicting process parameters mechanistically for this three-component formulation. Die temperature was significant for the die melt pressure, the die melt temperature (model not discussed but data shown in Table C-2 in the Supplemental Material section C) and the RTD parameters. Concerning the pellet size and shape parameter models, die temperature was included for both shape parameters (L/T and sphericity) and the uniformity index. For the uniformity index, also the interaction of the die temperature and throughput was improving the model when included as a factor. The same interaction was included in the model for die melt temperature, whereas all other interactions of the factor 'die temperature' were excluded from the statistical models.

Die Melt Pressure

Die melt pressure data gives a very good statistical model ($Q^2 = 0.962$, $R^2 = 0.981$). All included factors were significant (Table C-2): throughput, die temperature, formulation component fractions and the quadratic term of the NMD content. The contour plots across process and mixture parameters are

shown in Figure 4-7, where the strongly plasticizing effect of NMD on this response can be observed. Decreased viscosity of formulation compositions with high NMD and low HPMC fraction, results in lower pressure drop through the dies. EE also acts as a plasticizer in the formulation, but is plasticized itself by NMD. The contour plot across the investigated process parameter range (Figure 4-7 left) illustrates that die temperature is a feasible parameter for controlling the melt pressure in the die.

With regard to process stability, the melt pump has upper and lower boundaries for an acceptable melt pressure, which causes a process shut-down if they are crossed. The lower limit is set by the melt pressure before the melt pump (30 bar), which is a controller input variable for the pump's gear speed. Therefore, die melt pressures below 35 bar, including some safety margin, are considered critical in terms of process stability. High melt pressures are critical since the melt pressure sensor has a measurement range of up to 250 bar. If the measurement range is exceeded, the sensor membrane can be irreversibly damaged. Therefore, the acceptance limit for the melt pressure in this study was set to 150 bar.

Both limits were reached during the DoE. The upper limit was reached at the lowest throughput and die temperature, the minimum API and the maximum HPMC fraction (N20). The opposite limit was approached at a high throughput and die temperature, the maximum API and the minimum HPMC fraction (N1). Thus, this process response is highly sensitive to formulation composition changes and critical for process stability. Therefore, this parameter needs to be considered during design space definition. However, the ability of HME process and melt pump to recover from high and low pressure levels remaining just inside limits, was good, as indicated by the excellent reproducibility (0.995) of replicates (N29, N30, N31). An adequate process control strategy e.g. with appropriate alarm and action limits needs to be implemented to improve process performance in case of deviations.

Nevertheless, for the nominal formulation the process response was well inside critical limits, across the entire tested range of process settings.

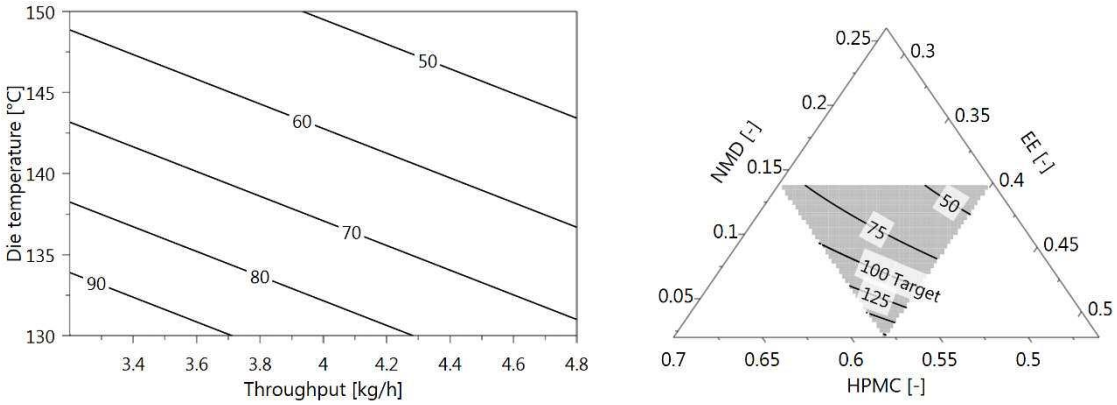

Figure 4-7. Contour plot of die melt pressure [bar] for process (left) and mixture parameters (right) (process parameter plot for nominal formulation, mixture plot for 3.2 kg/h and 140°C, intake speed ratio = 3.3 m·h/(kg·min) for both).

Pellet Size and Shape Properties

All pellet size and PSD responses, as well as L/T as a shape indicator, had skewed distributions across the DoE runs, requiring transformation of the responses (given in Table 4-3). However, some remaining skewness led to inferior statistical models compared to the process parameter models in general.

Pellet size was investigated as a CQA of the intermediate product. Two measures, i.e., the median D_A and median FL, were evaluated in statistical models, both of them showing good repeatability (0.966 and 0.988). FL yielded a slightly better model (Q^2 = 0.758, R^2 = 0.831) compared to D_A (Q^2 = 0.621, R^2 = 0.778). In both models, the throughput (mf), the formulation component fractions and the interaction terms between the throughput and each component fraction were included (Table C-3).

The significance of the interaction between the throughput and the formulation composition can be further examined if one considers strand temperatures in the pelletizer intake at various throughputs (Figure 4-8). The strand temperature measurements indicate that the main influence on this temperature is the time during which the strands are passing the cooling length between the machines (N1-N12 at 3.2 kg/h, N13 and N14 at 3.6 kg/h, N29-N31 at 4 kg/h, N15 and N16 at 4.4 kg/h and N17-N28 at 4.8 kg/h). However, the criticality of this temperature depends on the formulation composition. The formulation compositions with a high NMD content (14 wt% - dark red, red, dark orange and purple in Figure 4-8) were more prone to yield poor pelletization results at a high throughput. The formulation with 10 wt% API but a high EE content (N28), which too was highly sensitive to the throughput, is softer than the nominal formulation (yellow) as well. In contrast, N19 with a throughput of 4.8 kg/h, 6 wt% of NMD and low EE content in the melt, did not exhibit such sensitivity to the strand temperature (84°C) at the pelletizer inlet.

Differences in significant factors in the models for the two size parameters resulted in various trends of contour lines in the mixture diagram at low throughput (Figure 4-9 a) and d)). D_A indicates a main influence of NMD content on the pellet size at a low throughput. FL also has increased sensitivity to the EE content, while HPMC stabilizes it. However, the particle size prediction range and the relevance of both models at a low throughput across the different formulation compositions is significantly lower than at the highest throughput of 4.8 kg/h (in accordance with Figure 4-9 d and e). At a high throughput, median pellet size (for both parameters) depended mainly on the HPMC content, emphasizing the importance of this component in terms of mechanical stability of the strand in the intake zone of the pelletizer.

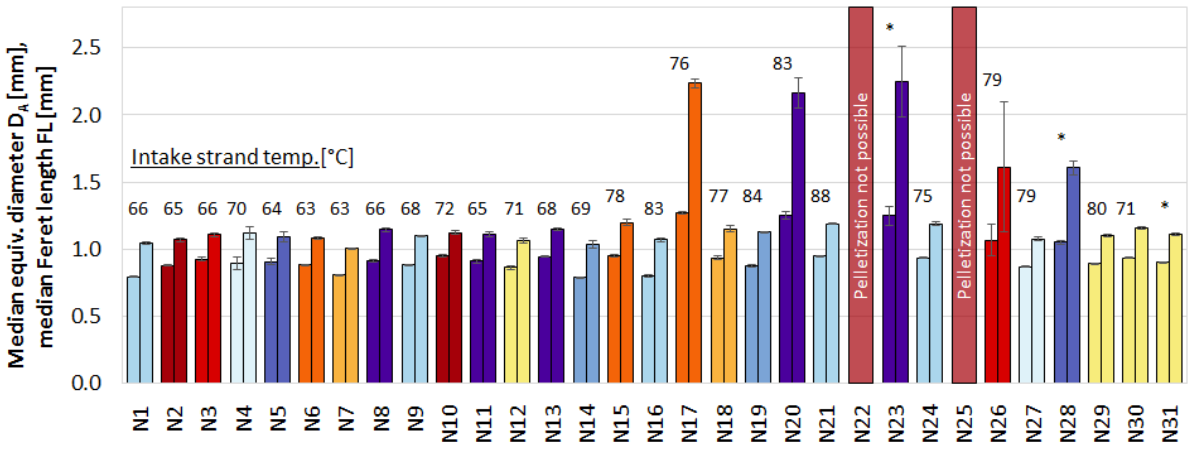

*Figure 4-8. Median pellet equivalent diameter D_A [mm] (left bar) and median pellet Ferret length FL [mm] (right bar) for all DoE runs (mean ± SD, n=4). Processing parameters and strand temperature measured in the pelletizer intake are shown as well. Colors according to formulation composition (color code see Figure 4-2). * No strand temperature data available.*

Contour plots for pellet sizes of the nominal formulation across the investigated process parameters window indicate the same trend of increasing size with an increasing throughput in both models (Figure 4-9 c) and f)). As a conclusion, throughput is the CPP affecting this critical intermediate quality attribute.

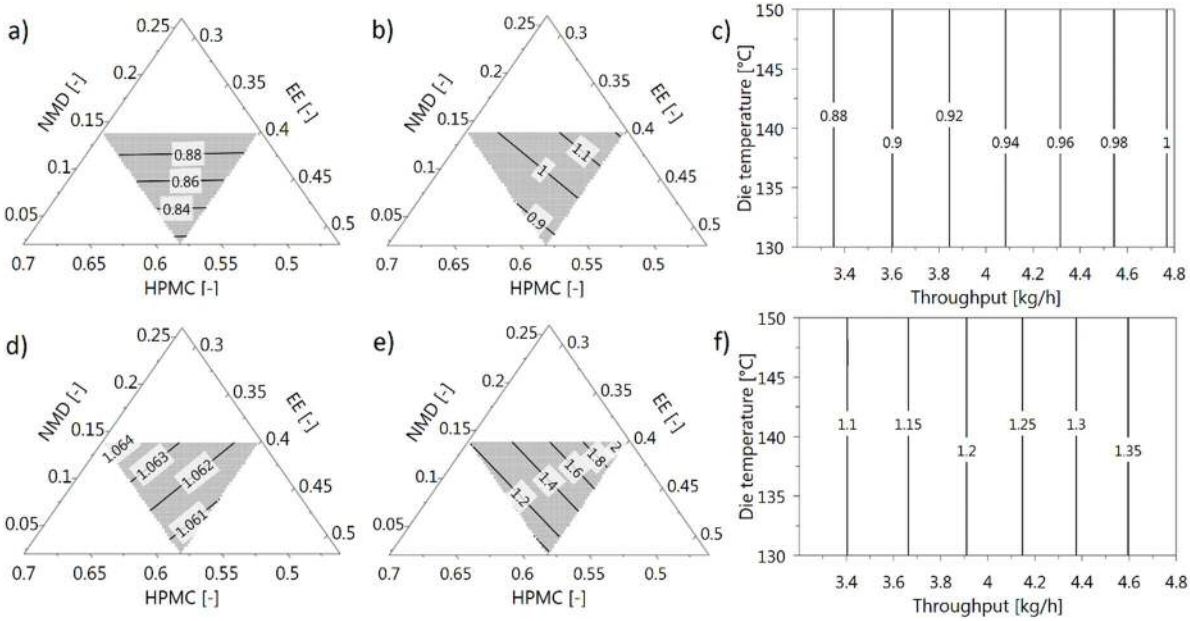

Figure 4-9. Mixture contour plots of D_A [mm] at a) 3.2 kg/h and b) 4.8 kg/h, and FL [mm] at d) 3.2 kg/h and e) 4.8 kg/h at 140°C. Process parameter contour plot of c) D_A and f) FL for nominal formulation. (Intake speed ratio = 3.3 m·h/(kg·min) for all).

Since both of the investigated size parameters offer similar conclusions regarding the effect of process parameters on the pellets, FL was chosen as the final size parameter. FL showed higher sensitivity (bigger absolute changes in the DoE) and yielded better model performance. Since the aim was to later compress the pellets into tablets, the maximum acceptable size of the pellets was chosen according to a rule of thumb for consistent die filling: the maximum dimension of a particle should be 1/10 of the tableting die diameter. For a target final tablet diameter of 8 mm, the maximum height of the

cylindrical pellet should be 0.8 mm. The maximum measurable Feret length of the corresponding cylinder (diameter D = 1 mm, height H = 0.8 mm) can be calculated as

$$FL_{max} = D\cos\alpha + H\cos\alpha \qquad \text{Eq. 4-6}$$

when oriented axially by angle α to the projection pane. The maximal FL is reached at $\alpha = 45°$, giving FL_{max} = 1.273 mm for the acceptable pellet size limit in design space definition.

Two PSD width parameters were evaluated, i.e., $span$ and UI. The limits set for both parameters ($span$ < 0.4 and UI < 60%) to distinguish between high- and low-quality products were already chosen based on the modality and skewness of the size distribution in the samples. UI and $span$ showed an excellent reproducibility ($span$: 0.967 and UI: 0.987), yielding good PLS models ($span$: Q^2 = 0.747, R^2 = 0.851 and UI: Q^2 = 0.689, R^2 = 0.880). However, while $TDie$ was not included as a factor for $span$, it was found to be significant for UI. Moreover, the interaction term of $mf * TDie$ was included for UI, resulting in different contour plots for the two responses, as shown in Figure 4-10. Since UI yielded a model with a better performance, this parameter was selected as the PSD width parameter. However, trends for the PSD width parameters as a pelletization process performance parameter were very similar to those of the pellet size evaluation.

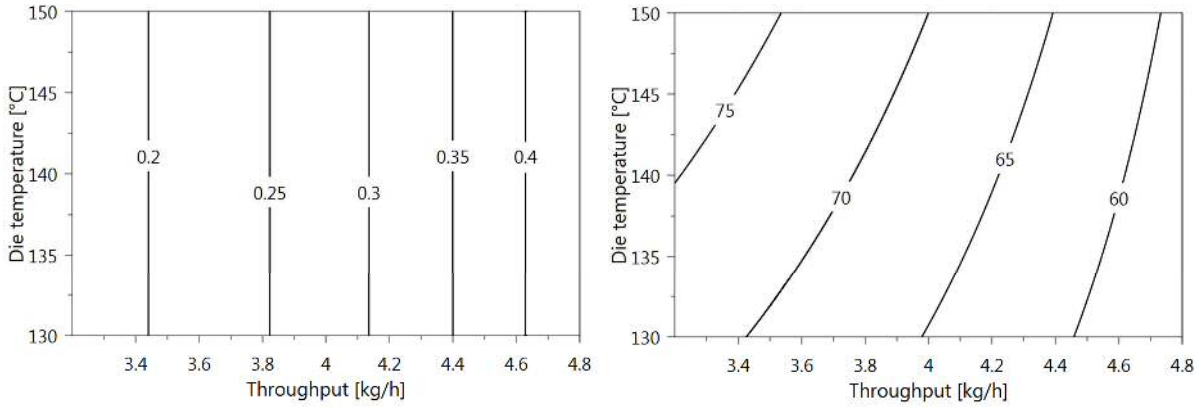

Figure 4-10. Contour plots of PSD span [mm] (left) and uniformity index [%] (UI) (right) for process parameters (nominal formulation).

Finally, the shape was evaluated using two parameters for statistical analysis, i.e., $sphericity$ and $L/T\ ratio$. The model fit for $sphericity$ was slightly better (Q^2 = 0.735, R^2 = 0.882) than for $L/T\ ratio$ (Q^2 = 0.605, R^2 = 0.767). Both responses show the same trends, with the effects of throughput, die temperature, formulation composition and interactions thereof. Since no additional insight or discrimination ability was gained by investigating these parameters in addition to FL and UI and the statistical models were of lower quality, both responses were not used further, nor as pelletization performance, neither as pellet quality indicators.

4.3.3. Design Space Definition

Information about the process stability limitations were used together with the product quality parameters to define a design space. The following critical constraints were given for this respective process and product:

- API release @ 30 min: > 85%
- Pellets size FL: < 1.273 mm
- PSD UI: > 60%
- die melt pressure: 35 -150 bar

The first two items refer to the (1) intermediate product quality, where API release was given by the requirement of IR and (2) the pellet size set to the limits acceptable for consistent die filling during subsequent tableting. The latter two points refer to the process stability limits. Process limits were assessed specifically using sweet spot analysis (shown in section V. in the Supplemental Material section C).

For the nominal formulation no HME processability limit was reached within the investigated process parameter range (Figure C-6 d in the Supplemental Material section C). The pelletization process does show a limit for processing the nominal formulation at throughput levels above 4.45 kg/h, as indicated by the PSD UI, which was used to detect strand fragments in the product.

Figure 4-11 shows the design space for various throughput and die temperature levels. The throughput limit of the design space was at 4.05 kg/h at 140°C die temperature, due to the acceptance limits in pellet size and PSD UI.

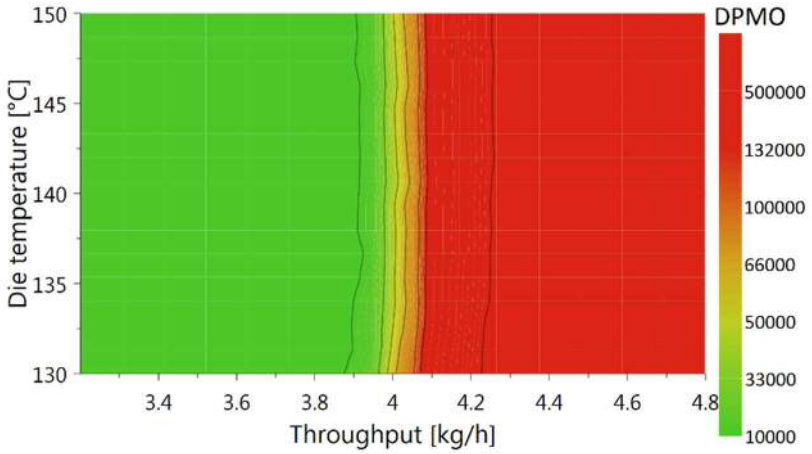

Figure 4-11. Design space for the production of immediate release pellets (nominal formulation, intake speed ratio constant at 3.3 m·h/(kg·min)) within the tested range of process parameters (DPMO level of 66,000).

The following conclusions can be drawn combining the results of product quality and process stability limit analysis:

i) If the throughput limitation is acceptable for the alignment with the downstream processes, the control action will include only a reduction but no increase of throughput.

ii) If required, the design space could be widened for higher throughputs by increasing the cooling efficiency along the given length before the pelletizer, e.g., by using a cooling channel.

iii) Investigating the design space across the mixture space (Figure 4-12 a) and b)), pellets with in-specification product performance could also be achieved at a higher throughput (4.3 kg/h shown) by slightly adapting the carrier composition. However, for this step, possible changes in the tabletability of the pellets need to be evaluated.

The set point optimization tests in MODDE indicated that the adaptation of HPMC content in the formulation to 56.4% and the die temperature to 150°C, would push the throughput limit up to 4.385 kg/h.

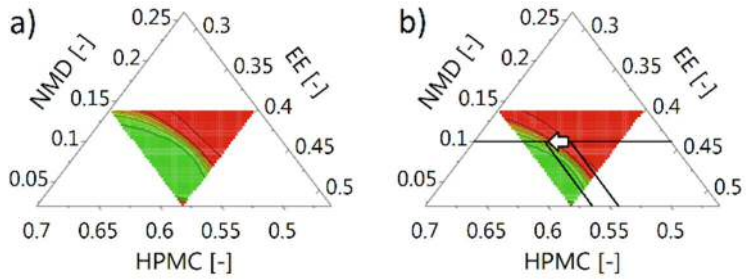

Figure 4-12. Design space for the production of intermediate release tablets with variable formulation composition at a throughput of a) 4.0 kg/h and b) 4.3 kg/h and 140°C (DPMO level of 66,000 - color code see Figure 4-11).

4.3.4. Sensitivity of Process Dynamics and API Content Monitoring

Investigation of RTD Sensitivity

RTD is an important process characteristic in CM, capturing the dynamics of the specific process. It is utilized to track the material and serves as a basis for the control strategy development (Byrn et al., 2015; Engisch and Muzzio, 2015; Rehrl et al., 2016). While the influence of HME process parameters, such as screw configuration, throughput and screw speed, on RTD has been studied extensively (Eitzlmayr et al., 2014; Gao et al., 1999; Puaux et al., 2000), the effect of pharmaceutical formulation compositions has not been duly researched. However, such effects are especially relevant if material tracking and material deviation decisions are based on RTDs.

The values of all RTD characteristics, i.e., dead time T_d, mean RT T_m and RTD standard deviation s_{RT}, are given in Table C-1 in the Supplemental Material section C. The overall variation of dead time in the DoE spans a range of 60 s to 90 s ($Q^2 = 0.623$, $R^2 = 0.886$), while mean RT and standard deviation of the RTDs range from 90 s to 160 s ($Q^2 = 0.810$, $R^2 = 0.935$) and 15 s to 40 s ($Q^2 = 0.917$, $R^2 = 0.886$), respectively. Investigating the statistical models for RTD process responses indicates that they are affected by throughput and, partially, die temperature (Figure 4-13), as well as the formulation composition and corresponding interactions (Table C-2 in the Supplemental Material section C).

The influence of throughput is represented in the statistical models by significant contributions of the factor throughput for T_m and s_{RT}, (for T_d just not significant ($p = 0.065$) for the confidence level of 95%, but with the maximal coefficient of all included factors or interactions). Concerning the effect of formulation composition however, it is actually known, that material transport efficiency of extrusion screws elements, the governing effect on RTD, does not depend on melt viscosity (Eitzlmayr et al., 2014; Eitzlmayr and Khinast, 2015). However, differences in viscoelastic properties have been shown to change the inherent volumetric flow in the free volume of the extrusion barrel by Elkouss et al. (2006). Strongly elastic contribution in the flow behavior leads to plug-flow type flow profiles. Therefore, the RTD is a function of formulation composition if elasticity of a melt is changed. In our previous work (Hörmann et al., 2018), oscillatory rheology measurements demonstrated, that the storage modulus exceeds the loss modulus when adding the 54 wt.% of HPMC to a formulation with NMD and EE.

Moreover, when comparing this study to the work of Rehrl et al. (2018), an effect of formulation composition on the appropriate structure of the transfer function to fit the tracer RTD curve was observed. In the experiments of Rehrl et al. with nominal formulation composition, a model of second order was found to fit the data well. In our study, a model structure of fourth order was required (according to Eq. 4-3) in order to capture the effect of entirely different formulation compositions on the RTD shape.

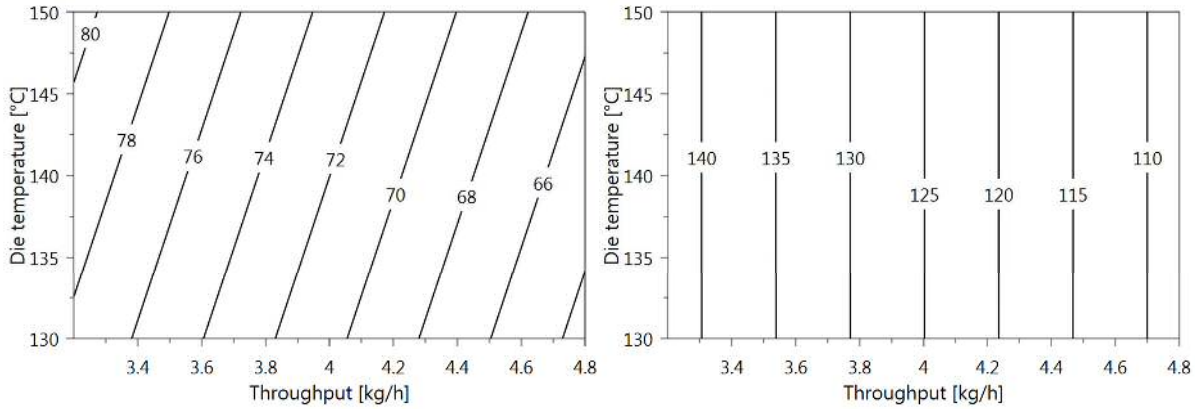

Figure 4-13. Contour plots of dead time [s] (T_d) and mean RT [s] (T_m) for process parameters (for nominal formulation).

In conclusion, the effects of throughput and die temperature need to be included into the RTD model utilized for material tracking, as well as the effect of formulation composition changes. An attempt to quantify the effect of formulation composition is taken, by comparing predictions from the surface response models for T_d and T_m at high and low HPMC and NMD content and for the nominal formulation composition (Table 4-5). The differences can be attributed to the effect of formulation composition.

Table 4-5. Comparison of dead time T_d and mean residence time T_m for equal process settings (3.2 kg/h throughput, 140°C die temperature) but different formulation compositions, as predicted from the response surface models or from measurement.

NMD fraction [-]	HPMC fraction [-]	EE fraction [-]	T_d [s]	T_m [s]
0.02	0.58	0.40	81.4	150.2
0.14	0.46	0.40	71.3	129.8
0.10	*0.54*	*0.36*	*79.1*	*142.3*
RTD measurement result (N12)				
0.10	*0.54*	*0.36*	*76.4*	*137.2*

While the effect of formulation composition on T_d is rather limited, the change in T_m is more pronounced with an increase of ~8 s in the case of lower API and higher HPMC content, and a decrease of 12.5 s in the case of higher API and lower HPMC content. However, when investigating the distance of the surface response model to the measured data, it is in the same order of magnitude as the composition based changes. Thus, this effect could be included in the definition of safety margins for start point and end point for material ejection considering measurement variability in general.

The RTD model captures the process dynamics from the extruder inlet, through the melt pump and down to the die plate holder melt channel, where the NIR probe was located. Since the pelletization process is not covered in the RTD measured, no effect of intake speed ratio is observed. However, since deviating material would be removed only after the pelletization unit, the RT of the pelletization process needs to be considered. It can be estimated via the intake speed v_{intake} and distance between

the extrusion die and the pelletizer knife (Eq. 4-7), when neglecting the pellet transfer time from the pelletizer intake into the collection vessel.

$$RT_{Pelletizer} = \frac{L_{Distance}}{v_{intake}} \qquad \textit{Eq. 4-7}$$

Transient Effects on RTD

To further investigate the sensitivity of the RTD to transient effects, Figure 4-14 shows the raw PC_1 data (as described in Section 4.2.6) of tracer experiments for the three replicates (N29, N30, N31).

The curves from the replicates exhibit some variability. While the RTDs determined in runs N29 and N31 agree well, N30 had a slightly lower lag time and a significantly narrower RTD width. Investigating the formulations processed in the extruder directly before (Table 4-2) it shows that N30 followed a DoE setting with a low API and a high HPMC content. In contrast, N31 was run at the beginning of a campaign and N29 was performed after a set point with high API content. The decreased residence times of the melt after running a formulation with a relatively high viscosity suggests that transient effects caused this deviation. Capillary rheology measurements for the nominal formulation, revealed the flow complex behavior of this melt (see section II in Supplemental Material). The viscosity data was fit by the CarPow model for highly-filled polymers (Geiger, 2009). It was observed that HPMC behaves as a filler, causing a power-law-like increase at low shear rates. This is a result of the yield point of HPMC, resulting in a lack of flow when embedded in a formulation with NMD and EE, due to the large differences in the viscosity of components. In case of HPMC content changes, zones of lower shear rate were therefore concluded to exhibit stagnant or slower traveling material at the wall. These zones, reduce the free cross section available at the melt volume flow, resulting in shorter RTs. While the extruder and the melt pump have a self-cleaning ability, there is a lack of forced flow in the interface regions, i.e., between the extruder outlet and the melt pump inlet, as well as in the melt channel from the melt pump outlet to the die plate.

This hypothesis for this origin of RTD replicate variability is supported by the work published by Rehrl et al. (2018) that addresses a soft sensor for API content in the die plate. In that work, the RTD of this respective HME process was characterized within the same throughput range of 3.2 to 4.8 kg/h but at the nominal formulation composition, showing better repeatability of replicates.

However, this demonstrates that the process dynamics are sensitive to the transient effects of formulation deviations. Therefore, a purely RTD-based approach for material tracking is not valid after formulation composition deviations to higher HPMC content for an unknown time. Thus, a second, independent measurement, such as NIR spectroscopy, should be used to determine at least the current API content after such composition deviations in real time.

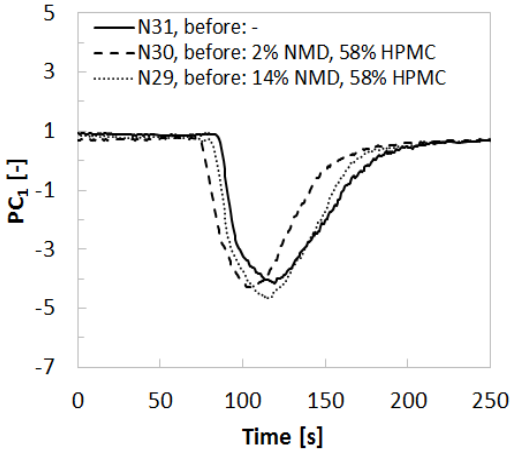

Figure 4-14. First principal components (PC_1) from tracer experiments in replicate runs N29, N30 and N3,1 indicating an effect of previously-processed formulation composition.

API Content Monitoring

A chemometric model was developed for real-time in-process API content monitoring. The model is based on the spectra collected during steady-state operation and the corresponding average API content is calculated based on the feeder data for each DoE setting. The model contained two principal components and had a good predictive power ($R^2 = 0.986$, $Q^2 = 0.981$, RMSEE = 0.533 and RMSECV = 0.608). However, the PCA score plots (Figure 4-15) of spectral variables showed that the correlation of spectra with the API content was overlaid by some correlation with the die melt pressure levels.

To refine the chemometric model, another one was developed, including time-resolved (i.e., an observation every second) and time-shifted feed-rate based API content and die melt pressure data. Time-shifting of feeder and pressure data was performed using lag-times determined by cross-correlation (time window of ±700 s) of process data and spectral data from a dynamic dataset run at 4 kg/h and a constant polymeric carrier ratio. The time-lag between API content and spectral data was cross-checked with RTD data and was in good agreement. The time-lag between spectral and melt pressure data was identified to be approximately -30 s. It was impossible to identify a physical reason for such an offset, since both sensors are located in the same axial position of the process. However, it is plausible that some negative time delay exists between the moment of the formulation change detection by the NIR probe and the change of flow resistance through the dies, which can only then be monitored by the pressure sensor. However, the half minute delay does not agree with delay times observed visually during the RTD determination using the red colored tracer.

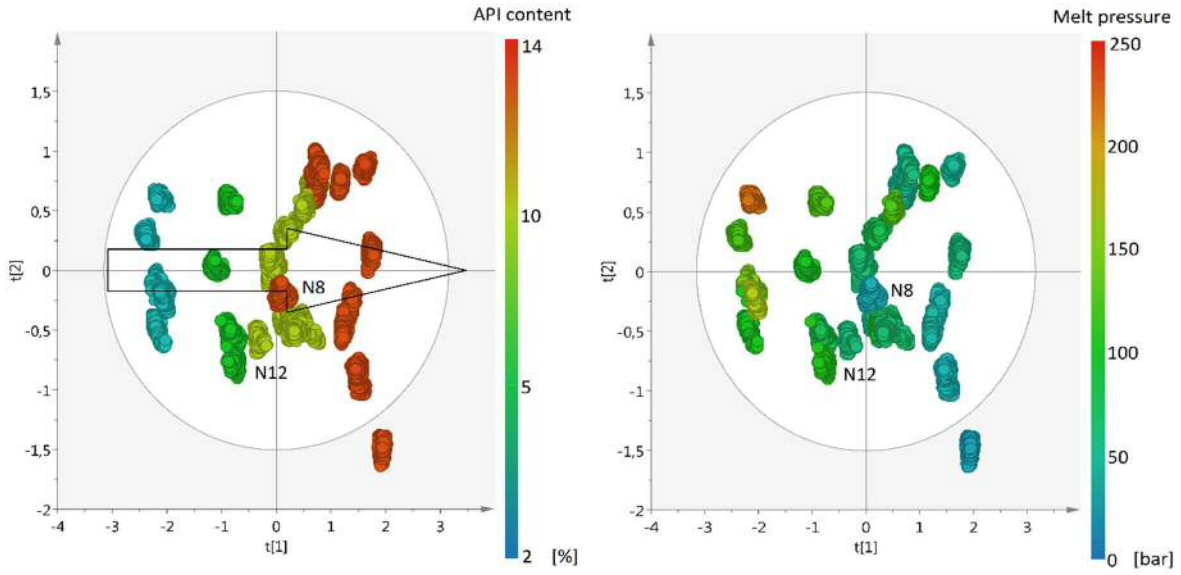

Figure 4-15. Score plots from PCA for steady-state spectral data. Left: color code according to average API content calculated from feeder data and right: color code according to average die melt pressure. Every cluster represents data belonging to one DoE setting. Clusters N8 and N12 representing an outlier due to the NIR probe window fouling.

The PLS regression of spectral variables with unit variance (UV)-scaled pressure and concentration data yielded a model with two PLS components and a good predictive power within the calibrated range (R^2 = 0.976, Q^2 = 0.969 (cross-validated), RMSEE = 0.699 and RMSECV = 0.784). The predictive performance of the model can be estimated by ±2*RMSECV ≈ ±1.6 %API. However, due to the material properties and their effect on the melt viscosity, it was impossible to completely separate the effect of material and pressure. Nevertheless, using the pressure sensor data as an additional input to the chemometric model (i.e., developing a hierarchical model on the spectral scores and the pressure data), allowed to refine the predictions in terms of RMSEE and RMSECV.

When investigating the predicted API content levels and API content as calculated based on the feeder feed rate data (Figure 4-16), especially strong deviations were observed in the cases of N12 (initially) and N8. By examining the process data collected in SIPAT for N12, the deviation in NIR predicted API content could be traced back to the process's start-up phase directly before this run. During the start-up, the API feeder was switched on for approx. 2 min after the excipient feeders. This way, the NIR probe interface was initially covered only by the carriers and afterwards not purged entirely by the more plasticized API containing melt. Therefore, the NIR process monitoring is sensitive to the HPMC fraction in the melt during process start-up. Similarly, the run processed before N8 was N25 with the same API content but the highest level of HPMC content. Even though the scattering in the API prediction and the lack of a trend over time indicate that some melt exchange must have taken place, the window fouling deteriorated the API content prediction. Thus, the state of control of this process monitoring method is again not guaranteed after formulation composition deviations to higher HPMC fractions.

Moreover, another source of uncertainty in this measurement is the effect of formulation composition on NIR sample size. The detection of lower API content may be the results of reduced sample size since the HPMC acts as a filler, increasing the melt opacity and reducing the penetration depth of the NIR. However, these effects should not deteriorate API content monitoring closely around the target formulation composition.

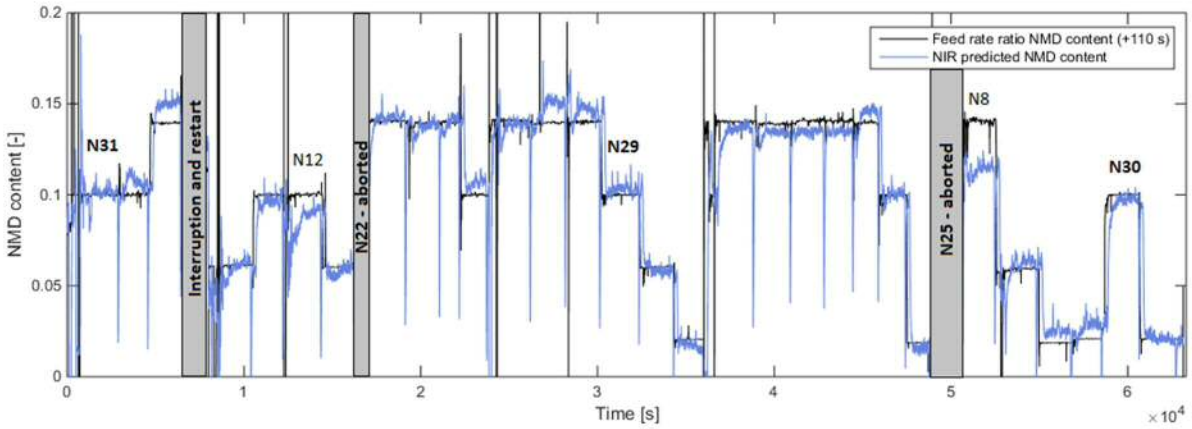

Figure 4-16. NMD content predictions based on chemometric PLS model with pressure and time resolved NMD content (calculated using the feeder data) for all DoE runs (for run order see Table 4-2). Replicates (N29, N30, N31) and runs with strongest deviations (N8, N12) labelled. The horizontal lines indicate a new start-up of process.

4.3.5. Process Control Strategy

Combining all information gained from the DoE concerning intermediate quality, process stability limits and process dynamics, a process control strategy for improving process robustness, as well as a control strategy for product quality monitoring can be developed. In general, it was possible to establish a design space for the production of pellets with nominal formulation composition, where the critical process parameter of die melt pressure, the RTD-model based material tracking and API content monitoring via NIR spectroscopy were found to perform very well in the absence of formulation deviations.

However, deviations to melts with higher HPMC fraction provoke pressure peaks potentially critical to process stability, as well as uncertainty in material tracking and NIR-based API content monitoring. Therefore, an adaptation in the process control strategy is suggested to eliminate formulation deviations to significantly higher HPMC contents: the application of feed rate control relative to the feed rate of the HPMC feeder for the two other feeders, as recently proposed by Hanson (2018). However, the dynamics of the two slave feeders and their controllers need to be well understood for this approach. A second approach to better control the risk of increased HPMC content would be the preparation of a premix of HPMC and API. By the API monitoring via NIR, the HPMC content would be indirectly monitored as well. However, a prerequisite for this approach is a stable, non-segregating blend of NMD and HPMC.

With regard to the control strategy for quality monitoring, NIR probe window fouling could be overcome by improving melt exchange in front of the probe, e.g. by decreasing the free channel volume in front of the probe as demonstrated in Wahl et al. (2013). However, this further increases the pressure drop across the extrusion die, reducing the stability window of the process.

Therefore, it is suggested to apply a soft sensor predicting current API content at the NIR probe based on the feed rate and formulation-resolved RTD model. Using this approach, steady-state offsets in the NIR spectral data, as caused by window fouling can be detected and corrected. The offset-corrected NIR data could still be used for the actual API content prediction. At the same time, a permanent comparison of spectral and soft sensor data on the time-shift from the material inlet to the NIR probe upon minor content variation allows to perform a real-time sanity check of the underlying RTD models. With this, a reduced free process volume due to stagnation in the flow channels, as observed in the replicate RTD curves in this study, can be detected.

Concerning the other CQAs of the intermediate pellets, size and size distribution were determined offline in this study, since the used particle sizer cannot handle the entire pellet throughput inline. Therefore, an at-line implementation could be done for the final manufacturing line, collecting samples on a regular basis. The measurement frequency can be low, since the main effects on size and size distribution were throughput and die temperature, both of which can be controlled well. However, since the downstream processing unit starts with a feeding process, which has been demonstrated to exhibit extensive wash-out times (Van Snick et al., 2019), deviating material forwarded to this unit may cause large amounts of rejected material. Thus, the measurement frequency could be chosen based on the size of feeder refill portions. For a refill portion of 0.5 kg, the production time is 7.5 min at 4 kg/h throughput during which sampling and at-line analysis can be performed, e.g. after 2 min for 5 s (an analysis time of ~3 min). Then, portions of the intermediate can be released to the subsequent downstream unit. In case of a pellet content or size deviations, the entire portion could be rejected by a rejection flap between the two units.

4.4. Conclusion

This study demonstrated the development of a design space and control strategy for a continuous HME and pelletization process for the production of pellets with IR for subsequent tableting. Thereby, the used formulation was challenging, since HPMC acted as a filler in the melt, resulting in complex viscoelastic properties. While a nominal set point had been identified for this process prior to this study, this work focused on the sensitivity of the product attributes, the stability limiting process state parameters and the process control tools to control actions or process deviations, i.e. feeder deviations.

HPMC content in the melt was found to be critical for process stability, as well as for the used process monitoring tools. Melt pressure limits were approached in the DoE, highlighting the need to include this process parameter in design space definition. NIR-based API content prediction was sensitive to window fouling during processing of melts with increased HPMC content. Similarly, RTD was sensitive to a reduction of free process volume due to flow stagnation on the channel walls in the absence of forced flow. To overcome the sensitivity of the whole process towards an increased HPMC content, a tight relative feed rate control between the HPMC feeder and the other two feeders, for NMD and EE, is recommended. Moreover, a combined approach of NIR and previously parameterized soft sensors was suggested to improve the robustness of the product quality control strategy.

With regard to the pelletization process, sensitivity to increased throughput levels was observed, due to a too-short cooling time before the pelletizer intake and cutting zone. Potential improvement can be achieved by using a strand cooling system between the HME and pelletization unit. The pelletizer's performance was directly related to the CQAs of the intermediate pellets: the pellet size and the size distribution width. However, the excellent robustness of the CQA of pellet dissolution performance highlights the benefit of a well-designed formulation. The design space for producing pellets of the nominal formulation and the current process setup was established in a throughput range of 3.2 to 4.05 kg/h, regardless of die plate temperature between 130 and 150°C. However, the design space could be widened by adjusting the carrier composition slightly (to a HPMC content of 56.4% in the formulation compensating the increased strand temperature at the pelletizer intake). This could be feasible, if the process has to be run at higher throughput, e.g., to fill up buffers to maintain a continuous operation of the downstream tableting unit.

Overall, this study emphasized the need to thoroughly understand the interplay of process and formulation parameters for guaranteeing a robust process performance. However, it also highlights that for continuous processes it is possible to gain deep process understanding and insight by performing a very compact set of experiments. All 31 DoE runs were performed within five working days, with real-time monitoring of process and partially also product quality data. This demonstrates

the ability of CM processes to speed up process development and time-to-market for new drug products.

4.5. References

Almaya, A., De Belder, L., Meyer, R., Nagapudi, K., Lin, H.R.H., Leavesley, I., Jayanth, J., Bajwa, G., DiNunzio, J., Tantuccio, A., Blackwood, D., Abebe, A., 2017. Control Strategies for Drug Product Continuous Direct Compression-State of Control, Product Collection Strategies, and Startup/Shutdown Operations for the Production of Clinical Trial Materials and Commercial Products. J. Pharm. Sci. 106, 930–943.

British Pharmacopoeia, 2009. British Pharmacopoeia (2009).

Byrn, S., Futran, M., Thomas, H., Jayjock, E., Maron, N., Meyer, R.F., Myerson, A.S., Thien, M.P., Trout, B.L., 2015. Achieving Continuous Manufacturing for Final Dosage Formation: Challenges and How to Meet Them May 20–21 2014 Continuous Manufacturing Symposium. J. Pharm. Sci. 104, 792–802.

Crowley, Michael M., Z.F., 2007. Pharmaceutical Applications of Hot-Melt Extrusion: Part I. Drug Dev. Ind. Pharm. 33, 909–926.

Desai, P.M., Hogan, R.C., Brancazio, D., Puri, V., Jensen, K.D., Chun, J.-H.H., Myerson, A.S., Trout, B.L., 2017. Integrated hot-melt extrusion – injection molding continuous tablet manufacturing platform: Effects of critical process parameters and formulation attributes on product robustness and dimensional stability. Int. J. Pharm. 531, 332–342.

Diaz, D.A., Colgan, S.T., Langer, C.S., Bandi, N.T., Likar, M.D., Van Alstine, L., 2016. Dissolution Similarity Requirements: How Similar or Dissimilar Are the Global Regulatory Expectations? AAPS J. 18, 15–22.

Eitzlmayr, A., Khinast, J., 2015. Co-rotating twin-screw extruders: Detailed analysis of conveying elements based on smoothed particle hydrodynamics. Part 1: Hydrodynamics. Chem. Eng. Sci. 134, 861–879.

Eitzlmayr, A., Koscher, G., Reynolds, G., Huang, Z., Booth, J., Shering, P., Khinast, J., 2014. Mechanistic Modeling of Modular Co-Rotating Twin-Screw Extruders. Int. J. Pharm.

Elkouss, P., Bigio, D.I., Wetzel, M.D., Raghavan, S.R., 2006. Influence of Polymer Viscoelasticity on the Residence Distributions of Extruders. AICHE J. 52, 1451–1459.

Engisch, W., Muzzio, F., 2015. Using Residence Time Distributions (RTDs) to Address the Traceability of Raw Materials in Continuous Pharmaceutical Manufacturing. J. Pharm. Innov. 64–81.

Engisch, W.E., Muzzio, F.J., 2014. Loss-in-Weight Feeding Trials Case Study: Pharmaceutical Formulation. J. Pharm. Innov. 10, 56–75.

Gao, J., Walsh, G.C., Bigio, D., Briber, R.M., Wetzel, M.D., 1999. Residence-Time Distribution Model for Twin-Screw Extruders. AiChE J. 45, 2541–2549.

Geiger, K., 2009. A New Heuristic Flow Law, in: 21. Stuttgarter Kunststoff-Kolloqium 2009. Stuttgart, pp. 1–15.

Ghebremeskel, A.N., Vemavarapu, C., Lodaya, M., 2007. Use of surfactants as plasticizers in preparing solid dispersions of poorly soluble API: selection of polymer-surfactant combinations using solubility parameters and testing the processability. Int. J. Pharm. 328, 119–29.

Gryczke, A., Schminke, S., Maniruzzaman, M., Beck, J., Douroumis, D., 2011. Development and evaluation of orally disintegrating tablets (ODTs) containing Ibuprofen granules prepared by hot melt extrusion. Colloids Surf. B. Biointerfaces 86, 275–84.

Grymonpré, W., De Jaeghere, W., Peeters, E., Adriaensens, P., Remon, J.P., Vervaet, C., 2016. The impact of hot-melt extrusion on the tableting behaviour of polyvinyl alcohol. Int. J. Pharm. 498, 254–262.

Hanson, J., 2018. Control of a system of loss-in-weight feeders for drug product continuous manufacturing. Powder Technol. 331, 236–243.

Hörmann, T.R., Jäger, N., Funke, A., Mürb, R.-K., Khinast, J.G., Paudel, A., 2018. Formulation Performance and Processability Window for Manufacturing a Dual-Polymer Amorphous Solid Dispersion via Hot-Melt Extrusion and Strand Pelletization. Int. J. Pharm. 553, 408–421.

Hughey, J.R., Keen, J.M., Miller, D.A., Brough, C., McGinity, J.W., 2012. Preparation and characterization of fusion processed solid dispersions containing a viscous thermally labile polymeric carrier. Int. J. Pharm. 438, 11–19.

International Conference on Harmonisation of Technical Requirements for Registration of Pharmaceuticals for Human Use, 2009. Pharmaceutical Development Q8(R2). ICH Harmon. Tripart. Guidel.

Jaeghere, W. De, Beer, T. De, Bocxlaer, J. Van, Remon, J.P., Vervaet, C., 2015. HOT-MELT EXTRUSION OF POLYVINYL ALCOHOL FOR ORAL IMMEDIATE RELEASE APPLICATIONS. Int. J. Pharm. 492, 1–9.

Khinast, J.G., Baumgartner, R., Roblegg, E., 2013. Nano-extrusion: A One-Step Process for Manufacturing of Solid Nanoparticle Formulations Directly from the Liquid Phase. AAPS PharmSciTech.

Kruisz, J., Rehrl, J., Sacher, S., Aigner, I., Horn, M., Khinast, J.G., 2017. RTD modeling of a continuous dry granulation process for process control and materials diversion. Int. J. Pharm. 528, 334–344.

Kulka, C., Duretek, I., Gonzalez-Gutierrez, J., Holzer, C., 2018. Rheology of Highly Filled Polymers, in: Rivera-Armenta, J.L., Salazar Cruz, B.A. (Eds.), Polymer Rheology. Intech Open, pp. 153–173.

LaFountaine, J.S., Prasad, L.K., Brough, C., Miller, D.A., McGinity, J.W., Williams, R.O., 2016. Thermal Processing of PVP- and HPMC-Based Amorphous Solid Dispersions. AAPS PharmSciTech 17, 120–132.

Lee, S.L., O'Connor, T.F., Yang, X., Cruz, C.N., Chatterjee, S., Madurawe, R.D., Moore, C.M. V, Yu, L.X., Woodcock, J., 2015. Modernizing Pharmaceutical Manufacturing: from Batch to Continuous Production. J. Pharm. Innov. 10, 191–199.

Meier, R., Thommes, M., Rasenack, N., Moll, K.P., Krumme, M., Kleinebudde, P., 2016. Granule size distributions after twin-screw granulation – Do not forget the feeding systems. Eur. J. Pharm. Biopharm. 106, 59–69.

Patwardhan, K., Asgarzadeh, F., Dassinger, T., Albers, J., Repka, M.A., 2015. A quality by design approach to understand formulation and process variability in pharmaceutical melt extrusion processes. J. Pharm. Pharmacol. 67, 673–684.

Puaux, J., Bozga, G., Ainser, A., 2000. Residence time distribution in a corotating twin-screw extruder. Chem. Eng. Sci. 55, 1641–1651.

Rehrl, J., Karttunen, A.-P., Nicolaï, N., Hörmann, T., Horn, M., Korhonen, O., Nopens, I., Beer, T. De, Khinast, J.G., 2018. Control of Three Different Continuous Pharmaceutical Manufacturing Processes: Use of Soft Sensors. Int. J. Pharm. 543, 60–72.

Rehrl, J., Kruisz, J., Sacher, S., Khinast, J., Horn, M., 2016. Optimized continuous pharmaceutical manufacturing via model-predictive control. Int. J. Pharm. 510, 100–115.

Reitz, E., Podhaisky, H., Ely, D., Thommes, M., 2013. Residence time modeling of hot melt extrusion processes. Eur. J. Pharm. Biopharm. 85, 1200–1205.

Roblegg, E., Jäger, E., Hodzic, A., Koscher, G., Mohr, S., Zimmer, A., Khinast, J., 2011. Development of sustained-release lipophilic calcium stearate pellets via hot melt extrusion. Eur. J. Pharm. Biopharm. 79, 635–45.

Roth, W.J., Almaya, A., Kramer, T.T., Hofer, J.D., 2017. A Demonstration of Mixing Robustness in a Direct Compression Continuous Manufacturing Process. J. Pharm. Sci. 106, 1339–1346.

Schenck, L., Troup, G.M., Lowinger, M., Li, L., McKelvey, C., 2010. Achieving a Hot Melt Extrusion Design Space for the Production of Solid Solutions. Chem. Eng. Pharm. Ind. 819–836.

Van Snick, B., Kumar, A., Verstraeten, M., Pandelaere, K., Dhondt, J., Di Pretoro, G., De Beer, T., Vervaet, C., Vanhoorne, V., 2019. Impact of material properties and process variables on the residence time distribution in twin screw feeding equipment. Int. J. Pharm. 556, 200–216.

Wahl, P.R., Treffer, D., Mohr, S., Roblegg, E., Koscher, G., Khinast, J.G., 2013. Inline monitoring and a PAT strategy for pharmaceutical hot melt extrusion. Int. J. Pharm. 455, 159–68.

Zheng, X., Yang, R., Tang, X., Zheng, L., 2007. Part I: Characterization of Solid Dispersions of Nimodipine Prepared by Hot-Melt Extrusion. Drug Dev. Ind. Pharm. 33, 791–802.

5. Tableting Formulation Development for the Compression of Elastic Hot-Melt Extruded Pellets[3]

Tableting remains a benchmark for new technologies in the manufacturing of oral solid dosage forms, due to excellent patient compliance, cost efficiency and the dominance of tableting equipment in industry. Thus, intermediates prepared by hot-melt extrusion (HME) need to be successfully formulated into tablets, in order to consider HME a platform technology. This study aims to develop a tableting formulation for compressing cylindrical HME pellets into mechanically stable tablets. Thereby, a final dose strength of 10 mg and an immediate release (IR) profile of the poorly water-soluble compound, nimodipine (NMD), was targeted. Additionally, the formulation should allow to process 4 kg/h of pellets on a rotary tablet press, as the tableting process was developed as part of a continuous manufacturing line.

In a first step, the mechanical properties of the pure pellet bed, as well as the binders, Avicel® PH101 (PH101), Avicel® PH102 (PH102) and Kollidon® VA64 (PVP/VA) were characterized on a compaction simulator. Heckel plots and compactability, tabletability and compressibility (CTC) profiles revealed the soft and elastic nature of the NMD-pellets. The pure pellets formed compacts due to solid bond formation, resulting in a lack of disintegration performance. PH102 was selected as the most promising external excipient for the preparation of binary blends. Deformation and disintegration characterization at different pellet fractions showed that PH102 was able to improve mechanical strength and the disintegration of the compacts. Nevertheless, disintegration was still too slow and a disintegrant, Kollidon® CL (K-CL) was added to the formulation.

The optimization of this adapted formulation and determination of the best tableting parameters was performed on a laboratory rotary tablet press. A design of experiments (DoE) was performed to screen the effect of the formulation components systematically, using different compression force settings. The formulation composition was varied in a range of 40 wt.% to 60 wt.% for PH102 and 0 to 20 wt.% for K-CL. Tablet mass uniformity, hardness, friability and disintegration time data was analyzed. Eventually, it was possible to identify the best formulation composition at a pellet fraction of 40 wt.% in 49.5 wt.% PH102, 10 wt.% K-CL and 0.5 wt.% magnesium stearate, providing IR of NMD and acceptable mechanical tablet strength.

[3] This chapter contains data from a Master's Thesis (Fölzer, 2017) which was co-supervised by the author of this doctoral thesis. Moreover, it is currently prepared for publication in the International Journal of Pharmaceutics.

5.1. Introduction

The vast majority of all oral dosage forms are tablets, since they are the first choice for patients and manufacturers (Ghebre-Sellassie, 1994). Yet, active pharmaceutical ingredients (APIs) frequently need to be modified prior to tableting to enhance or tailor drug release. Poorly soluble APIs are therefore typically pre-processed to enhance bioavailability, e.g. by preparing amorphous solid dispersions (ASD). Hot-melt extrusion (HME), is a technology to generate ASDs with improved bioavailability by embedding the API in a polymeric carrier. Moreover, HME has the advantage of being an inherently continuous process. Continuous manufacturing (CM) is considered to accelerate process development by reducing scale-up effort, to provide increased efficiency at steady-state operation and it facilitates the application of in-line quality control (Breitenbach, 2002).

In the majority of cases, the extruded material is (cryo-)milled prior to tableting (Agrawal et al., 2016; Boersen et al., 2014; Iyer et al., 2013; Jijun et al., 2010; Mohammed et al., 2012). However, it is not possible to perform this process step continuously, whereas pelletization allows to continuously produce HME intermediates. Moreover, the preparation of tablets from pellets, that is the preparation of a multiple unit pellet system (MUPS), has several biopharmaceutical advantages (Abdul et al., 2010; Bhad et al., 2010; Bodmeier, 1997; Dukić-Ott et al., 2009). Compared to monolithic tablets, disintegration of MUPS into pellets shortens the transit time in the stomach, providing a faster onset of the therapeutic effect, and better distribution of the API in the gastrointestinal (GI) tract. The distribution effect reduces the risk of mucosal irritation and recrystallization of poorly water-soluble APIs.

From a quality-by design (QbD) perspective, it is crucial to understand, how critical product quality attributes (CQAs) are related to critical material attributes (CMAs) of the raw materials and the critical process parameters (CPPs) (FDA, 2004). The quality target product profile (QTPP) summarizes the requirements, e.g. regarding tablet appearance, potency, identity of the API (i.e. crystalline polymorph or amorphous API), uniformity of dosage units, dissolution performance, as well as mechanical tablet strength. If HME pellets are used for tablet compression, some of these properties are already fixed by the properties of the pellets. The dissolution profile for example, is primarily determined by the ASD and the size of the pellets, as long as a fast tablet disintegration can be achieved. However, other CQAs, such as the uniformity of dosage units (UDU) and the mechanical tablet strength, that is the tensile strength and friability, are determined by the tableting formulation and process.

With regard to the UDU, the excellent flowability of pellets is beneficial. However, there is an increased risk of segregation when compressing pellets with powder-sized excipients. Moreover, pellet size determines the achievable content and weight uniformity, since large pellets exhibit a higher relative influence on total API content and weight of the tablet (Beckert et al., 1998). There are three

approaches to control segregation and variability in content uniformity: i) the use of slightly cohesive, fibrous excipients, such as Avicel® PH101 (Wagner et al., 2000, 1999), ii) the use of pellet volume fractions in the range of 30% to form percolation clusters with minimum segregation tendency (Beckert et al., 1998), and iii) the use of granulated excipients with a particle size similar to that of the pellets (Beckert et al., 1998). All the approaches have positive and negative effects e.g. on maximum achievable drug load, die filling consistency and mechanical tablet strength. Thereby, the granulation of excipients is the least preferred option, since an additional process step is needed and the granulated excipients could reduce tablet strength by a reduction of bonding sites in the compact (Lundqvist et al., 1997).

One of the main critical aspects in tablet compression of HME pellets, is the achievable mechanical strength of the tablets. HME processed materials have been exposed to high temperature and pressure, resulting in dense products with low molecular mobility. This is beneficial for the generation of stable ASDs, but causes a lack of further densification ability upon tablet compression (Iyer et al., 2013; Young et al., 2005). Moreover, the glassy state, or an increasing amorphous content of HME products have been reported to cause problematic compressibility. Thus, it is understood that decreased tensile strength is observed for tablets with a high content of HME processed materials, milled as well as pelletized (Agrawal et al., 2016; Boersen et al., 2014; Démuth et al., 2015; Grymonpré et al., 2016; Young et al., 2005). However, even though there is a limited amount of polymers available for preparing ASDs via HME, there is a lack of literature on intrinsic deformation characteristics of these polymers. Appropriate tableting formulations, compensating for the properties of the HME-processed intermediates therefore need to be developed empirically.

Extruded intermediates have been formulated using binders and fillers such as microcrystalline cellulose (MCC), lactose, mannitol, polyvinylpyrrolodine/vinyl acetate copolymers (PVP/VA) and anhydrous dicalcium phosphate (DCP) (Agrawal et al., 2016, 2013; DiNunzio et al., 2012; Feng et al., 2012; Gryczke et al., 2011; Jijun et al., 2011). Thereby, especially MCC has been reported to provide good tablet strength, due to its superior ability to form compacts by plastic deformation. Disintegrants tested in combination with HME intermediates were cross-linked polyvinylpyrrolidone (Kollidon® CL, K-CL), croscarmellose sodium and sodium starch glycolate (Agrawal et al., 2016, 2013; Gryczke et al., 2011; Jijun et al., 2010). A thorough investigation of the effect of disintegrants upon compression with milled ASD extrudates, was published by Gryczke, highlighting the excellent performance of K-CL in terms of disintegration and tablet strength (Gryczke et al., 2011).

The aim of this study was to identify a tableting formulation for the compression of cylindrical pellets to mechanically stable tablets in a CM line. For an integration of the tableting process in the line, it had to be aligned with the upstream HME-pelletization unit, or specifically with its pellet production rate

of 4 kg/h. The produced pellets contained an ASD of a poorly water-soluble API, nimodipine (NMD), in HPMC E5 and Eudragit® E, providing an IR dissolution profile. In order to provide IR also from the final tablets, fast tablet disintegration was desired.

In a first step, pellets and selected binders, that is Avicel® PH101 (PH101), Avicel® PH102 (PH102) and Kollidon® VA64 (PVP/VA), were compressed on a compaction simulator to characterize their deformation behavior. Heckel parameters, compactability, tabletability and compressibility (CTC) profiles, as well as the disintegration performance of the compacts from pure pellets were determined. The excipient expected to compensate best for the limitations of pellets, in terms of tabletability and disintegration, was selected for the preparation of binary mixtures. Deformation behavior and disintegration performance of binary blends with different pellet fractions were characterized to gain understanding on the contribution of each component on tablet quality. Finally, the formulation was further adapted by adding a disintegrant, Kollidon® CL (K-CL), and transferred to a laboratory rotary tablet press.

In the second step, different formulation compositions were screened on the rotary tablet press, applying a design of experiments (DoE). The effect of formulation composition on tablet quality attributes, such as mass uniformity, tensile strength, friability and disintegration was determined. Sweet spot analysis eventually yielded an optimal formulation composition, for the production of tablets with desired properties. Concluding, an experimental run using the optimal tablet composition and selected compression settings was performed to validate the statistical models.

5.2. Materials and Methods

5.2.1. Used Materials

The pellets used in this work were produced from the nominal formulation composition and at the nominal set point of the HME-pelletization process described in Chapters 3 and 4. The pellets comprise 10 wt.% of nimodipine (NMD), 54 wt.% of Methocel™ E5 (HPMC) and 35 wt.% Eudragit® E (EE), which were supplied by Bayer (Germany), Dow Chemicals (USA) and Evonik AG (Germany). In order to remove dust and to agglomerates, the pellets were sieved, using 800 and 1200 µm sieves. The fraction between the sieves was further used. Since NMD is light sensitive, pellets and pellet blends were stored protected from light.

The Heckel parameters and compression characteristics of a wide range of binders/fillers were examined in a master's thesis (Fölzer, 2017) (as part of this project), in order to investigate the effect of excipients with different deformation behavior, when compressed with the NMD-pellets. This work at hand, shows only data from the most relevant binders: Avicel® PH101 (PH101) and Avicel® PH102 (PH102) (both FMC BioPolymer, USA) and Kollidon® VA64 (PVP/VA) (BASF, Germany). Methocel™ E5 (HPMC) (Dow Chemical, USA) was characterized as well, in order to understand the deformation properties of the neat polymer making up the main fraction of the HME pellets. Kollidon® CL (K-CL) (BASF, Germany) was used as disintegrant in the formulation screening and magnesium stearate (MgSt) (Sigma-Aldrich, Chemicals Company, USA) was added for tablet press lubrication.

5.2.2. Blend Preparation

All blends were prepared in a tumble blender (Turbula® T2F Shake Mixer, WAB) at a speed of 75 rpm. Binary blends for the characterization of deformation properties were prepared at pellet volume fractions of 30, 50 and 70 vol.% using a blending time of 10 min. Blend preparation for the formulation screening DoE was performed using 1 kg portions of each formulation and two blending steps to avoid over-lubrication: first, all components, except MgSt, were blended for 10 min and subsequently, 0.5 wt.% of MgSt were added for another 1 min of blending at 75 rpm.

5.2.3. Tableting Equipment

Investigations on deformation characteristics of raw materials and binary blends were carried out on a compaction simulator Stylcam 200R (Medelpharm, France), using round, flat-faced 8 mm punches (Natoli, USA). Formulation optimization was executed on a laboratory rotary press Fette 102i with eight punch stations and round, flat-faced EU1" punches with 8 mm diameter (Fette Compacting, Germany).

The data from compaction simulation was exported from the machine software and evaluated in Excel (Microsoft, USA). Process data from the rotary press Fette 102i was collected via a process analytical technology (PAT) software solution SIMATIC SIPAT 4.0 (Siemens, Germany), pre-processed in Excel and used for statistical evaluation in MODDE 11 (Umetrics, Sweden).

5.2.4. Excipient, Pellet and Tablet Characterization

Particle Size and Size Distribution

Particle size of PH101, HPMC and MgSt was determined using the HELOS/KR laser diffraction system (Sympatec, Germany) and the size of PH102 and K-CL with the QICPIC image analysis system (Sympatec, Germany), both particle sizers were equipped with a RODOS/L dispersion unit (Sympatec, Germany). The size of unsieved pellets was determined using the PartAn^{3D} image analyzer (Microtrac, USA). From both systems, the median volume-equivalent diameter d_{50} and the particle size distribution (PSD) $span = (d_{90} - d_{10})/d_{50}$ were determined. The sphericity of pellets was 0.92.

Density Measurements

True density (n=3, AccuPyc1340, Micromeritics, Germany) and initial bulk density and porosity in the compaction simulator die (for a mass of approx. 200 mg) were used to determine the relevant characteristics for Heckel analysis (Table 5-1). The true density $\rho_{true,M}$ of binary mixtures (with components *A* and *B)* was calculated according to Eq. 5-1. Therein, the component true densities are given by $\rho_{true,A}$ and $\rho_{true,,}$, and φ_A and φ_B are the respective volume fractions.

$$\rho_{true,M} = \rho_{true,A} \cdot \varphi_A + \rho_{true,B} \cdot (1 - \varphi_A) \qquad \text{Eq. 5-1}$$

Table 5-1 True density ρ_{tr} (mean, n=3), initial bulk density $\rho_{b,0}$, initial porosity ε_0, particle size and PSD span of used materials.

Substance	True density ρ_{tr} [g/cm³]	Bulk density $\rho_{b,0}$ [g/cm³]	Initial porosity ε_0 [-]	Size d_{50} [µm]	PSD $span$ [-]
PH101	1.562 ± 0.001	0.28	0.82	60.80	1.73
PH102	1.563 ± 0.003	0.31	0.80	136.88	1.86
PVP/ VA	1.201 ± 0.000	0.33	0.72	85.26	1.83
HPMC E5	1.284 ± 0.000	0.33	0.74	91.07	1.43
NMD-pellets	1.204*	0.55	0.54	908**	0.24**
K-CL	1.234 ± 0.001	n.d.	n.d.	117.56	1.41
MgSt	1.085 ± 0.002	n.d.	n.d.	7.66	2.92

* True density calculated from pvT-data determined in Chapter 4. ** Determined for unsieved pellets.

Tablet Mass Uniformity and Mechanical Tablet Strength

Tablet weight was determined using an analytical balance directly after tablet compression and the tablets stored for at least 72 h prior to further analysis. After full elastic recovery, tablet height was measured using a micrometer caliper (Mitutoyo, Japan). Tablet hardness (i.e. resistance to crushing) and diameter were determined using a PTB 311E Hardness Tester (Pharma Test, Germany) in diametral compression tests. For the compaction simulator experiments all tablets were characterized. For the formulation screening DoE, ten tablets (n=10) were used for determining mass, dimensions and hardness at each set point.

Tablet friability was investigated for 6.5 g of tablets for samples from the formulation screening DoE. Tests were performed in a PTF 10E Friability Tester (Pharma Test, Germany) using 100 rounds, according to Ph.Eur. 2.9.7. (European Pharmacopoeia Commission, 2014).

Tablet Disintegration

Tablets prepared for compaction analysis, were compressed at three distinct compression force levels (5, 10 and 15 kN), in order to investigate the effect of excipient fraction and compression force on tablet disintegration. Disintegration testing was performed according to Ph. Eur. 2.9.1. (European Pharmacopoeia Commission, 2014), using a PTZ-S Single Basket Tablet Disintegration Tester with sinker disks (Pharma Test, Germany) and testing six tablets (n=6) at a time in water at a temperature of 37°C.

Tablet Dissolution

Tablet dissolution performance was determined for tablets from the finally selected formulation, produced in the final validation run. Dissolution testing (n=3) was performed in sink conditions using a USP II apparatus (DT820LH Dissolution Tester, Erweka, Germany) with 100 rpm paddle speed and 500 mL of sodium acetate buffer with pH 4.5 ± 0.1 and 0.3% sodium lauryl sulfate (SLS) at 37°C. Samples of 1.5 mL were collected automatically at 0, 5, 15, 30, 45, 60 and 90 min and filtered through 0.10 µm poroplast filters. The dissolved API concentration in the dissolution medium over time was determined via UV/Vis spectroscopy (Lambda 950, PerkinElmer, USA). Absorbance measurements were carried out in 10 mm polymethyl methacrylate (PMMA) semi-micro cuvettes at 360 nm against pure dissolution medium from the same vessel.

For direct comparison of tablet and pellet dissolution profile, the profiles were normalized using an API content according to the target pellet fraction in the tablets and 10 wt.% API content in the pellets.

Compaction Analysis

Tablets of approx. 200 mg were prepared on the compaction simulator by filling the die manually, using pre-set filling heights. The filling heights were adjusted based on the initial bulk density of each material or blend. No pre-compression was used and tableting was performed at a tableting speed

setting of 25 tablets per minute (165 mm/s compression rate). Main compression forces between 5 to 20 kN were used for preparing 12 to 15 tablets, and another 12 to 15 tablets were prepared in a force range below 5 kN for out-of-die Heckel analysis. Heckel plots for pellets, selected excipients were generated from in-die as well as from out-of-die data. For binary blends, only in-die Heckel plots were produced. Moreover, CTC profiles were determined for all materials and binary blends. Further details on the influence of compression speed on the tableting parameters and from a wider range of excipients and binary blends can be found in (Fölzer, 2017).

In-Die Compaction Analysis

The punch distance data $d(F)$ reported by the compaction simulator software was corrected for machine deformation, using Eq. 5-2. Therein, d_{corr} is the corrected distance between upper and lower punch in [mm] and F the compression force in [kN]. The correction equation was fit to data collected during machine deformation characterization using a steel gauge block.

$$d_{corr} = d + 0.00009 \cdot F^3 - 0.0024 \cdot F^2 + 0.0354 \cdot F + 0.0104 \qquad \textit{Eq. 5-2}$$

Heckel constants were determined by linear regression, using Eq. 5-3. Pressure P and punch distance-based porosity data ε collected at high compression pressures were used, in order to resolve the whole force-range in which a linear trend was observed in the Heckel plots. The linear range (for $R^2 \geq 0.993$), the slope of the linear fit K, the Heckel yield pressure $P_y = 1/K$ and the intercept A were evaluated.

$$\ln\frac{1}{\varepsilon} = -\ln\varepsilon = A + K \cdot P \qquad \textit{Eq. 5-3}$$

Moreover, the densification factor B was evaluated using the intercept A of the linear fit and initial porosity ε_0 Eq. 5-4.

$$A = \ln\frac{1}{\varepsilon_0} + B = -\ln\varepsilon_0 + B \qquad \textit{Eq. 5-4}$$

Out-of-Die Compaction Analysis

The apparent tablet density ρ_{app} was determined from weight and dimension data of each finished tablet after elastic recovery. Out-of-die porosity ε_{OD} was calculated according to Eq. 5-5 for out-of-die Heckel analysis.

$$\varepsilon_{OD} = 1 - \frac{\rho_{app}}{\rho_{true}} \qquad \textit{Eq. 5-5}$$

Elastic recovery of the finished tablets was evaluated using the axial elastic relaxation index (ER) according to (Armstrong and Haines-Nutt, 1974), as given in Eq. 5-6:

$$ER\ [\%] = \frac{t_1 - t_0}{t_0} \cdot 100\ [\%] \qquad \textit{Eq. 5-6}$$

with t_1 being the thickness of the final tablet and t_0 the minimum punch distance between the punches during tablet compression.

Compactability, Tabletability and Compressibility (CTC) Profiles

CTC profiles were generated using the maximum compression force in each compression cycle, the out-of-die porosity and the tensile strength of the generated tablet. The radial tablet tensile strength σ_t was calculated from the tablet hardness F, diameter D and thickness t of each tablet as given in Eq. 5-7.

$$\sigma_t = \frac{2F}{\pi D t} \qquad \textit{Eq. 5-7}$$

Compactability profiles were fit by the Ryshkewitch-Duckworth equation (Eq. 5-8). Thereby, σ_0 is the theoretical tensile strength of the compact at porosity $\varepsilon = 0$ and b a constant.

$$\sigma = \sigma_0 \cdot e^{-b \cdot \varepsilon} \qquad \textit{Eq. 5-8}$$

5.2.5. Formulation Screening

The formulation screening was performed, applying a D-optimal DoE with a linear mixture design and duplicate center point (G-efficiency 86.67 and condition number 1.59). Eight different formulation compositions were investigated. Formulation compositions were varied in terms of NMD-pellet, PH102 and K-CL content as given in Table 5-2. MgSt content was kept constant at 0.5 wt.%. In total, twelve runs were performed and during each run the compaction force settings were varied in a two-level full factorial design with duplicate center point. The pre-compression force was varied between 0.5 to 2 kN and the main compression force from 10 to 25 kN. The center point compression settings were applied first and last, in order to assess the influence of segregation on the tablet characteristics. The sequence of used compression force settings is given in Table 5-3. The force levels were set by manually adjusting the minimal punch distance in each run. Automatic force control was deactivated during the runs. The actual average compression forces were calculated from the data collected in SIPAT for further analysis.

For all runs, the feed frame and the turret speed were set constant to 50 rpm and 83 rpm, respectively. The turret speed was selected based on the pellet production rate of 4 kg/h upstream of the tableting unit. The tablet weight was adapted for each formulation composition, in order to reach a final tablet dose strength of 10 mg, that is a pellet weight of 100 mg in each tablets, at every pellet fraction (Table 5-2). Tablet weight was set by manual adjustment of the filling depth during the experiments.

Table 5-2. Formulation compositions for all DoE runs (MgSt fraction constant at 0.5 wt.%), with different target tablet weights and calculated total throughput.

Exp.	Run Order	K-CL fraction [wt.%]	PH102 fraction [wt.%]	Pellet fraction [wt.%]	Tablet weight [mg]	Throughput [kg/h]
N1	1	20	30	49.5	202	8.08
N4	2	20	40	39.5	253	10.13
N2	3	0	60	39.5	253	10.13
N10	4	10	50	39.5	253	10.13
N6	5	10	30	59.5	168	6.72
N9	6	0	50	49.5	202	8.08
N3	7	0	60	39.5	253	10.13
N7	8	0	40	59.5	168	6.72
N12	9	10	40	49.5	202	8.08
N8	10	0	40	59.5	168	6.72
N5	11	20	40	39.5	253	10.13
N11	12	10	40	49.5	202	8.08

Table 5-3. Full-factorial variation of compression force settings, applied at each formulation screening DoE run.

Force setting	Run order	Pre-compression force [kN]	Main compression force [kN]
P1	2	0.5	10
P2	3	2	10
P3	4	0.5	25
P4	5	2	25
P5	6	1.25	17.5
P6	1	1.25	17.5

The tablet responses collected during the DoE were tablet mass uniformity, tensile strength, friability and disintegration time. Mas uniformity was evaluated by calculating the relative standard deviation (RSD) of tablet weights from ten tablets (n=10). Tablet tensile strength was determined for ten tablets (n=10) as well, and the mean value used in statistical analysis. Friability testing was performed as given above in section 5.2.4, with 6.5 g of tablets. The loss of tablet mass after friability testing in [%] was used as response. Disintegration testing was performed using the fixed number of six tablets, evaluating the disintegration time by which the last tablet was fully disintegrated.

Friability and disintegration time were log-transformed to a better distribution of the responses in statistical analysis. Partial least squares (PLS) models were fit in MODDE for the tablet responses from tablets produced at the compression force settings of P3. Model fine tuning was performed manually. Finally, sweet spot analysis was performed in order to identify the optimal formulation composition for the production of mechanically stable, IR tablets from NMD pellets.

Finally, tablets were prepared for validating the fitted statistical models from the formulation screening. The optimal formulation composition was used and compressed to tablets over a run time of 30 min using the compression forces settings, selected during the DoE screening. Turret speed and feed frame speed were set to 83 and 40 rpm speed, respectively to mimic the continuous production at the target CM line throughput. The tablet press hopper fill level was kept quasi-constant at 80% of total hopper height, by frequent, manual refilling.

5.3. Results

5.3.1. Pellet Characterization

As a first step in tableting formulation development, the NMD-pellets were characterized with regard to their tableting behavior. Surprisingly, it was possible to form stable compacts even at low compression forces. Thereby, the maximal tensile strength that was reached was around 3 MPa (equal to a breaking force of ~140 N in diametral compression). Pellet CTC profiles are shown in Figure 5-1.

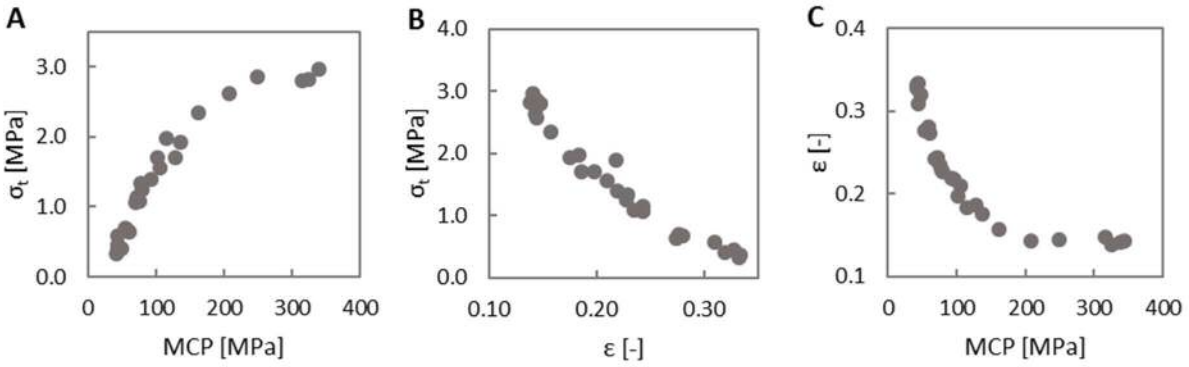

Figure 5-1. Tabletability (A), compressibility (B) and compactability (C) profiles of NMD pellets. (MCP…main compression pressure)

Tabletability profiles indicate the ability of a material to form compacts of specific strength upon different main compression pressures (MCP). However, it does not elucidate the mechanisms or reasons for the generation of a weak or strong compact. Thus, compressibility profiles are used to evaluate the degree of densification the material exhibits after compression. It contains information on how much particle-particle contact was generated for inter-particle bond formation by applying a specific pressure. Lastly, compactability allows to analyze the strength of inter-particle bonds, as it displays the tablet tensile strength as a function of porosity.

The formation of stable compacts from NMD-pellets was surprising, since extruded materials were reported to exhibit poor tableting properties, due to their dense microstructure. EE, which is contained in the pellets with 36 w.% has been reported to behave elastically during compression, causing inter-particle bond rupture upon decompression (Grymonpré et al., 2017b). Regarding cellulosic carriers, such as hydroxypropyl methylcellulose (HMPC), which was contained in the pellets with 54 wt.%, no literature is available on the deformation characteristics after HME processing. This may be associated to the challenges in HME processing of pure HPMC, due to its propensity for degradation. Neat HPMC however, is classified as deforming plastically in tablet compaction (Ritschel and Bauer-Brandl, 2002). Comparing the CTC profiles of HPMC E5 (Figure D-2 in the Supplemental Material section D) and the pellets, it can be observed, that HPMC exhibits better tabletability and compactability, as expected. However, the compressibility of pellets was slightly better than of HPMC, as lower porosity was

reached at high compression pressures. This may be attributed to a reduced elastic recovery after tablet ejection.

It has been reported, that the addition of plasticizers, or plasticizing APIs to polymers, alters CTC profiles and every so often improves tabletability (Grymonpré et al., 2017b, 2017a; Mohammed et al., 2012). The pellet formulation used in this study, formed a phase separated ASD in vacuum compressed (VCM) specimen, as indicated by two to three glass transitions (Hörmann et al., 2018). Even though the phase separation was less pronounced, i.e. multiple T_gs were not detectable, after the intensive mixing in HME, the lowest T_g around 30°C pertained. This T_g was attributed to a NMD-EE rich phase and indicates, that at least two phases were present also after HME processing. The T_g of the NMD-EE-rich phase was close to room temperature and the fast deformation during tablet compression is expected to soften this phase significantly. Therefore, the formation of stable compacts was attributed to the formation of solid bonds by fusion. This is not desired for two reasons: First, because the tablets prepared from pure pellets did not disintegrate anymore, even after 40 min of disintegration testing (Figure 5-2). This results in a loss of the IR properties of the single pellets. Second, there is an increased risk of recrystallization of the amorphous API upon melting and re-solidification of the ASD material.

Figure 5-2. Tablet compressed at 5 kN from NMD-pellets after 40 min of disintegration testing.

Thus, excipients were required to avoid fusion of the pellets during tablet compression and to provide rapid disintegration. Heckel analysis was applied to evaluate the deformation behavior of the pellet bed and to select a suitable excipient.

5.3.2. Heckel Constants of Pellets and Selected Excipients

Out-of-die Heckel plots (Figure 5-3 shows the plots for NMD-pellets) contain the exactly same information as compressibility plot, but displayed with a logarithmic y-axis. By evaluating the linear region in the plot (with slope K_{OD}), conclusions on the plastic deformability of the material bed can be drawn. Above the linear region, the profile flattens until a plateau is reached where higher compression pressures do not decrease porosity (after elastic recovery) of the finished tablet further.

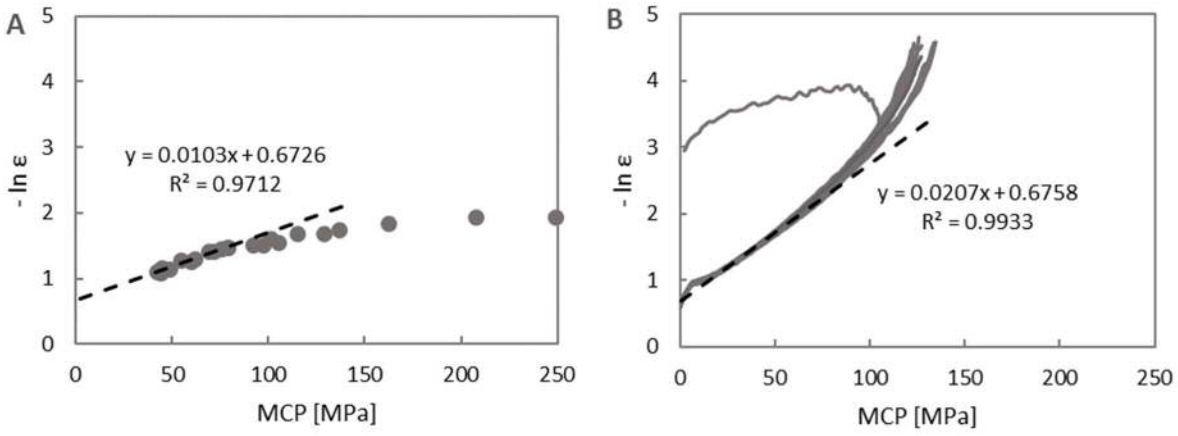

Figure 5-3. Out-of-die (A) and in-die (B –compression cycles with different maximum main compression pressure (MCP)) Heckel plots of NMD pellets with linear fit of the region with plastic deformation.

In-die Heckel plots, can be generated from each single compression cycle, using the decreasing bulk porosity, i.e. decreasing volume between the two punches, and the increasing compression force associated with this densification. Therefore, this plot does not contain the contribution of elastic relaxation of the compact after ejection from the die. This results in a steeper slope in the in-die Heckel plot compared to the slope of the out-of-die Heckel plot, i.e. the in-die yield pressure P_y is lower than the out-of-die yield pressure $P_{y,OD}$. The relevant parameters of in-die and out-of-die Heckel analysis are given in Table 5-4. The in-die Heckel plots of the pellets and all investigated excipients are shown together in Figure 5-4. Excipient Heckel plots from compression cycles with different maximal compression pressures and the CTC profiles of all materials are shown in Figure D-1 and Figure D-2 in the Supplemental Material section D.

Table 5-4 Heckel constants and related parameters, elastic relaxation and zero-porosity tensile strength for all raw materials.

Substance	Linear range [MPa]	P_y [MPa]	A [-]	B [-]	$P_{y,OD}$ [MPa]	ER [%]	σ_0 [MPa]
HPMC E5	10 – 85	42.9	0.668	0.367	82.0	23.6 ± 0.5	9.4
NMD-pellets	15 – 80	48.3	0.676	0.060	97.1	23.2 ± 1.5	12.8
PVP/VA	5 – 100	61.3	0.542	0.213	103.1	18.5 ± 1.1	9.5
PH101	12 – 180	69.4	0.488	0.290	102.2	15.5 ± 1.0	18.5
PH102	50 – 230	81.3	0.624	0.401	101.0	11.9 ± 1.0	16.7

In-die Heckel analysis allows to investigate the different phases and mechanisms occurring during tablet compression. The bulk material undergoes the following steps during tableting: i) rearrangement of primary particles, ii) densification of particles, iii) plastic, elastic and viscoelastic deformation, or fracture and attrition of particles, iv) inter-particle bond formation by surface forces (Van der Waals forces), mechanical interlocking or solid bond formation and finally, v) elastic recovery in the die upon release of the compression pressure.

Depending on the properties of the material, different mechanisms are involved in the formation of a stable compact and their contribution can be evaluated by means of the yield pressure P_y, the linear range in the in-die Heckel curves, Heckel constant A and the rearrangement parameter B (all given in Table 5-4). The yield pressure P_y in the linear range of the Heckel plot is an indicators for the deformation mechanism. High yield pressures are observed in brittle materials, while a low yield pressure is associated with plastically or elastically deforming materials (Nokhodchi, 2005). The pellets exhibited a low yield pressure P_y, but higher than that of the neat HPMC. Both materials exhibit a steep increase after the linear range, an effect, that has been attributed to elastic deformation (Sun and Grant, 2001). The earlier the onset of this increase was observed, i.e. the shorter the linear range, and the steeper the increase, the more elastic deformation occurred during compression. Comparing the upper end of the linear range with the elastic recovery ER of finished tablets (Table 5-4), an inverse correlation was observed for the investigated materials. This indicates PH102 to exhibit the least elastic contribution to the deformation behavior. The elastic behavior of materials can also be observed in the decompression phase in the Heckel plots. A horizontal trend in this phase indicates a higher degree of plastic deformation, whereas a decreasing trend is caused by the elastic recovery of the material during the decompression process. The Heckel plot of pellets Figure 5-3 illustrates such a case of immediate elastic recovery. The same is observed in the plots for HPMC and PVP/VA, whereas the MCC grades show a clear horizontal trend (Figure D-1 in the Supplemental Material section D).

PH102 exhibited the highest yield pressure, indicating some brittle deformation. However, compared to inorganic materials, such as dicalcium phosphate with a P_y value of 625 MPa (Fölzer, 2017), all used materials were classified as soft materials with plastic/elastic deformation. This is in good agreement with published data (Grymonpré et al., 2017b; Klevan et al., 2010; Zhang et al., 2003).

The parameter B is an indicator for the degree of densification achieved by particle bed rearrangement and fragmentation in the initial phase of the compression cycle. In general, larger particle sizes are considered to exhibit more propensity of fragmentation and rearrangement in the particle bed. Surprisingly, the NMD pellets yielded the lowest of all B values. While an absence of fragmentation was presumed, due to the rather soft, than brittle nature of the pellets, significant rearrangement of the pellet bed was expected, especially due to the cylindrical shape of the pellets. Investigating the

initial phase in the Heckel plot (Figure 5-4), a kink can be observed between the rearrangement phase and the onset of plastic deformation, which falsifies the evaluation of the initial rearrangement phase by the parameter B. The other materials showed expected behavior, with obtained rearrangement/ fragmentation factors B in the order of PH101 < HPMC E5 < PH102. This correlates well with the median particle size of the materials. PVP has been reported already to exhibit little rearrangement and fragmentation upon compression (Klevan et al., 2010).

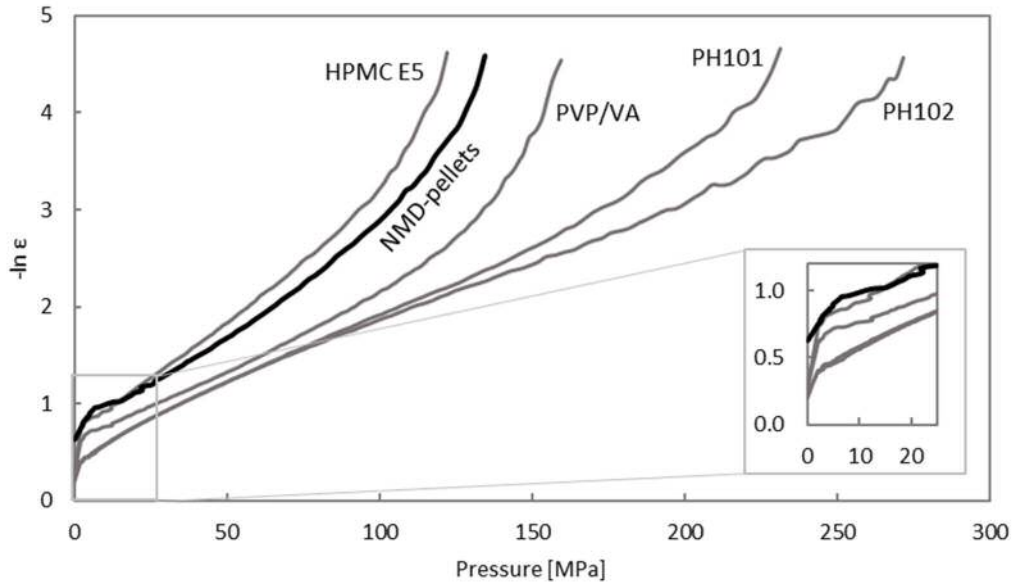

Figure 5-4. Comparison of in-die Heckel plots, averaged from compression cycles with high maximal main compression forces, for all raw materials and zoomed rearrangement region.

An appropriate binder had to be selected, to compensate for the elastic behavior of NMD-pellets and to improve the disintegration performance of tablets. PVP/VA was excluded due to its soft, elastic nature. Moreover, PVP/VA provides less disintegrating effects itself and would only aid disintegration by acting as a cushioning material between the pellets. Finally, the PH102 MCC grade was chosen, even though CTC profiles of the two grades were very similar and PH101 was reported to be beneficial to avoid segregation. However, in order to ensure, that the blend of cylindrical pellets and powder remains well flowable, when processing the blend on a rotary tablet press, PH102 was preferred for further investigations.

In the work of Fölzer, also binary blends of NMD-pellets with PVP/VA, Starch® 1500 and DI-CAFOS® D160 were investigated (Fölzer, 2017). Their performance was inferior to the performance of PH102-blends, and the data therefore not shown.

5.3.3. Compaction Analysis and Disintegration Testing of Binary Mixture

Heckel plots of the binary mixtures with different fractions of NMD-pellets and PH102 are shown in Figure 5-5 A. Initial bulk density and porosity data, and the calculated true density of the binary mixtures used for generating the Heckel plots are given in Table D-1 in the Supplemental Material section D. The Heckel plots of the binary blends were located between the Heckel plots of raw materials, correlating with the component fractions. Similar behavior could be observed in the compactability plots from out-of-die characterization (Figure 5-5 B). However, in this case, the slope of the linearized compactability profiles of the binary blends was almost the same as for the pellets. This indicated, that the relatively lower strength of bonds formed by the pellets determined the final strength of the tablet at a given porosity, even at the lowest pellet content.

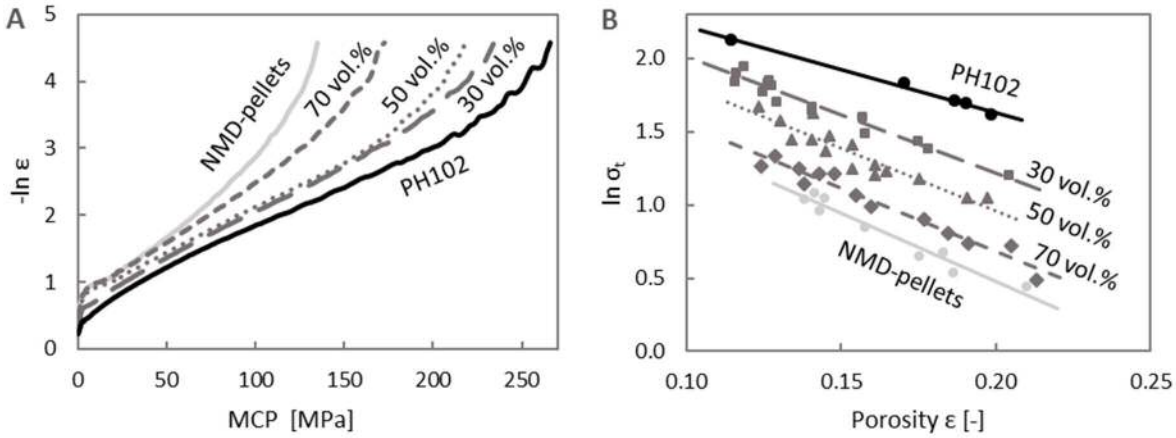

Figure 5-5. In-die Heckel plots (A) and compactability profiles (B) of pure materials and binary mixtures with different fractions of NMD-pellets and PH102. Specified vol.% gives pellet content in blend.

The fact that the binary blend behaves similar to an “ideal mixture”, was beneficial for two reasons: First, this allows to efficiently improve properties, such as compressibility and compactability by adding the binder PH102. Second, it indicates a stable blending state, which is also supported by pictures taken from the finished and the hardness tested tablets (Figure 5-6) Therein, the binder and pellets are well distributed given the fact, that the tablets were produced from manual die filling by skimming the material over the tableting die until it was completely filled.

Figure 5-6. Tablets made of binary blends with different fractions of NMD-pellets and PH102:70 vol.% (left), 50 vol.% (middle) and 30 vol.% (right) of NMD-pellets.

However, a rough surface of the pellets was observed, caused by the elastic recovery of the pellets in the tablets. Surprisingly, this did not cause any lamination of the binder phase in these tablets. A clear correlation of axial elastic recovery of the finished tablets with the pellet content was also observed in the ER data (Table 5-5).

Table 5-5. Heckel plot yield pressures, elastic recovery and disintegration times of binary blends of NMD-pellets and PH102.

	Pellet content [% v/v]	P_y [MPa]	ER index [%]	Disintegration time*		
				5 kN	10 kN	15 kN
PH102	0	81.3	11.9 ± 1.0	2 - 7	10 - ∞	20 - ∞
	30	71.9	15.3 ± 0.9	1 - 8	26 - ∞	∞
	50	74.6	17.0 ± 0.9	7 - 18	∞	∞
	70	57.5	20.0 ± 1.5	∞	∞	∞
NMD-pellets	100	48.3	23.2 ± 1.5	∞	∞	∞

* ∞ indicates that tablet disintegration takes longer than 40 minutes.

The disintegration data revealed an influence of maximal compression pressure, as well as pellet content. Increasing maximum compression pressure reduces the porosity of the compact, and thus, increased disintegration time by reducing water ingress velocity (Yassin et al., 2015).Above a pellet fraction of 70 vol.% (equivalent to a pellet mass fraction of 64 wt.%), tablets did not disintegrate anymore, even at low compression pressures. This indicated again, the formation of solid bridges between the pellets, with higher strength than the swelling pressure of MCC in water. The average packing fraction of a random, loose bed of cylindrical particles is 0.56 (Nolan and Kavanagh, 1995). Assuming a random close packing for much smaller spherical excipient particles (packing fraction 0.64), approximately 28 vol.% of excipient are needed to fill the voids in the pellet bed. A powder fraction of 30 vol%, just slightly above this threshold, is obviously not sufficient to act as a separation layer between the pellets.

Conclusion from the Compaction Simulation Study

Compression of pure NMD-pellets surprisingly demonstrated, that stable tablets could be formed. However, the compacts did not disintegrate at all during disintegration testing, indicating that solid bonds were formed by fusion during the tableting. Moreover, a significant elastic contribution was observed in the deformation of pellets.

Binary mixtures with PH102 formed mechanically stable tablets without any visible defects at different pellet fractions. The best trade-off between acceptable tensile strength (~3 MPa) and the best disintegration time (<10 min) was reached for a pellet fraction of 30 vol.%, when compressed at the lowest compression pressure of 5 kPa.

However, tablets compressed at 10 kN partially failed to disintegrate. Thus, a disintegrant had to be added to the formulation. To that end, K-CL was selected, since it has been shown to provide excellent

disintegration performance while simultaneously increasing tablet hardness for a formulation with milled extrudate of ibuprofen and EE (Gryczke et al., 2011).

In order to gain understanding on the formulation performance in the final tableting process, the composition screening of the adapted formulation was performed on a rotary tablet press. Different compression force profiles, and die filling regime often change critical tablet properties (hardness, disintegration, weight uniformity), when transferring a formulation from compaction simulators to rotary presses (Braun, 2003; Ritschel and Bauer-Brandl, 2002). This is especially critical for elastically deforming materials and segregating blends. Feed frame (FF) speed influences die filling consistency and intra-tablet segregation, an effect that cannot be mimicked by manual die filling in the compaction simulator. Moreover, the machine vibrations and the FF speed in the rotary tablet press may have an effect on inter-tablet segregation over time.

5.3.4. Formulation Screening

The formulation screening was executed with K-CL fractions in a range between 0 and 20 wt.%, in order to receive a clear response for positive/negative effects of the disintegrant addition. The pellet fractions were varied between 39.5 and 59.5 wt.%. The upper limit was equal to a pellet fraction of 62.6 to 65.5 vol.% in the formulation, depending on the external excipient composition. This was just below the pellet content, for which solid bridge formation was observed during the compaction simulation runs. The lower limit for pellet content was given by the target to produce tablets of decent size, i.e. in the range of 250 mg. In order to achieve the desired dose strength of 10 mg of NMD, approx. 40 wt.% of pellets were required (44.2 to 46.3 vol% of pellets).

Tableting Process Data

The tablet press process data of each DoE run was collected via SIPAT (data from formulation N10 shown in Figure 5-7). The blends were filled into the tablet press hopper and the press was started for a short time in order to fill the entire empty volume. Then, the fill height was manually adjusted by producing tablets for a short period of time and determining the weight of the collected tablets. After adjusting the weight, the run at the first process set point (P6) was started, manipulating the punch distance for pre- and main compression to provide the desired compression force levels (around 08:44 in Figure 5-7). When the desired force levels were reached, tablets were collected for approx. 30 s for later analysis and the press was stopped. Then, the run at the next process setting (P1) was started, adjusting the tablet press parameters as described before. The first and the last process set points (P6 and P5) were the duplicate center point settings. Comparing the tablet properties from these two runs, the influence of segregation on the data was assessed. After the last process set point (P5), the tablet press was run empty and cleaned before filling the next formulation into the tablet press hopper.

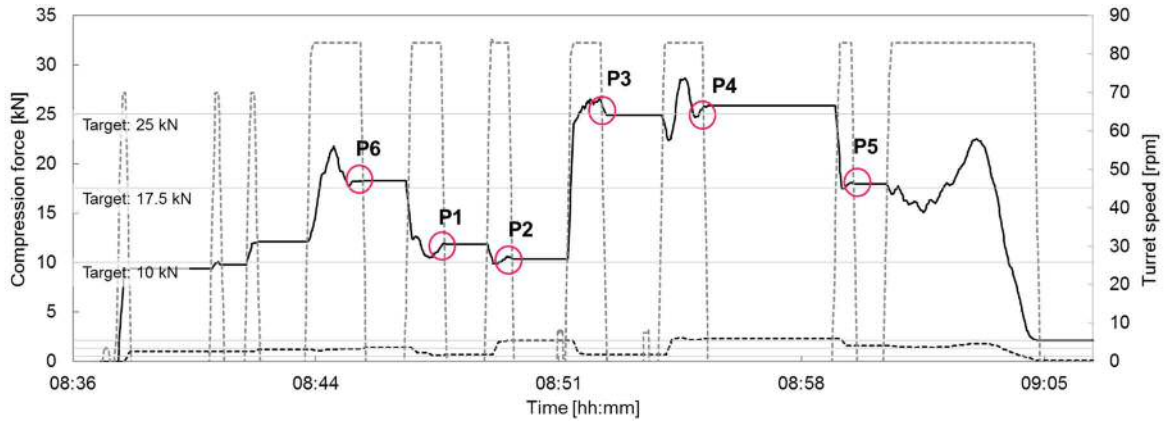

Figure 5-7. Process data (solid black line: main compression force [kN], dashed black: pre-compression force [kN] and dashed grey: turret speed) of tableting experiment with formulation N10. Circles indicating sampling of tablets.

Tablet Properties

Tablet weight uniformity, tensile strength, friability and disintegration time were determined. The data for all runs is given in Table D-2 and Table D-3 in the Supplemental Material section D. Tensile strength and friability data for formulations with low pellet content (39.5 wt.%) are shown in Figure 5-8. An approximately 5-fold reduction of tablet strength was observed in tablets without K-CL (N3), when comparing them to the pellet and PH102 containing tablets produced on the compaction simulator. With regard to friability, higher values were observed with increasing pellet content, as well as decreasing K-CL content. Higher compression force settings appeared to decrease friability to some degree, especially for tablets with higher pellets contents (Figure D-4 in the Supplemental Material section D). The increased friability in tablets without K-CL in the formulation was related to lamination which occurred in the absence of K-CL even at low pellet content (Figure 5-8).

Concerning segregation, differences in the tablet properties of runs P5 and P6 (duplicates) were investigated. It can be observed, that P6 was providing tablets with higher tensile strength in all cases. This indicates, that initially produced tablets contained an increased excipient fraction. In some cases (N1, N3), this effect is overlaid by the effect of the hopper already running empty during the last process set point (P5). This led to reduced compression forces, due to insufficient die filling, and significantly changed tablet properties. However, the data clearly shows, that some segregation occurred in all formulations, especially at the beginning and end of the experiments. Therefore, the data from tablets produced in the middle of the experiment, that is at process set point P3, were considered most representative for the formulations performance and used for statistical analysis.

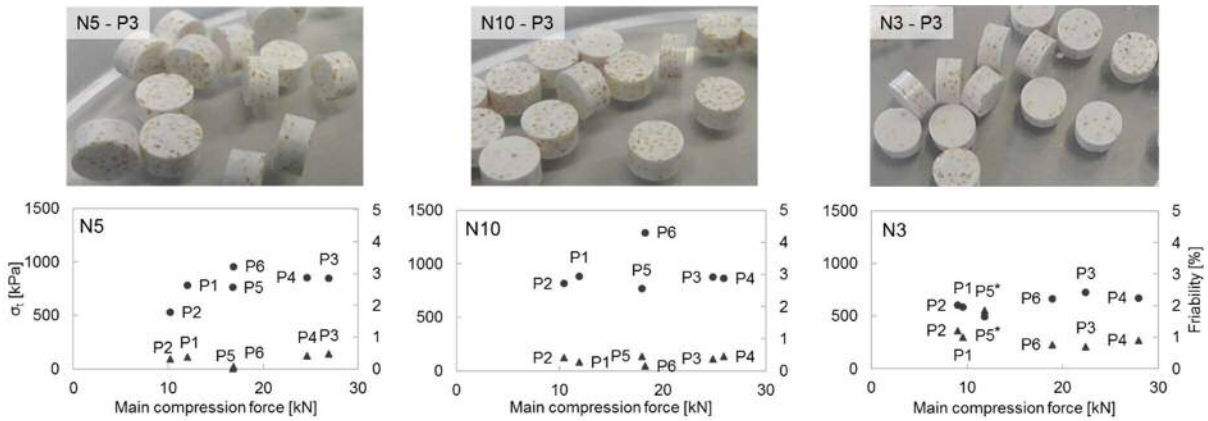

Figure 5-8. Tensile strength and friability data for formulations with 39.5 wt.% NMD-pellet content: N5 with 20 wt.%, N10 with 10 wt.% and N3 with no K-CL in the formulation. Pictures showing tablets after friability testing. (Indicates data from samples were the hopper was already running empty during tablet sampling.)*

Statistical Modelling

Models with linear and quadratic terms were fit for all responses. Excellent models were achieved for tensile strength (R^2 = 0.98 and Q^2 = 0.96) and friability (R^2 = 0.94 and Q^2 = 0.90). Mass uniformity data could be fit with a satisfactory model (R^2 = 0.73 and Q^2 = 0.52), while disintegration time data yielded a very poor model (R^2 = 0.39 and Q^2 = 0.15). An attempt was made to improve the statistical models by including actual average tablet weight (m_{Tablet}) and actual main compression force (MCF) as uncontrolled factors into the worksheet. This did not significantly improve any model performance and thus, these factors were always kept excluded. However, tablet mass did show positive correlation with mass uniformity and tensile strength, while there was a negative correlation observed with friability and disintegration time. Correlations of factors and responses (Table D-4), the coefficient plots (Figure D-5), with error bars indicating the statistical significance of each factor, and PLS model details (Table D-5) and are given in the Supplemental Materials section D.

Contour plots of all responses are shown in Figure 5-9. All contour plots demonstrate the strong influence of pellet content on tablet quality. High pellet content resulted in lower mass RSD (Figure 5-9 A), lower tensile strength (Figure 5-9 B), higher friability (Figure 5-9 C) and a tendency to longer disintegration times (Figure 5-9 D). While the variation in tablet mass RSD and disintegration was rather low, there was strong and critical variation observed in the parameters associated with mechanical tablet strength. Overall, the higher porosity of tablets produced on the rotary tablet press, compared to tablets prepared on the compaction simulator, resulted in significantly shorter disintegration times.

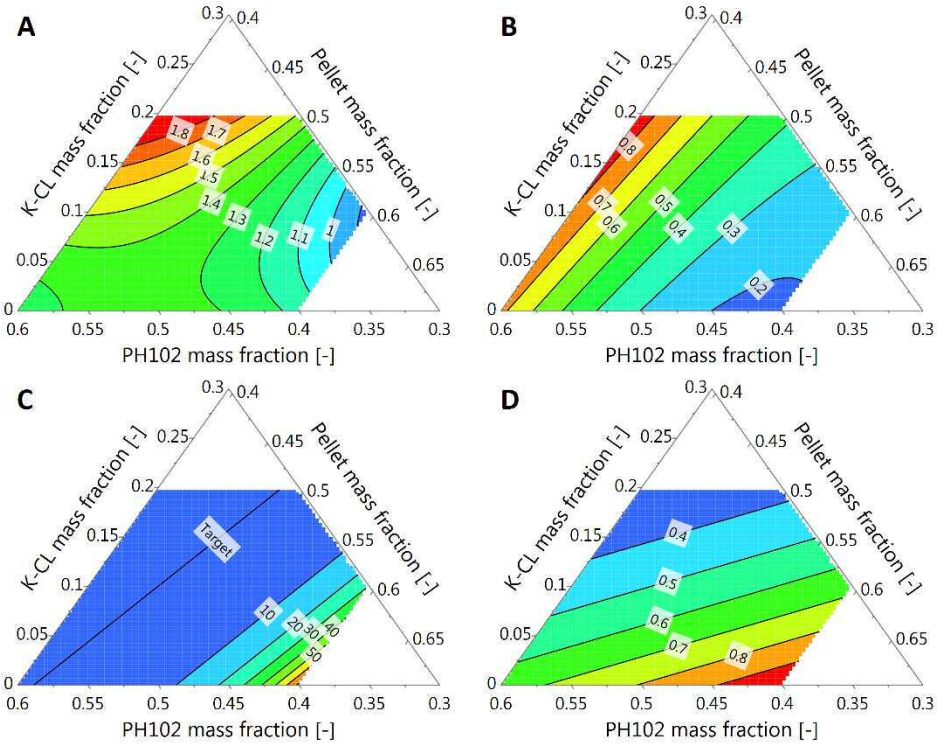

Figure 5-9. Contour plots for mass uniformity (RSD) [%] (A), tensile strength [MPa] (B), friability [%] (C) and disintegration time [s] (D) from tablets produced at process setting P3.

Nevertheless, K-CL content did of course affect disintegration time. However, also a positive effect on tensile strength and friability was observed. Tablet weight RSD though, was slightly negatively affected, by increased fractions of the cohesive K-CL. However, this effect was only observed at low pellet fractions. For PH102, the expected positive effect on mechanical tablet strength was confirmed in the models. No statistically significant effect of PH102 was indicated for mass RSD and disintegration time.

Sweet Spot Analysis

The ultimate aim of the statistical analysis was to identify the sweet spot for the final tableting formulation composition. The following limits were used for specifying the sweet spot:

- Mass uniformity (RSD): < 1.6%
- Tensile strength: > 0.75 MPa
- Friability: < 1%

Disintegration time was not included as a limit, since all formulations disintegrated in less than 1 min. Thus, IR of API from the tablets was predicted for all formulation compositions.

The acceptable friability level was chosen according to Ph.Eur. 2.9.7. (European Pharmacopoeia Commission, 2014), while the limits for tensile strength and mass uniformity were chosen specifically to identify the best composition for this formulation. Commonly, a tensile strength above 1 MPa is required to allow industrial handling of the tablets and a mass RSD below 2% should be achieved. Since this tensile strength was not reached by any formulation composition and this weight variability limit never exceeded, the sweet spot thresholds were selected to reflect on the best performing regions in the investigated range of formulation compositions.

The sweet spot plot is shown in Figure 5-10 A. The sweet spot was framed by two specification limits: mass uniformity and tensile strength. The sweet spot was located at the lowest pellet fraction and at medium K-CL content. K-CL obviously played a beneficial role in taking up the elastic recovery of the pellets after tablet ejection. The plastically deforming binder PH102 was not able to compensate sufficiently for the pellet's behavior.

The final formulation was consequently defined at 40 wt.% NMD pellets, 10 wt.% K-CL, 49.5 wt.% of PH102 and 0.5 wt.% MgSt. A pellet mass fraction of 40% was chosen, in order to receive a target tablet weight of 250 mg. Compression settings were selected based on the flat trend of tensile strength across the different compression forces for this formulation composition (N10 in Figure 5-8). Since higher compression forces were not increasing tensile strength (flat profile), pre- and main compression force were set to 0.5 kN and 12 kN.

PLS model predictions of tablet quality for the final formulation (compression forces not contained in models), yielded the following values: 1.5% mass RSD, 0.77 MPa tensile strength, 0.36% friability and a disintegration time of 0.45 min.

Finally, validation tableting runs were performed for 30 min, using this formulation and the selected compression force settings. The tablets exhibited an average tensile strength of 0.67 ± 0.01 MPa (n=5 samples of 10 tablets) and an average tablet weight RSD of 1.30 ± 0.35% (max. value 2.1%, in n=21 samples of 10 tablets). Friability and disintegration were not tested, since they were not limiting the sweet spot. However, dissolution tests were performed for tablets (n=3) sampled at different time points. Immediate API release from the tablets was confirmed, as shown in Figure 5-10 B.

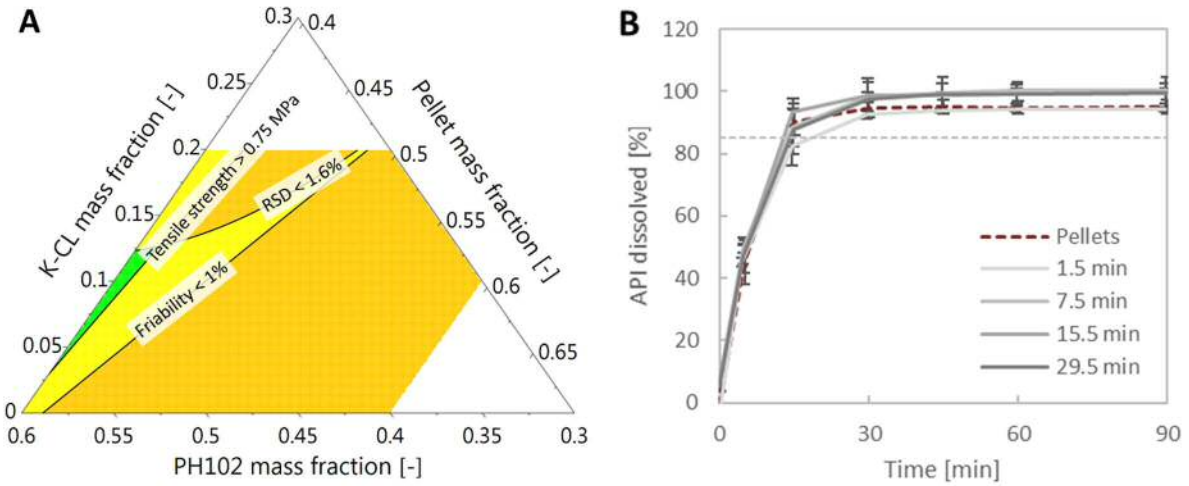

Figure 5-10. Sweet spot of formulation composition (A) at process settings P3 (green: sweet spot, yellow: 3 criteria met and orange: 2 criteria met) and dissolution profiles (B) of tablets from finally selected formulation and compression settings, sampled over a tableting run time of 30 min.

5.4. Conclusions

HME is a key technology for the production of ASDs with improved bioavailability. In order to become a platform technology, a strategy is required for the robust tableting of HME products. Démuth has attributed the low number of ASD products in tablet form to a knowledge gap in this field (Démuth et al., 2015). Thus, the preparation of tablets from HME prepared ASD pellets was investigated in this study. Acceptable mechanical stability (hardness, friability) of tablets could be achieved for relatively low pellet content (≤ 40 wt.%) and when using appropriate binders (PH102 and K-CL) for the given NMD-pellets (D_{50} ~ 0.9 mm). In formulations with high pellet content, the elastic properties of the pellets caused tablet lamination, when processed in a rotary tablet press. Surprisingly, especially the disintegrant K-CL was effective in reducing this effect, by increasing the elasticity of the powder matrix.

Concluding, the tableting formulation development was successful in providing a formulation for the continuous preparation of tablets with a dose strength of 10 mg NMD and immediate API release. Nevertheless, the segregation tendency and tablet strength remain critical points with regard to the compression of HME pellets to tablets.

5.5. References

Abdul, S., Chandewar, A. V, Jaiswal, S.B., 2010. A flexible technology for modified-release drugs: multiple-unit pellet system (MUPS). J. Control. Release 147, 2–16.

Agrawal, A., Dudhedia, M., Deng, W., Shepard, K., Zhong, L., Povilaitis, E., Zimny, E., 2016. Development of Tablet Formulation of Amorphous Solid Dispersions Prepared by Hot Melt Extrusion Using Quality by Design Approach. AAPS PharmSciTech 17, 214–232.

Agrawal, A.M., Dudhedia, M.S., Patel, A.D., Raikes, M.S., 2013. Characterization and performance assessment of solid dispersions prepared by hot melt extrusion and spray drying process. Int. J. Pharm. 457, 71–81.

Armstrong, N.A., Haines-Nutt, R.F., 1974. Elastic recovery and surface area changes in compacted powder systems. J. Pharm. Pharmacol. 9, 287-290.

Beckert, T.E., Lehmann, K., Schmidt, P.C., 1998. Compression of enteric-coated pellets to disintegrating tablets: uniformity of dosage units. Powder Technol. 96, 248–254.

Bhad, M.E., Abdul, S., Jaiswal, S.B., Chandewar, A. V, Jain, J.M., Sakarkar, D.M., 2010. MUPS Tablets – A Brief Review. Int. J. PharmTech Res. 2, 847–855.

Bodmeier, R., 1997. Tableting of coated pellets. Eur. J. Pharm. Biopharm. 43, 1–8.

Boersen, N., Lee, T.W.-Y., Shen, X. (George), Hui, H.-W., 2014. A preliminary assessment of the impact of hot-melt extrusion on the physico-mechanical properties of a tablet. Drug Dev. Ind. Pharm. 40, 1386–1394.

Braun, M., 2003. Einflussfaktoren bei der Tablettierung magensaftresistent überzogener Pellets auf Exzenter- und Rundlauftablettenpresse. Friedrich-Wilhelms-Universität Bonn.

Breitenbach, J., 2002. Melt extrusion: from process to drug delivery technology. Eur. J. Pharm. Biopharm. 54, 107–117.

Démuth, B., Nagy, Z.K., Balogh, A., Vigh, T., Marosi, G., Verreck, G., Van Assche, I., Brewster, M.E., 2015. Downstream processing of polymer-based amorphous solid dispersions to generate tablet formulations. Int. J. Pharm. 486, 268–286.

DiNunzio, J.C., Schilling, S.U., Coney, A.W., Hughey, J.R., Kaneko, N., McGinity, J.W., 2012. Use of highly compressible CeolusTM microcrystalline cellulose for improved dosage form properties containing a hydrophilic solid dispersion. Drug Dev. Ind. Pharm. 38, 180–189.

Dukić-Ott, A., Thommes, M., Remon, J.P., Kleinebudde, P., Vervaet, C., 2009. Production of pellets via extrusion–spheronisation without the incorporation of microcrystalline cellulose: A critical review. Eur. J. Pharm. Biopharm. 71, 38–46.

European Pharmacopoeia Commission, 2014. European Pharmacopoeia 8.0, European Council, Strasbourg.

FDA, 2004. Pharmaceutical CGMPS for The 21st Century- A Risk-Based Approach. Final Report.

Feng, J., Xu, L., Gao, R., Luo, Y., Tang, X., 2012. Evaluation of polymer carriers with regard to the bioavailability enhancement of bifendate solid dispersions prepared by hot-melt extrusion. Drug Dev. Ind. Pharm. 38, 735–743.

Fölzer, L., 2017. The Influence of Different Tableting Aids on the Performance of Tablets Prepared from Hot-Melt Extruded Pellets. Graz University of Technology.

Ghebre-Sellassie, I., 1994. Mulitparticulate Oral Drug Delivery, 1st ed. Marcel Dekker, London.

Gryczke, A., Schminke, S., Maniruzzaman, M., Beck, J., Douroumis, D., 2011. Development and evaluation of orally disintegrating tablets (ODTs) containing Ibuprofen granules prepared by hot melt extrusion. Colloids Surf. B. Biointerfaces 86, 275–84.

Grymonpré, W., Bostijn, N., Herck, S. Van, Verstraete, G., Vanhoorne, V., Nuhn, L., Rombouts, P., Beer, T. De, Remon, J.P., Vervaet, C., 2017a. Downstream processing from hot-melt extrusion towards tablets: A quality by design approach. Int. J. Pharm. 531, 235–245.

Grymonpré, W., De Jaeghere, W., Peeters, E., Adriaensens, P., Remon, J.P., Vervaet, C., 2016. The impact of hot-melt extrusion on the tableting behaviour of polyvinyl alcohol. Int. J. Pharm. 498, 254–262.

Grymonpré, W., Verstraete, G., Van Bockstal, P.J., Van Renterghem, J., Rombouts, P., De Beer, T., Remon, J.P., Vervaet, C., 2017b. In-line monitoring of compaction properties on a rotary tablet press during tablet manufacturing of hot-melt extruded amorphous solid dispersions. Int. J. Pharm. 517, 348–358.

Hörmann, T.R., Jäger, N., Funke, A., Mürb, R.-K., Khinast, J.G., Paudel, A., 2018. Formulation Performance and Processability Window for Manufacturing a Dual-Polymer Amorphous Solid Dispersion via Hot-Melt Extrusion and Strand Pelletization. Int. J. Pharm. 553, 408–421.

Iyer, R., Hegde, S., Zhang, Y.-E., Dinunzio, J., Singhal, D., Malick, A., Amidon, G., 2013. The Impact of Hot Melt Extrusion and Spray Drying on Mechanical Properties and Tableting Indices of Materials Used in Pharmaceutical Development. J. Pharm. Sci. 102, 3604–3613.

Jijun, F., Lili, Z., Tingting, G., Xing, T., Haibing, H., 2010. Stable nimodipine tablets with high bioavailability containing NM-SD prepared by hot-melt extrusion. Powder Technol. 204, 214–221.

Jijun, F., Lishuang, X., Xiaoli, W., Shu, Z., Xiaoguang, T., Xingna, Z., Haibing, H., Xing, T., 2011. Nimodipine (NM) tablets with high dissolution containing NM solid dispersions prepared by hot-melt extrusion. Drug Dev. Ind. Pharm. 37, 934–944.

Klevan, I., Nordström, J., Tho, I., Alderborn, G., 2010. A statistical approach to evaluate the potential use of compression parameters for classification of pharmaceutical powder materials. Eur. J. Pharm. Biopharm. 75, 425–435.

Lundqvist, A.E.K., Podczeck, F., Newton, J.M.., 1997. Influence of disintegrant type and proportion on the properties of tablets produced from mixtures of pellets. Int. J. Pharm. 147, 95–107.

Mohammed, N.N., Majumdar, S., Singh, A., Deng, W., Murthy, N.S., Pinto, E., Tewari, D., Durig, T., Repka, M.A., 2012. Klucel™ EF and ELF polymers for immediate-release oral dosage forms prepared by melt extrusion technology. AAPS PharmSciTech 13, 1158–69.

Nokhodchi, A., 2005. An Overview of the Effect of Moisture on Compaction and Compression. Pharm. Technol. January, 46–66.

Nolan, G.T., Kavanagh, P.E., 1995. Random Packing of non-spherical particles. Powder Technol. 84, 199–205.

Ritschel, W.A., Bauer-Brandl, A., 2002. Die Tablette: Handbuch der Entwicklung, Herstellung und Qualitätssicherung. ECV-Editio-Cantor-Verlag.

Sun, C., Grant, D.J.W., 2001. Influence of Elastic Deformation of Particles on Heckel Analysis. Pharm. Dev. Technol. 6, 193–200.

Wagner, K.G., Krumme, M., Beckert, T.E., Schmidt, P.C., 2000. Development of disintegrating multiple-unit tablets on a high-speed rotary tablet press. Eur. J. Pharm. Biopharm. 50, 285–292.

Wagner, K.G., Krumme, M., Schmidt, P.C., 1999. Investigation of the pellet-distribution in single tablets via image analysis. Eur. J. Pharm. Biopharm. 47, 79–85.

Yassin, S., Goodwin, D.J., Anderson, A., Sibik, J., Wilson, D.I., Gladden, L.F., Zeitler, J.A., 2015. The Disintegration Process in Microcrystalline Cellulose Based Tablets, Part 1: Influence of Temperature, Porosity and Superdisintegrants. J. Pharm. Sci. 104, 3440–50.

Young, C.R., Dietzsch, C., McGinity, J.W., 2005. Compression of Controlled Release Pellets Produced by a Hot Melt Extrusion and Spheronization Process. Pharm. Dev. Technol. 1, 133–139.

Zhang, Y., Law, Y., Chakrabarti, S., 2003. Physical properties and compact analysis of commonly used direct compression binders. AAPS PharmSciTech 4, 489–499.

6. Residence Time Distributions of a Powder-Pellet Blend in a Continuous Blending and Tableting Unit[4]

Material traceability throughout the process line is an integral part in the adoption of continuous manufacturing (CM) in the pharmaceutical industry. This can be achieved by utilizing residence time distributions (RTDs) of each process unit for convoluting them to a manufacturing line RTD. Additionally, RTDs characterize the back-mixing ability and dynamic behavior of a continuous process. In the presented study, the RTDs of a continuous blender (Modulomix, Hosokawa) and laboratory rotary tablet press (Fette 102i) were determined. Both units were part of a CM line for the preparation of tablets from hot-melt extruded (HME) pellets. Thus, the RTDs were determined at the nominal line throughput ± 20%, investigating the effect of throughput changes on the process dynamics of each unit. Thereby, the RTDs of powder-sized excipients (Avicel® PH102 and Kollidon® CL) and pellets were characterized separately to elucidate differences relevant for material tracking.

The RTD was determined by means of tracer experiments, where the formulation components were dyed with red food color to act as tracers. Tracer signals were evaluated via colorimetric analysis of video frames from monitoring the processed material at the unit operation's outlet. Material attributes of raw materials and tracers, relevant for the processing behavior were characterized to ensure representative RTD results.

The blender characterization revealed short and well controlled RTDs for the powder components, across all throughput levels. The dead time of pellets was similar, but the mean residence time T_m and RTD width were significantly larger than for powders and also subjected to increased variability. The effect of throughput on the RTD was also less clearly pronounced. This was attributed to inconsistent powder flow across the weir in the blender, caused by the larger particle size of pellets. The tablet press characterization revealed an extensive degree of back-mixing in the feed-frame for both, pellets and powders. The RTD of pellets was less influenced by varying process parameters, but exhibited poorer repeatability in general. The colorimetric analysis of pellet tracer concentration in tablets exhibited a low signal-to-noise ratio, which may have affected the RTD results. Nevertheless, it could be identified, that pellets passed the feed frame faster than powders.

Moreover, a recirculation zone at the interface of the tablet press hopper and the feed fame was identified, further provoking a tailing of the RTD. Thus, the RTD investigations highlighted the need for CM optimized feed frame designs.

[4] This chapter is based on data from a Master's Thesis (Waldenhofer, 2017), co-supervised by the author of this doctoral thesis. Some of the data in this chapter is contained in a ECCPM joint publication (Karttunen et al., 2019).

6.1. Introduction

The characterization of the residence time distribution (RTD) of pharmaceutical processes has gained significant attention over the past years, due to the increasing adoption of continuous manufacturing (CM). In CM, material continuously enters and leaves the process, undergoing transformation as it moves along the process. The RTD is the probability distribution of time it takes for a material portion to exit the process. Therefore, it characterizes how long the material remains exposed to the different process conditions, such as a specific shear stress. It is the basis for tracking materials through the process and to assign measured quality control data to a final product portion. Consequently, it can also be used to divert specific material portions which do not fulfill the desired quality attributes along the process line (Engisch and Muzzio, 2015; Gao et al., 2012). Additionally, RTDs contain information on the characteristics of a process, e.g. if there are dead zone or bypass-zones present, or which degree of convective and diffusive mixing is provided. This information is relevant during process development and also severs in the specification of appropriate measurement frequencies for process analytical technologies (PAT) (Engisch and Muzzio, 2015).

RTDs have been extensively characterized for linear continuous blenders, across a large variety of configurations, process settings and materials (Ammarcha et al., 2017; Berthiaux et al., 2008; Gao et al., 2011; Kruisz et al., 2017; Marikh et al., 2017; Osorio et al., 2014; Osorio and Muzzio, 2016; Portillo et al., 2010, 2009, 2008). For tablet presses and parts thereof in contrast, fewer literature is available (Dülle et al., 2018a, 2018b; Manley and Shi, 2018; Martinetz et al., 2018). For both processes, most studies investigated the RTDs of pharmaceutical powders. The RTDs of particle blends containing significantly different particle size ranges, such as pellets in powder, have not been reported yet, neither for continuous blending, nor for tableting. Multiple unit pellet system (MUPS) tablets, utilize such blends to provide many small units containing the active pharmaceutical ingredient (API) within one single dosage form. This has biopharmaceutical advantages, such as shorter passage times in the stomach and a better distribution of the API in the gastrointestinal (GI) tract (Bodmeier, 1997).

Typically, the RTD is determined by means of tracer experiments. Thereby, APIs, or other well detectable tracers are used to provoke an impulse, or a step-change response of the system. Spectral methods, such as inline near-infrared spectroscopy (NIR) (Escotet-Espinoza et al., 2019a; Manley and Shi, 2018; Martinetz et al., 2018; Simonaho et al., 2016; Van Snick et al., 2019) and chemical imaging (Kumar et al., 2014; Martinetz et al., 2018), or manual sampling and offline analysis (Abouzeid et al., 1974; Dülle et al., 2018a) have been used to monitor the system's response. Another attractive option is image analysis in combination with colorimetric evaluation (Ammarcha et al., 2017; Kruisz et al., 2017; Kumar et al., 2006; Wahl et al., 2017), due to the low investment costs for high-performance cameras. A comparison of these different measurement approaches, including benefits and

disadvantages of the different methods, was recently published (Karttunen et al., 2019). The responses are typically used for fitting an RTD model. Different RTD model types are available, which can be selected depending on their later use: i) analytical solutions of the Taylor axial dispersion model or Fokker-Planck equation for defined initial boundary conditions (Danckwerts, 1953; Levenspiel, 1999) or tanks-in-series models (Levenspiel, 1999) to gain understanding of the mixing mechanisms in the process, ii) statistical distributions, such as the Weibull function, to represent the RTD empirically by a continuous function (Potente and Lappe, 1986), or iii) transfer function models of different order to represent linear time-invariant systems in control engineering (Johansson, 2011; Ljung, 1999). Moreover, the latter model allows to use arbitrary (but well defined) input functions for provoking the system's response, such as block signals, or pseudo random binary sequence signals (Nicolaï et al., 2018).

The effect of tracer material properties on the RTD characteristics of continuous blending equipment has recently been discussed by Escotet-Espinoza et al. (Escotet-Espinoza et al., 2019a, 2019b). They observed different RTDs when using materials of different properties as tracer for a specific base material. They elucidated, that bulk properties, such as flow function coefficient, bulk density and basic flow energy must be similar for tracer and bulk material in order to receive representative RTD parameters. Thus, it is vital to use appropriate tracer materials. Additionally, this highlights, that RTDs of blend components with significantly different properties should be characterized separately, in order to accurately track them through the process.

In general, narrow RTDs are desired for CM processes. This simplifies material tracking and minimizes the amount of material that needs to be rejected in case of a deviation or when changing set points. The back-mixing, that is needed to dampen feeder fluctuations should be provided by specific process units, i.e. blenders, where the degree of back-mixing can be controlled independently from other product quality attributes. Thus, the design of equipment that was originally developed for batch processing, may need to be revisited for optimized behavior in CM. For example, tablet press feed frames have been optimized to provide consistent bulk densities above the tableting dies in batch processing, independent of the decreasing hopper fill level, i.e. overhead pressure. Hoppers were designed to provide large empty volumes, in order to produce a large quantity of tablets in one batch. For CM in contrast, hoppers with small empty volumes are desired to shorten start-up time and reduce in-process material. Thereby, the feed frame design should provide well controlled residence times, whereas the bulk density conditioning is less critical due to the basically constant fill levels in the hopper during tablet manufacturing. Nevertheless, it is worth mentioning, that back-mixing in the feed frame has also been utilized to improve the micro- and macroscopic blend homogeneity (Van Snick et al., 2018, 2017). In these studies, it was highlighted though, that intensified mixing in the feed frame has to be carefully balanced, due to the risk of over-lubrication decreasing tablet hardness and wetting.

Another implication of CM on tablet press operation originates from the need to align the throughputs of all units. Thus, processes ideally allow to slow down, or speed up the production, depending on events upstream and downstream of the respective unit. Martinetz et al. investigated the use of the tablet press as slave (instead of master) in the control loop of a CM line, by changing turret speed inside a limited range (Martinetz et al., 2017). A main concern when using such a control strategy is the effect of tableting speed on tablet quality attributes. The sensitivity of quality attributes to such speed changes depends on the formulation properties, as demonstrated by Grymonpré et al. (2018b). However, also the effect on the process dynamics, i.e. the RTD, is of interest.

The aim of this study was, to determine the RTD of pellet and powder blend components in a blending and tableting unit for the production of immediate release (IR) tablets in a continuous manufacturing line (Figure 6-1). RTDs were determined in a range of ± 20% around the nominal process set point to elucidate the effect of throughput changes on the process dynamics of the given units. RTDs were determined using red colored formulation components as tracers for colorimetric video evaluation. Thereby, the RTDs of powder components and pellets were characterized separately to study potential differences in material behavior in the process units. The blending process was characterized in full continuous operation. The RTDs of the tablet press were evaluated in batch experiments using a throughput range relevant for continuous operation. Furthermore, the effect of different feed frame speeds and tracer layer positions was investigated in tablet press RTD characterization. Transfer function models were fit to tracer color intensity curves, for later use in process control strategy development and for the calculation of RTD characteristics, elucidating the effect of material and process settings.

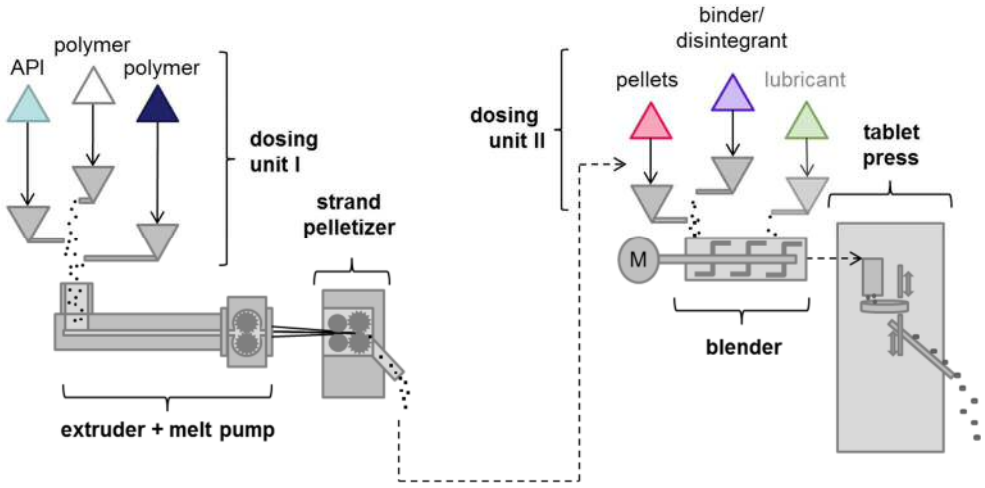

Figure 6-1. Continuous manufacturing line for the preparation of MUPS tablets from strand-pelletized HME pellets. Dashed lines indicate, that material was transferred manually between the process units, i.e. the process units were not directly connected. The lubricant feeder was not mounted on the blender during blender characterization.

6.2. Materials and Methods

6.2.1. Used Materials

The formulation for tableting of the cylindrical hot-melt extruded (HME) pellets was optimized (see Chapter 5), in order to provide IR of the active pharmaceutical ingredient (API) from mechanically stable tablets. The pellets (mean particle size 912.09 µm) contained 10 wt.% of a poorly water-soluble API, nimodipine (NMD, Bayer AG, Germany), 36 wt.% Eudragit® E (Evonik AG, Germany) and 54 wt.% Methocel™ E5 (Dow Chemical, USA) and exhibited a yellow color. The production of the cylindrical pellets was performed in a HME and strand pelletization unit at the nominal settings described in Chapter 4. External components made up 60 wt.% of the tableting formulation, where 49 wt.% consisted of Avicel® PH102 (PH102, FMC Biopolymer, USA) acting as binder, 10 wt.% of Kollidon® CL (K-CL, BASF, Germany) acting as disintegrant and binder, and 0.5 wt.% of magnesium stearate (MgSt, SIGMA-ALDRICH Chemicals Company, USA) as lubricant.

Tracer Materials

Red colored pellets and powder components (except MgSt) were used as tracers in the RTD characterization experiments. Red food colors (No-Taste Red Icing Color, Wilton industries USA and Color Flo Red, Rainbow Dust Colors Ltd, UK) were used to dye the raw pellets, PH102 and K-CL. For the pellets pure food color was applied by thoroughly kneading it onto the pellets in a plastic bag. The color was diluted with water for PH102 and with ethanol for K-CL tracer preparation to achieve a more homogeneous color distribution after kneading. Afterwards, the tracers were dried (40°C for pellets and 50°C for powders) and de-agglomerated by sieving (1200 µm screen for pellets and 430 µm screen for powders). Pictures from the raw and colored raw materials are shown in Figure 6-2.

Figure 6-2. Raw and colored formulation components.

Pre-Blend Preparation

Blender characterization experiments were performed feeding a powder pre-blend and the pellets separately. Pre-blending of the powders was performed in a tumble blender (Turbula® T2F, WAB AG, Switzerland) at a speed of 75 rpm for 10 min. MgSt was not added for the blender runs, in order to maintain full color intensity of tracers for video recording. For the tableting runs, the whole formulation was pre-blended. Pellets, PH102 and K-CL were mixed in a first step as given above, and MgSt was added in a second step to avoid over-lubrication, using only 1 min of blending time.

6.2.1. Material Characterization

To ensure representative behavior of the tracer, raw and colored materials were characterized with regard to relevant material properties. Particle size and size distribution were determined by means of image analysis (QICPIC with a dispersion unit RODOS, Sympatec GmbH, Germany). Angle of repose was measured according to the United States Pharmacopeia (U.S.P.) 35 (The United States Pharmacopeial Convention, 2012). Bulk and tapped density were determined in a graduated volumetric cylinder and a tapped density tester (PT-TD200, PharmaTest, Germany) according to Ph.Eur. 2.9.34. (Council of Europe, 2014). Hausner ratio was calculated as a measure for flowability. Permeability tests were performed on a FT4 powder rheometer (Freeman Technology, UK).

6.2.2. Used Process Equipment

Two KT20 twin-screw loss-in-weight (LIW) feeders (Coperion-K-Tron, Switzerland) were used to feed the continuous blender (Modulomix, Hosokawa Micron, The Netherlands). The blender was equipped with seven forward-conveying paddle pairs, mounted at an angle of 45° on to rotating shaft. Before the last two paddle pairs and the outlet, a weir was installed to increase the hold-up of material in the process. The blender was operated in the fluidized regime at 1000 rpm, which was found to provide a homogeneous distribution of pellets in the material stream and limited dust formation. A black conveyor belt (Geppert, Germany) was used to collect the processed material below the blender outlet. After the conveyor belt, a catch-scale (PW22C3MR, HBM, Germany) was placed, weighing the processed material during the experiments to determine when steady state was reached before starting the RTD characterization tests.

Tableting was performed in a laboratory rotary tablet press Fette 102i (Fette Compacting, Germany). The tablet press was equipped with eight pairs of flat faced punches with 8 mm diameter (EU1'', Fette Compacting, Germany) and a feed frame with three rotating wheels (Fill-O-Matic). The original tablet press hopper was replaced by a straight hopper with reduced volume (100 mm diameter and 450 mm height). The compression settings of the tablet press were set to a pre-compression force of 0.5 kN, a main compression force of 12 kN and a fill-depth for a target tablet weight of 250 mg, according to the findings in Chapter 5. At the beginning of each tableting run, tableting parameters where manually set to reach the desired tablet weight and compression forces. Then, automatic force control was activated and used throughout the tableting runs, allowing the tablet press to adjust the filling depth of the tableting dies to maintain a constant main compression force. The produced tablets were collected on the black conveyor belt, which was also used in the blending experiments. After running the hopper empty, the tablet press was vacuum cleaned before refilling the hopper for the next experiment.

6.2.3. Residence Time Distribution Characterization

Blender Tracer Experiments

After reaching steady state in throughput, tracer impulses were injected manually into the inlet port through which the formulation components were fed to the blender. The portions of powder and pellet tracer, were quickly poured from a small container with pre-weighed tracer mass. For the pellet tracer a mass of 5 g was used, for the powder tracer 3 g. The optimal tracer mass was chosen in preliminary experiments with regard to sufficient detectability of the tracer signal in the video and a minimal disturbance of the process. The RTD experiments for pellets and powder components were performed in duplicate at throughput levels of 8, 10 and 12 kg/h (run order given in Table E-1 in the Supplemental Material section E).

At a distance of 56 cm from the outlet, a camera (Nikon E5200, Nikon, Japan) was installed above the conveyor belt. The time delay caused by the distance of the camera to the blender outlet, was corrected for during the RTD data evaluation. The video was recorded with a frame rate of 25 frames/s. The analysis of the tracer concentration in the material stream was performed via colorimetric analysis of a defined pixel region in the video frames, using an in-house programmed script (MATLAB® 2015b, The MathWorks, USA). The same script has already been used for determining the RTD of a melt extrusion process (Wahl et al., 2017).

The results from the colorimetric analysis over time were used for fitting a transfer function model. The model structures giving the best fit for the RTDs of powder and pellet tracers are given in Eq. 6-1 and in Eq. 6-2 respectively.

$$P(s) = \frac{k(1+sT_1)}{(1+sT_2)(1+sT_3)(1+sT_4)(1+sT_5)} e^{-sT_d} \qquad \textit{Eq. 6-1}$$

$$P(s) = \frac{k(1+sT_1)}{(1+sT_2)(1+sT_3)(1+s*T_4)} e^{-sT_d} \qquad \textit{Eq. 6-2}$$

In the transfer function models k is a scaling factor, T_d the dead time and T_x are flow rate-dependent time constants.

Tablet Press Tracer Experiments

The operating points of the tablet press turret speed were adapted to the desired overall CM line throughput levels between 8 and 12 kg/h, i.e. to five different turret speeds (68, 75, 83, 92 and 100 rpm). In order to assess the back-mixing effect of the feed frame, its speed was varied in three levels of 40, 60 and 80 rpm. Additionally, tracer layers were placed at two different positions Figure 6-3, to capture the effect of back-mixing above the feed frame. Position A was at the bottom of the hopper, i.e. just above the feed frame. Position B was at 30% of the total hopper height. The process settings were distributed in a D-optimal experimental design (runs N1 to N17) with duplicated center point (N18, N19). One additional run (R20) was performed at an initial hopper fill level of 100% using powder tracer, to assess the effect of more wash-out material and time until the hopper was running empty. However, for pellet tracer only a reduced number of RTD runs were performed at the higher tracer layer position (B), due to limited tracer detectability. Moreover, several runs (runs 8-14) were performed with a 10-fold mass of MgSt in the formulation, among them the center point runs. This critically affected the mechanical stability of the tablets, and the effect on RTD data was investigated by repeating the center point runs with the correct composition (R19) and comparing the resulting RTD. An overview of all tableting runs is given in Table E-2 in the Supplemental Material section E.

Tracer layers were placed at the specified levels by filling the uncolored formulation in the feed frame and manually rotating the wheels for ten times. Then, the hopper was filled to the desired level and the tracer layer added evenly. Above the tracer, uncolored formulation was used to fill up the hopper to 80% of its total height. The tablet press was characterized in batch mode, washing out the tracer layer with the uncolored formulation.

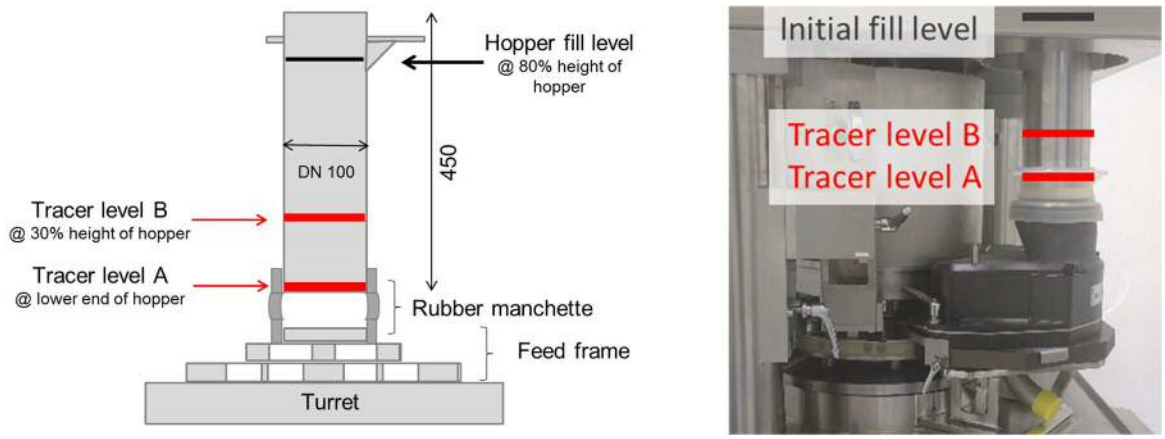

Figure 6-3. Tracer layer positions A and B for RTD determination in the tablet press.

Since the RTDs of the two different components were determined separately, the tracer layer was either composed of red powder and uncolored pellets when testing the powder RTD, or of uncolored powder and red tracer pellets for pellet RTD characterization. Again, tracer mass was chosen with regard to detectability in the final tablets. A total tracer layer mass of 177.5 g was used for the pellet

tracer and 59.1 g for the powder tracer. Thus, the tracer was added as a block function in this case. The "duration" of this block function was given by the tracer layer mass and the throughput.

The product was again collected on the conveyor belt, with the camera installed at a distance of 66 cm from the tablet press outlet for video recording. The colorimetric analysis of the powder tracer concentration was performed using the same evaluation tool as for the blender RTD characterization runs. However, a different approach had to be used for the pellet tracer runs. In that case, the colorimetric evaluation of the videos was adapted in a MATLAB script. Frequency density values of different color space values were combined and used for a principal component analysis (PCA) to increase the sensitivity to color changes in a low number of pixels in the video frames. The first principal component (PC1) over time was used to fit the transfer function model. The details of this evaluation are described in the results section 6.3.2.

In the tablet press runs, the same model structure was used for fitting the responses of both tracers. The structure is given in Eq. 6-3.

$$P(s) = \frac{k}{(1 + sT_1)(1 + sT_2)(1 + s * T_3)} e^{-sT_d} \qquad \textit{Eq. 6-3}$$

Calculation of the RTD and its Characteristics

The RTD, that is the probability density distribution of residence times $E(t)$ in a process, is defined by

$$E(t) = \frac{c(t)}{\int_0^\infty c(t)\, dt} \qquad \textit{Eq. 6-4}$$

where $c(t)$ is the momentary concentration of a tracer material.

Under the assumption, that the results from colorimetric analysis are linearly related to the concentration of the tracer (Peng et al., 1994), $E(t)$ can be determined directly from the impulse response (with scaling factor $k = 1$) of the fit transfer function model. The validity of this assumption is discussed for the different RTD characterization experiments in section 6.3.2.

In order to compare the RTD of powder components and pellets at different throughputs, the dead time T_d, and RTD characteristics, such as mean residence time T_m and the standard deviation s_{RT} were calculated according to Eq. 6-5 and Eq. 6-6.

$$T_m = \int_0^\infty t\, E(t)\, dt \qquad \textit{Eq. 6-5}$$

$$s_{RT} = \int_0^\infty (t - T_m)^2\, E(t)\, dt \qquad \textit{Eq. 6-6}$$

6.3. Results

This section is structured in the following way: First, the results from the raw material and tracer characterization are given. Next, details of experimental conditions and the colorimetric analysis for RTD characterization are shown. Finally, the RTD results for powder and pellets in blending and tableting are investigated with regard to the effect of particle size and process parameters.

6.3.1. Tracer Characterization

The properties of raw materials and colored tracers were determined to evaluate how the dying of the particles affected their bulk properties and consequently, the RTD measurement results. The properties of raw bulk materials and the bulk after coloring of the particles are given in Table 6-1. Minor differences in median particle size were observed in the tracer materials, attributed to some agglomeration during dying (K-CL) and to the sieving step after tracer coloring (pellets). Some changes were observed for PH102 in terms of flowability classification according to Hausner ratio (HR) and significant changes in K-CL permeability. Permeability is a relevant material attribute for die filling and pre-compression, and was also shown to influence the powder flow and residence time in the feed frame (Van Snick et al., 2018). However, since K-CL is present in the formulation only with a fraction of 10 wt.%, this change is considered negligible. The slightly increased HR of PH102 indicated minor changes in compressibility and flowability of the PH102 tracer. The angle of repose (AOR) test showed the opposite trend in flowability though. Thus, the tracer property characterization indicates, that the dyed tracers are suitable to produce representative data during blender and tablet press RTD characterization.

Table 6-1. Averaged material characterization results (n=3, except for PSD data with n=1) for raw materials and tracers.

Material	x_{50} [µm]	span [-]	AOR [%]	Flowability (AOR)	HR [-]	Flowability (HR)	PD@1kPa [mbar]
			PH102				
Raw	134.6	1.31	38.03 ± 0.26	Fair	1.33	Passable	0.54 ± 0.02
Tracer	118.2	1.41	35.55 ± 0.49	Fair	1.40	Poor	0.57 ± 0.10
			K-CL				
Raw	114.1	1.61	37.23 ± 0.73	Fair	1.40	Poor	0.99 ± 0.10
Tracer	123.4	1.62	36.23 ± 1.54	Fair	1.42	Poor	0.35 ± 0.08
			Pellets				
Raw	912.1	0.40	37.11 ± 0.76	Fair	1.09	Excellent	-
Tracer	887.7	0.30	37.50 ± 0.37	Fair	1.07	Excellent	-

x_{50}…median particle size, span…$(x_{90}-x_{10})/x_{50}$, AOR…angle of repose, HR…Hausner ratio, PD…pressure drop

6.3.2. Experimental Conditions, Colorimetric Analysis and Model Fitting

Except for representative behavior of the tracer material, there are several other aspects that need to be considered, in order to receive reliable information on a material's RTD in a process. Here, a list of aspects is given, which needed special attention in this study:

i) The process in characterization needs to operate in (quasi-) steady state.
ii) The tracer must not disturb the process, or alter the process dynamics.
iii) Representative sampling must be applied when measuring the process response.
iv) The quantity used for evaluating the process response (e.g. color intensity, spectral peak height) must be linearly related to the concentration of the tracer in the material stream.

A more complete set of underlying assumptions and prerequisites for accurate RTD characterization was published by Escotet-Espinoza et al. (2019a).

Experimental Conditions and Sampling

Regarding the first two points, the data from the reference catch-scale confirmed that the process was in steady state before, and not disturbed by the addition of the tracer. Process data of the blender RTD runs is shown in Figure E-1 in the Supplemental Material section E. There was only a very short increase in throughput detected when the tracer left the process and no further instabilities in powder flow were observed.

Process data from an exemplary tableting run is shown in Figure E-3 in the Supplemental Material section E. Quasi-steady state of the process parameters was observed after 1 min of process time, when the automatic compression force control of the press was activated. The quasi-steady state lasted for approx. 2/3 of the total run time, i.e. time for emptying the hopper of the press. After that, an increase in main compression force standard deviation and fill depth (adjusted by automatic compression force control) was observed. This indicated inhomogeneous and decreasing bulk density in the feed frame, due to insufficient overhead pressure. For tableting runs with the highest level of feed frame speeds (80 rpm), this phase was furthermore accompanied by tablet press shut-downs, caused by single punch overloads (Figure 6-4). This was an indicator for irregular die filling, or segregation of the formulation. Increased die filling variability at high feed frame paddle speed has also been reported for another tablet press (Grymonpré et al., 2018b). The duration of such interruptions was excluded from the colorimetric analysis data, in order to evaluate the tracer signal over process time correctly. In general, the tablet press characterization in batch-mode was expected to exhibit some deviations from the results which would be received from continuous operation of the press. Especially, the degree of tailing in the RTD may appear different, if the hopper is constantly refilled during operation. However, it still delivers valuable information on the different behavior of pellets and powders.

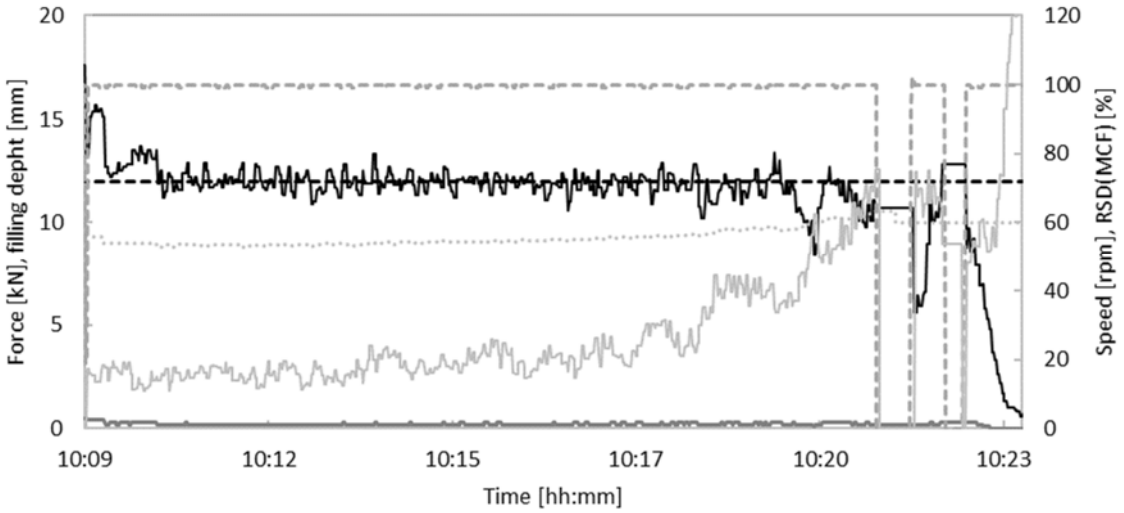

Figure 6-4. Tablet press data collected via SIPAT (run N16 with a feed frame speed of 80 rpm): main compression force (MCF – solid black), pre-compression force (solid dark gray), RSD of MCF (solid light gray), MCF set point (dashed black), die filling depth (dotted gray) and turret speed (dashed gray). Process interruptions occurred in the last third of process time due to single punch overloads. These interruption durations were removed for RTD analysis. (Activation of compression force control around 10:10)

With regard to representative sampling of the processed material stream, an appropriate pixel region position and size was selected for colorimetric analysis in each video (50 x 700 pixels for blending and 50 x 800 pixels for tableting). The length of the region was selected to cover the whole width of the material stream on the conveyor belt. The width of the region in the direction of the conveyor movement was as short as possible, in order to avoid a strong smoothing of the color intensity over time, while still minimizing noise in the measurement.

Colorimetric Analysis and RTD Modeling

The pixels inside the selected video frame region were analyzed regarding their average L*a*b*-color space values (L*=lightness, a*=red/green and b*=yellow/blue). Pixels showing the black conveyor belt were excluded using a threshold in the L*-value.

For the blender characterization, the averaged a*-value (redness) in the analysis region of each frame was used to evaluate the concentration of the red tracer. The a*-value curve over time was offset-corrected and used to fit the transfer function models.

When using these models directly for evaluating the RTD, a linear relationship between the color intensity and the tracer concentration was assumed. Wahl et al. demonstrated the validity of this assumption for low color tracer concentrations (weight fraction < 1%) (Wahl et al., 2017). In the given blender characterization runs, the maximum tracer content at the outlet was calculated to remain below 0.5% (w/w). This estimation was based on a convolution of the momentary tracer concentration at the blender inlet upon tracer addition with the determined RTD. Exemplary color intensity curves with fit models for a pellet and a powder tracer impulse are shown in the Supplemental Material

section E (Figure E-2). The model parameters of fit transfer function models are given in the same section in Table E-1.

The RTD characterization of the tablet press required some adaptations in the video data analysis and model fitting.

First, the material was not presented as a continuous stream to the camera, but the tablets were visible as discrete spots on the black conveyor belt. Thus, it was necessary to filter out frames, where only small parts of a low number of tablets was inside the analysis region and most of the pixels were excluded as background. These frames, where filtered out by a threshold for the average lightness L*-value, reducing the measurement noise. Moreover, the resulting curve was smoothed using a moving average function over 25 frames (1 s). With regard to the linear relationship of the redness of tablets with the actual tracer concentration, the maximum tracer content at the outlet was again estimated to remain below 0.5% (w/w).

Second, an entirely different strategy was needed for the colorimetric evaluation of the pellet tracer runs. The color intensity of the red pellets on the tablet surfaces was very low and the red-green space value (a*) could therefore not be used to reliably determine the tracer concentration. The improve the sensitivity of the colorimetric analysis, the background and shadowy edges of the tablets in the video frames were removed entirely. Then, probability distribution histograms of color intensities in several color spaces (RGB, L*a*b* and HSV) were determined for the remaining pixels. Quantiles of these distributions were evaluated over process time and this allowed to increase the sensitivity to color changes in a small number of pixels. The x_{10} and x_{50} quantiles of the H-value histograms and the x_{10} of the b*-value (yellow-blue space) were found to contain the highest sensitivity to the presence of tracer pellets in the tablets. For a few pellet tracer RTD runs other quantiles yielded better RTD curves: for N15_E1 the x_{90} of the b*-value was used instead of x_{10}, for N17_E2 the x_{90} of the a*-value instead of the x_{10} of b*, and for N2_E17 the x_{50} of the a*-value instead of H-value and the x_{90} of the a*-value instead of the x_{10} of b*. In general, the sensitivity of the b*-value suggests, that in this case the reduced number of yellow raw pellets visible on the tablet surface was a more reliable indicator for increased tracer concentration, than the redness value (a*). In order to increase the robustness of the colorimetric analysis, a principal component analysis (PCA) was applied to combine several quantiles of color space values for RTD evaluation. However, it is important to notice, that this approach does not directly measure the concentration of the tracer anymore, but purely a change in color due to changing tablet composition (e.g. also by segregation effects). Thus, the validity of this approach to determine pellet tracer concentration in tablets needs to be further investigated in the future.

Third, with regard to model fitting, another interesting observation was made during powder RTD characterization in the tablet press. A second peak in tracer color intensity was observed at the end of

several tableting run (Figure 6-5 A). Upon close inspection, the appearance of this peak could be correlated to the moment, where the hopper fill level reached the interface between the tablet press hopper and the inlet of the feed frame. In this zone, a recirculating pattern of material was observed (Figure 6-5 B), which only started to wash out when the hopper fill level reached this level. The tracer material caught inside this recirculation zone was therefore released only when the whole pattern collapsed. Upon collapsing, the tracer entered the feed frame and gave a second peak-signal in color intensity. Since this effect would not occur during continuous operation of the tablet press, this second peak was truncated from the color intensity curve over time before model fitting. In continuous operation, the tracer material inside this circulation pattern is expected to wash out very slowly, elongating the tail of the RTD curve further.

The presence of this circulating pattern may be related to the design of the interface, which is schematically shown in Figure 6-5 C. The interface between the hopper and the feed frame is gradually reducing in size, yielding in a kidney-shaped opening to the upper feeding wheel of the feed frame. The chambers of this wheel are filled with new material when they emerge from the covered section and excess material is scraped off when the wheel moves under the cover again. Thereby, the inclination of the cover surface causes the material to move upwards, forming a circulating pattern at this location. However, it was not possible to correlate the appearance of the intensity of this effect to any process parameters or combinations thereof. Moreover, it did not or significantly less pronounced occur when tracer pellets were used. Thus, this effect should be further investigated before drawing final conclusions on how to avoid it.

An exemplary set of powder and pellet color analysis data and model fits is shown in Figure E-4 in the Supplemental Material section E. The model parameters from all fit transfer functions are given in Table E-2 in the same section.

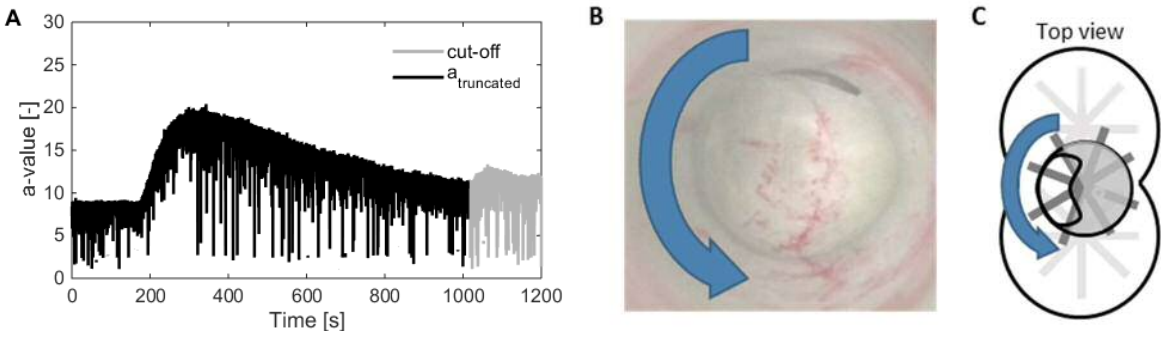

Figure 6-5. The second peak in the tablet press RTD occurred when the hopper was running empty (A). Top view on the material surface with red powder tracer with an arrow indicating the direction of the rotational movement of the distributing wheel below the powder surface at the moment where the interface section was running empty (B). The kidney shaped interface with the underlying distributor and feed frame wheels is shown schematically in (C).

6.3.1.RTD Characterization Results

Continuous Blending

The RTD curves $E(t)$ and RTD characteristics for powder and pellet tracer impulses at all throughput levels are shown in Figure 6-6 and Figure 6-7. The RTD characteristics of all runs are given in Table E-1 in the Supplemental Material section E.

The repeatability of powder tracer runs was found to be excellent (Figure 6-6 A). In Figure 6-7, it can be observed, that the dead time became slightly shorter and RTD narrower with increasing throughput, which was of course expected. For the pellet tracer, higher variability was observed in the repeated RTD characterization runs. Moreover, no consistent trend was observed across the tested throughput range. Compared to the powder, the pellets exhibited a significantly wider RTD, resulting in longer mean RTs. This is an interesting observation, since Escotet-Espinoza et al. observed a negative correlation of tracer particle size with the mean RT in continuous blending (Escotet-Espinoza et al., 2019a). A similar effect was reported by Ammarcha et al., where coarse couscous was leaving the blender first during start-up, while fine particles accumulated in the system, until they started to exit (Ammarcha et al., 2017). Since a non-fluidizing blender was used in both cases though, the different results are likely caused by the profoundly different powder flow regime in the process. For the given blender, the increased variability and larger degree of back-mixing of pellets was attributed to the effect of the weir mounted before the outlet of the blender. The weir leaves only a narrow gap for the material to reach the outlet zone of the blender. The larger particle size of the pellets may require a larger gap to ensure more consistent passage of the material. However, the blender was operated at the lower end of its throughput specification range (specified for 4 to 200 kg/h) and better control of the blending process is expected at higher throughputs.

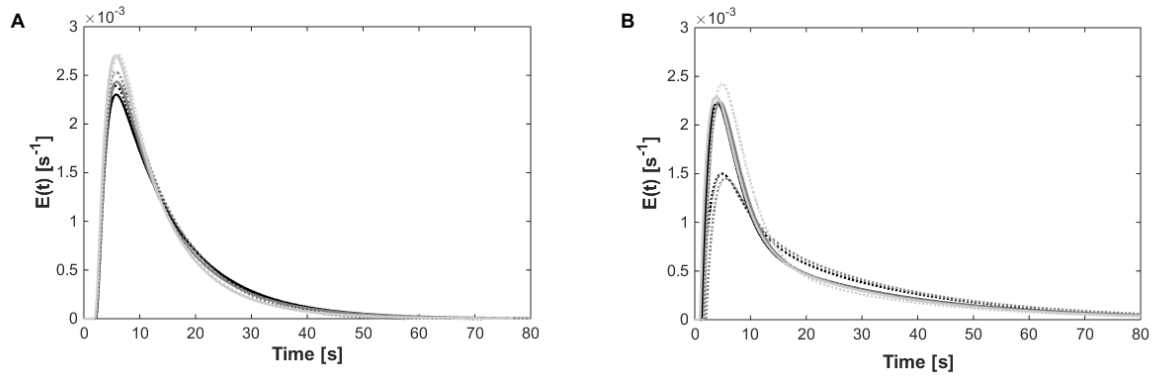

Figure 6-6. Duplicates (dashed and solid) of powder (A) and pellet (B) RTD measurements at different throughput levels: 8 kg/h (light grey), 10 kg/h (grey) and 12 kg/h (black).

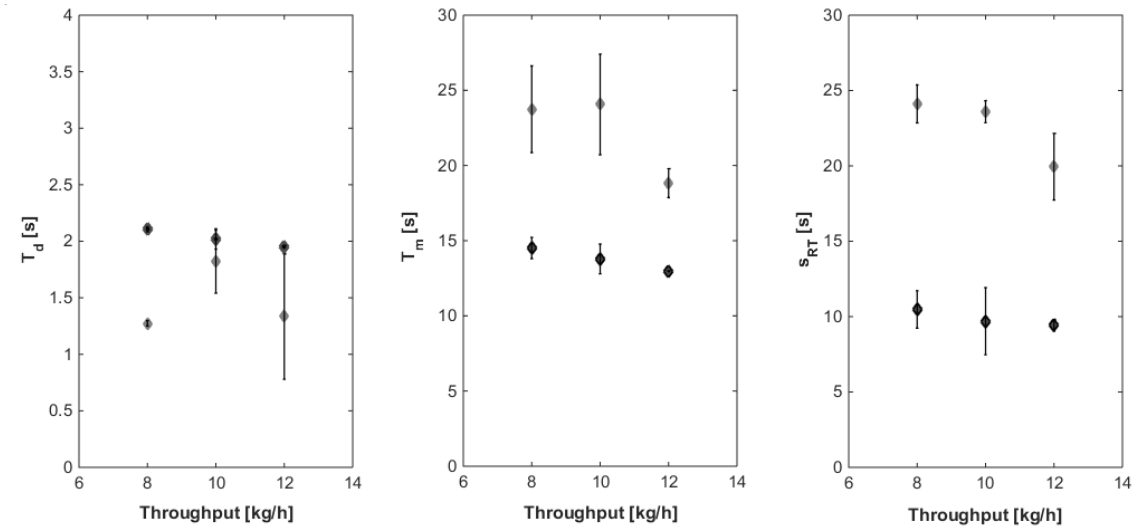

Figure 6-7. Averaged RTD parameters for pellets (grey) and powder components (black) (error bars indicating the measurement span for n=2) at different throughput levels.

Overall, the blending process was found to provide limited back-mixing with a powder and pellet RTD width around 10 s and 23 s, respectively. Thus, long-term feeder fluctuations cannot be dampened by this blender. However, the tested throughput changes of ±20% do not critically affect the degree of back-mixing that is provided by the blending process, when applying it in a CM line.

Tablet Press Characterization

Tablet press RTD characterization already yielded some interesting insight in flow patterns at the interface between the hopper and the feed frame. In this section, the effect of throughput, feed frame speed, position of the tracer layer and, of course, of the component particle size (powder vs. pellets) is discussed.

The repeatability and representativeness of the RTD characterization runs were investigated by duplicate RTD characterization runs (N18, N19) and a repetition of the center point with a higher initial hopper fill level of 100% (R20 – powder tracer only). The offset-corrected color intensity $a^*(t)$ and the first principal component ($PC_1^*(t)$) curves of respective powder and pellet tracer runs are shown in Figure 6-8. Thereby, some variability, especially in dead time was observed for both tracer types. However, the shape and width of the curves was similar. Run R20, with a higher hopper fill level yielded a very similar RTD to run N18, indicating that more wash-out time does not significantly change the RTD. Moreover, Figure 6-9 shows the color intensity curves of the repeated center point run, with the correct formulation. N18 and N19 were executed with a 10-fold amount of MgSt in the formulation. Runs R19 exhibited a powder tracer RTD, basically framing both replicate runs. Thus, no clear trend in T_d or T_m could be observed for the increased MgSt content, while RTD width was widened. It was concluded that the disturbance of MgSt content deviations on the RTD was in a similar range to other sources of disturbance in the experiments, such as initial material packing in the feed frame.

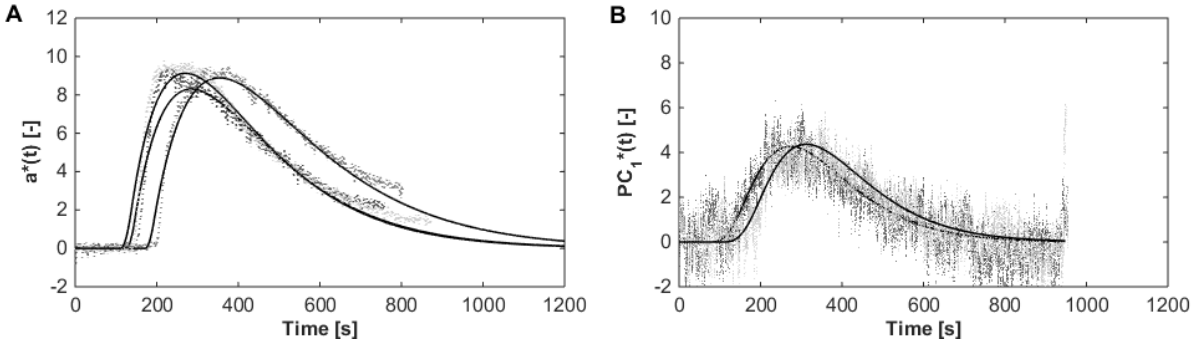

Figure 6-8. Replicate center point runs with model fits (solid black) for color intensity of powder tracer (A) and PC_1 of pellet tracer runs (B): N18 (dark gray dots) and N19 (gray dots) with 80% and R20 (light gray dots) with 100% hopper fill level.

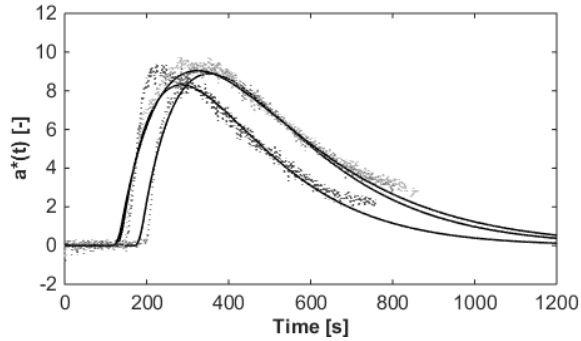

Figure 6-9. Color intensity of powder tracer center point runs N18 (dark gray) and N19 (gray) with 10-fold MgSt content in formulation, compared to run R19 (light gray) with correct composition.

The effect of tracer layer position was investigated by comparing run N17 to the center point runs, since they only differed in this factor. The powder tracer RTD exhibited a longer dead time and reduced RTD width Figure 6-10. The latter could be a result of the shorter wash-out time, which was problematic for model fitting. For the pellet tracer, the higher tracer level (TL B) resulted in a significantly shortened RTD curve. This was attributed to a lack of detectability of pellets in the videos though and was the reason, why no additional pellet RTD characterization runs were performed at this level anymore (run N15 done before – results shown in Supplemental Material section E).

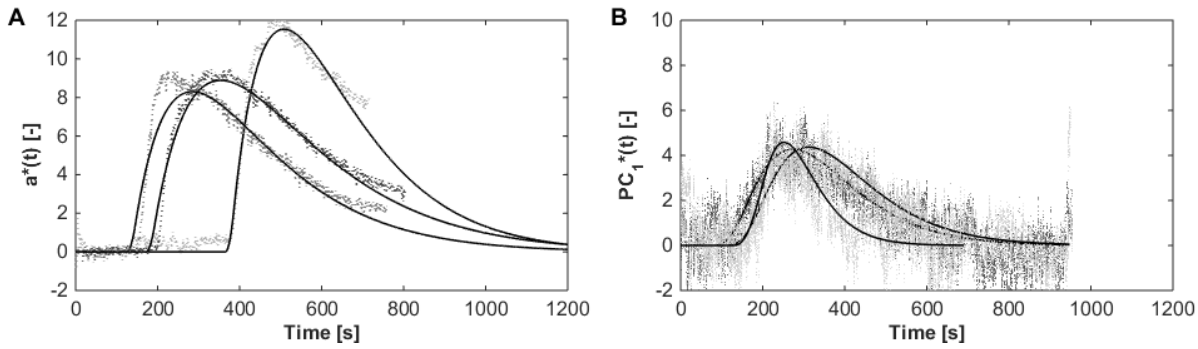

Figure 6-10. Comparison of TL A (N18 – gray, N19 – dark gray) and TL B (light gray) color intensity for powder tracer (A) and PC_1 for pellet tracer (B) with fit models (solid black) at medium turret and feed frame speed (TS 83 rpm, FF60).

Finally, Figure 6-11 shows RTD characteristics of powder and pellet tracer for different turret speeds and initial tracer layer positions at a feed frame speed of 60 rpm. The plots generated at other feed frame speeds are shown in Figure E-5 and Figure E-6 in the Supplemental Material section E.

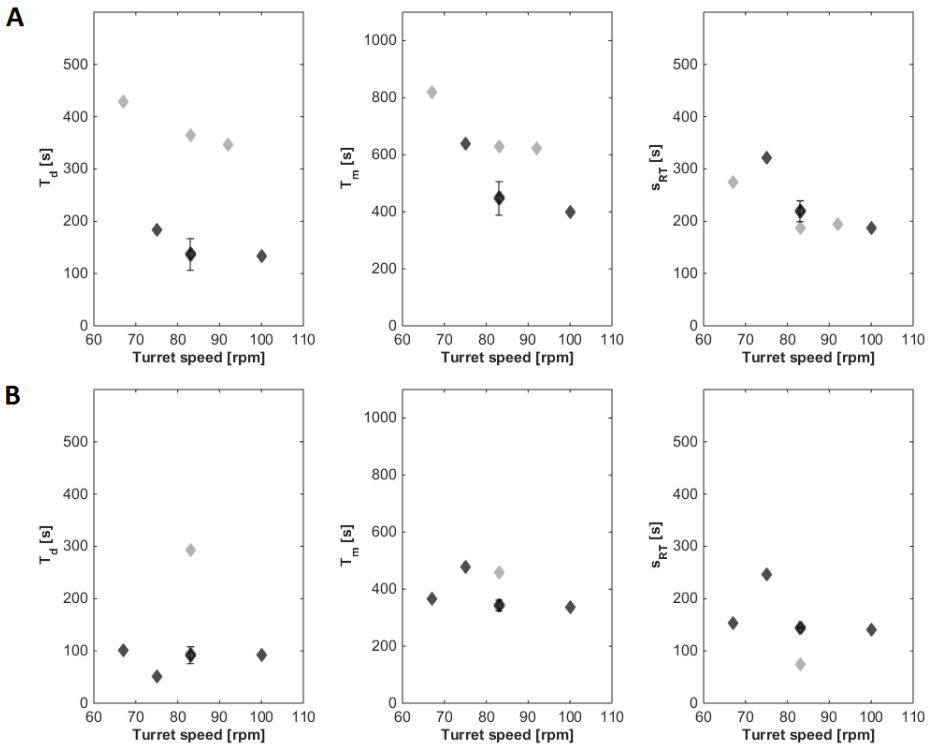

Figure 6-11. RTD characteristics of powder (row A) and pellet tracers (row B) in the tablet press across different turret speed levels and initial tracer layer positions (black – tracer level A, grey – tracer level B). (CP run error bars indicating span of n=2.)

It can be clearly observed, that increasing turret speed, i.e. throughput, decreases dead time T_d, mean RT (T_m) and the width s_{RT} of the powder tracer RTD. For pellet tracers, surprisingly there was no such effect observed. Only T_m did show the expected trend at the lowest feed frame speed of 40 rpm (Figure E-6 in the Supplemental Material section E). Mateo-Ortiz et al. reported that size segregation was reduced at higher feed frame speeds (Mateo-Ortiz et al., 2014). This undoubtedly positive effect may be the reason, why the detectability of pellets on the tablet surfaces was reduced, resulting in more variable RTD results at higher feed frame speeds.

Regarding the effect of feed frame speed on the RTD, Dülle et al. have reported that the T_m of MCC in this exact feed frame was independent of feed frame speed (using a throughput of 7.2 kg/h) (Dülle et al., 2018a). This was in line with our findings on powder tracer RTD (Figure E-5 in the Supplemental Material section E).

For powder tracer, the different tracer layer positions allowed to investigate the effect of back-mixing at the lower end of the hopper, or the hopper-feed frame interface. Dead time increased with a higher position of the initial tracer level (B), as expected. However, s_{RT} indicated, that the width of the RTD was narrower with higher initial tracer layer position. This may support the hypothesis, that the second peak in the tracer intensity curve was caused by a circulating zone at the interface between the hopper and the feed frame. While for the lower tracer layer position A, some of the tracer materials may have been entrapped in this zone, the tracer materials inserted at the higher position B appear to have passed this zone faster, i.e. they were not entrapped into the circulation to the same degree. However, a second possible reason for this observation was the reduced wash-out time of the tracer and consequently, the reduced part of the RTD curve that was available for model fitting. Thus, additional experiments, or simulations should be performed to better investigate this interface.

Finally, when comparing the RTDs for powder and pellet tracer, the RTD characteristics of pellets were harder to evaluate, due to less pronounced trends in the data across different process settings. In contrast to the blender results, this could not be attributed only to the process, but also to the reduced reliability of the colorimetric RTD analysis. Nevertheless, the RTD width (s_{RT}) of pellet tracer were clearly narrower and dead time T_d shorter, when compared to the powder tracers. This emphasizes, that component specific RTDs should be used to track the respective materials through the process.

6.4. Conclusions

This study demonstrated, that formulation components with significantly different particle size, such as pellets and powders, travel differently through a continuous blender and tableting process, resulting in distinct RTDs. This is of crucial importance for material tracking and quality control in CM.

The effect of throughput changes on the process dynamics of the given process equipment was investigated as well, to elucidate the criticality of control actions on material traceability. Thereby, the blender dynamics were identified to be very robust across the tested range of ± 20% around the nominal throughput of 10 kg/h. The tablet press in contrast, did exhibit RTD parameter alteration upon such throughput changes, especially detected for the powder components. However, further investigations in continuous operation of the tablet press are suggested to decrease variability in the data, before drawing final conclusions on acceptable throughput changes. Moreover, the effect of such changes on tablet quality has not been investigated and is expected to pose further boundaries to the final CM line control strategy.

With regard to other tableting parameters, feed frame speed was concluded to best remain in a range of 40 to 60 rpm. The RTD of the process was not affected by changing feed frame speed, yet, at higher feed frame speed, process instabilities occurred, indicating inconsistent die filling behavior.

Additionally, the RTD characterization of the tablet press revealed, that a recirculating pattern of material was formed at the interface between the hopper and the feed frame. Thus, a first-in-first-out principal was not fulfilled. This poses a challenge in material tracking for CM lines, and the design of this interface should therefore be optimized for CM. Moreover, a reduction of the feed frame empty volume would be desired to provide a narrower RTD and to reduce in-process material.

6.5. References

Abouzeid, A.-Z.M.A., Mika, T.S., Sastry, K.V., Fuerstenau, D.W., 1974. The Influence of Operating Variables on the Residence Time Distribution for Material Transport in a Continuous Rotary Drum. Powder Technol. 10, 273–288.

Ammarcha, C., Gatumel, C., Dirion, J.L., Cabassud, M., Berthiaux, H., 2017. Continuous powder mixing of segregating mixtures under steady and unsteady state regimes: Homogeneity assessment by real-time on-line image analysis. Powder Technol. 315, 39–52.

Berthiaux, H., Marikh, K., Gatumel, C., 2008. Continuous mixing of powder mixtures with pharmaceutical process constraints. Chem. Eng. Process. Process Intensif. 47, 2315–2322.

Bodmeier, R., 1997. Tableting of coated pellets. Eur. J. Pharm. Biopharm. 43, 1–8.

Council of Europe, 2014. 2.9.34. Bulk Density and Tapped Density of Powders, in: European Pharmacopoeia 8.0. European Commission, pp. 343–346.

Danckwerts, P.V., 1953. Continuous Flow Systems - Distribution of Residence Times. Chem. Eng. Sci. 2, 1–13.

Dülle, M., Özcoban, H., Leopold, C.S., 2018a. Investigations on the residence time distribution of a three-chamber feed frame with special focus on its geometric and parametric setups. Powder Technol. 331, 276–285.

Dülle, M., Özcoban, H., Leopold, C.S., 2018b. Analysis of the powder behavior and the residence time distribution within a production scale rotary tablet press. Eur. J. Pharm. Sci. 125, 205–214.

Engisch, W., Muzzio, F., 2015. Using Residence Time Distributions (RTDs) to Address the Traceability of Raw Materials in Continuous Pharmaceutical Manufacturing. J. Pharm. Innov. 64–81.

Escotet-Espinoza, M.S., Moghtadernejad, S., Oka, S., Wang, Y., Roman-Ospino, A., Schäfer, E., Cappuyns, P., Van Assche, I., Futran, M., Ierapetritou, M., Muzzio, F., 2019a. Effect of tracer material properties on the residence time distribution (RTD) of continuous powder blending operations. Part I of II: Experimental evaluation. Powder Technol. 342, 744–763.

Escotet-Espinoza, M.S., Moghtadernejad, S., Oka, S., Wang, Z., Wang, Y., Roman-Ospino, A., Schäfer, E., Cappuyns, P., Van Assche, I., Futran, M., Muzzio, F., Ierapetritou, M., 2019b. Effect of material properties on the residence time distribution (RTD) characterization of powder blending unit operations. Part II of II: Application of models. Powder Technol. 344, 525–544.

Gao, Y., Muzzio, F.J., Ierapetritou, M.G., 2012. A review of the Residence Time Distribution (RTD) applications in solid unit operations. Powder Technol. 228, 416–423.

Gao, Y., Vanarase, A., Muzzio, F., Ierapetritou, M., 2011. Characterizing continuous powder mixing using residence time distribution. Chem. Eng. Sci. 66, 417–425.

Grymonpré, W., Vanhoorne, V., Van Snick, B., Blahova Prudilova, B., Detobel, F., Remon, J.P., De Beer, T., Vervaet, C., 2018. Optimizing feed frame design and tableting process parameters to increase die-filling uniformity on a high-speed rotary tablet press. Int. J. Pharm. 548, 54–61.

Johansson, R., 2011. System Modeling & Identification, 2nd Edition ed. Prentice Hall, Lund.

Karttunen, A.-P., Hörmann, T.R., De Leersnyder, F., Ketolainen, J., De Beer, T., Hsiao, W.-K., Korhonen, O., 2019. Measurement of residence time distributions and material tracking on three continuous manufacturing lines. Int. J. Pharm. 563, 184–197.

Kruisz, J., Rehrl, J., Sacher, S., Aigner, I., Horn, M., Khinast, J.G., 2017. RTD modeling of a continuous dry granulation process for process control and materials diversion. Int. J. Pharm. 528, 334–344.

Kumar, A., Ganjyal, G.M., Jones, D.D., Hanna, M. a., 2006. Digital image processing for measurement of residence time distribution in a laboratory extruder. J. Food Eng. 75, 237–244.

Kumar, A., Vercruysse, J., Toiviainen, M., Panouillot, P.-E., Juuti, M., Vanhoorne, V., Vervaet, C., Remon, J.P., Gernaey, K. V., De Beer, T., Nopens, I., 2014. Mixing and transport during pharmaceutical twin-screw wet granulation: Experimental analysis via chemical imaging. Eur. J. Pharm. Biopharm. 87, 279–289.

Levenspiel, O., 1999. Chemical Reaction Engineering, 3rd ed. John Wiley & Sons, Inc.

Ljung, L., 1999. System Identification - Theory for the User, 2nd Edition ed. Prentice Hall, Inc., Upper Saddle River, NJ.

Manley, L., Shi, Z., 2018. Characterizing drug product continuous manufacturing residence time distributions of major/minor excipient step changes using near infrared spectroscopy and process parameters. Int. J. Pharm. 551, 60–66.

Marikh, K., Berthiaux, H., Gatumel, C., Mizonov, V., Barantseva, E., 2017. Influence of stirrer type on mixture homogeneity in continuous powder mixing: A model case and a pharmaceutical case. Chem. Eng. Res. Des. 86, 1027–1037.

Martinetz, M.C., Karttunen, A.-P., Sacher, S., Wahl, P., Ketolainen, J., Khinast, J.G., Korhonen, O., 2018. RTD-based material tracking in a fully-continuous dry granulation tableting line. Int. J. Pharm. 547, 469–479.

Martinetz, M.C., Rehrl, J., Aigner, I., Sacher, S., Khinast, J., 2017. A Continuous Operation Concept for a Rotary Tablet Press Using Mass Flow Operating Points. Chemie-Ingenieur-Technik 89, 1006–1016. doi:10.1002/cite.201700017

Mateo-Ortiz, D., Muzzio, F.J., Méndez, R., 2014. Particle size segregation promoted by powder flow in confined space: The die filling process case. Powder Technol. 262, 215–222.

Nicolaï, N., De Leersnyder, F., Copot, D., Stock, M., Ionescu, C.M., Gernaey, K. V., Nopens, I., De Beer, T., 2018. Liquid-to-solid ratio control as an advanced process control solution for continuous twin-screw wet granulation. AIChE J. 64, 2500–2514.

Osorio, J.G., Muzzio, F.J., 2016. Effects of processing parameters and blade patterns on continuous pharmaceutical powder mixing. Chem. Eng. Process. Process Intensif. 109, 59–67.

Osorio, J.G., Stuessy, G., Kemeny, G.J., Muzzio, F.J., 2014. Characterization of pharmaceutical powder blends using in situ near-infrared chemical imaging. Chem. Eng. Sci. 108, 244–257.

Peng, J., Huff, H.E., Hsieh, F., 1994. An RTD Determiantion Method for Extrusion Cooking. J. Food Process. Preserv. 18, 263–277.

Portillo, P.M., Ierapetritou, M.G., Muzzio, F.J., 2009. Effects of rotation rate, mixing angle, and cohesion in two continuous powder mixers—A statistical approach. Powder Technol. 194, 217–227.

Portillo, P.M., Ierapetritou, M.G., Muzzio, F.J., 2008. Characterization of continuous convective powder mixing processes. Powder Technol. 182, 368–378.

Portillo, P.M., Vanarase, A.U., Ingram, A., Seville, J.K., Ierapetritou, M.G., Muzzio, F.J., 2010. Investigation of the effect of impeller rotation rate, powder flow rate, and cohesion on powder flow behavior in a continuous blender using PEPT. Chem. Eng. Sci. 65, 5658–5668.

Potente, H., Lappe, H., 1986. Analysis of the residence time distribution in conventional plasticising extruders. Plast. rubber Process. 6, 135.

Simonaho, S.-P., Ketolainen, J., Ervasti, T., Toiviainen, M., Korhonen, O., 2016. Continuous manufacturing of tablets with PROMIS-line — Introduction and case studies from continuous feeding, blending and tableting. Eur. J. Pharm. Sci. 90, 38–46.

The United States Pharmacopeial Convention, 2012. <1174> Powder Flow, in: U.S. Pharmacopoeia. pp. 801–804.

Van Snick, B., Grymonpré, W., Dhondt, J., Pandelaere, K., Di Pretoro, G., Remon, J.P., De Beer, T., Vervaet, C., Vanhoorne, V., 2018. Impact of blend properties on die filling during tableting. Int. J. Pharm. 549, 476–488.

Van Snick, B., Holman, J., Vanhoorne, V., Kumar, A., De Beer, T., Remon, J.P., Vervaet, C., 2017. Development of a continuous direct compression platform for low-dose drug products. Int. J. Pharm. 529, 329–346.

Van Snick, B., Kumar, A., Verstraeten, M., Pandelaere, K., Dhondt, J., Di Pretoro, G., De Beer, T., Vervaet, C., Vanhoorne, V., 2019. Impact of material properties and process variables on the residence time distribution in twin screw feeding equipment. Int. J. Pharm. 556, 200–216.

Wahl, P.R., Hörl, G., Kaiser, D., Sacher, S., Rupp, C., Shlieout, G., Breitenbach, J., Koscher, G., Khinast, J.G., 2017. In-line measurement of residence time distribution in melt extrusion via video analysis. Polym. Eng. Sci.

Waldenhofer, K., 2017. Characterization of a Blender-Tableting Unit for Compaction of Hot-Melt Extruded Pellets. Graz University of Technology.

7. Conclusions and Future Directions

7.1. Conclusions

The purpose of this thesis was to provide a use case for the application of continuous manufacturing (CM) in the pharmaceutical industry. Main drivers for the implementation of CM are cost efficiency, time-to-market (i.e. reduced product development time) or in some cases, the possibility to manufacture more complex dosage forms from active pharmaceutical ingredients (APIs), which were previously excluded from the development pipeline due to bioavailability or manufacturability limitations.

Hot-melt extrusion (HME) is an inherently continuous process and was investigated as a platform technology for the preparation of intermediates for later tableting. HME allows to increase the bioavailability of poorly water-soluble APIs by generating an amorphous solid dispersion (ASD) of drug molecules in a polymer matrix. In this study, nimodipine (NMD) was used as model drug, which is basically insoluble in water. The continuous HME process transforms small volumes of materials by melting and shearing, as they move along the process in a tightly controlled manner. This allows to disperse the formulation components to a degree, that recrystallization of the API is hindered upon solidification. However, the lifetime of this thermodynamically unstable state depends on many factors, such as the carrier substance, other formulation components and the process conditions. In order to consider HME a platform technology for manufacturing oral solid dosage forms (OSDFs), the produced intermediates should be suitable for tableting. Tablets are the most relevant OSDF, due to high patient compliance and their ease of manufacturing. Thus, the goal was to develop an entire continuous process line, starting with the raw materials for extrusion and ending with the final (uncoated) tablet, using the principles of quality-by-design (QbD).

Chapter 2 details on the miniaturized ASD formulation screening that was performed to identify a suitable ASD carrier system. The aim was to achieve a physically stable ASD with immediate release profile from pellets at a drug load of 10 wt.% and with properties suitable for the continuous production of the pellets via strand pelletization. There is only a limited number of polymers available on the market, which are processable in HME and approved for oral use. From that selection, it was not possible to identify a polymer that fulfilled all requirements. Therefore, a dual-polymeric carrier approach was used to overcome the limitations of the single carrier polymers. Combinations of Eudragit® E (EE), an amorphous cationic statistical co-polymer of di-methyl-amino-ethyl-methacrylate, butyl-methacrylate and methyl-methacrylate monomers, and Methocel™ E5 (HPMC), a non-ionic cellulose with hydroxyl-propyl and methoxy-side groups, were screened for their optimum composition with regard to ASD stability, dissolution performance and processability in strand

pelletization. Thorough understanding of the contribution of each component and the process conditions in three different ASD preparation methods (in-situ quench cooling, vacuum compression molding and benchtop extrusion) was gained by characterizing solid state and phase arrangement by thermal and spectroscopic methods. ASD stability and dissolution was found to depend on the presence of shear during ASD generation. This was due to HPMC, which exhibits a yield point and highly viscous behavior. Thus, shear was required to distribute the molecules homogeneously, i.e. to minimize local variation in ASD stability. However, HPMC was required to improve the processability of the formulation by increasing the mechanical stability of the extruded strand at processing temperature. EE in contrast, was solubilizing and stabilizing the amorphous NMD by molecular interaction, forming a separate phase with low glass transition temperature (T_g) in the cellulosic carrier.

A crucial aspect when setting up the pilot-scale HME and pelletization unit for processing this formulation (Chapter 3) was to produce pellets of smallest possible size. Pellet size strongly determines the downstream processability in the tableting unit. Pelletization was applied, since it is the only technology continuously producing intermediates of extruded ASDs, suitable for tableting. Commonly, HME products are milled before tableting. Yet, ASDs often exhibit a T_g, that does not allow to mill them directly after the extruder due to the risk of softening. Thus, cryo-milling is typically used for ASDs, which also minimizes the risk of solid-state transformation, i.e. recrystallization. However, no technology is available for continuous cryo-milling. Consequently, some effort was taken to select the ideal pelletization technology. Die-face pelletization was tested as an alternative technology to strand pelletization. An advantage of die-face over strand pelletization is the possibility to produce rounded, instead of cylindrical pellets. However, cutting the melt directly at the die face, links the pelletization to the thermal state of the extrusion dies. While the pelletization process requires sufficient cooling to avoid sticking and agglomeration of the pellets, the extrusion dies must remain at sufficiently high temperatures, in order to maintain a consistent melt flow through the small die channels at acceptable pressure drop. The development of a thermally-decoupled die-plate largely had resolved this issue for pharmaceutical polymers (Treffer, 2016). Yet, for the given formulation with two phases of very distinct T_gs no process window could be identified. Consequently, strand pelletization was used downstream of the HME process. A process parameter screening was performed to establish a process knowledge space. One important finding of the screening was that the HME screw speed directly influenced the degradation of HPMC in the formulation. The nominal settings of the process were selected accordingly. Thus, while the use of HPMC in a formulation requires some shear, in order to disperse the molecules well, high shear stress provokes degradation.

In the next step, a sensitivity analysis was executed in order to identify a design space for the HME and pelletization process (Chapter 4). The goal was to produce pellets with an immediate release (IR) profile and in a size range feasible for tablet compression. Process parameters were varied around the nominal process settings and formulation composition to assess the sensitivity of the process state and product quality to control actions and feeding deviations in the final CM line. The pelletization process was found to be sensitive when throughput was increased, due to insufficient cooling in the given setup. Thus, control actions changing the line throughput can be performed only below this limit. Feeding deviations in the split-feeding unit, resulting in significantly altered formulation composition were found to be critical especially, if they were related to increased HPMC content. High fractions of HPMC caused high pressure drop levels in the extrusion die plate, approaching even the pressure limits of the used melt pump (250 bar). Moreover, residence time distribution (RTD) characterization and inline API content monitoring via near-infrared (NIR) spectroscopy revealed that high HPMC content was critical also for real-time quality control and material tracking. The increased viscosity of the melt upon such deviations carries the risk of window fouling and flow stagnation in melt flow channels. The process could poorly wash out this deviating melt due to the lower viscosity of the nominal formulation composition. Thus, the application of a relative feed rate control in the split-feeding unit was suggested as an important measure to avoid such events. Moreover, the use of a soft sensor for predicting API content based on feeder feed rates was identified as a viable option for backing up the information from the NIR sensor.

Then, deformation properties of the produced pellets were characterized, in order to select appropriate excipients for the compression of the pellets to mechanically stable tablets with immediate API release (Chapter 5). The pellets were found to deform mainly elastically, forming solid bridges by fusion if compressed purely. Thus, binders were selected for compensating the elastic deformation behavior, i.e. for providing sufficient tablet strength, and for separating the pellets from each other during compression to ensure fast tablet disintegration. It was possible to identify an optimal composition of pellets, Avicel® PH102 (PH102), Kollidon® CL (K-CL) and magnesium stearate (MgSt) in a design of experiments (DoE). The generated surface response model also predicted the properties of tablets well, that were produced in a semi-continuous tableting run over 30 min.

Finally, the RTDs of the processes downstream of HME and pelletization, that is blending and tableting, were determined (Chapter 6). This was highly relevant for material traceability through the process, which is the basis for quality control in CM. Special attention was put on identifying potential differences in RTDs of pellets and powders in these units. Such differences were observed in both units, highlighting the need to consider this in future control strategy development and process monitoring systems. Moreover, RTDs give important information on the back-mixing in a process. While back-mixing is desired in continuous blenders, the RTD should be narrow and well controlled in other unit

operations. In this case, the tablet press exhibited a very wide RTD though, indicating a significant amount of back-mixing. In that context, a recirculation zone was observed in the material flow at the interface between the hopper and the feed frame. In continuous operation the material entrapped in this zone would leave the process only after long process times. Thus, when setting up the entire, integrated CM line containing the characterized process units, a material ejection valve should be placed before the tablet press. This valve would allow to eject material from the process, if it was out-of-specification (OOS), e.g. in blend uniformity. If the material was rejected only after the tablet press, the amount of material that needs to be discarded would be significantly larger, due to the amount of back-mixing in the process.

7.1.1. Conclusions on Continuous Manufacturing

Regarding the advantage of CM in time-to-market, this study demonstrated that CM allows to apply QbD principles during process development in a time- and material-sparingly manner. Time and API demand during HME process development (Chapters 3 and 4) were compared to the development of a batch fluidized bed granulation process (Table 7-1). The reference data was kindly provided by Bayer (Germany), a project partner in this consortium use case.

Table 7-1. Comparison of time and API demand during the development of a continuous process for the preparation of ASD pellets and a batch process for the preparation of granules.

Continuous HME & pelletization process			**Batch fluidized bed granulation**		
Task	**Time demand [working days]**	**API demand [kg]**	**Task**	**Time demand [working days]**	**API demand [kg]**
1) Process setup runs	2 (experimental)	2.4	1) Lab-scale process development (screening)	10 (experimental) + 10 (analytics)	1.5
2) Process screening	2 (experimental) + 4 (analytics)	4.8	2) Lab-scale process development (optimization)	20 (experimental) + 10 (analytics)	4
3) Process sensitivity analysis	4 (experimental) + 8 (analytics)	12	3) Scale-up to pilot scale (50 kg)	6 (experimental) + 5 (analytics)	15
4) Validation runs	1 (experimental) + 2 (analytics)	2.4	4) Concurrent validation at pilot scale	4 (experimental) + 5 (analytics)	10
Total	**~23 days**	**21.6 kg**		**~70 days**	**30.5 kg**

Assumption for analytical time demand: all tests/evaluations can be done in parallel; Assumption for API demand: 10% nominal API load in 4 kg/h nominal throughput;

The comparison includes several stages of the process development, starting with experiments for selecting the CM process setup and lab-scale screening runs for batch granulation and ending with the design space validation in pilot scale (data not shown in this thesis). The category “experimental” refers

to the experimental run time, while “analytics” refers to the analysis of process data as well as analytical lab work for product characterization. During the setup experiments in this study, qualitative information was used to make decisions on the optimal setup, thus no specific time could be assigned to the analytics category.

The reduced time demand of the continuous process highlighted the benefit of performing several DoE runs by dynamically changing set points in one experimental set. This is not possible in batch manufacturing, where a new set point can be tested only after emptying and cleaning the equipment from the previous run (as it was performed in the tableting process development in Chapters 5 and 6). With regard to API demand, it has to be mentioned that the scale-up of the batch process to commercial scale requires further extensive amounts of API. For continuous processes, basically the same or slightly larger equipment could be used to produce commercial volumes by scaling up in process time.

However, these advantages of CM in time and material savings strongly depend on the readiness of process monitoring systems and inline process analytical technology (PAT). The ability to reliably measure the effects of process conditions and material attributes on product quality is mandatory for a risk-based approach in product development. In cases, where such systems need to be newly implemented and tested, development time and material demand will expand significantly.

7.1.2. Conclusions on Hot-Melt Extrusion as a Platform Technology

Concerning the application of HME and pelletization as a platform technology for the production of tableting intermediates, it was concluded that it will remain attractive only for specialized products. Yet, it offers to take full advantage of CM in cases, where this technology is chosen, e.g. due to superior product performance compared to less complex manufacturing routes. The following observations in this project led to this conclusion:

i) HME formulation development for the preparation of ASDs requires special attention due to the complex interdependencies of material attributes and process conditions. Even though the miniaturized formulation approach via quench-cooling, vacuum compression molding and benchtop extrusion in Chapter 2 was successful in estimating performance and processability on pilot scale, experience was required to interpret the results. Thus, some risk remains when transferring the formulation to the final process, especially when using thermo-labile materials, such as cellulosic carriers.

ii) Extrusion equipment is typically not available in many pharmaceutical companies and thus, the equipment needs to be purchased. Therefore, the adoption of this process and implementation of required PAT and control strategy systems cannot compete economically with other CM lines (direct compression, dry granulation), for which

knowledge and parts of equipment are normally readily available. Nevertheless, it is worth mentioning that extrusion technology comes with a wide range of auxiliary equipment, which allows to tailor the process to the specific requirements of a product (see Chapter 3). The application of such equipment, e.g. side feeders and melt pumps, has not been fully utilized for pharmaceutical production yet. Moreover, HME is a very capable process with the ability to recover from deviations, as long as material does not lose its flowability, e.g. due to thermal degradation (see Chapter 4).

iii) In general, the compressibility of HME-processed materials is challenging, due to their dense and often elastic nature, as shown in Chapter 5. Nevertheless, the compression of pellets to tablets was possible. Yet, the final tablets did not exhibit the same product robustness as common tablets and especially segregation remained a risk. Moreover, the inline monitoring of API, or tracer content in pellet-powder blends or tablets is challenging (Chapter 6). Image-based measurements, or measurements in reflectance mode suffer from the low representation of the API-containing pellets at accessible surfaces. However, this is mainly relevant during process development, when the effect of segregation needs to be evaluated. The application of multispectral ultraviolet (UV) surface imaging has already been demonstrated to provide robust quality control of multiple unit pellet system (MUPS) tablets, that could also be utilized inline during production (Novikova et al., 2016). Concluding, this route is considered viable only, if it provides significant biopharmaceutical benefits or if the adoption of CM offers significant economic advantages.

7.2. Future Directions

7.2.1. Material Science

Hot-Melt Extruded Amorphous Solid Dispersions

The selection of ASD formulation components in this study was performed mainly empirically with significant experimental work. The main concern when formulating ASDs is the stability of the solid state. Physical stability is determined by the miscibility (thermodynamic contribution) and molecular mobility (kinetic contribution) of the system. A prediction of drug-polymer miscibility based on Hansen solubility parameters via group contribution methods did not deliver useful estimations. Such methods cannot capture the miscibility contribution of ionic, or specific directional intermolecular H-bond interactions (Brunsteiner et al., 2018) and no kinetically stabilizing effects of course. Moreover, for commercial HPMC grades the exact molecular structure is normally not known and only ratios of substitution side groups are specified. However, molecular dynamics simulation was recently used to rank several combinations of small molecule drugs and polymers with regard to physical stability based on both, thermodynamic and kinetic descriptors (Brunsteiner et al., 2018). Moreover, this method provides insight whether thermodynamics or molecular mobility is the aging rate limiting factor, which is an important step towards the in-silico prediction of the relative stability of ASD systems.

For the used experimental approach, i.e. assessing melting point depression, reduction in enthalpy of fusion, number and position of ASD glass transition points and spectroscopic evaluation of molecular interactions, it was crucial to select sample preparation methods which mimic the final manufacturing process. The combination of different methods for small-scale screening during ASD formulation development (in-situ quench cooling, vacuum compression molding, benchtop extrusion) provided sufficient insight in the role of each formulation component and of preparation conditions. However, the intensity of molecular interactions in the system was found to depend on the molecular mixedness (Hörmann et al., 2018). Thus, an unknown state of mixing in the micro-scale is a critical point when screening the ASD properties experimentally. In that regard, spectroscopic monitoring of interactions during sample preparation could be an interesting option. Time-resolved data during ASD preparation would provide insight whether steady state, that is a thermodynamic equilibrium, was reached by diffusion after holding a sample at a specific elevated temperature for a defined amount of time. Moreover, state transformations could be monitored while applying a temperature programs similar to the thermal history in HME processing. This may allow to assess the effect of thermal processing history on molecular interactions, or on the degradation of specific components.

HMPC Extrusion

In the context of degradation, also the sources and kinetics of HPMC degradation during HME processing remain a relevant aspect for future research. HPMC is a versatile excipient, since it is available in many different grades of substitution. The different degrees of substitution, variability in substitution side groups and in molecular weight offer a wide range of applications, e.g. for stabilizing supersaturation of poorly soluble drugs during dissolution (Hughey et al., 2012; Xie and Taylor, 2016) or for providing different release profiles (Meena et al., 2014; Nokhodchi et al., 2012; Siepmann and Peppas, 2001). Moreover, aiming for fully integrated CM of ASD-containing tablets, the dual-polymeric carrier system with HPMC yielded promising results in improving processability for strand pelletization.

It is well known, that cellulosic polymers tend to degrade under increased thermal and mechanical stress (Hughey et al., 2012; Meena et al., 2014). Accordingly, processes are commonly designed by empirically balancing barrel temperature, screw speed and throughput, minimizing the total stress input on the material to avoid degradation. Yet, alone the effect of screw speed, which is directly related to shear stress, local temperature peaks by dissipative heat generation and the residence time in fully filled zones (i.e. kneading blocks), is highly complex and depends on the specific formulation (viscoelastic, rheological and conductive properties).

Here, simulation tools, such as 3D smoothed-particle hydrodynamics (SPH), or 1D mechanistic models offer valuable insight, by making local stress conditions virtually accessible. Nevertheless, there is some development required for these simulations tools, to accurately capture stress and temperature conditions in the critical spots, i.e. the gap region (Eitzlmayr, 2015). Especially, the complex non-Newtonian flow properties of HPMC and phase separation pose substantial challenges in this context. However, even simplified estimations of local temperatures, shear rates and residence times in combination with kinetic models for the degradation of the respective HPMC grade under different stress conditions, would allow a more rational design of HME processes for HPMC extrusion.

Another aspect for further investigation is the volume fraction of HPMC required in a formulation to improve mechanical stability of the strand. Observations during formulation development (Chapter 2) and sensitivity analysis at changing formulation composition (Chapter 4) suggest, that a certain fraction is required to form a stabilizing network of HPMC molecules in the melt. Thus, percolation theory may aid in understanding the minimal required HPMC volume fraction.

Tablet Compression of Pellets

The investigation of deformation behavior and tabletability of HME pellets in this study was very much focused on the identification of a formulation suitable for the generation of mechanically stable and fast disintegrating tablets. Thus, many interesting research questions remain unanswered. An investigation of the effect of ASD carrier composition and microstructure (as a function of HME process conditions) on the deformation behavior of the pellets would be important to understand the consequences of upstream process variability on the final product quality (Grymonpré et al., 2016).

Moreover, physical stability of the final tablets was not characterized specifically, i.e. potential long-term effects of tableting on ASD stability were not investigated. Downstream tableting of ASDs has been reported to cause both, decreased or enhanced physical stability depending on the material system used (Démuth et al., 2015). Thus, this aspect definitely requires additional examination. Additionally, interactions of ASDs with tableting excipients and subsequent effects on ASD stability in solid state and during dissolution were observed (Leane et al., 2013). The relatively high content of the hygroscopic Kollidon® CL in this study's final tableting formulation may be seen critical in that context.

Finally, the effect of using cylindrical, instead of spherical pellets was not investigated specifically. In published studies round pellet have been considered a prerequisite, i.e. spheronization was applied prior to tableting (Young et al., 2002), and no comparative study on pellet shape has been published yet. Since there is no technology available for spheronizing pellets continuously, and strand pelletization is more robust compared to die-face pelletization, this research question is of special relevance for the CM of MUPS tablets. To that end, also the effect of pellet aspect ratio and size may be further investigated.

7.2.2. Continuous Manufacturing

This section contains topics that were relevant to all investigated CM use cases of the ECCPM consortium, thus aiming for a wider validity, than for the use case of HME. A fully integrated continuous process line with connecting interfaces, PAT tools, material deviation points and control concept was not established in any of the use cases. This was mainly related to: i) a lack of well characterized interfaces between continuous process units, ii) a shortcoming of PAT tools for real-time analysis during process development, and iii) issues in continuous feeding. These three aspects will be discussed specifically in the following sections.

Using this thesis as an example, it was not possible to install the blender directly above the tablet press, due to limitations in space. However, the risk of segregation of the pellet-powder blend in an interfacing horizontal connection system was unknown and did therefore, not allow a timely integration. Concerning the lack of inline PAT tools, the limitations in real-time API content or tracer detection in the tablets prepared from powder and pellets have been discussed above already. With regard to powder feeding, no severe challenges were encountered in this use case. However, the selection of the appropriate equipment and its setup was performed purely based on experience.

Process Integration, Material Traceability and Process Analytical Technology

Critical process parameters and process dynamics of single continuous units, such as blenders, granulators, extruders, roller compactors and tablet presses have been characterized and are relatively well understood (Dülle et al., 2018b; Kruisz et al., 2017; Liu et al., 2017; Toson et al., 2019; Treffer et al., 2013; Vanarase and Muzzio, 2011). However, even if there are a few publications available using entire continuous process lines (Lakio et al., 2017; Pawar et al., 2016; Simonaho et al., 2016), there is little, or no information contained on the effect of interfacing connections. Nevertheless, the type of connection (by gravity, pneumatically, by vacuum or by screw) and its parameter settings are expected and have been reported to have an effect on intermediate product properties (De Leersnyder et al., 2018). Moreover, their residence time distributions (RTDs) need to be characterized to ensure material traceability throughout the entire process line.

In that context, it is also important to mention, that feeders often represent the interface between process units. Their RTD has largely been disregarded up to now. Only one recent publication (Van Snick et al., 2019) covers this important aspect of CM. Currently, loss-in-weight (LIW) feeding is the only option, to measure and control a flow of particulate material in a process line. Thus, for any kind of intermediate that requires the continuous addition of external excipients, feeding must be performed to achieve an accurate ratio of the components in the final product. An alternative approach was taken in the continuous wet granulation line ConsiGma™ (GEA, Belgium): By splitting the continuous material stream after granulation into small portions, so-called product keys (PKs), no

granule feeding step is required. These PKs are separately transferred through a weighing section into a mini batch-blender, were the needed amount of external excipients is added by twin-screw LIW dispensing. After batch-blending, the PKs are merged on top of each other in the tablet press hopper. In both approaches, the intermediate feeding approach, or the PK approach, convolution of single unit RTDs are the basis for material tracking and the probability-based assignment of PAT measurements to specific portions of final product.

With regard to PAT, the use cases exhibited very different degrees of implementation (Karttunen et al., 2019; Rehrl et al., 2018). In general, the application of inline PAT tools mainly focused on determining API or tracer content, which was required to characterize the RTD of the process units. However, especially for future process development, it is desirable to determine as many quality attribute (QAs) as possible inline. The insight in dynamic correlations of process parameters (PPs) and QAs gives valuable insight in process robustness and deepens process and product understanding. However, the effort for calibration, maintenance and data handling around such a fully PAT equipped line must not be underestimated. Based on the additionally gained knowledge on the criticality of PPs and QAs, it is expected though, that the final production process can be operated in a state of control inside the design space with significantly reduced PAT. Ideally, only sensors required for feedback or feed-forward control and real-time release testing (RTRT) should remain in the final process line.

Processability of Pharmaceutical Materials

Finally, the feeding issues, that were encountered in the use case of continuous wet granulation, shall not be ignored in the context of CM. Batch-to-batch variation, caused by different primary manufacturing routes of an API, critically affected the feedability of the granulation pre-blend (Stauffer et al., 2019). This case highlighted, that not only the final product quality, but also the feasibility of CM largely depends on the ability to feed all required materials consistently into the process line. Accordingly, with an increasing adoption of CM in pharmaceutical production, an increasing number of publications focusses on powder feeding (Bostijn et al., 2019; Santos et al., 2018; Stauffer et al., 2019; Van Snick et al., 2017; Wang et al., 2017).

The follow up project of the consortium as well, the European Consortium of Continuous Pharmaceutical Manufacturing (ECCCPM) 2.0, investigates the processability of different pharmaceutical materials in feeding. Furthermore, an attempt will be made to identify mechanistic relations between intrinsic, chemical material properties, micromeritics and geometrical properties of particles to their bulk behavior and consequently to their processability.

7.3. References

Bostijn, N., Dhondt, J., Ryckaert, A., Szabó, E., Dhondt, W., Van Snick, B., Vanhoorne, V., Vervaet, C., De Beer, T., 2019. A multivariate approach to predict the volumetric and gravimetric feeding behavior of a low feed rate feeder based on raw material properties. Int. J. Pharm. 557, 342–353.

Brunsteiner, M., Khinast, J., Paudel, A., 2018. Relative Contributions of Solubility and Mobility to the Stability of Amorphous Solid Dispersions of Poorly Soluble Drugs: A Molecular Dynamics Simulation Study. Pharmaceutics 10, 101.

De Leersnyder, F., Vanhoorne, V., Bekaert, H., Vercruysse, J., Ghijs, M., Bostijn, N., Verstraeten, M., Cappuyns, P., Van Assche, I., Vander Heyden, Y., Ziemons, E., Remon, J.P., Nopens, I., Vervaet, C., De Beer, T., 2018. Breakage and drying behaviour of granules in a continuous fluid bed dryer: Influence of process parameters and wet granule transfer. Eur. J. Pharm. Sci. 115, 223–232.

Démuth, B., Nagy, Z.K., Balogh, A., Vigh, T., Marosi, G., Verreck, G., Van Assche, I., Brewster, M.E., 2015. Downstream processing of polymer-based amorphous solid dispersions to generate tablet formulations. Int. J. Pharm. 486, 268–286.

Dülle, M., Özcoban, H., Leopold, C.S., 2018. Analysis of the powder behavior and the residence time distribution within a production scale rotary tablet press. Eur. J. Pharm. Sci. 125, 205–214.

Eitzlmayr, A., 2015. Modeling of High-Viscous Flow and Mixing in Co-Rotating Twin-Screw Extruders. Graz University of Technology.

Grymonpré, W., De Jaeghere, W., Peeters, E., Adriaensens, P., Remon, J.P., Vervaet, C., 2016. The impact of hot-melt extrusion on the tableting behaviour of polyvinyl alcohol. Int. J. Pharm. 498, 254–262.

Hörmann, T.R., Jäger, N., Funke, A., Mürb, R.-K., Khinast, J.G., Paudel, A., 2018. Formulation Performance and Processability Window for Manufacturing a Dual-Polymer Amorphous Solid Dispersion via Hot-Melt Extrusion and Strand Pelletization. Int. J. Pharm. 553, 408–421.

Hughey, J.R., Keen, J.M., Miller, D.A., Brough, C., McGinity, J.W., 2012. Preparation and characterization of fusion processed solid dispersions containing a viscous thermally labile polymeric carrier. Int. J. Pharm. 438, 11–19.

Karttunen, A.-P., Hörmann, T.R., De Leersnyder, F., Ketolainen, J., De Beer, T., Hsiao, W.-K., Korhonen, O., 2019. Measurement of residence time distributions and material tracking on three continuous manufacturing lines. Int. J. Pharm. 563, 184–197.

Kruisz, J., Rehrl, J., Sacher, S., Aigner, I., Horn, M., Khinast, J.G., 2017. RTD modeling of a continuous dry granulation process for process control and materials diversion. Int. J. Pharm. 528, 334–344.

Lakio, S., Ervasti, T., Tajarobi, P., Wikström, H., Fransson, M., Karttunen, A.-P., Ketolainen, J., Folestad, S., Abrahmsén-Alami, S., Korhonen, O., 2017. Provoking an end-to-end continuous direct compression line with raw materials prone to segregation. Eur. J. Pharm. Sci. 109, 514–524.

Leane, M.M., Sinclair, W., Qian, F., Haddadin, R., Brown, A., Tobyn, M., Dennis, A.B., 2013. Formulation and process design for a solid dosage form containing a spray-dried amorphous dispersion of ibipinabant. Pharm. Dev. Technol. 18, 359–366.

Liu, H., Galbraith, S.C., Ricart, B., Stanton, C., Smith-goettler, B., Verdi, L., Connor, T.O., Lee, S., Yoon, S., 2017. Optimization of critical quality attributes in continuous twin-screw wet granulation via design space validated with pilot scale experimental data. Int. J. Pharm. 525, 249–263.

Meena, A., Parikh, T., Gupta, S.S., Serajuddin, A.T.M., 2014. Investigation of Thermal and Viscoelastic Properties of Polymers Relevant to Hot Melt Extrusion - II: Cellulosic Polymers. J. Excipients Food Chem. 5, 46–55.

Nokhodchi, A., Raja, S., Patel, P., Asare-Addo, K., 2012. The role of oral controlled release matrix tablets in drug delivery systems. BioImpacts 2, 175–187.

Novikova, A., Carstensen, J.M., Rades, T., Leopold, P.D.C.S., 2016. Multispectral UV imaging for surface analysis of MUPS tablets with special focus on the pellet distribution. Int. J. Pharm. 515, 374–383.

Pawar, P., Wang, Y., Keyvan, G., Callegari, G., Cuitino, A., Muzzio, F., 2016. Enabling real time release testing by NIR prediction of dissolution of tablets made by continuous direct compression (CDC). Int. J. Pharm. 512, 96–107.

Rehrl, J., Karttunen, A.-P., Nicolaï, N., Hörmann, T., Horn, M., Korhonen, O., Nopens, I., Beer, T. De, Khinast, J.G., 2018. Control of Three Different Continuous Pharmaceutical Manufacturing Processes: Use of Soft Sensors. Int. J. Pharm. 543, 60–72.

Santos, B., Carmo, F., Schlindwein, W., Muirhead, G., Rodrigues, C., Cabral, L., Westrup, J., Pitt, K., 2018. Pharmaceutical excipients properties and screw feeder performance in continuous processing lines: A Quality by Design (QbD) approach. Drug Dev. Ind. Pharm. 44, 2089–2097.

Siepmann, J., Peppas, N.A., 2001. Modeling of drug release from delivery systems based on hydroxypropyl methylcellulose (HPMC). Adv. Drug Deliv. Rev. 48, 139–157.

Simonaho, S.-P., Ketolainen, J., Ervasti, T., Toiviainen, M., Korhonen, O., 2016. Continuous manufacturing of tablets with PROMIS-line — Introduction and case studies from continuous feeding, blending and tableting. Eur. J. Pharm. Sci. 90, 38–46.

Stauffer, F., Vanhoorne, V., Pilcer, G., Chavez, P.F., Schubert, M.A., Vervaet, C., De Beer, T., 2019. Managing active pharmaceutical ingredient raw material variability during twin-screw blend feeding. Eur. J. Pharm. Biopharm. 135, 49–60.

Toson, P., Lopes, D.G., Paus, R., Kumar, A., Geens, J., Stibale, S., Quodbach, J., Kleinebudde, P., Hsiao, W.-K., Khinast, J., 2019. Model-based approach to the design of pharmaceutical roller-compaction processes. Int. J. Pharm. X 1, 100005.

Treffer, D., Wahl, P., Markl, D., Koscher, G., Roblegg, E., Khinast, J., 2013. Hot Melt Extrusion as a Continuous Pharmaceutical Manufacturing Process, in: Repka, M.A., Langley, N., DiNunzio, J. (Eds.), Melt Extrusion - Materials, Technology and Drug Product Design. American Association of Pharmaceutical Scientists, New York.

Treffer, D.F., 2016. Pharmaceutical Hot Melt Extrusion - Novel Tools for Screening and Processing. Graz University of Technology.

Van Snick, B., Holman, J., Vanhoorne, V., Kumar, A., De Beer, T., Remon, J.P., Vervaet, C., 2017. Development of a continuous direct compression platform for low-dose drug products. Int. J. Pharm. 529, 329–346.

Van Snick, B., Kumar, A., Verstraeten, M., Pandelaere, K., Dhondt, J., Di Pretoro, G., De Beer, T., Vervaet, C., Vanhoorne, V., 2019. Impact of material properties and process variables on the residence time distribution in twin screw feeding equipment. Int. J. Pharm. 556, 200–216.

Vanarase, A.U., Muzzio, F.J., 2011. Effect of operating conditions and design parameters in a continuous powder mixer. Powder Technol.

Wang, Y., Li, T., Muzzio, F.J., Glasser, B.J., 2017. Predicting feeder performance based on material flow properties. Powder Technol. 308, 135–148.

Xie, T., Taylor, L.S., 2016. Improved Release of Celecoxib from High Drug Loading Amorphous Solid Dispersions Formulated with Polyacrylic Acid and Cellulose Derivatives. Mol. Pharm. 13, 873–884.

Young, C.R., Koleng, J.J., McGinity, J.W., 2002. Production of spherical pellets by a hot-melt extrusion and spheronization process. Int. J. Pharm. 242, 87–92.

A. Supplemental Material - Formulation Performance and Processability Window for Manufacturing a Dual-Polymer Amorphous Solid Dispersion via Hot-Melt Extrusion and Strand Pelletization

I. Material Properties

Table A-1. Particle size distribution quantiles of raw material determined via laser diffraction in a dry dispersion unit (Helos and Rodos, Sympathec GmbH, Germany).

Component	x_{10} [µm]	x_{50} [µm]	x_{90} [µm]
NMD	22.18 ± 2.06	122.98 ± 9.66	268.53 ± 15.46
EE	1.97 ± 0.05	8.65 ± 0.05	16.34 ± 0.01
HPMC	27.71 ± 0.07	68.83 ± 0.75	178.15 ± 1.47

Table A-2. Average pellet diameter (by calliper), mass (from n=10) and calculated surface measured.

No.	Avg. pellet diameter [mm]	Avg. surface per pellet [m²]	Avg. mass per pellet [mg]
F1	1.12 ± 0.12	1.93E-05	3.77
F3	1.24 ± 0.09	1.91E-05	4.24
F5	1.48 ± 0.01	2.28E-05	8.23
F6	1.53 ± 0.03	2.76E-05	9.21
F9	1.83 ± 0.01	3.09E-05	14.61

II. Polarized Light Microscopy Images

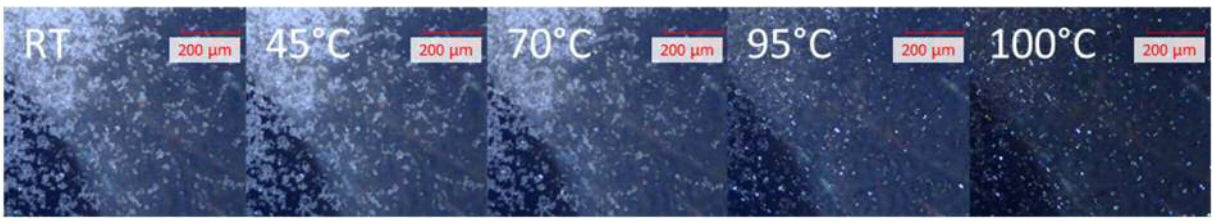

Figure A-1. Polarized light hot-stage microscopy images of EE particles recorded during a heating ramp at 5 K/min and 40°C to 120°C. Softening of the particles is evidenced by an increasing transparency of particles after Tg at 48°C. Coalescence and flow of the particles is observed only at above 95°C, indicating a relaxation of main block chains in the polymers.

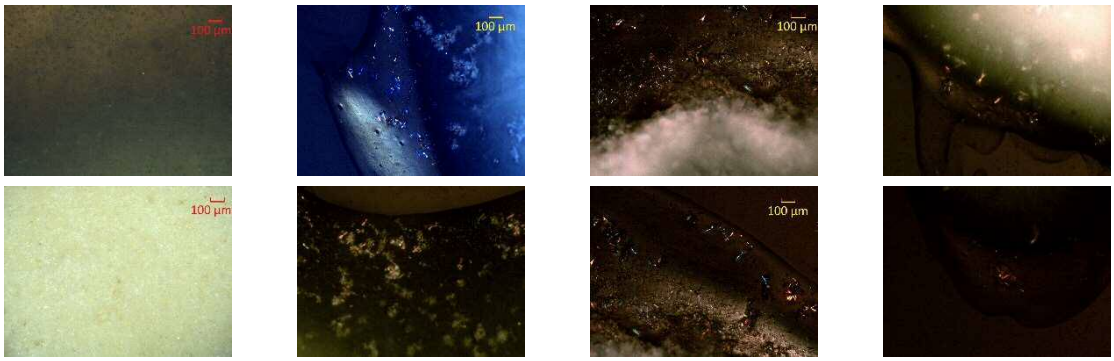

Figure A-2. Polarized light microscopy images of VCM discs of the binary formulation with HPMC (F9). From left to right: before dissolution testing and after 20 min, 45 min and 70 min of dissolution testing showing NMD crystals at the sample surface upon contact with the dissolution medium. Top and bottom showing same sample at different position/settings.

III. Benchtop Extrusion Process Data

Table A-3. Torque levels averaged over the processing time in benchtop extrusion. Due to different powder flowability of the premixes used for feeding the extruder manually, the throughput is not exactly known and varying for the different formulations. The absolute values are therefore, giving a trend only. The torque data file of formulation F6 was corrupted and could not be evaluated.

No.	EE:HPMC	EE in carrier [% w/w]	Torque [Nm]
F1	- (EE)	100	4.2 ± 0.3
F3	2:1	67	4.4 ± 0.9
F5	1:1	50	4.5 ± 0.2
F6	2:3	40	-
F9	- (HPMC)	0	6.5 ± 0.3

IV. Additional mDSC Data and Thermograms

Table A-4. Measured T_g values (rev. HF) (mean ± span, n=2) for QC and VCM ASDs for all formulations and HME ASD formulations.

No.	NMD	EE in carrier	QC ASD	VCM ASD			HME ASD	
	[% w/w]	[% w/w]	T_g [°C]	$T_{g,1}$ [°C]	$T_{g,2}$ [°C]	$T_{g,3}$ [°C]	$T_{g,1}$ [°C]	$T_{g,2}$ [°C]
F1	10	100	36.6 [b]	42.5 ± 0.8	94.2 ± 1.2[a]	-	36.7 ± 0.4	96.0 ± 1.5 [a]
F2	10	80	34.9 ± 0.6	39.2 ± 0.2	96.1 ± 2.2	-		
F3	10	67	35.2 ± 0.3	37.4 ± 0.1	102.0 ± 2.4	-	34.3 ± 0.3	-
F4	10	60	32.4 ± 1.2	36.2 ± 1.0	105.5 ± 1.5	148.0 ± 2.1		
F5	10	50	35.6 ± 0.3	34.2 ± 0.1	101.6 ± 0.6	150.0 ± 0.9	36.7 ± 3.7	-
F6	10	40	34.7 ± 2.3	31.8 ± 0.1	-	146.8 ± 1.2	29.5 ± 1.6	-
F7	10	33	32.5 ± 0.1	28.8 ± 1.6	-	146.1 ± 0.1		
F8	10	20	31.3 ± 1.3	28.6 ± 0.2	-	143.8 ± 1.9		
F9	10	0	97.0 ± 0.1	47.3 ± 3.0	103.7 ± 0.8	149.4 ± 1.8	95.1 ± 3.3	-
F10	20	50	29.4 ± 0.0	23.8 ± 1.1	-	144.5 ± 0.8		
F11	30	50	22.1 ± 0.9	20.3 ± 0.9	-	149.6 ± 0.3		

[a] Thermal event other than T_g; [b]data for one sample (n=1);

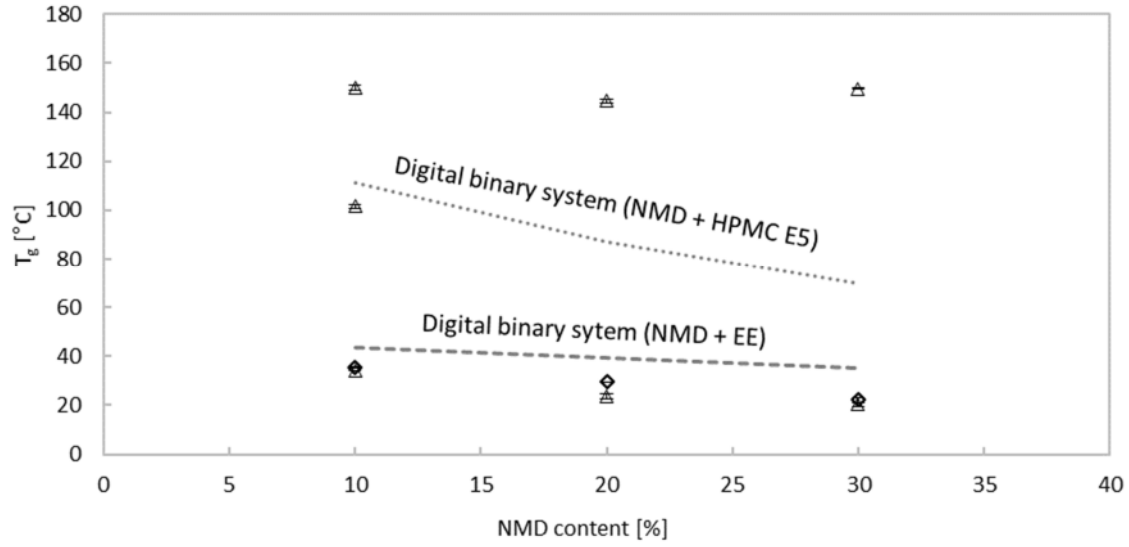

Figure A-3. mDSC measured Tg values (rev HF) (mean ± span, n=2) at varying NMD content in a carrier polymer ratio of 1:1 (EE:HPMC) for QC ASD (◊) and VCM ASD (Δ) versus "digital" values calculated using the Gordon-Taylor binary mixtures of NMD and EE (dashed line) and NMD and HPMC (dotted line).

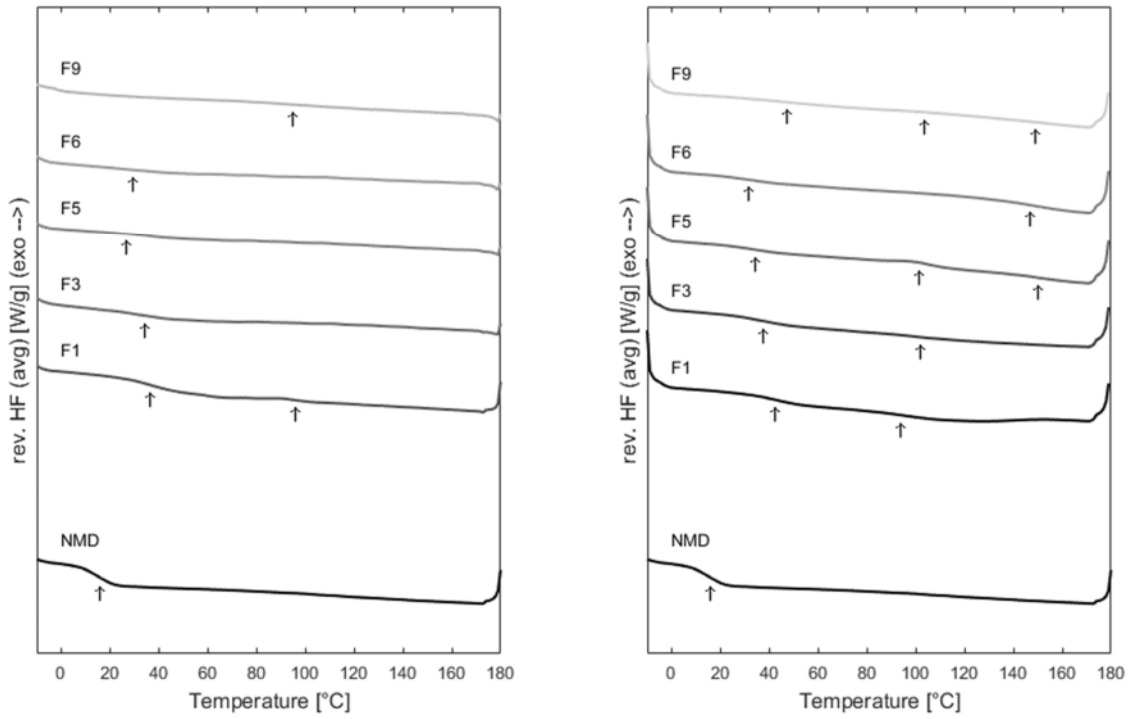

Figure A-4. Comparison of mDSC thermograms (n=2) for HME ASDs (left) and VCM ASDs (right) with Tgs. For HME ASDs, the reversing heat flow of the second heating run is shown.

V. ATR-FTIR Spectra

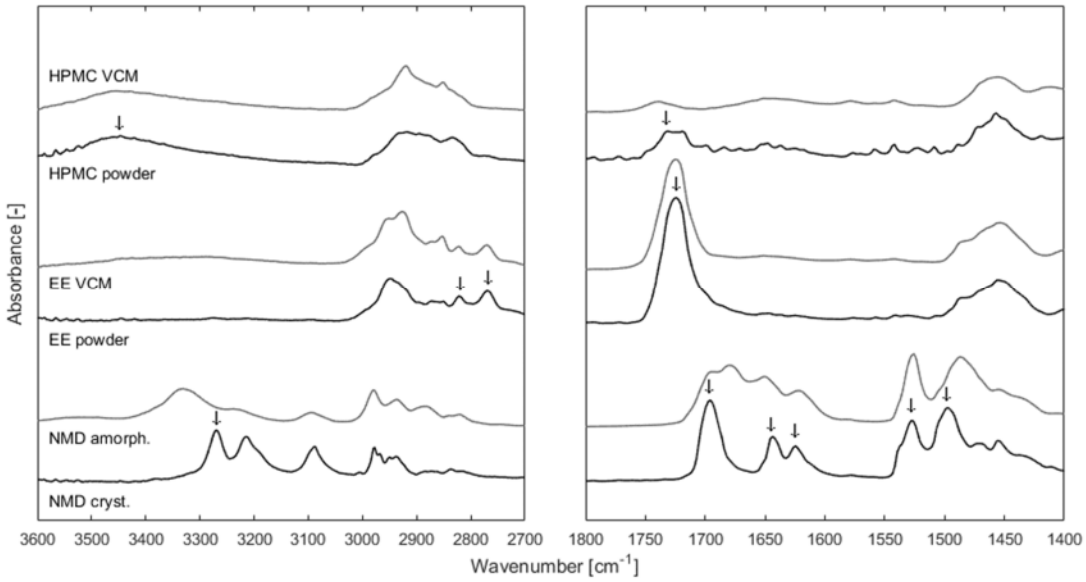

Figure A-5. Averaged ATR-FTIR-spectra (n=3) of powder-shaped (black), VCM-prepared polymers and amorphous API (grey). Arrows indicate the bands of interest for the analysis of molecular interactions. Since for HPMC the spectrum at low wavenumbers is very weak, the noise is magnified in the plot.

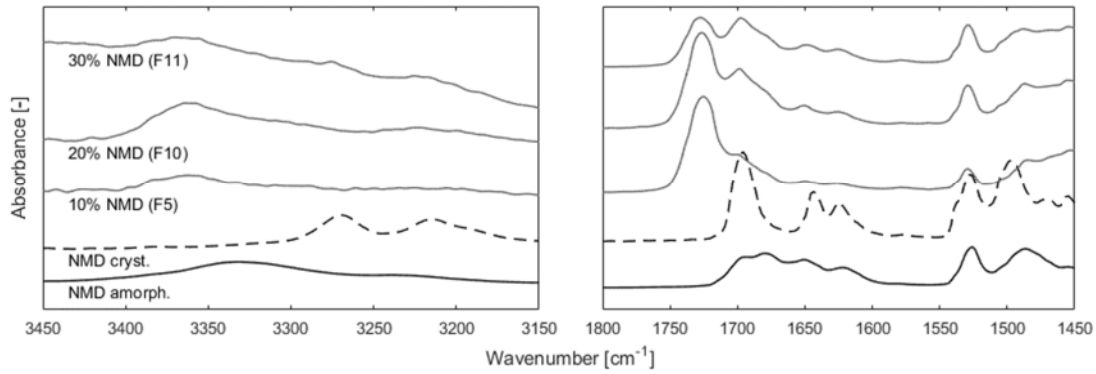

Figure A-6. ATR-FTIR-spectra (averaged, n=3) of VCM ASDs containing 10%, 20% and 30% (w/w) of NMD with a polymer ratio of 1:1 EE: HPMC (F6, F10, F11). (F11 VCM from duplicate (n=2))

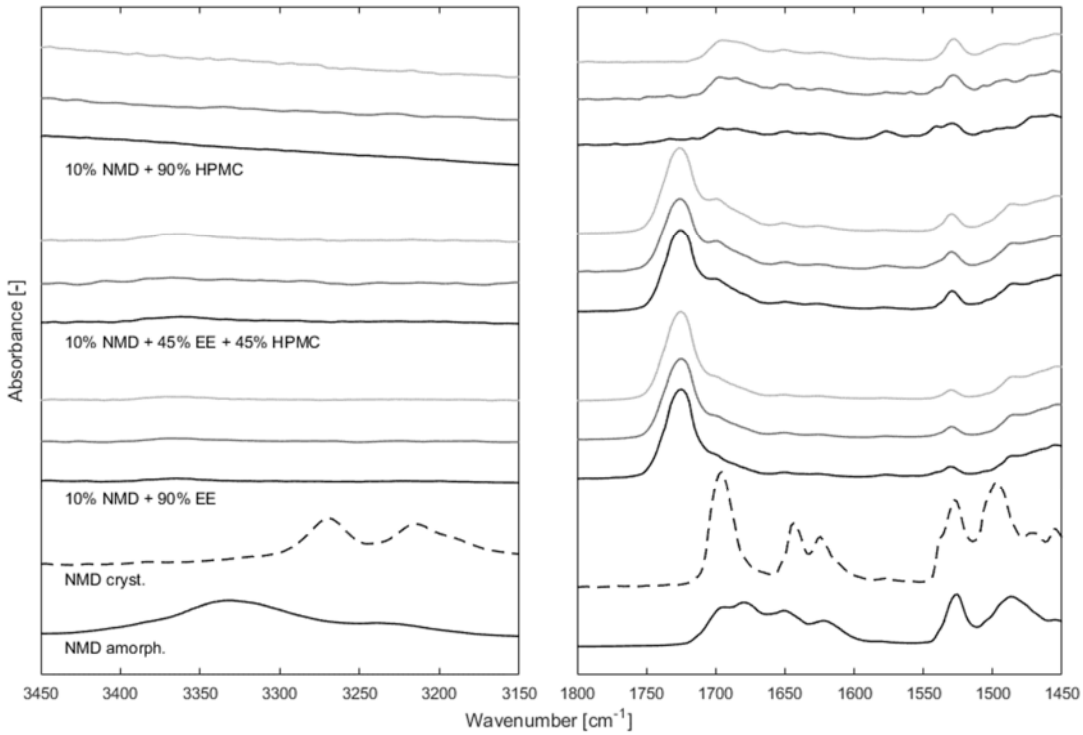

Figure A-7. Averaged ATR-FTIR-spectra (n=2) of stability-tested VCM tablets of binary formulations (F1, F9) and the formulation containing a polymer ratio of 1:1 (F5) before stress conditions (black), after one week (grey) and four weeks (light grey) under accelerated conditions (40°C and 75% RH).

VI. Formulation-Intrinsic Dissolution Testing

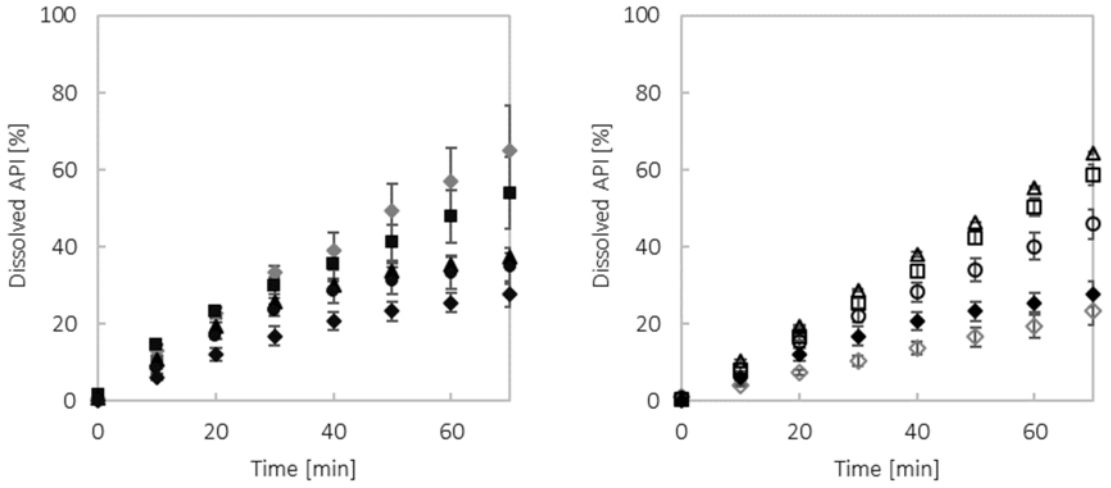

Figure A-8. Left: Formulation-intrinsic dissolution profiles (mean ± SD, n=3) of formulations with 10% API and more EE: (◆) binary with EE (F1), (■) 4:1 EE:HPMC (F2), (▲) 2:1 EE:HPMC (F3), (●) 3:2 EE:HPMC (F4), (◆) 1:1 EE:HPMC (F5). Right: Formulation-intrinsic dissolution profiles of formulations with 10% API and more HPMC: (Δ) 1:2 EE:HPMC (F7), (□) 1:4 EE:HPMC (F8), (○) 2:3 EE:HPMC (F6), (◆) 1:1 EE:HPMC (F5), (◊) binary with HPMC (F9).

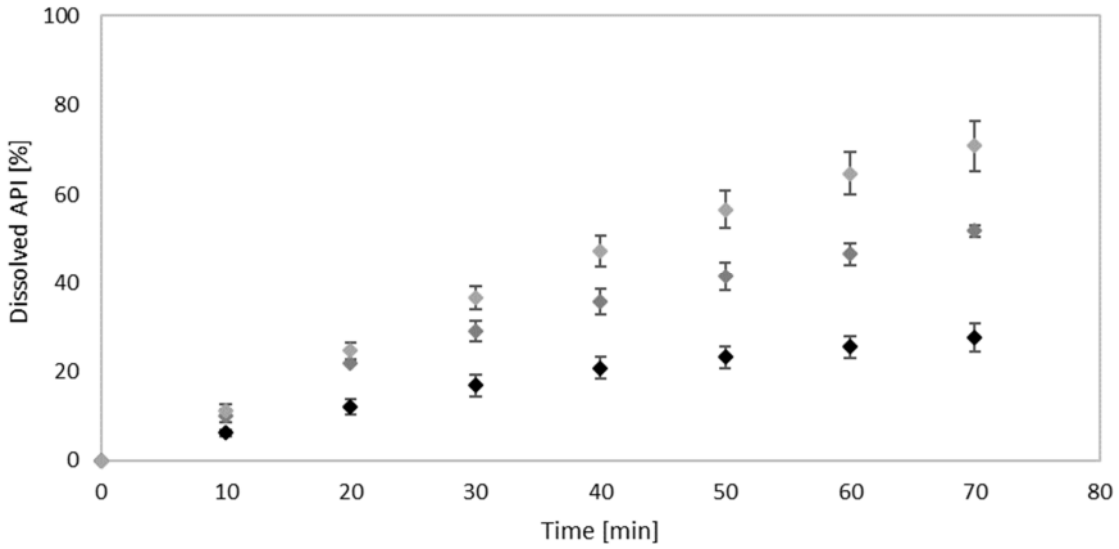

Figure A-9. Intrinsic dissolution profiles (n=3) of formulations with a polymer ratio of 1:1 (EE:HPMC) and 10% API (◆ – F5), 20% API (◆ – F10) and 30% API (◆ – F11) content.

B. Supplemental Material - Hot-Melt Extrusion and Pelletization Process Setup and Parameter Screening

Table B-1. API content and content uniformity of pellets from all DoE runs (n=10).

Exp.	Average recovery [%]	SD of recovery	RSD of recovery [%]	AV [%]
N2	103.23	1.0	1.0	3.9
N3	**103.18**	**0.5**	**0.5**	**2.6**
N4	103.16	1.0	1.0	4.0
N5	101.96	0.9	0.9	2.6
N6	99.25	4.3	4.3	10.4
N7	**100.71**	**0.9**	**0.9**	**2.0**
N8	100.60	0.9	0.9	1.9
N9	**101.62**	**0.8**	**0.8**	**1.8**
N12	102.70	1.1	1.1	3.1
N13	103.14	1.0	1.0	3.4
N14	102.87	2.1	2.0	6.1

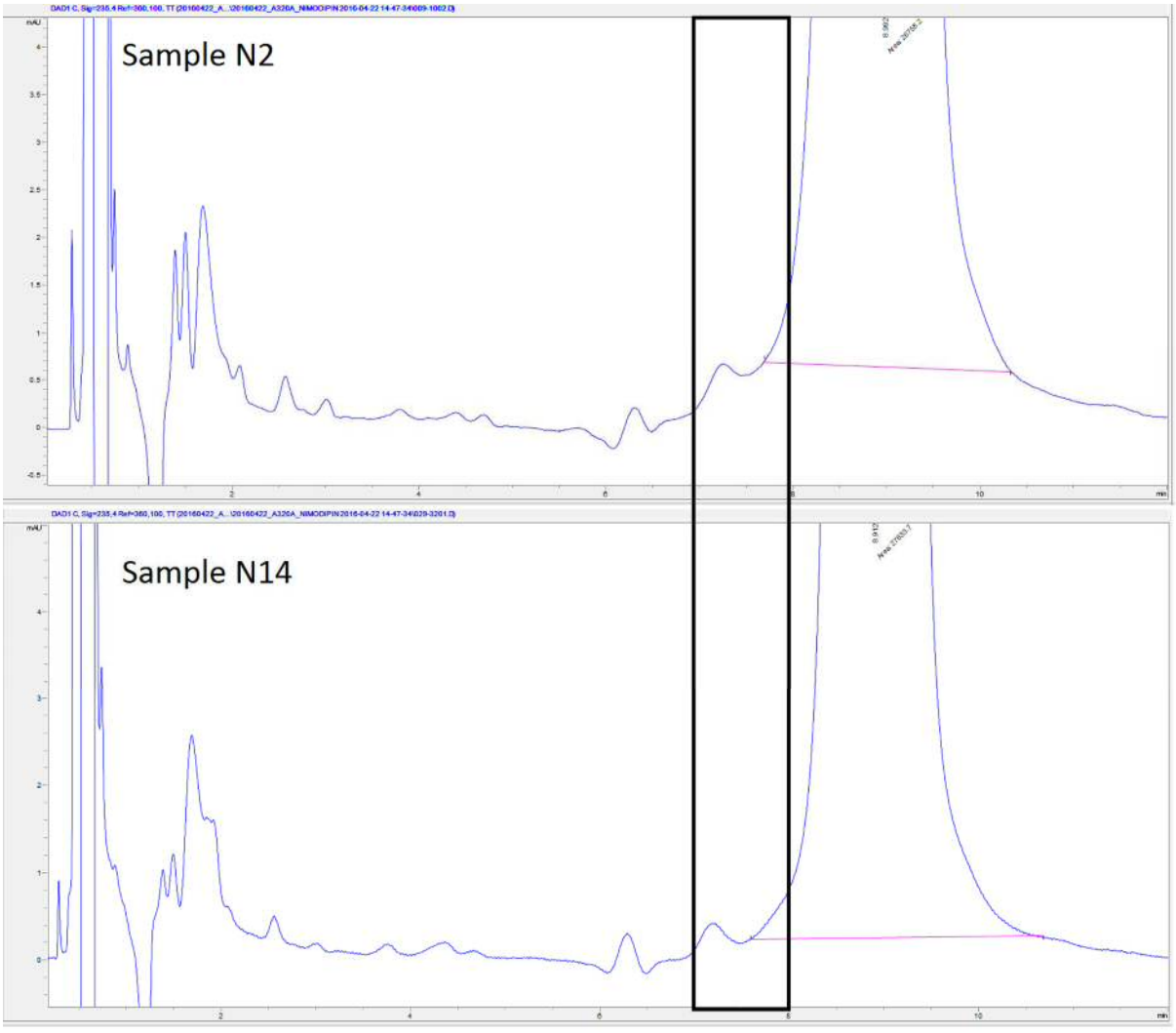

Figure B-1. HPLC chromatograms from pellet analysis for DoE runs with lowest (N2) and highest (N14) stress conditions. The black box is indicating the retention time of impurity A according to the monograph for nimodipine in the Ph. Eur. (Council of Europe, 2014a).

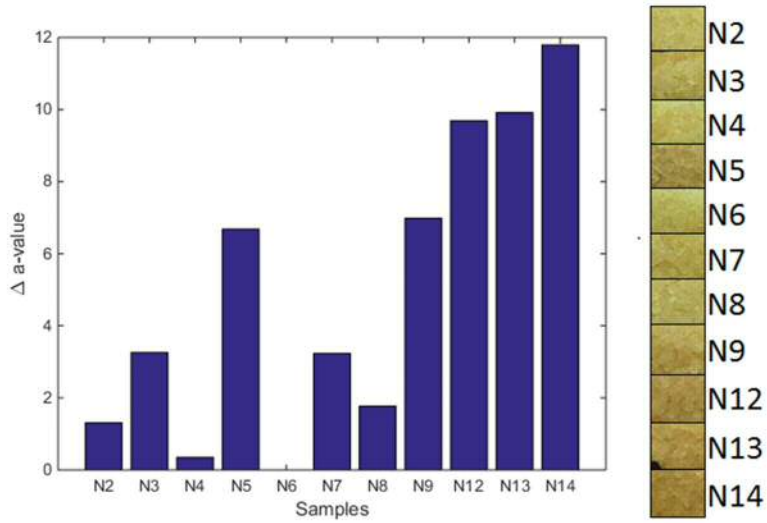

Figure B-2. Change in pellet average a-value in Lab color space relative to the pellets with the lowest a*-value (N6).*

Table B-2. Correlation matrix of factors and responses used in the screening DoE. Green cells showing correlations (>0.3) between responses and factors or responses, red cells showing correlations between factors and grey cells indicate self-correlation.

	SS	MP	DPT	DA	SS*MP	SS*DPT	MP*DPT	Color change	Sphericity	D50	Span~	ML	DMP	DMP SD	# of strands
SS	1.00	-0.16	0.16	-0.29	-0.16	0.16	0.16	0.95	0.76	-0.34	-0.25	-0.32	0.47	0.02	0.28
MP	-0.16	1.00	0.16	0.65	-0.16	0.16	0.16	-0.09	-0.58	0.29	0.59	0.90	-0.23	-0.15	-0.48
DPT	0.16	0.16	1.00	-0.41	0.16	-0.16	-0.16	0.12	0.13	-0.08	-0.02	-0.10	-0.72	-0.73	-0.06
DA	-0.29	0.65	-0.41	1.00	-0.29	0.06	0.06	-0.33	-0.63	0.34	0.68	0.80	0.12	0.12	-0.57
SS*MP	-0.16	-0.16	0.16	-0.29	1.00	0.16	0.16	-0.08	0.31	-0.30	-0.56	-0.03	-0.36	-0.54	0.61
SS*DPT	0.16	0.16	-0.16	0.06	0.16	1.00	-0.16	0.27	0.13	-0.25	-0.30	0.05	0.07	0.33	0.15
MP*DPT	0.16	0.16	-0.16	0.06	0.16	-0.16	1.00	0.23	0.13	0.13	0.29	0.18	0.11	-0.10	0.04
Color change	0.95	-0.09	0.12	-0.33	-0.08	0.27	0.23	1.00	0.69	-0.18	-0.28	-0.23	0.49	0.13	0.37
Sphericity	0.76	-0.58	0.13	-0.63	0.31	0.13	0.13	0.69	1.00	-0.68	-0.70	-0.69	0.25	-0.16	0.56
D50	-0.34	0.29	-0.08	0.34	-0.30	-0.25	0.13	-0.18	-0.68	1.00	0.62	0.45	-0.02	0.24	-0.32
Span~	-0.25	0.59	-0.02	0.68	-0.56	-0.30	0.29	-0.28	-0.70	0.62	1.00	0.62	-0.08	0.01	-0.68
ML	-0.32	0.90	-0.10	0.80	-0.03	0.05	0.18	-0.23	-0.69	0.45	0.62	1.00	-0.08	-0.09	-0.33
DMP	0.47	-0.23	-0.72	0.12	-0.36	0.07	0.11	0.49	0.25	-0.02	-0.08	-0.08	1.00	0.70	0.31
DMP SD	0.02	-0.15	-0.73	0.12	-0.54	0.33	-0.10	0.13	-0.16	0.24	0.01	-0.09	0.70	1.00	-0.03
# of strands	0.28	-0.48	-0.06	-0.57	0.61	0.15	0.04	0.37	0.56	-0.32	-0.68	-0.33	0.31	-0.03	1.00

SS…screw speed, MP…melt pump inlet pressure, DPT…die plate temperature, DA…die age, D50…median equivalent diameter, ML…motor load, DMP…die melt pressure, DMP SD…die melt pressure standard deviation

Table B-3. PLS model coefficients for process and product quality responses with p values (red numbers indicating no significance for 95% confidence interval) from ANOVA.

Responses	**Color change**		**Sphericity**		**D50**		**Span**		**Motor load**		**Die melt pressure**		**Die melt pressure SD**		**# of stable strands**	
N=11	**Coeff.**	**p value**	**Coeff.**	**p value**	**Coeff.**	**p value**	**Coeff.**	**p value**	**Coeff.**	**p value**	**Coeff.**	**p value**	**Coeff.**	**p value**	**Coeff.**	**p value**
Constant	5.00	4.27E-06	0.928	5.29E-16	0.962	2.06E-06	-0.477	3.35E-07	44.0	4.64E-18	129	7.34E-09	6.35	8.04E-05	6.909	3.34E-09
SS	3.87	4.90E-05	0.008	1.59E-03	-0.012	0.646	-	-	-	-	17.4	0.013	0.095	0.832	-	-
MP	-	-	-0.003	0.158	0.012	0.801	-	-	1.42	8.90E-05	-	-	-0.271	0.562	-	-
DPT	-	-	-	-	-0.003	0.942	-	-	-	-	-24.9	1.81E-03	-1.24	0.045	-	-
DA	-	-	-0.003	0.170	0.011	0.843	0.112	0.016	-	-	-	-	-	-	-0.836	0.030
SS*MP	-	-	0.003	0.071	-0.009	0.706	-	-	-	-	-	-	-0.926	7.49E-02	-	-
SS*DPT	-	-	-	-	-0.015	0.535	-	-	-	-	-	-	0.650	0.168	-	-
MP*DPT	-	-	-	-	-	-	-	-	-	-	-	-	-	-	-	-
Model performance																
Q^2	0.826		0.811		0.127		0.433		0.798		0.7		0.461		0.346	
R^2	0.853		0.903		0.312		0.492		0.833		0.796		0.847		0.426	

SS…screw speed, MP…melt pump inlet pressure, DPT…die plate temperature, DA…die age, D50…median equivalent diameter

C. Supplemental Material - Sensitivity of a Continuous Hot-Melt Extrusion and Strand Pelletization Line to Control Actions and Composition Variation

I. Experimental Setup and Nominal Process Settings

The HME process setup and screw configuration were optimized prior to this study. The final screw and temperature profile (Figure C-1) with a long intake zone for slow material compression ensured a robust intake performance. To avoid HPMC degradation, the thermal and mechanical stress was kept low in the melting zone, consisting of forward-conveying kneading elements. After another conveying zone, the mixing zone was equipped with four toothed mixing elements to achieve mixing with a low shear energy input. A narrow, neutral kneading element was employed at the end of the mixing zone to increase the residence time of the material in this zone. Atmospheric devolatilization was applied to remove vapor and other volatiles in the melt. The end of the screw had small-pitched conveying elements to increase the pressure build-up efficiency at the interface to the melt pump.

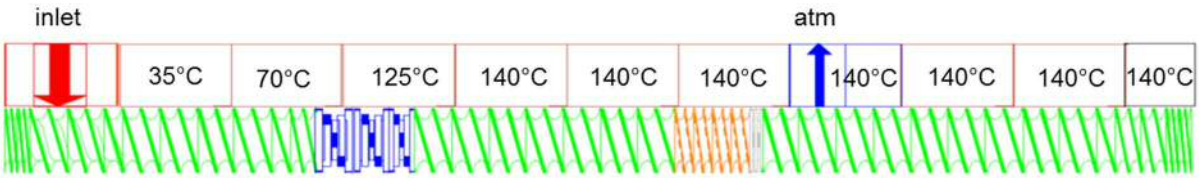

Figure C-1. Screw configuration with the melting zone, the low shear stress mixing zone (with toothed elements), the barrel temperature profile (max 140°C) and the barrel configuration (inlet in barrel 1 and atmospheric devolatilization in barrel 8).

Melt pressure at the melt pump inlet was controlled by automatically adjusting the rotational speed of the pump gear wheels. To that end, a pressure sensor was mounted directly before the melt pump (Figure C-2). After the melt pump, an adapter plate held the die plate. The adapter was temperature-controlled and in tight contact with the dies. Therefore, the die temperature can be assumed to be equal to the adapter plate temperature.

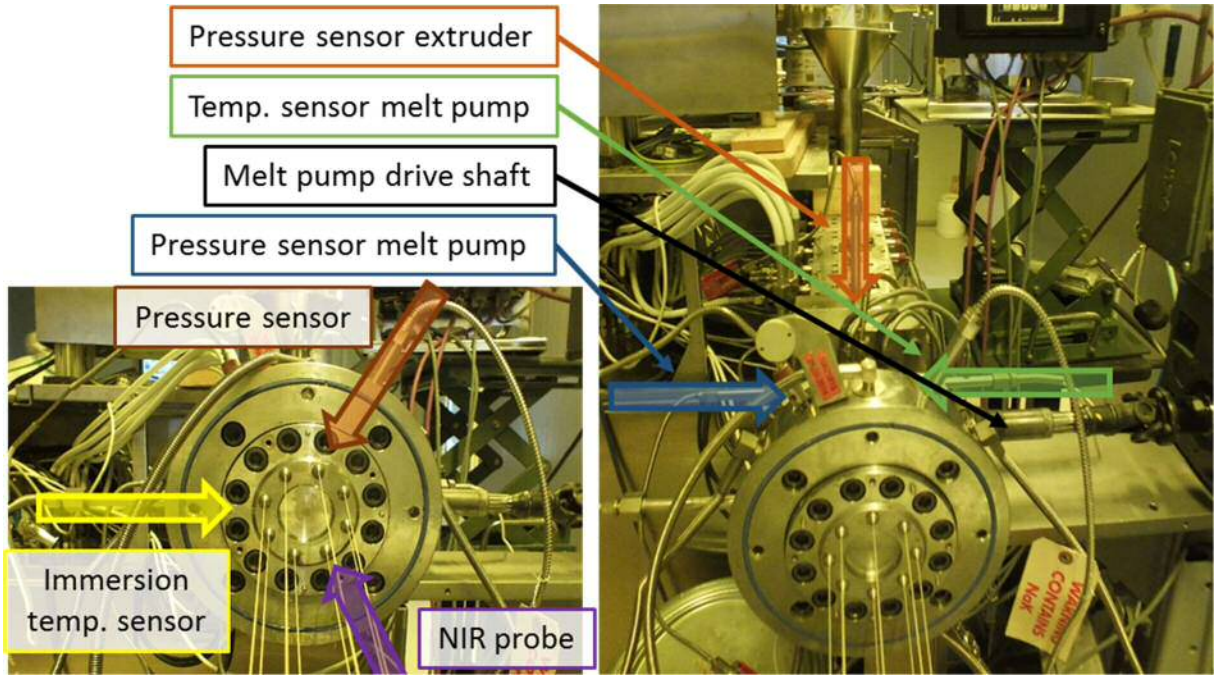

Figure C-2. Melt sensor setup in extruder, melt pump and extrusion die plate.

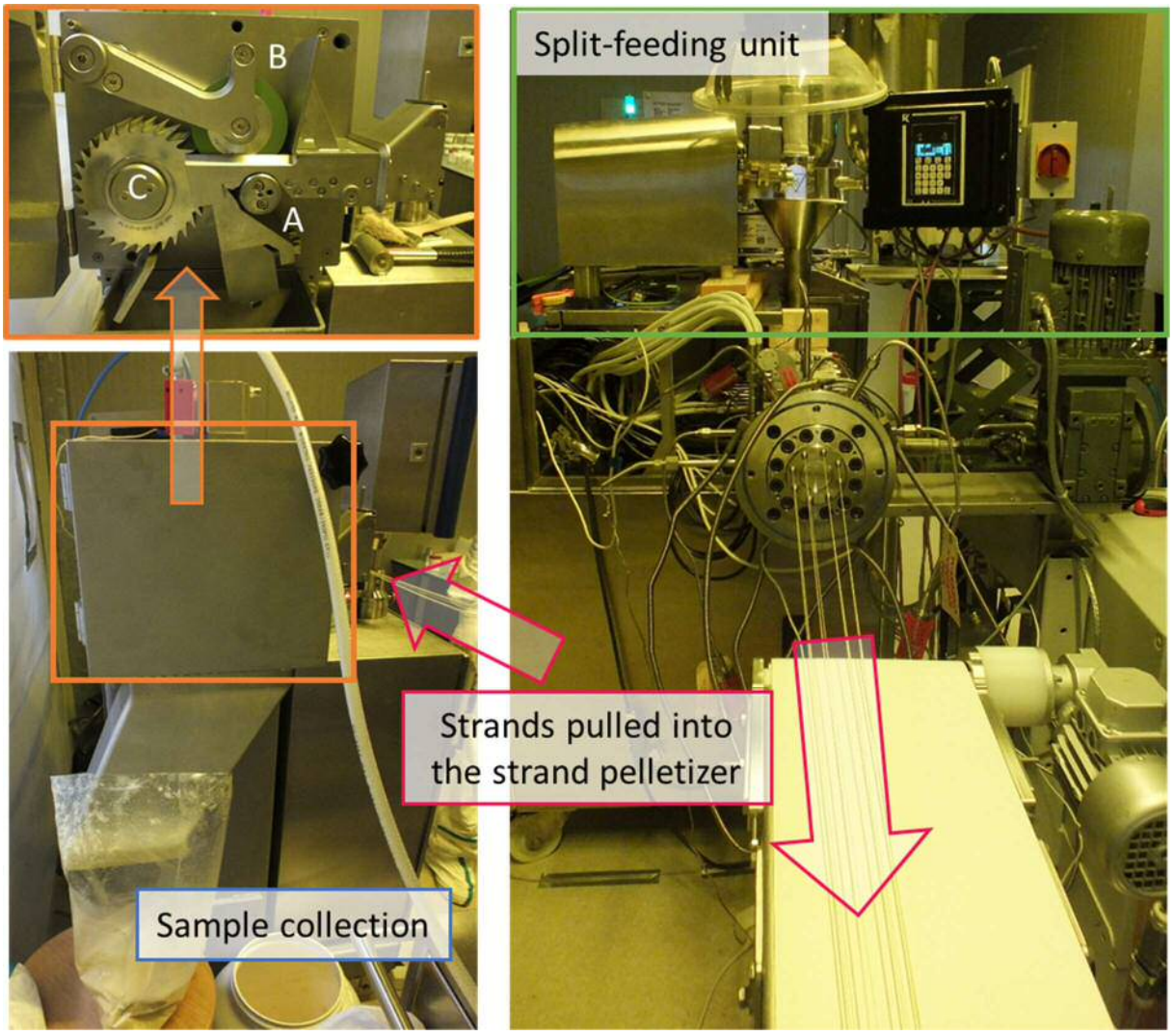

Figure C-3. Process setup with split-feeding unit, extruder and strand pelletizer (top-left: opened view with driven (A) and passive (B) intake wheel and knife roll (C)).

In the strand pelletizer, the strands were seized by the two intake wheels (Figure C-3) and conveyed into the cutting region at a specified speed, i.e., the intake speed. The lower wheel is motor driven (wheel A) and has a grooved surface to ensure a good grip. The upper wheel (wheel B) is passively driven and made of rubber, pressing the strand down using its weight. The cutting knife roll (C) is equipped with 30 knives rotating at a specific rotational speed. The rotational speed adjustment of the rotating knife roll is performed automatically based on the intake speed and the pellet size settings. After the cutting region, the pellets exit the pelletizer due to gravity. To improve the transport of pellets from the cutting region, an air flow pointed downwards from the knife roll to the pelletizer outlet.

Nominal extrusion settings were determined in a process screening DoE. The screw speed, melt pump pressure and die temperature were varied for a constant throughput of 4 kg/h and the nominal formulation composition. Based on the results of the screening a fixed screw speed of 120 rpm was established, which was the lowest speed the extruder can run at. The screw speed was set at this level in order to avoid degradation of HPMC, which was observed at higher screw speeds (200 and 280 rpm) and led to browning of the pellets. The pressure level before the melt pump was fixed at 30 bar to reduce back-pressure length of the melt in the sheared environment of the extruder and to extend the lower range of possible melt pressure levels in the extrusion die. Since the pressure difference across the pump must be positive, a low pressure set point also widens the process window in the presence of formulation composition deviations, resulting in a lower viscosity. Although adapter temperature influenced the die melt pressure, it did not have any significant effect on the pellet size and shape within the investigated range (120-140°C). Therefore, a nominal setting of 140°C was chosen to widen the process window for highly-viscous melts using this parameter.

The nominal intake speed setting of the pelletizer was equal to the intake speed-to-throughput ratio of 3.3 m·h/(kg·min). In these settings, the strands bridged the distance between the extrusion dies and the pelletizer hanging freely, bending by their internal stress. Thus, the only elongation of strands after the extrusion dies was caused by gravity. At higher intake speed ratio, the strands were dilated (stretched) between the machines, resulting in a stronger dilatation and thinning in the diameter. At lower intake speed ratios, the strands were touching the conveyor belt below and reducing the elongating effect of gravity on the strands.

II. Nominal Formulation Characterization

Understanding the flow behavior of a melt is crucial when designing HME and pelletization processes. In our previous work (Hörmann et al., 2018) phase separation was observed in this formulation, with HPMC-rich and NMD and EE-rich phases. Capillary rheology measurements performed in this study, revealed the complex rheology of this formulation.

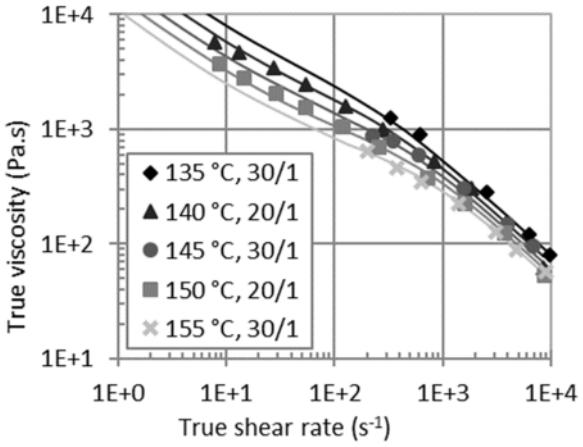

Figure C-4. Capillary rheology viscosity data of the nominal formulation, fitted by CarPow viscosity model.

In contrast to typical polymeric melts, the formulation does not have a zero-viscosity plateau, with the viscosity values steadily increasing at decreasing shear rates (Figure C-4). The CarPow model considers the viscous behavior of highly-filled polymers (Geiger, 2009). Fitting measurement data under consideration of the horizontal shift factor $a_T(T) = 1$ for time-temperature superposition at a reference temperature of 150°C, results in the following equation:

$$\eta\left(\dot{\gamma}|_{Tref=150°C}\right) = \frac{a_T(T)\cdot d}{\dot{\gamma}^n} + \frac{a_T(T)\cdot a}{(1 + a_T(T)\cdot b\cdot\dot{\gamma})^c} = \frac{13523.6}{\dot{\gamma}^{0.72}} + \frac{674.0}{(1 + 1.83\cdot 10^{-3}\cdot\dot{\gamma})^1} \qquad \textit{Eq. C-1}$$

where $a = \eta_0(T)$ is the zero-viscosity, b is the inverse of the critical shear rate ($b = 1/\dot{\gamma}_{crit}$ with $\dot{\gamma}_{crit} = 674.0$ s^{-1}) and the horizontal shift factor $a_T(T)$ according to Williams et al. (1955) (Eq. C-1).

$$ln\left(a_T(T)\right) = \frac{-C_1\cdot(T - T_{Ref})}{C_2 + T - T_{Ref}} \qquad \textit{Eq. C-2}$$

The second term in Eq. C-1 is equivalent to the Carreau model for shear-thinning polymer melts, while the first term describes the rise of viscosity at low shear rates due to the non-flowing filler component by a power law model. Clearly, HPMC behaves as a filler and does not flow when embedded in a formulation with NMD and EE due to the large differences in the viscosity of components. This has two implications on the extrusion process development:

i) Simulation tools, such as 1-dimensional codes for the prediction of residence times and HME process state variables, as proposed by Eitzlmayr et al. (2014), cannot be applied without significant adaptations for viscoelastic melts (Elkouss et al., 2006).

ii) It is mandatory to ensure uniform melt flow throughout the whole extrusion process (e.g., in melt channels) to avoid permanently stagnating material. Therefore, the ability of the process to recover from a composition fluctuation was investigated.

The characterization of the formulation's complex melt rheology further emphasized the need for an experimental evaluation of process sensitivity to throughput and formulation changes.

III. Process Responses

Table C-1. Steady-state process responses and RTD model parameters from all DoE runs.

Run	Motor load [%]	Die melt pressure [bar]	T_d [s]	T_m [s]	s_{RT} [s]	T [b] [s]
N1	50.2	220.0	77.6	151.9	36.8	18.6
N2	35.3	104.7	84.0	150.9	33.3	16.7
N3	31.9	47.7	85.4	141.2	27.9	14.0
N4	43.9	99.6	84.8	144.7	30.0	15.0
N5	34.0	47.9	79.1	141.8	31.3	15.7
N6	30.2	59.5	72.8	134.7	30.9	15.5
N7	39.0	129.2	79.7	147.6	33.8	17.0
N8	27.3	28.7	69.4	131.3	30.9	15.5
N9	49.9	127.1	85.6	150.7	32.4	16.3
N10	34.2	62.2	85.1	146.7	30.7	15.4
N11	28.0	48.6	73.8	130.9	28.5	14.3
N12	36.3	82.1	76.4	137.2	30.4	15.2
N13	29.3	50.1	65.7	118.8	26.6	13.3
N14	42.6	130.6	72.7	137.7	32.5	16.3
N15	31.5	30.6	72.3	119.0	23.4	11.7
N16	55.2	148.3	68.0	122.8	27.4	13.7
N17	35.3	41.4	62.1	105.8	21.9	10.9
N18	42.0	98.0	65.2	111.2	23.0	11.5
N19	46.4	109.5	64.1	118.0	26.9	13.5
N20	32.9	22.1	70.1	114.0	21.9	11.0
N21	57.3	102.2	59.4	101.2	20.9	10.5
N22[a]	33.5	37.3	74.5	106.0	15.7	7.9
N23	33.5	37.5	66.1	113.7	23.8	11.9
N24	57.4	169.3	62.4	109.7	23.6	11.8
N25 [a]	35.7	42.4	60.7	96.8	18.1	9.0
N26	34.4	35.6	66.2	102.9	18.3	9.2
N27	49.5	81.2	65.1	106.2	20.6	10.3
N28	38.6	49.9	63.7	107.3	21.8	10.9
N29	*37.7*	*67.2*	*72.5*	*125.1*	*26.3*	*13.1*
N30	*37.1*	*62.2*	*68.7*	*114.5*	*22.9*	*11.5*
N31	*37.4*	*65.6*	*74.0*	*130.8*	*28.4*	*14.2*

[a] *data averaged over 3-4 min only;* [b] time constant from transfer function model

IV. PLS Model for Motor Load

Motor load is a potentially critical process parameter for process stability since at a level above 80% an emergency shut down is triggered. The critical level was not reached in any case, with motor loads between 20% and 60%. Therefore, the HME process is robust across the investigated range. Reproducibility of this response in comparison to the overall variability in the dataset was excellent (0.998), and highly accurate models could be fitted (Q^2 = 0.968, R^2 = 0.988). One of the replicate center runs (N29) was performed after a run with 14% API content and high HPMC level (N10), another one after a run with 2% API content and high HPMC level (N21) and one after starting up the empty extruder (N30) (see run sequence in Table 2). The excellent repeatability of the replicate center runs indicates robustness of this process in terms of recovery from the formulation deviations without alteration, confirming the self-cleaning ability and forced melt flow provided by the extrusion screws.

However, a strong correlation of motor load with formulation composition was observed. With increasing HPMC content and throughput, the motor load rises (Figure C-5). As such, in cases where the momentary formulation composition exceeds the investigated range, e.g., due to a drastic feeding deviation, motor overload is still possible. In contrast, high API fractions decrease the motor load significantly, which is in agreement with the known plasticizing effect of NMD.

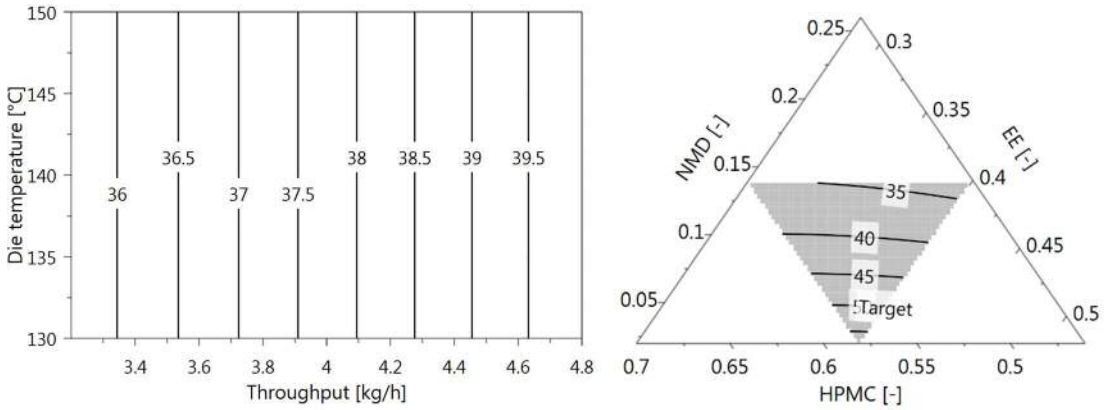

Figure C-5. Contour plot of motor load [%] for process (left) and mixture parameters (right) (process parameter plot for nominal formulation, mixture plot for 4.8 kg/h and 140°C, intake speed ratio = 3.3 m·h/(kg·min) for both).

V. Process Stability Sweet Spot

Statistical process analysis was used to define a sweet spot specifically for understanding process stability limits. The HME process limits were given by

- the motor load limit of the extruder (<80%) and
- a two-sided die melt pressure limit (35 bar < p_{Die} < 150 bar).

Concerning pelletization process, no machine parameters posed any limitations. However, the appearance of strand rupture or a lack of sufficient strand cooling before the intake zone of the pelletizer is critical. Therefore, the PSD width is used as a process performance indicator using the limit of 60% for UI to detect strand-cutting failures. This limit value was correlated to the occurrence of a second peak of larger-sized pellets or, to be more specific, fragments in the intermediate product.

For the nominal formulation no HME processability limit was reached within the investigated process parameter range Figure C-6 d)). Therefore, the HME process can be considered robust in the presence of changes made as control actions. The pelletization process does show sensitivity to throughput levels above 4.45 kg/h, given by the pellet PSD UI.

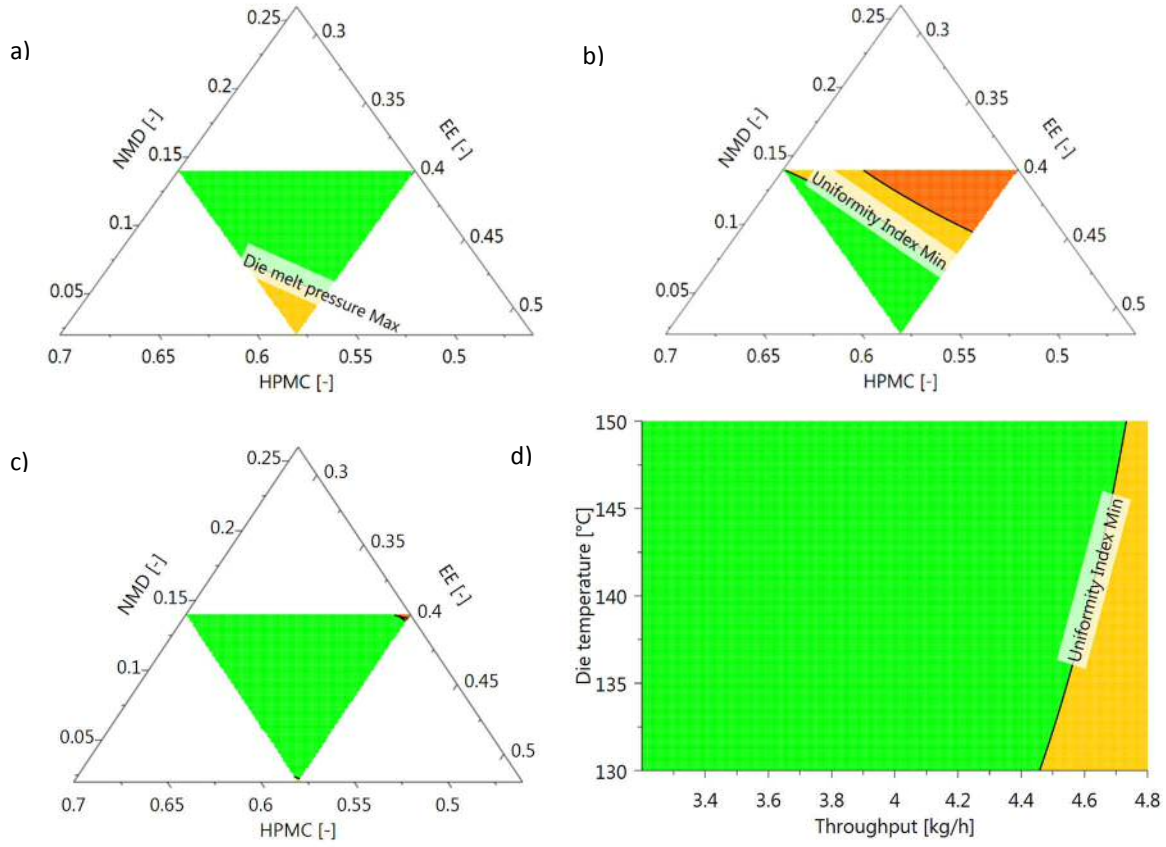

Figure C-6 Sweet spot for HME and pelletization process stability for full range of investigated formulation compositions and selected process settings: a) 130°C and 3.2 kg/h, b) 150°C and 4.8 kg/h, and c) 140°C and 4.0 kg/h. d) Sweet spot for HME and pelletization process stability across the full range of investigated process parameters (nominal formulation).

However, the sweet spot analysis for the full range of investigated formulation compositions (Figure C-6 a)-c)) shows process limitations for both HME and pelletization, suggesting that the process stability is sensitive to feeder fluctuations and the resulting formulation composition changes in general. The upper and lower melt pressure limits were reached in the tested parameter space at the two extreme ends of formulation viscosities. Formulations with a high HPMC and low EE fraction approach the maximum melt pressure level if the throughput is low (Figure C-6a). A low throughput results in decreased shear rates in the die and a weaker shear thinning effect on carrier rheology. Thus, a significantly higher pressure drop occurs across the die.

Moreover, the lower melt pressure limit for the melt pump is approached for high fractions of plasticizing components, NMD and EE, at simultaneously high throughput levels (orange spot Figure C-6 b)). Such a combination puts the correct operation the melt pump at risk, since a negative pressure drop in conveying direction is generated.

The pelletization process limit (UI) can be observed as well in the mixture diagram contour plot for throughput levels from 4 kg/h onwards (the limit visible in the top right corner of mixture range in Figure C-6 c)).

VI. Product Responses

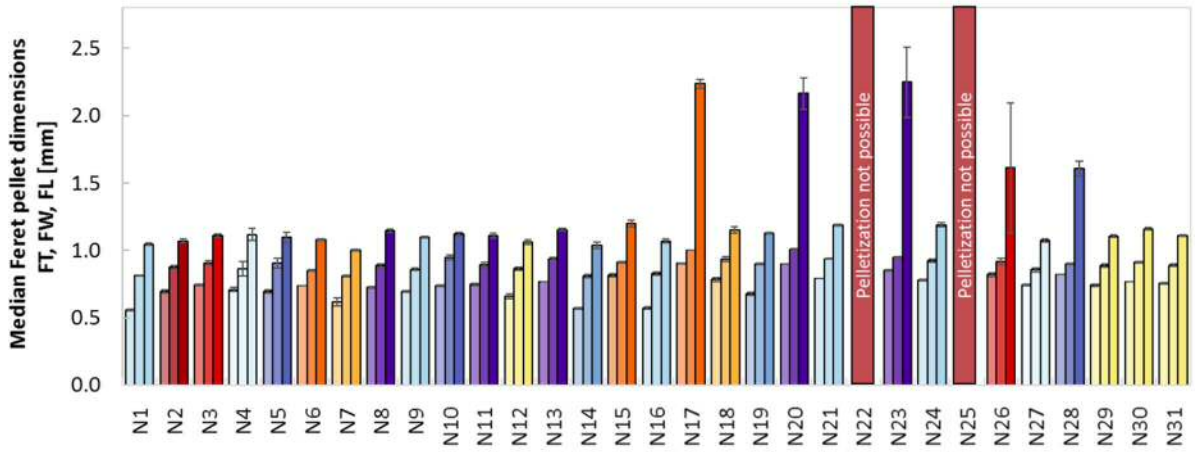

Figure C-7. Median Feret dimensions (thickness, width, length) of pellet samples (mean ± SD, n=4) for all DoE runs (color code for formulation composition see Figure 4-2).

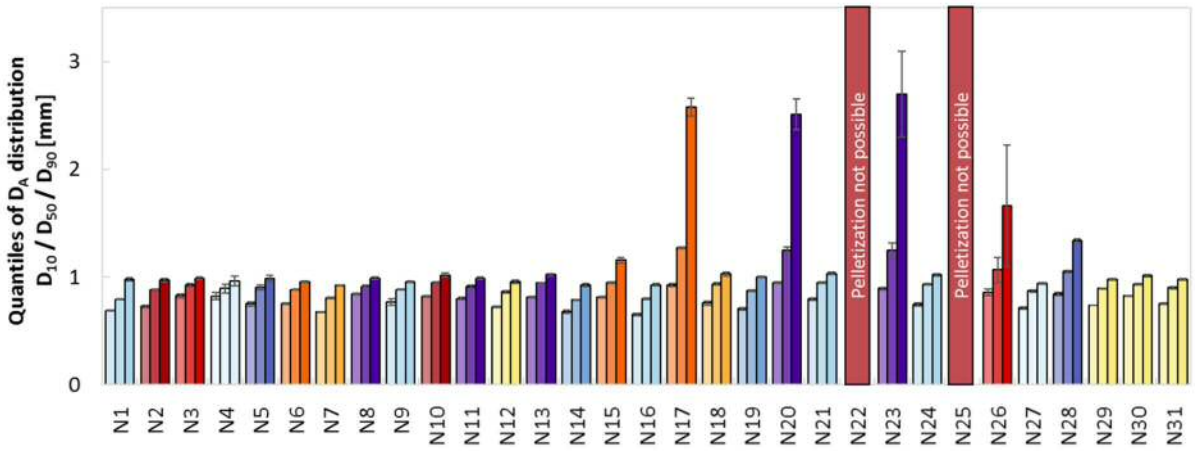

Figure C-8. 10%, 50% and 90%-quantiles of equivalent diameter distribution of pellet samples (mean ± SD, n=4) for all DoE runs (color code for formulation composition see Figure 4-2).

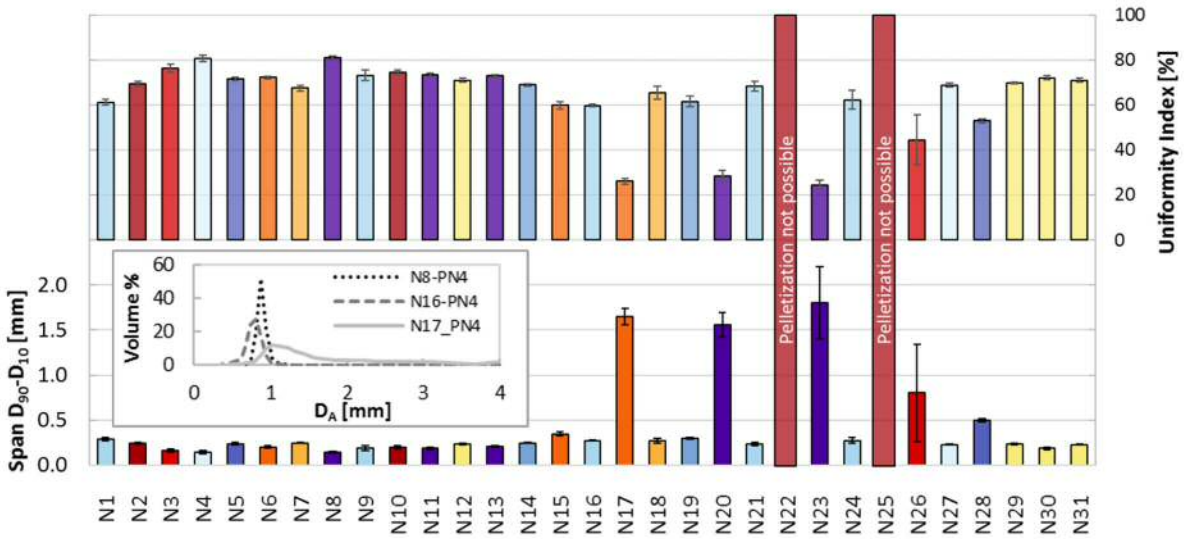

Figure C-9. PSD span [mm] and uniformity index {%] (mean ± SD, n=4) of D_A distributions for all DoE runs (color code for formulation composition see Figure 4-2). Small diagram: Volume-based density distribution of D_A for exemplary unimodal (N8, N16) and multimodal (N17) sample distributions.

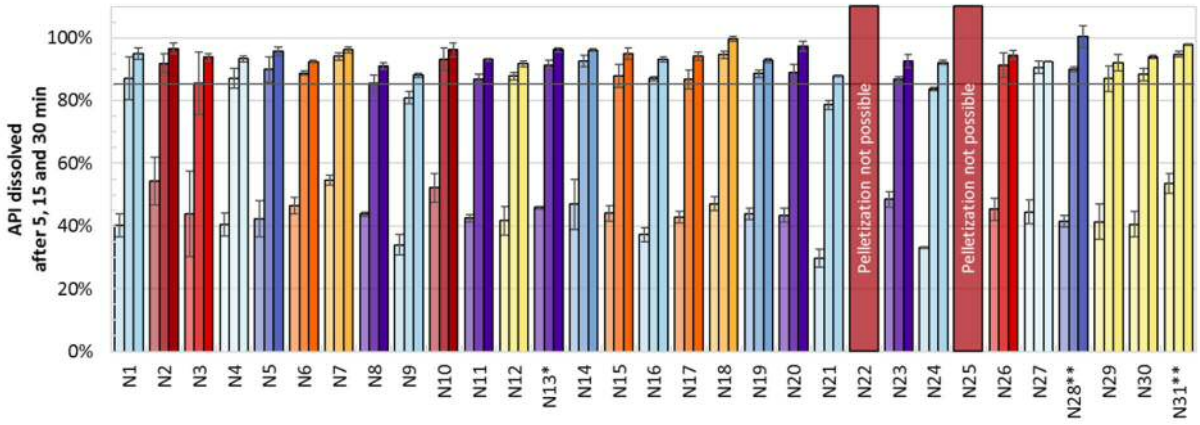

Figure C-10. Dissolved API [%] (mean ± SD, n=3) from pellets in all DoE runs. The horizontal line represents the 85% threshold for immediate release after 30 min (color code for formulation composition see Figure 4-2). *n=2, **measured with different UV/Vis spectrometer.

VII. PLS Model Coefficients

Table C-2. PLS model coefficients for process responses with p values (red numbers indicating no significance for 95% confidence interval) from ANOVA. (Reference mixture for centering: nominal formulation)

Responses	**10Log(ML)**		**10Log(DMP)**		**DMT**		**T_d**		**T_m**		**s_{RT}**	
N=31	**Coeff.**	**p value**	**Coeff.**	**p value**	**Coeff.**	**p value**	**Coeff.**	**p value**	**Coeff.**	**p value**	**Coeff.**	**p value**
Constant	1.576	1.9E-01	1.80	4.6E-20	143.29	0.0E+00	71.925	2.2E-17	124.99	1.4E-19	26.502	5.7E-14
mf	0.024	5.6E-02	-0.07	1.1E-09	0.343	1.8E-02	-6.359	6.5E-02	-15.44	3.8E-03	-4.486	1.5E-02
T_{Die}	-	-	-0.11	4.6E-14	4.531	4.7E-22	1.388	3.3E-02	-2.47	5.6E-03	-1.170	1.3E-03
v_{in}/mf	-	-	-	-	-	-	-	-	-	-	-	-
API	0.213	5.9E-02	-0.15	7.6E-05	-1.103	5.1E-09	-0.083	8.8E-01	0.76	1.2E-01	-1.158	5.3E-04
HPMC	0.296	2.4E-06	0.08	1.0E-13	0.326	2.4E-04	0.954	8.3E-03	-0.44	4.9E-01	-0.025	8.9E-01
EE	0.261	3.5E-04	-0.04	7.2E-07	-0.173	9.7E-02	-1.332	5.3E-03	-	-	0.339	1.5E-01
API*API	-	-	0.03	5.8E-03	-	-	-	-	-	-	-	-
HPMC*HPMC	0.006	1.3E-01	-	-	-	-	-	-	-	-	-	-
EE*EE	0.007	4.9E-02	-	-	-	-	-	-	-	-	-	-
mf*T_{Die}	-	-	-	-	-0.486	1.1E-03	-	-	-	-	-	-
mf*(v_{in}/mf)	-	-	-	-	-	-	-	-	-	-	-	-
mf*API	-0.002	2.2E-01	-	-	-	-	1.380	1.9E-02	1.95	2.3E-02	0.343	2.4E-01
mf*HPMC	-0.005	4.9E-04	-	-	-	-	-1.125	1.6E-03	-2.09	1.3E-04	-0.470	9.1E-03
mf*EE	0.007	5.8E-05	-	-	-	-	1.233	5.9E-03	2.45	3.6E-04	0.576	1.3E-02
T_{Die}*(v_{in}/mf)	-	-	-	-	-	-	-	-	-	-	-	-
T_{Die}*API	-	-	-	-	-	-	-	-	-	-	-	-
T_{Die}*HPMC	-	-	-	-	-	-	-	-	-	-	-	-
T_{Die}*EE	-	-	-	-	-	-	-	-	-	-	-	-
API*HPMC	-	-	-	-	-	-	-	-	-	-	-	-
API*EE	-	-	-	-	-	-	-	-	-	-	-	-
HPMC*EE	0.017	1.3E-02	-	-	-	-	-	-	-	-	-	-
Model performance												
Q^2	0.968		0.962		0.955		0.623		0.81		0.753	
R^2	0.988		0.981		0.981		0.866		0.935		0.917	

ML…motor load, DMP…die melt pressure, DMT…die melt temperature, T_d…dead time RTD model, T_m…mean RT from RTD model, s…standard deviation of RT from RTD model, mf…total mass flow (throughput), T_{Die}…die plate temperature, v_{in}/mf…intake speed to throughput ratio, API…NMD fraction, HPMC…HPMC fraction, EE…EE fraction

Table C-3. PLS model coefficients for pellet responses with p values (red numbers indicating no significance for 95% confidence interval) from ANOVA. (Reference mixture for centering: nominal formulation)

Responses	**10Log(10$x_{50}(D_V)$+0.01)**		**10Log(x_{50}(FL)+0.01)**		**10Log(L/T+0.01)**		**Sphericity**		**10Log(Span(x_{90}-x_{10})+0.001)**		**-10Log(10-0.1*UI)**	
N=29	**Coeff.**	**p value**	**Coeff.**	**p value**	**Coeff.**	**p value**	**Coeff.**	**p value**	**Coeff.**	**p value**	**Coeff.**	**p value**
Constant	0.970	3.9E-21	0.090	6.3E-02	0.253	2.5E-04	0.919	2.4E-03	-0.564	2.2E-02	-0.506	2.1E-04
mf	0.031	2.9E-01	0.058	2.2E-01	0.030	3.7E-01	-0.016	8.2E-02	0.195	1.5E-01	-0.110	1.0E-01
T_{Die}	-	-	-	-	-0.012	7.0E-02	0.006	1.0E-03	-	-	0.033	1.3E-02
v_{in}/mf	-	-	-	-	-	-	-	-	-	-	-	-
API	0.024	7.2E-05	0.031	9.6E-04	0.006	8.2E-01	0.005	8.4E-01	0.115	3.1E-01	-0.046	4.1E-01
HPMC	-0.010	4.7E-03	-0.021	7.0E-04	-0.004	4.4E-01	0.008	7.4E-01	-0.024	2.6E-01	0.002	8.3E-01
EE	0.007	8.7E-02	0.019	8.5E-03	0.013	1.3E-02	0.002	9.4E-01	0.045	3.1E-02	-0.018	7.3E-02
API*API	-	-	-	-	0.010	2.5E-01	-	-	0.042	2.1E-01	-0.026	1.2E-01
HPMC*HPMC	-	-	-	-	-	-	-	-	-	-	-	-
EE*EE	-	-	-	-	-	-	3.1E-04	9.0E-01	-	-	-	-
mf*T_{Die}	-	-	-	-	-	-	-	-	-	-	-0.016	1.7E-01
mf*(v_{in}/mf)	-	-	-	-	-	-	-	-	-	-	-	-
mf*API	0.010	6.0E-02	0.030	1.1E-03	0.022	1.1E-03	-0.005	4.8E-03	0.101	2.0E-04	-0.050	2.4E-04
mf*HPMC	-0.009	1.3E-02	-0.020	6.1E-04	-0.014	1.0E-03	0.004	2.5E-03	-0.060	4.6E-04	0.028	8.1E-04
mf*EE	0.008	3.9E-02	0.018	7.1E-03	0.012	1.1E-02	-0.003	2.0E-02	0.052	8.6E-03	-0.024	1.4E-02
T_{Die}*(v_{in}/mf)	-	-	-	-	-	-	-	-	-	-	-	-
T_{Die}*API	-	-	-	-	-	-	-	-	-	-	-	-
T_{Die}*HPMC	-	-	-	-	-	-	-	-	-	-	-	-
T_{Die}*EE	-	-	-	-	-	-	-	-	-	-	-	-
API*HPMC	-	-	-	-	-	-	-	-	-	-	-	-
API*EE	-	-	-	-	-	-	0.002	6.3E-01	-	-	-	-
HPMC*EE	-	-	-	-	-	-	-	-	-	-	-	-

Model performance						
Q^2	0.621	0.758	0.605	0.735	0.747	0.689
R^2	0.778	0.831	0.767	0.882	0.851	0.880

$x_{50}(D_V)$= $x_{50}(D_A)$…median projection area equivalent diameter, x_{50}(FL)…median Feret length, L/T…length-to-thickness ratio, UI…uniformity index, mf…total mass flow (throughput), T_{Die}…die plate temperature, v_{in}/mf…intake speed to throughput ratio, API…NMD fraction, HPMC…HPMC fraction, EE…EE fraction

D. Supplemental Material - Tableting Formulation Development for the Compression of Elastic Hot-Melt Extruded Pellets

I. In-Die Heckel Plots of Binders

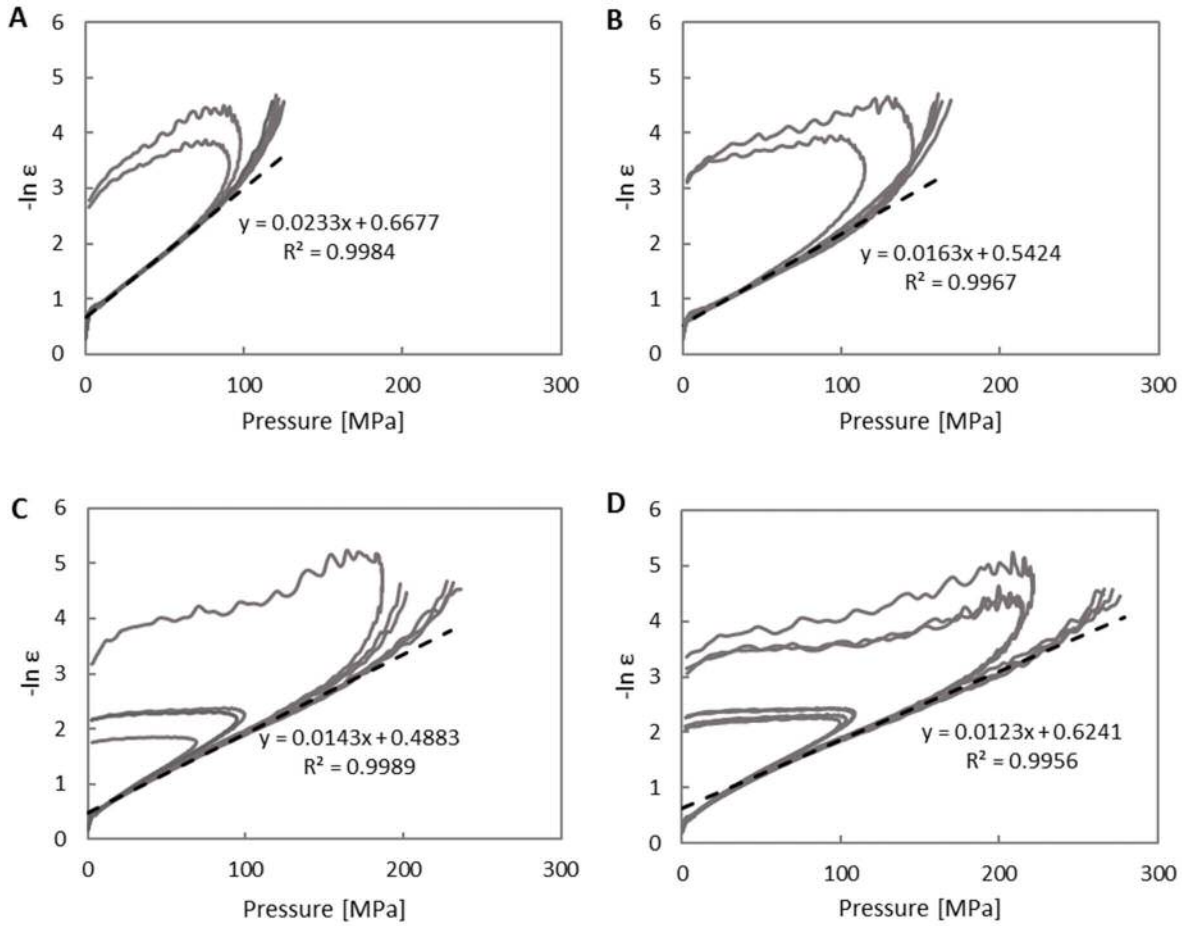

Figure D-1. In-die Heckel plots of Methocel™ E5 (A), Kollidon® VA64 (B), Avicel® PH101 (C) and Avicel® PH102 (D).

II. CTC Profiles of Pellets and Binders

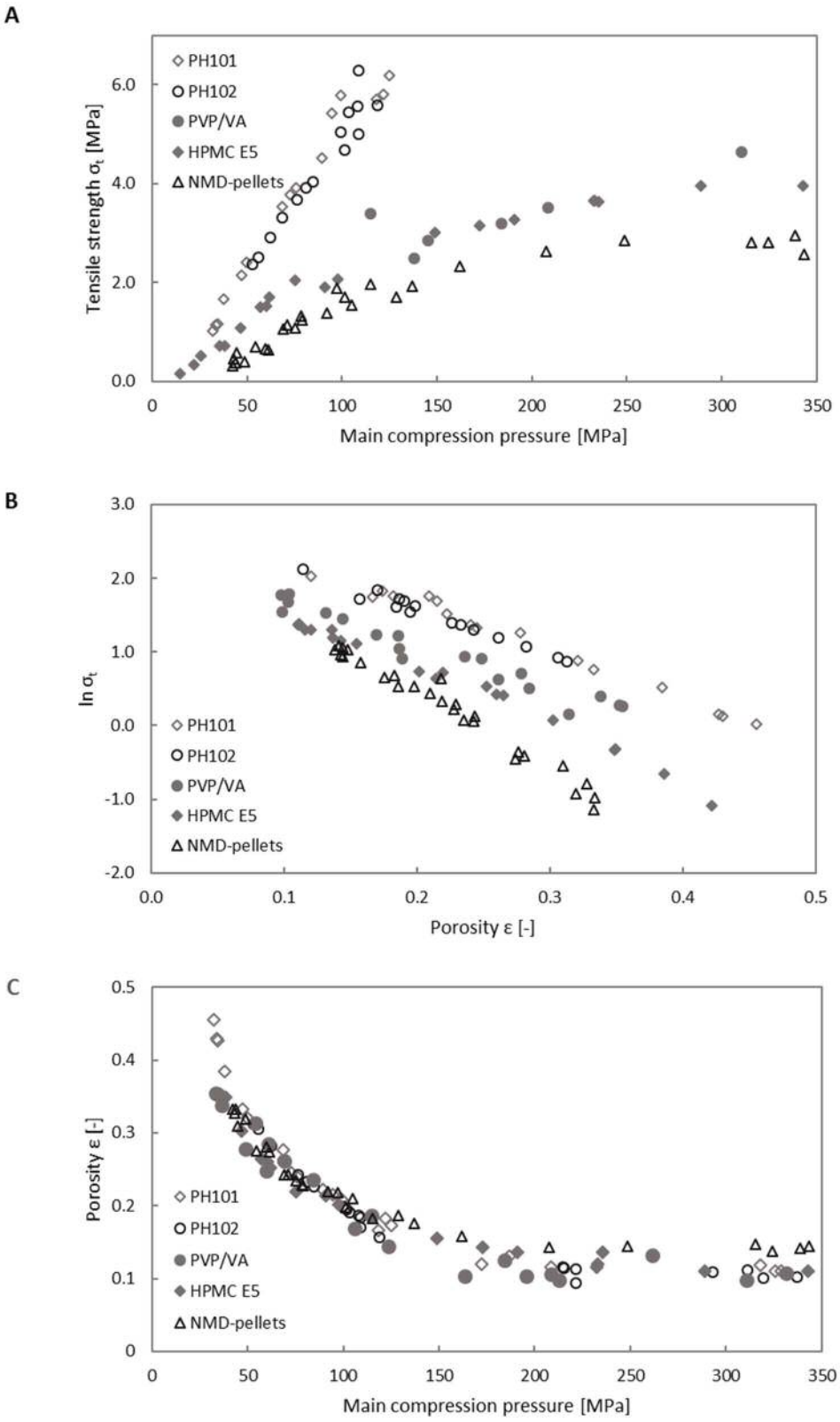

Figure D-2. Tabletability (A), linearized compactability (B) and compressibility (C) profiles for all raw materials. Tabletability and compactability not showing tensile strength data from PH101 and PH102 tablets produced at high main compression pressures, because tablet hardness was exceeding measurement range of hardness tester.

III. Additional Data for Binary Blend Compaction Analysis

Table D-1 Initial bulk density, true density and initial porosity of binary mixtures compared to pure substances.

	Pellet content [% v/v]	True density ρ_{tr} [g/cm³]	Initial bulk density $\rho_{b,0}$ [g/cm³]	Initial porosity ε_0 [-]
PH102	0	1.563	0.31	0.80
	30	1.455	0.39	0.73
	50	1.384	0.42	0.70
	70	1.312	0.52	0.60
NMD-pellets	100	1.204	0.55	0.54

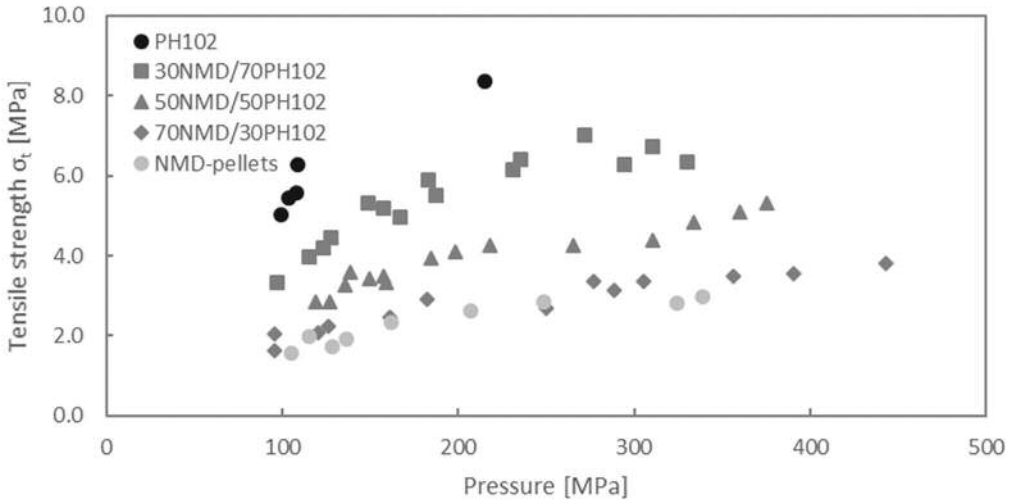

Figure D-3. Tabletability profiles of raw materials and binary blends from NMD-pellets and PH102. Ratios given in vol.%.

IV. Additional Data for Formulation Screening

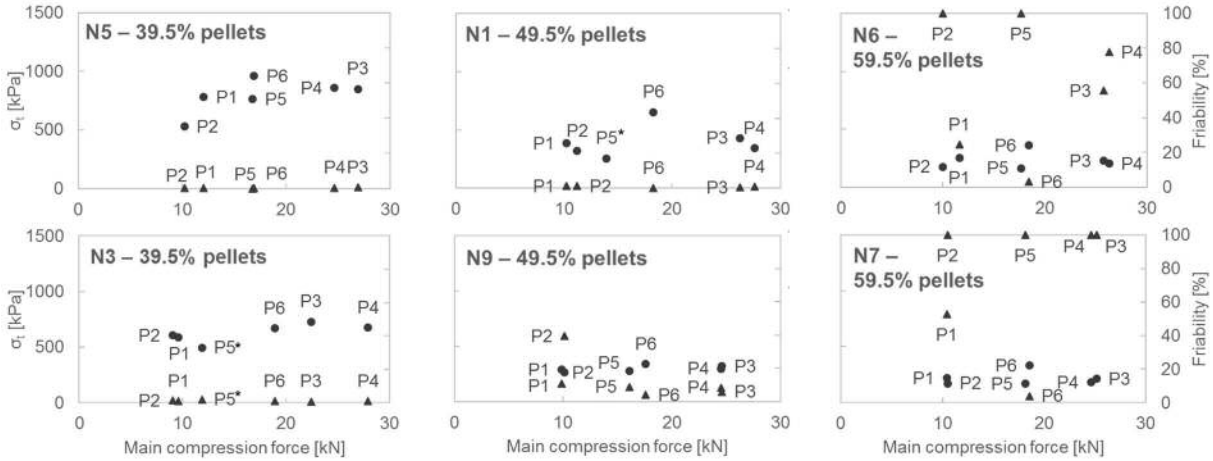

Figure D-4. Tensile strength (circles) and friability data (triangles) from selected formulations in the DoE. Pellet content in the respective formulations is given in the diagrams, formulations N5 and N1 contained 20 wt.%, N6 10 wt.% and N3, N9 and N7 with no K-CL. (Indicates data from samples were the hopper was already running empty during tablet sampling.)*

Table D-2. Compression force and tablet property data from formulation screening DoE runs.

	PCF [kN]	MCF [kN]	Avg. weight [mg]	MU (RSD) [%]	RC [N]	TS [MPa]	FR [%]	DT [min]
P1								
N1	0.50	10.22	211.0	1.80	19.36	0.387	1.24	0.28
N2	0.62	13.05	260.6	1.27	37.28	0.656	0.51	0.45
N3	0.43	9.57	253.6	1.29	33.09	0.588	1.01	0.33
N4	0.66	10.43	229.9	2.24	39.47	0.750	0.26	0.15
N5	0.67	12.05	232.1	1.18	41.67	0.780	0.33	0.25
N6	0.57	11.65	171.3	1.20	10.4	0.255	24.51	0.27
N7	0.54	10.45	172.1	0.92	8.71	0.219	52.56	0.00
N8	0.49	9.97	172.6	1.19	7.12	0.178	81.65	0.58
N9	0.54	9.88	194.9	1.03	12.98	0.290	11.04	0.45
N10	0.70	11.93	238.5	2.19	47.18	0.884	0.26	0.18
N11	0.62	10.24	210.4	1.35	17.18	0.346	2.79	0.15
N12	0.56	10.71	201.5	1.04	14.42	0.313	7.50	0.35
P2								
N1	2.09	11.2	212.1	0.95	15.99	0.320	1.28	0.25
N2	2.47	11.46	267.4	2.60	30.24	0.509	1.38	0.68
N3	2.00	9.02	251.5	0.76	32.81	0.605	1.21	0.27
N4	2.19	11.57	237.9	1.19	37.39	0.688	0.28	0.55
N5	2.22	10.21	231.4	3.28	29.05	0.529	0.27	0.22
N6	2.19	9.99	171.8	1.32	7.33	0.177	100.00	0.28
N7	2.03	10.51	172.4	1.11	6.96	0.174	100.00	0.57
N8	2.09	10.75	173.4	1.09	6.85	0.170	89.83	0.60
N9	1.95	10.15	197.2	0.93	11.91	0.263	39.52	0.62
N10	2.12	10.43	242.9	2.14	44.68	0.815	0.41	0.23
N11	1.86	9.76	206.3	1.37	15.79	0.325	3.55	0.17
N12	2.08	10.24	200.0	1.25	12.2	0.268	14.39	0.35
P3								
N1	0.52	26.27	208.9	1.31	20.71	0.430	0.48	0.38
N2	0.43	23.6	257.3	1.24	39.21	0.710	0.66	0.85
N3	0.47	22.41	242.2	1.01	37.53	0.728	0.70	0.58
N4	0.62	26.05	240.0	2.02	45.69	0.848	0.11	0.53
N5	0.67	26.9	244.3	2.10	47.18	0.849	0.42	0.32
N6	0.59	25.74	172.3	1.12	9.06	0.227	55.41	0.65
N7	0.58	25.18	171.7	1.44	8.37	0.213	100.00	0.53
N8	0.49	24.81	172.8	0.93	6.87	0.173	77.13	2.02
N9	0.46	24.63	193.9	1.52	13.95	0.319	5.94	1.28
N10	0.68	24.88	245.6	1.62	47.51	0.874	0.38	0.22
N11	0.53	24.8	204.6	1.26	18.19	0.387	1.54	0.22
N12	0.48	25.23	200.1	1.04	13.47	0.298	3.95	0.80
P4								
N1	2.11	27.61	210.5	1.56	16.78	0.343	0.87	0.43
N2	2.26	28.4	263.8	1.14	33.22	0.582	0.98	0.72
N3	1.99	27.92	246.4	1.21	35.49	0.674	0.91	0.78
N4	2.27	27.33	241.0	2.67	46.1	0.854	0.06	0.32
N5	1.99	24.63	242.5	1.08	46.92	0.856	0.37	0.23
N6	2.16	26.29	173.6	0.91	8.22	0.202	77.81	0.63
N7	2.07	24.62	173.6	1.45	7.18	0.181	100.00	2.32
N8	2.00	25.62	172.4	2.07	6.19	0.158	91.47	2.38
N9	1.96	24.55	194.4	1.52	13.02	0.298	8.43	1.18
N10	2.29	25.94	254.0	1.32	48.21	0.862	0.44	0.00
N11	1.96	25.23	204.8	1.03	17.56	0.373	2.09	0.32
N12	1.87	24.08	197.8	1.10	13.56	0.307	5.17	0.97

Table D-3. Compression force and tablet property data from formulation screening DoE runs (continued).

	PCF [kN]	MCF [kN]	Avg. weight [mg]	MU (RSD) [%]	RC [N]	TS [MPa]	FR [%]	DT [min]
P5								
N1	0.91	13.93	206.9	3.58	12.51	0.257	-	0.38
N2	0.60	8.56	-	-	-	-	-	-
N3	0.73	11.85	236.5	6.60	25.90	0.495	1.86	0.52
N4	0.68	9.41	227.1	7.60	23.78	0.395	8.21	0.28
N5	1.16	16.78	230.9	2.82	40.31	0.762	0.00	1.00
N6	1.42	17.67	175.6	1.05	6.79	0.163	100.00	0.00
N7	1.31	18.14	172.4	0.85	6.69	0.169	100.00	1.65
N8	1.22	17.73	-	-	-	-	-	-
N9	1.13	16.11	192.1	0.92	11.93	0.274	8.94	1.20
N10	1.61	17.99	251.8	1.15	42.94	0.767	0.46	0.18
N11	1.29	18.11	204.4	1.30	15.55	0.329	2.14	0.38
N12	1.14	16.62	194.6	1.14	13.60	0.312	4.10	0.82
P6								
N1	1.23	18.27	205.4	1.13	30.92	0.653	0.06	0.55
N2	1.38	18.22	255.1	1.15	50.07	0.918	0.21	0.55
N3	1.27	18.89	258.2	0.92	37.94	0.667	0.76	0.53
N4	1.58	18.88	229.3	1.74	46.87	0.911	0.00	0.40
N5	1.16	16.89	224.6	1.66	48.78	0.958	0.02	0.20
N6	1.16	18.43	168.4	1.32	6.79	0.362	3.16	0.98
N7	1.19	18.58	172.5	1.28	13.13	0.333	4.01	0.92
N8	1.18	18.86	171.3	1.05	12.35	0.315	6.67	1.97
N9	1.51	17.59	211.1	0.97	16.16	0.340	4.04	0.62
N10	1.37	18.31	235.2	1.22	65.61	1.291	0.15	0.18
N11	1.32	18.05	211.9	0.91	20.77	0.425	1.19	0.22
N12	1.35	18.76	201.3	1.32	17.72	0.390	2.65	0.73

PCF…pre-compression force, MCF…main compression force, MU (RSD)…mass uniformity, RC…resistance to crushing, TS…tensile strength, FR…friability, DT…disintegration time

Table D-4. Correlations of factors and responses in the formulation screening DoE (tablets from process setting P3)

	m_{Tablet}	MCF	KF	AF	PF	KF*KF	AF*AF	PF*PF	MU (RSD)	TS	FR	DT
m_{Tablet}	1	-0.187	0.277	0.596	-0.980	0.326	0.603	-0.972	0.452	0.952	-0.892	-0.412
MCF	-0.187	1	0.792	-0.816	0.170	0.773	-0.836	0.164	0.585	-0.027	-0.058	-0.278
KF	0.277	0.792	1	-0.590	-0.304	0.957	-0.586	-0.315	0.593	0.393	-0.568	-0.571
AF	0.596	-0.816	-0.590	1	-0.590	-0.516	0.994	-0.579	-0.080	0.467	-0.301	0.137
PF	-0.980	0.170	-0.304	-0.590	1	-0.348	-0.586	0.998	-0.499	-0.944	0.923	0.409
KF*KF	0.326	0.773	0.957	-0.516	-0.348	1	-0.510	-0.355	0.665	0.439	-0.597	-0.455
AF*AF	0.603	-0.836	-0.586	0.994	-0.586	-0.510	1	-0.575	-0.124	0.464	-0.304	0.140
PF*PF	-0.972	0.164	-0.315	-0.579	0.998	-0.355	-0.575	1	-0.491	-0.927	0.933	0.415
MU (RSD)	0.452	0.585	0.593	-0.080	-0.499	0.665	-0.124	-0.491	1	0.623	-0.535	-0.441
TS	0.952	-0.027	0.393	0.467	-0.944	0.439	0.464	-0.927	0.623	1	-0.870	-0.498
FR	-0.892	-0.058	-0.568	-0.301	0.923	-0.597	-0.304	0.933	-0.535	-0.870	1	0.529
DT	-0.412	-0.278	-0.571	0.137	0.409	-0.455	0.140	0.415	-0.441	-0.498	0.529	1

m_{Tablet}…avg. tablet weight, MCF…avg. main compression force, KF…K-CL mass fraction, AF…PH102 mass fraction, PF…pellet mass fraction, MU (RSD)…mass uniformity, TS…tensile strength, FR…friability, DT…disintegration time

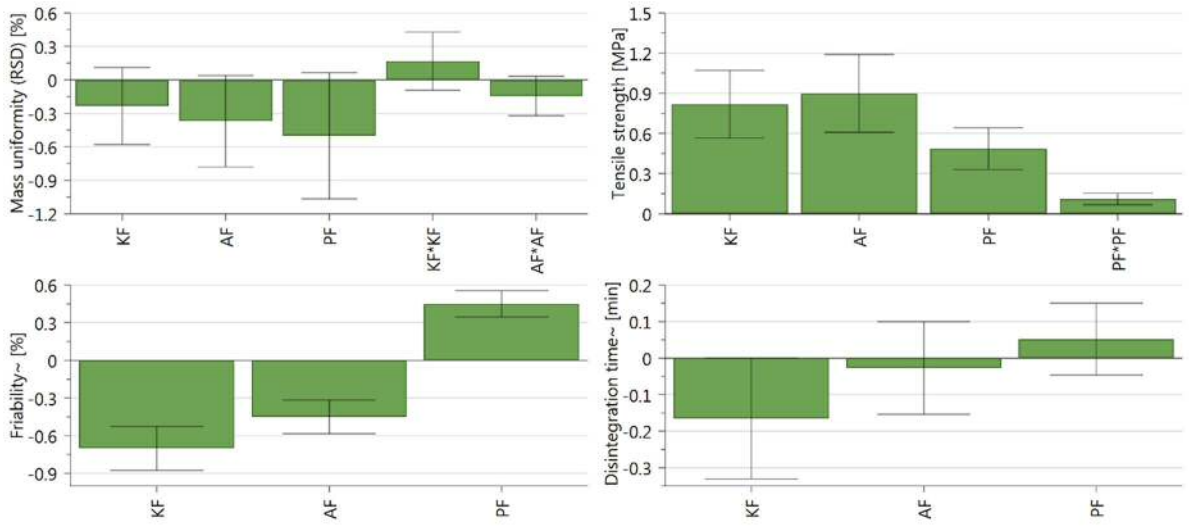

Figure D-5. Coefficient plots of PLS models for all tablet responses.

Table D-5. PLS model coefficients for tablet responses with p values (red numbers indicating no significance for 95% confidence interval) from ANOVA. (Reference mixture for centering: 10 wt.% K-CL, 40 wt.% PH102, 49.5 wt.% NMD-pellets)

Responses	**MU (RSD)**		**TS**		**10Log(FR)**		**10Log(DT)**	
N=12	**Coeff.**	**p value**	**Coeff.**	**p value**	**Coeff.**	**p value**	**Coeff.**	**p value**
Constant	1.36	3.26E-02	0.4	6.97E-04	0.397	1.06E-01	-0.247	3.46E-01
m_{Tablet}	-	-	-	-	-	-	-	-
MCF	-	-	-	-	-	-	-	-
KF	-0.234	1.53E-01	0.82	7.16E-05	-0.701	8.46E-06	-0.165	5.06E-02
AF	-0.370	6.97E-02	0.90	9.69E-05	-0.450	3.39E-05	-0.027	6.40E-01
PF	-0.501	7.41E-02	0.49	9.02E-05	0.450	4.48E-06	0.052	2.64E-01
KF*KF	0.166	1.74E-01	-	-	-	-		
AF*AF	-0.144	9.49E-02	-	-	-	-		
PF*PF	-	-	0.11	3.06E-04	-	-		
Model performance								
Q^2	0.520		0.956		0.900		0.151	
R^2	0.725		0.984		0.943		0.386	

m_{Tablet}…avg. tablet weight, MCF…avg. main compression force, KF…K-CL mass fraction, AF…PH102 mass fraction, PF…pellet mass fraction, MU (RSD)…mass uniformity, TS…tensile strength, FR…friability, DT…disintegration time

E. Supplemental Material - Residence Time Distributions of a Powder-Pellet Blend in a Continuous Blending and Tableting Unit

I. Continuous Blending Process and RTD Data

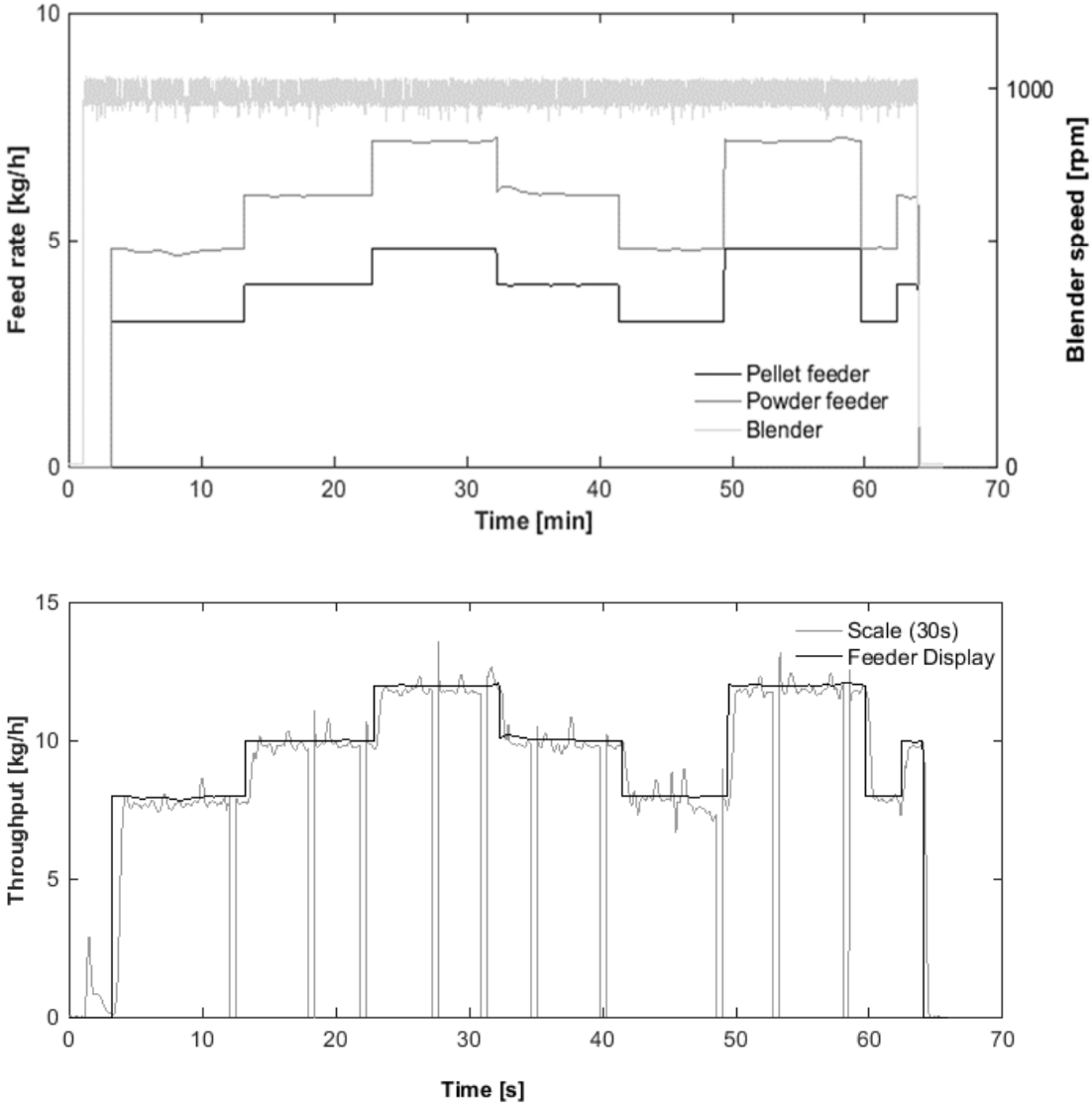

Figure E-1. Top: Equipment data collected via SIPAT during the RTD characterization runs; some disturbance in powder feed rate could be observed after refilling the hopper at approx. 32 min. Bottom: Comparison of total throughput calculated from feeder data and from the weight increase on the reference catch-scale (smoothed over 30s). Only minor deviations were observed after tracer addition (e.g. at approx. 8, 10, 17, 19 min etc.) without subsequent throughput variations. Interruptions in throughput calculated from scale data indicate an exchange of the collecting bowl on the scale. (Waldenhofer, 2017)

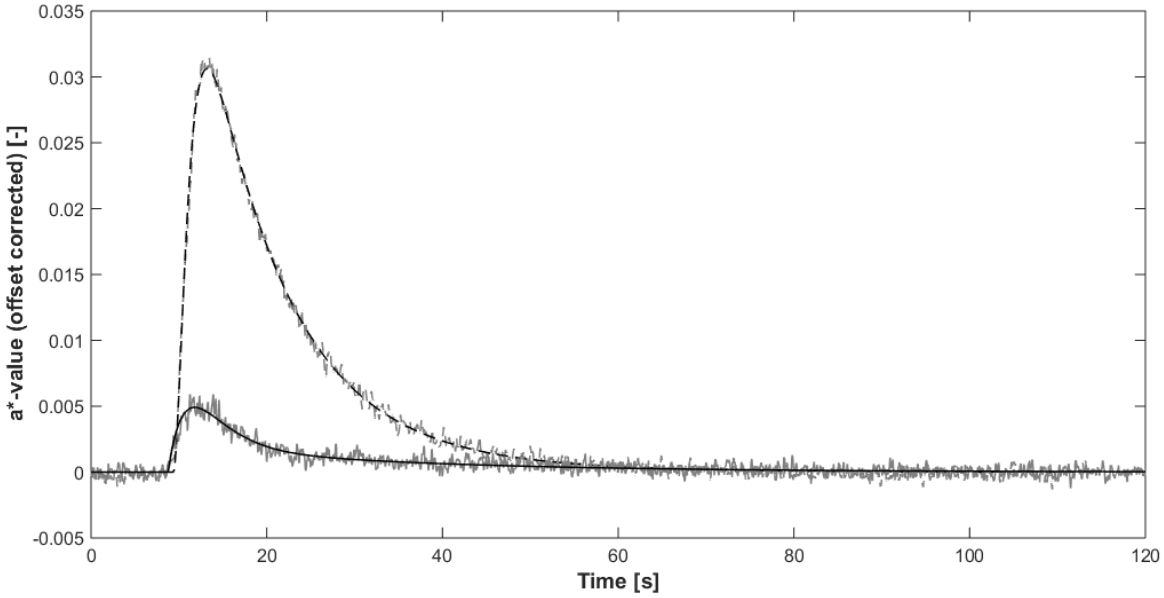

Figure E-2.Color intensity curves from powder (dashed grey – run 3) and pellet tracer (solid grey – run 4) with fit transfer function models (black) determined at a throughput of 10 kg/h.

Table E-1. Blender RTD characterization results: transfer function model parameters and RTD characteristics.

Run order	Throughput [kg/h]	Tracer	T_d [s]	T_1	T_2	T_3	T_4	T_5	k	T_m [s]	s_{RT} [s]
1	8	Powder	2.12	11.59	0.86	13.16	0.86	9.65	4.70	15.01	11.36
2	8	Pellets	1.29	10.48	2.40	26.61	2.40		0.54	21.70	23.22
3	10	Powder	1.96	8.55	1.01	12.56	1.01	6.52	4.22	14.48	11.27
4	10	Pellets	1.62	10.86	2.50	26.33	2.48		0.49	21.69	23.08
5	12	Powder	1.96	11.63	0.98	13.38	0.98	7.42	3.93	12.99	9.70
6	12	Pellets	0.94	10.54	2.52	24.65	2.52		0.46	18.15	18.38
7	10	Powder	2.08	26.33	0.89	10.72	0.88	24.14	4.44	13.09	8.12
8	10	Pellets	2.02	6.01	2.49	25.97	2.49		0.61	26.43	24.11
9	8	Powder	2.09	26.31	0.86	11.06	0.87	25.12	4.87	14.01	9.60
10	8	Pellets	1.26	7.31	2.75	26.63	2.75		0.69	25.78	25.01
11	12	Powder	1.94	2.94	1.55	9.30	1.56	1.56	3.69	12.95	9.15
12	12	Pellets	1.73	14.05	2.88	26.39	2.92		0.48	19.51	21.51

II. Tablet Press Process and RTD Data

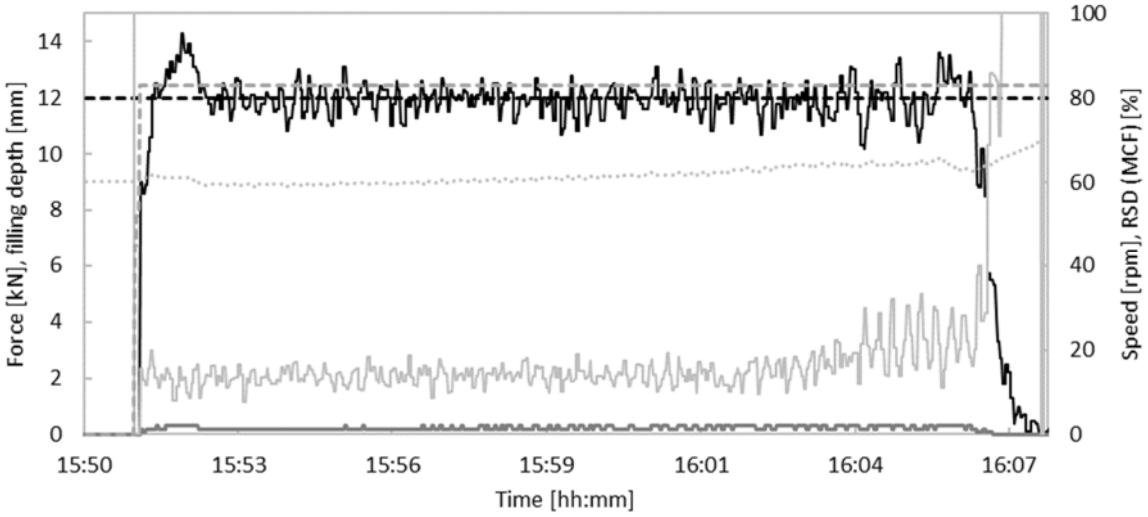

Figure E-3. Exemplary process data from powder tracer tableting run (N19-E14 – TS 83 rpm (dashed gray) and 60 rpm FF). Consistent process parameter values indicated that quasi-steady state of main compression force (MCF - solid black), and pre-compression force (solid dark gray) after approximately 1 min (activation of automatic force control at 12 kN MCF (set value - dashed black)) and was maintained over approximately 10 min of run time. During the last 5 min of operation, an increase in relative standard deviation of the MCF (solid light gray) and in filling depth (dotted light gray) was observed.

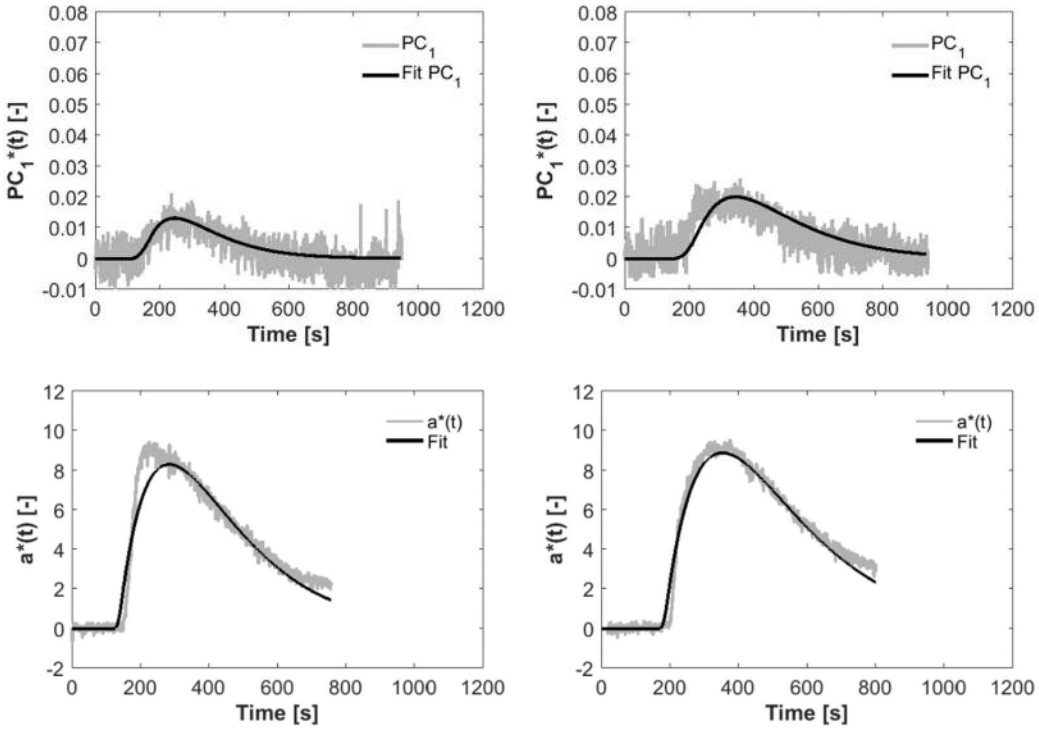

Figure E-4.Curves from colorimetric analysis of pellet (top left: run N18, top right: run 19) and powder tracer content (top left: run N18, top right: run 19) with fit transfer function models (black) determined at a throughput of 10 kg/h, 60 rpm FF and TL A (center point runs).

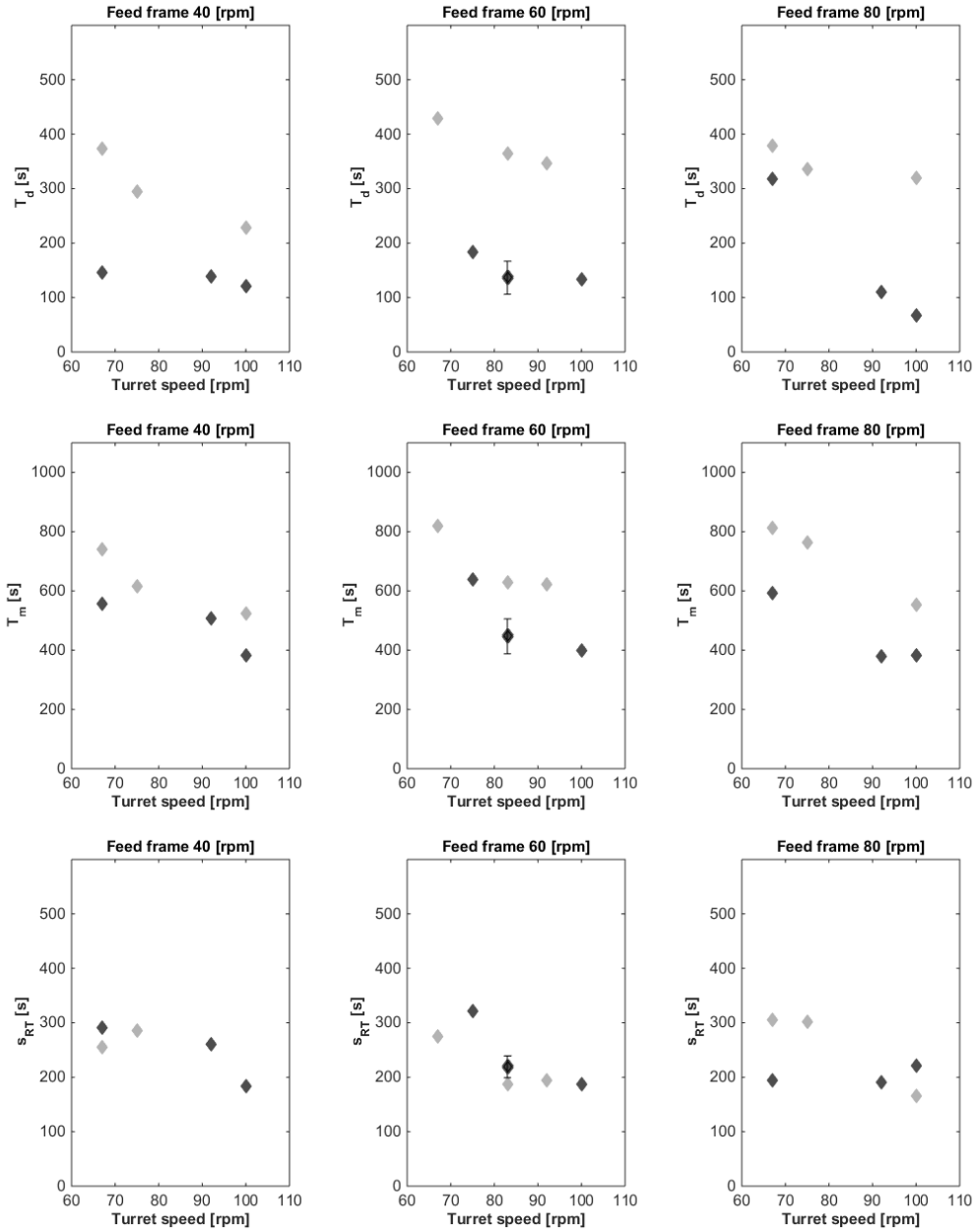

Figure E-5. All tablet press powder RTD characteristics.

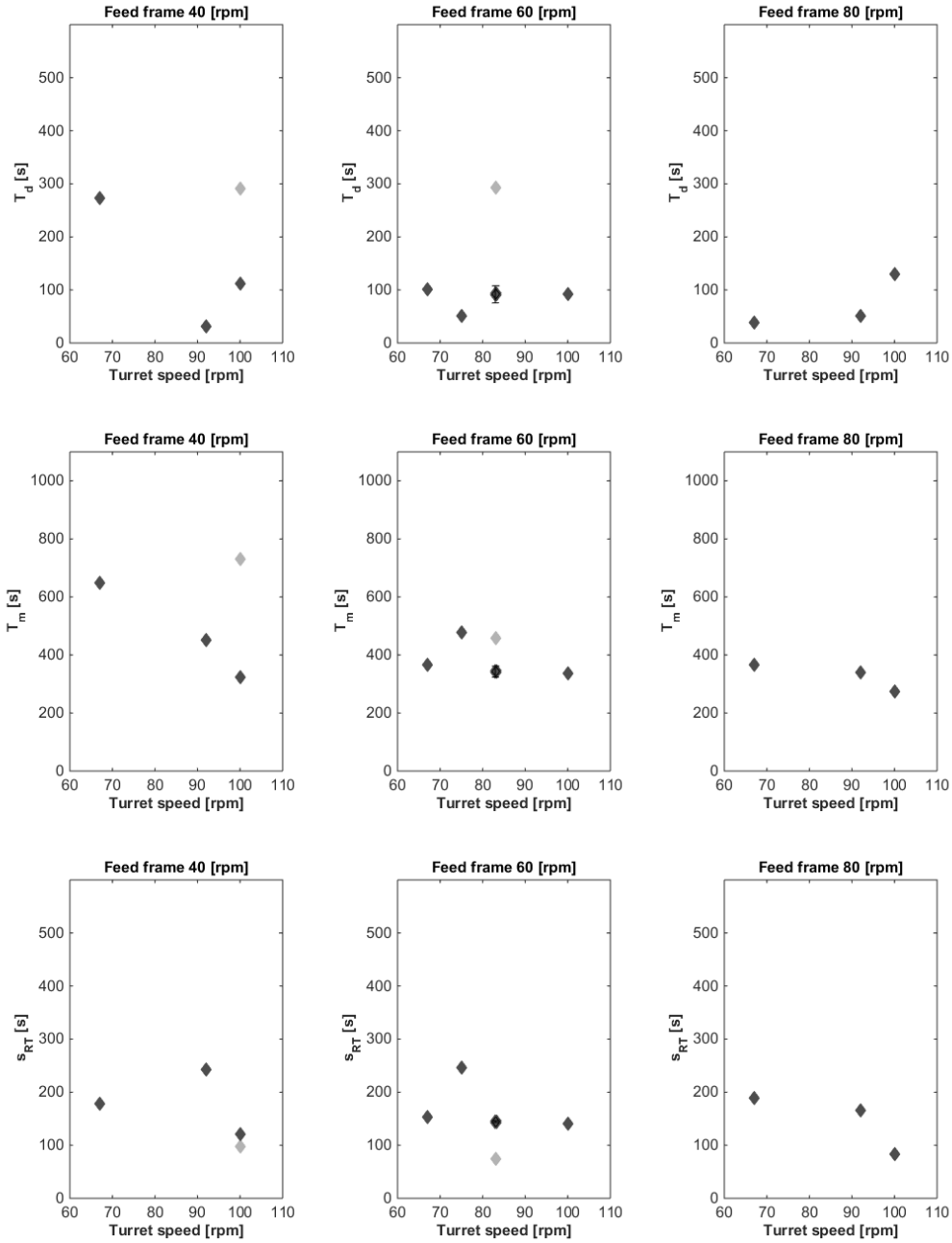

Figure E-6. All tablet press pellet RTD characteristics.

Table E-2. Tableting run settings, fit model parameters and RTD characteristics.

Exp.	Run Order	FF	T	TL	Powder							Pellets						
					k	T_1	T_2	T_3	T_d	T_m	s_{RT}	k	T_1	T_2	T_3	T_d	T_m	s_{RT}
N1	3	40	67	A	203.3	0.5	205.4	205.4	146.6	558.0	290.4	20.9	103.0	103.0	103.0	272.8	649.4	178.4
N2	17	80	67	A	140.8	0.3	137.4	137.4	317.2	592.3	194.3	17.1	109.0	109.0	109.0	38.8	365.9	188.8
N3	6	60	75	A	225.2	0.5	227.5	227.5	182.8	638.1	321.1	33.2	141.8	141.8	141.8	51.1	476.4	245.5
N4	18	40	92	A	238.8	0.4	185.0	185.0	138.1	508.0	260.1	46.4	139.7	139.7	139.7	31.2	450.3	241.9
N5	5	80	92	A	160.3	0.4	134.7	134.7	109.3	379.0	190.3	25.8	95.9	95.9	95.9	51.5	339.2	166.1
N6	7	40	100	A	189.1	0.3	129.8	129.8	121.5	381.3	183.5	20.2	70.2	70.2	70.2	111.8	322.5	121.7
N7*	9	80	100	A	205.4	0.4	157.8	157.8	67.6	383.2	222.0	12.9	48.4	48.4	48.4	129.0	274.3	83.9
N8*	10	60	100	A	113.7	0.1	132.2	132.2	134.0	398.6	186.9	24.7	81.4	81.4	81.4	92.8	337.1	141.1
N9	19	40	67	B	155.9	5.0	181.0	181.0	373.1	739.9	255.3							
N10*	8	80	67	B	209.6	0.4	218.0	218.0	378.2	813.3	305.3							
N11*	11	60	67	B	187.3	1.4	195.1	195.1	428.7	819.8	274.9	15.1°	88.0°	88.0°	88.0°	100.8°	364.8°	152.4°
N12	16	40	75	B	161.7	23.4	309.8	0.2	294.7	616.0	286.0							
N13*	12	80	75	B	197.5	0.6	214.2	214.2	335.8	764.8	302.6							
N14	15	60	92	B	199.8	0.4	137.8	137.8	346.6	622.5	194.8							
N15	1	40	100	B	127.6	37.8	128.0	128.0	228.8	522.2	184.1	17.7	56.5	56.5	56.5	290.8	730.4	97.8
N16	4	80	100	B	153.8	0.4	117.3	117.3	319.2	554.1	165.6							
N17	2	60	83	B	201.8	1.0	132.2	132.2	364.5	629.8	186.8	11.7	43.4	43.4	43.4	292.8	458.0	75.1
*N18**	*13*	*60*	*83*	*A*	*157.5*	*0.2*	*148.7*	*148.7*	*124.6*	*422.1*	*210.2*	*21.9*	*82.6*	*82.6*	*82.6*	*75.7*	*323.5*	*143.0*
*N19**	*14*	*60*	*83*	*A*	*193.9*	*0.5*	*171.4*	*171.4*	*170.9*	*514.1*	*242.1*	*20.9*	*84.6*	*84.6*	*84.6*	*107.8*	*361.5*	*146.4*
R19	21	60	83	A	223.7	0.4	193.3	193.3	119.1	506.0	273.0							
R20	20	60	83	A	167.9	0.4	145.1	145.1	113.7	404.3	205.2							

* RTD measurement performed with 10-fold MgSt mass in formulation; ° data determined for tracer level A;

F. List of Publications

I. Peer-Reviewed Papers Containing Parts of this Thesis

Hörmann, T.R., Jäger, N., Funke, A., Mürb, R.-K., Khinast, J.G., Paudel, A., 2018. Formulation Performance and Processability Window for Manufacturing a Dual-Polymer Amorphous Solid Dispersion via Hot-Melt Extrusion and Strand Pelletization. Int. J. Pharm. 553, 408–421.

Hörmann, T.R., Rehrl, J., Scheibelhofer, O., Schaden, L.-M., Funke, A., Makert, C., Khinast, J.G.. Sensitivity of a Hot-Melt Extrusion and Strand Pelletization Line to Control Actions and Composition Variation. Int. J. Pharm, submitted.

Karttunen, A.-P., Hörmann, T.R., De Leersnyder, F., Ketolainen, J., De Beer, T., Hsiao, W.-K., Korhonen, O., 2019. Measurement of residence time distributions and material tracking on three continuous manufacturing lines. Int. J. Pharm. 563, 184–197.

II. Other Peer-Reviewed Papers

Rehrl, J., Karttunen, A.-P., Nicolaï, N., Hörmann, T., Horn, M., Korhonen, O., Nopens, I., Beer, T. De, Khinast, J.G., 2018. Control of Three Different Continuous Pharmaceutical Manufacturing Processes: Use of Soft Sensors. Int. J. Pharm. 543, 60–72.

Treffer, D., Wahl, P.R., Hörmann, T.R., Markl, D., Schrank, S., Jones, I., Cruise, P., Mürb, R.-K., Koscher, G., Roblegg, E., Khinast, J.G., 2014. In-line implementation of an image-based particle size measurement tool to monitor hot-melt extruded pellets. Int. J. Pharm. 466, 181–9.

III. Book Chapter Contributions

Laske, S., Hörmann, T.R., Witschnigg, A., Koscher, G., Wahl, P., Hsiao, W.K., Khinast, J., 2017a. Continuous Melt Extrusion and Die-Face Pelletization, in: Kleinebudde, P., Khinast, J.G., Rantanen, J. (Eds.), Continuous Manufacturing of Pharmaceuticals. Wiley & Sons, NJ, USA, p. 337.

IV. Oral Presentations

Hörmann, T.R., Laske, S., Koscher, G., Khinast, J.G., 2015. Development of Immediate-Release Tablets Processed via Hot-Melt Extrusion, in: PPS 2015. Polymer Processing Society, Graz: 23.09.2015.

Hörmann, T.R., Laske, S., Koscher, G., Khinast, J.G., 2015. Continuous Manufacturing of Immediate-Release Tablets from Hot-Melt Extruded Pellets, in: 2015 AIChE Annual Meeting. AIChE, Salt Lake City: 11.11.2015.

Hörmann, T.R., Scheibelhofer, O., Rehrl, J., Aigner, I., Khinast, J.G., 2017. Design Space Definition for a Pharmaceutical Hot-Melt Extrusion and Pelletization Process, in: PSSRC Annual Meeting. PSSRC, Graz: 28.06.2017.

Hörmann, T.R., Scheibelhofer, O., Rehrl, J., Funke, A., Paudel, A., Khinast, J.G., 2018b. Development of a tablet manufacturing line via hot-melt extrusion and strand pelletization, in: 2018 AIChE Annual Meeting. AIChE, Pittsburgh: 30.10.2018.

V. Poster Presentations

Hörmann, T.R., Laske, S., Koscher, G., Khinast, J.G., 2016. Process Development for Continuous Extrusion and Pelletization of a Heat and Shear-Sensitive Formulation, in: 2016 AIChE Annual Meeting. AIChE, San Francisco: 14.11.2016.

Hörmann, T.R., Tausendschön, J., Schmid, T., Koscher, G., Khinast, J.G., 2016. Optimization of a Micro-Feeding Unit in a Continuous Pharmaceutical Process Line, in: 2016 PARTEC Conference. VDI Wissensforum, Nuremberg: 21.04.2016.

VI. Academic Thesis

Hörmann, T.R., 2014. An Investigation of the Impact of Feeder Fluctuations on the Content Uniformity of Hot-Melt Extruded Drug Products. Master's Thesis, Graz University of Technology.

Hörmann, T.R., 2012. Continuous Particle Size Monitoring. Bachelor's Thesis, Graz University of Technology.